# Preparation, Characterization, and Reactivity of Ruthenium Protic *N*-Heterocyclic Carbene Complexes

Sarah Elizabeth Flowers

A dissertation

submitted in partial fulfillment of the

requirements for the degree of

Doctor of Philosophy

University of Washington

2017

Reading Committee:

Brandi M. Cossairt. Chair

D. Michael Heinekey

Julia A. Kovacs

Program Authorized to Offer Degree:

Department of Chemistry

University of Washington

## Abstract

Preparation, Characterization, and Reactivity of Ruthenium Protic N-Heterocyclic Carbene Complexes

Sarah Elizabeth Flowers

Chair of the Supervisory Committee:
Professor Brandi M. Cossairt
Department of Chemistry

As carbon dioxide levels continue to rise in our atmosphere, scientific interest has peaked around the capture and utilization of $CO_2$. Not only does $CO_2$ have the potential to be used as a C1 building block for the production of value added chemicals, but $CO_2$ also has the potential to be used as a carbon neutral hydrogen storage material in the form of formic acid. Although catalysts for $CO_2$ reduction exist, many of these catalysts require the use of high temperatures and pressures and are not stable for prolonged exposure to the reaction conditions. Therefore, the challenge of making robust catalysts for $CO_2$ hydrogenation that can operate under mild conditions with high activity remains outstanding.

With the goal of generating a robust and highly active $CO_2$ hydrogenation catalyst in mind, this thesis describes the fundamental metalation chemistry of a novel tripodal bis(protic *N*-Heterocyclic carbene)-phosphine ligand with ruthenium precursors and the reactivity of the resulting organometallic complexes with $CO_2$. Chapter 1 provides a brief overview of $CO_2$ in the earth's atmosphere, a glimpse at $CO_2$ hydrogenation chemistry, and an introduction to traditional and protic *N*-heterocyclic carbene (PNHC) chemistry. Chapter 2 describes the synthesis and characterization of PNHC Ru complexes utilizing $[Cp^*RuCl]_4$ as the ruthenium precursor. Chapter 3 investigates the coordination chemistry and synthesis of PNHC Ru complexes stemming from [(Arene)Ru] precursors. Chapter 4 describes both stoichiometric and catalytic reactivity studies of complexes synthesized in Chapters 2 and 3 with $CO_2$. Finally, Chapter 5 dives into an entirely new subject and discusses the crystallographic structure determination of an unprecedented $In_{37}P_{20}$ nanocluster.

# TABLE OF CONTENTS

# LIST OF FIGURES

# LIST OF SCHEMES

# LIST OF TABLES

# ACKNOWLEDGEMENTS

These last five and a half years have gone by so fast. There are so many people who have helped me get to where I am today. First of all, I would like to thank my high school chemistry teacher Mrs. Allen, who first sparked my interest in chemistry especially for offering an organic chemistry class to high school students!

I would like to thank my undergraduate research advisor Richard Schrock for giving me the opportunity to work in his lab. In his lab, not only did I get discover my interest in organometallic chemistry, but I had the opportunity to work with several amazing graduate students who would teach me, encourage me, inspire me, kindle my interest in chemistry, and serve as my role models as chemists. I cannot thank them enough: Smaranda Marinescu, thank you for teaching me how to be a chemist, for your patience, guidance, and wisdom; Laura Gerber, thank you for being a fantastic mentor, helping guide me through my final year of college, and making me a better chemist.

To my graduate research advisor, Brandi Cossairt, thank you for letting me be one of your first students, for your guidance, your support, and your wisdom. Who would have thought, that when you drew that bimetallic molecule on the white board five years ago in the lab, that I would end up making it and it would be the topic of an entire thesis? You have been an incredible mentor and have really brought out the best in me, I have learned so much. You have let me work on projects that are interesting to me, even if that has meant putting my main project on hold for a while, that has also been so valuable to me. Thank you for letting me help guide my own project and helping me grow as a person and as a chemist.

Werner Kaminsky, I am so thankful that I got the opportunity to work as the Crystallography TA under you. You have taught me so much! You have been such a wonderful mentor, sharing your love of both crystallography and classical music with me, while teaching me valuable life lessons.

Thank you to my undergraduate mentees Yuting Lin and Ashley Matthews and my high school student Zephyr Pitre: you have all taught me more than I have taught you.

Cecilia Johnson, you're my only hope! Thanks for continuing on with my project, the future is in your hands.

Mike Heinekey, thank you so much for having your door open, letting me stroll in, and discussing my chemistry with you.

To my family: my mom, Beth Flowers; my dad, Fort Flowers; my siblings, Caroline, Elaine, Daniel, and Abigail; my grandfather, Dan Flowers; and my grandmother, Jeanie Flowers thank you for all of your love and support throughout my graduate school career, I could not have done it without you. I love you all, always! Also, Echo, you are such a good boy dog, I am so lucky to have you! Keep being good!

To my boyfriend Tyler, thanks for taking the dog out, encouraging me to always eat lunch, talking to me about my chemistry, and being there for me over the last four years.

I would also like to thank the entire Cossairt lab. Thank you for being there every day! What an amazing group!

# DEDICATION

To my family.

You are the best part of me.

# Chapter 1. INTRODUCTION

## 1.1 OVERVIEW: CARBON DIOXIDE

Planet earth has a natural carbon cycle that for millions of years has kept $CO_2$ levels in check. But since the dawn of the industrial revolution, human activity has annually exceeded the natural carbon cycle and therefore $CO_2$ levels in our atmosphere have been on the rise.[1, 2] In 2013 the $CO_2$ concentration in the Earth's atmosphere passed 400 ppm for the first time in the scientific record and levels have continued to rise.[2] It is well accepted that the burning of fossil fuels has led to this increase and it is well accepted in the scientific community that rising levels of $CO_2$ has the potential to have catastrophic consequences on our climate.

In response to these studies, there has been a growing interest in the scientific community for methods to capture and utilize $CO_2$ as a C1 building block for the production of value added chemicals.[3-5] Beyond its obvious use as a feedstock for chemicals such as formate or methanol, $CO_2$ also has the potential to be used as a hydrogen storage material in the form of formic acid.[6]

## 1.2 HOMOGENOUS REDUCTION OF CARBON DIOXIDE TO FORMATE

First reported in 1976, the homogenous hydrogenation of $CO_2$ to formic acid has developed rapidly.[7] With the reverse reaction, the dehydrogenation of formic acid, also being well characterized, the possibility of using formic acid as a carbon neutral hydrogen storage material emerges.[8-10] When designing an effective catalyst for either the forward or reverse transformation, it is important to understand the mechanism of the proposed transformation. While several mechanisms for $CO_2$ hydrogenation have been proposed, the ones that will be

focused on here are the hydrogenation of $CO_2$ and $CO_2$ reduction to formate by transfer hydrogenation.

### 1.2.1 *Hydrogenation of $CO_2$ with hydrogen gas*

The most commonly proposed mechanism for $CO_2$ hydrogenation involves three main steps: 1) hydrogen addition to the catalyst metal center; 2) deprotonation of the metal hydrogen complex with an external base to form a metal hydride, and 3) hydride transfer from the metal center to $CO_2$ (Scheme 1.1).[11] Jeletic *et. al.* demonstrate, using a series of cobalt and rhodium complexes, that the driving force for $CO_2$ hydrogenation is dependent upon the thermodynamic properties of the catalyst, specifically the free energy of $H_2$ addition to the metal center, the $pK_a$ of the corresponding $MH_2$ species, and the hydricity of the M-H complex.[11]

**Scheme 1.1. Generalized catalytic cycle for $CO_2$ hydrogenation, based on a schematic by Jeletic *et. al.*[11]**

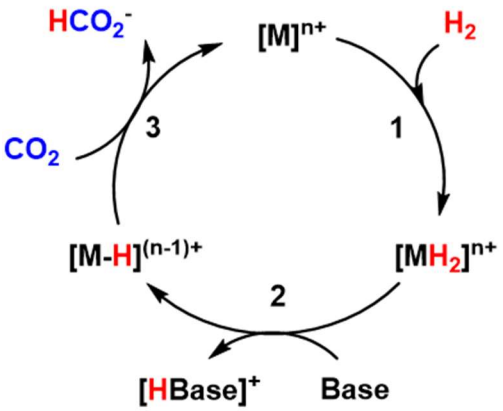


The need for base to access the key M-H intermediate in this most basic mechanism motivates the exploration of chemically non-innocent atmospheric ligand scaffolds that

incorporate basic sites, several of which have been well established.[12, 13] In these examples, the proposed mechanism for $CO_2$ hydrogenation follows the same general steps outlined in Scheme 1.01, but the order of steps changes.[12, 13] In these complexes, an external base deprotonates the ligand scaffold and then hydrogen addition occurs across the metal-ligand center directly creating a metal hydride and a re-protonated ligand backbone.

### 1.2.2 *$CO_2$ reduction to formate by transfer hydrogenation*

Although the vast majority of $CO_2$ hydrogenation chemistry involves the use of hydrogen gas as a source of protons and electrons, there are other reports of using alternative hydrogen atom sources for producing formic acid from $CO_2$. In 2010, Peris and coworkers reported $CO_2$ reduction to formate using *i*PrOH via a proposed transfer hydrogenation mechanism.[14]

Transfer hydrogenation is a type of hydrogen transfer reaction that is typically used for the reduction of ketones to alcohols or imines to amines (Scheme 1.2). There are two proposed mechanistic pathways for these hydrogen transfer reactions: 1) the direct transfer route and 2) the hydridic route.[15]

**Scheme 1.2. Hydride transfer reaction resulting in hydrogenation of $CO_2$ with an alcohol hydrogen source. Adapted from Brandt *et al.*[16]**

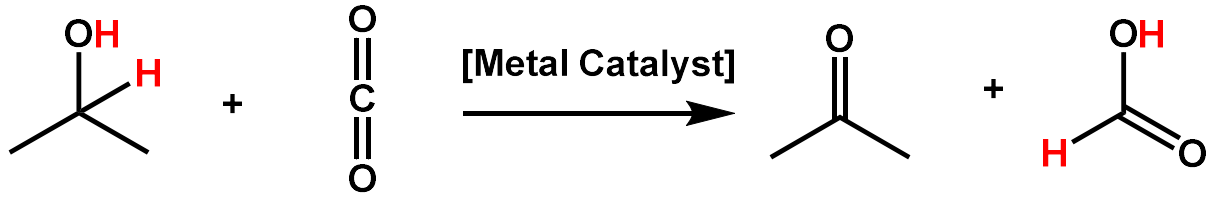

The direct hydrogen transfer mechanism involves coordination of both the donor and the acceptor species to the metal center, and direct hydrogen atom transfer from the donor to the acceptor. This mechanism is characterized by a six coordinate metallacycle transition state. This mechanism is best exemplified by the Meerwein-Ponndorf-Verley (MVP) reduction, in which an aluminum alkoxide catalyzes a hydride shift from the β-carbon on an alcohol donor to the carbonyl carbon of an acceptor (Scheme 1.3).[16]

**Scheme 1.3. MPV reduction "direct transfer" mechanism, adjusted to display $CO_2$ reduction to formic acid. Figure adapted from Brandt *et al.*[16]**

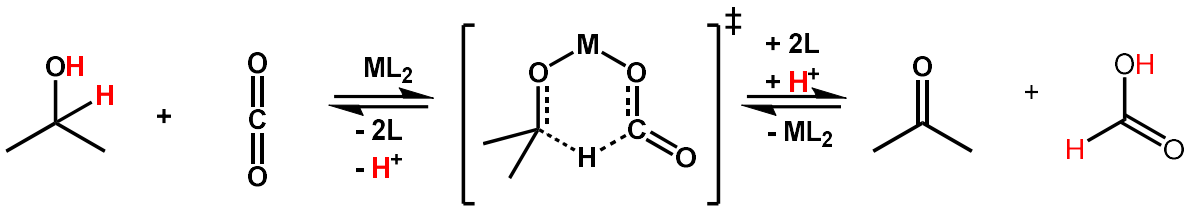


The hydridic route is characterized by a metal hydride intermediate. The hydrogen donor species will bind to the metal center and donate its beta hydrogen atom to form a metal hydride and the oxidized donor species. The metal hydride is then proposed to transfer the hydride and reduce the acceptor species (Scheme 1.4).[15]

**Scheme 1.4 "Hydridic" mechanistic route of transfer hydrogenation based on work from Brandt *et al*,[16] and Zassinovich *et al*.[15]**

Monohydride Route

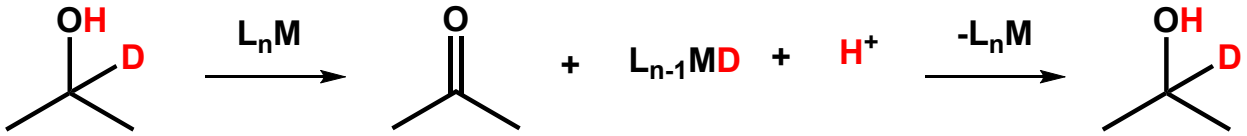


Dihydride Route


## 1.3 N-HETEROCYCLIC CARBENES

N-heterocyclic carbenes (NHCs) are well known, strongly sigma electron donating ligands that can coordinate metal centers to create thermally robust metal complexes. These properties make NHCs excellent candidates for ligands for $CO_2$ hydrogenation reactions, which often occur at high temperatures and pressures.[17-19]

### 1.3.1 *Electronic physical structure of N- heterocyclic carbenes*

Functionalized imidazolium-type carbenes are, perhaps, the most studied subtype of NHCs and will therefore be the subject of the following description. A schematic of a typical imidazolium carbene can be seen in Figure 1.1. The structural and electronic properties of the imidazolium stabilize the carbene and determine the binding properties of the NHC to a metal center, all of which can be readily tuned by synthetic substitution.[18, 20]

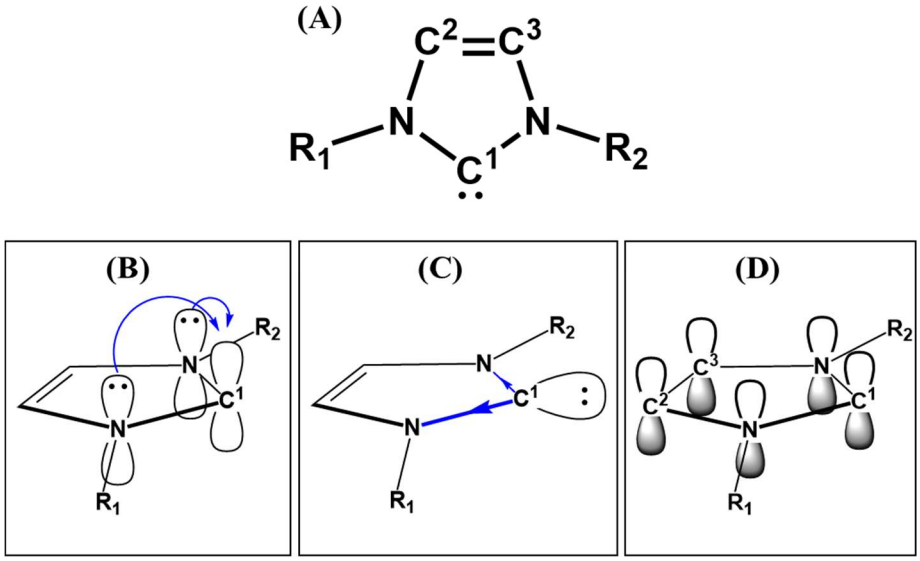


Figure 1.1. Structural and electronic features of N-Heterocyclic carbenes. A) General accepted structure of a free NHC. B) Nitrogen lone pair π-donating to stabilize the empty p-orbital on $C^1$. C) Nitrogen σ-withdrawing effect which stabilizes the singlet carbene. D) Aromaticity of heterocyclic ring stabilizes the NHC by delocalizing three pairs of electrons among four p-oribitals. Figure adapted from Hopkinson *et.al*. [18]

The singlet carbene located at position C(1) has a highest occupied molecular orbital consisting of a lone pair in a hybridized $sp^2$-like orbital in the plane of the heterocycle, with an empty p-orbital perpendicular to the ring (Figure 1.1C). The two adjacent nitrogen atoms to the carbene provide both σ- electron withdrawing character plus stabilizing π- electron-donating character from the lone pairs on the nitrogen atoms, which partially stabilizes the empty p-orbital on the carbene (Figure 1.1B). The aromatic backbone of the imidazole, carbons C(2) and C(3), has been shown to further stabilize an NHC by providing aromatic character to the heterocycle once the carbene has formed (Figure 1.1D).[21] The N-substituents can further enable electronic tenability to the NHC scaffold, influencing carbene stability, as well as sterically preventing dimerization of the free carbene due to Wanzlick equilibrium.[18]

### 1.3.2 *Synthesis of traditional NHC Transition Metal Complexes*

Perhaps the most common way to synthesize metal-NHC complexes is by ligand substitution at the metal center. For this method a free or *in situ* generated carbene can be combined with the appropriate metal precursor to produce a metal carbene complex (figure 1.2).[17] *In Situ* generated carbenes are synthesized by adding an appropriately strong base to an imidazolium salt to deprotonate the carbon at the C(1) position. According to experimental and theoretical studies, the $pK_a$ of the proton at the C(1) position of imidazolium salts vary from 20 to 40 dependent upon the solvent, nitrogen substituents, and aromaticity of the heterocyclic ring.[22, 23]

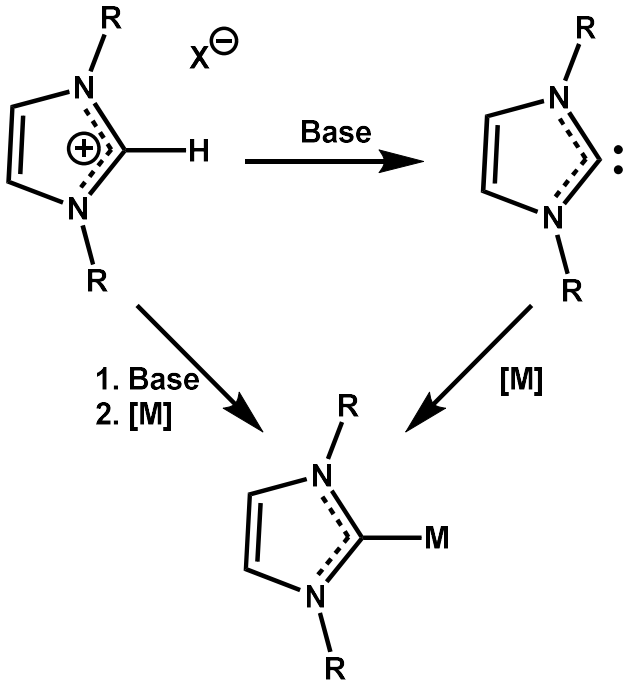


Figure 1.2 Metal-NHC synthesis by ligand substitution based on a figure from Hahn *et al*.[17]

Ligand substitution, however, is not the only method for the preparation of metal-NHC complexes. Other popular methods for NHC metalation with imidazolium salts include trans-

metalation using silver oxide,[17, 24] and direct oxidative addition of the imidazolium salt to a transition metal center.[25]

## 1.4 Protic N-Heterocyclic Carbenes

Protic NHCs or (PNHCs) are a subclass of NHCs which, when bound to a metal center, feature an N-H unit β to the metal center. This N-H position offers the potential to act as a directing group during catalysis, but the proton in this position can also act as a Bronsted-acid for direct cooperation with the substrate.[26, 27]

PNHCs, unlike traditional NHCs, can rarely be isolated as free carbenes and therefore coordination by simple ligand substitution is not an option for these complexes. The synthesis of transition metal PNHC complexes is covered in several reviews, [26-30] but briefly these metalation techniques include acid or base catalyzed tautomerization,[31-33] the use of lithiated azoles for transmetalation,[34, 35] protection-deprotection chemistries,[36] or through oxidative addition of the imidazole.[37, 38]

Chelating PNHCs reported in the literature often do not use an acid or base to promote metalation but proceed through a tether-assisted "redox tautomerization" mechanism.[39-49] In the known examples, a chelating ligand incorporating a neutral electron donor group that binds to the metal center is used and coordination of this donor group is postulated to occur before oxidative addition of the C(1)-H leading to intermediate M-H and M-C bonds that quickly reductively eliminate to form the PNHC (Scheme 2). [42-49]

**Scheme 1.5. A proposed mechanism for tether-assisted oxidative addition followed by reductive elimination to form protic NHC metal complexes figure based on figure by Hahn *et al.*[50]**

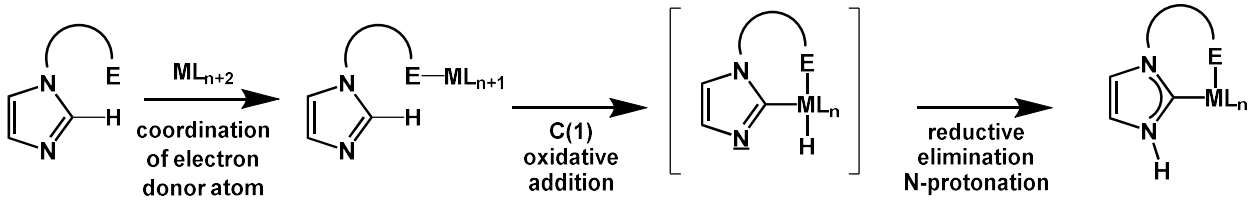


## 1.5 DISSERTATION SUMMARY

The following chapters describe the synthesis, characterization, and reactivity of ruthenium complexes containing tridentate bis(PNHC)-phosphine complexes. This work focuses around the metalation of a bis-imidazole phosphine ligand **L** (Scheme 1.6) to create mono- and bimetallic complexes supported by a tripodal bis(PNHC)-phosphine ligand (Scheme 1.6). Chapter 2 describes the synthesis and characterization of PNHC Ru complexes utilizing $[Cp^*RuCl]_4$ as the ruthenium precursor. Chapter 3 investigates the coordination chemistry and synthesis of PNHC Ru complexes stemming from [(Arene)Ru] precursors. Chapter 4 describes the stoichiometric and catalytic reactivity studies of complexes synthesized in Chapters 2 and 3 with $CO_2$. Finally, Chapter 5 dives into an entirely new subject and discusses the crystallographic structure determination of an unprecedented $In_{37}P_{20}$ nanocluster.

**Scheme 1.6. Ligand (L) and theoretical M-L PNHC complex.**

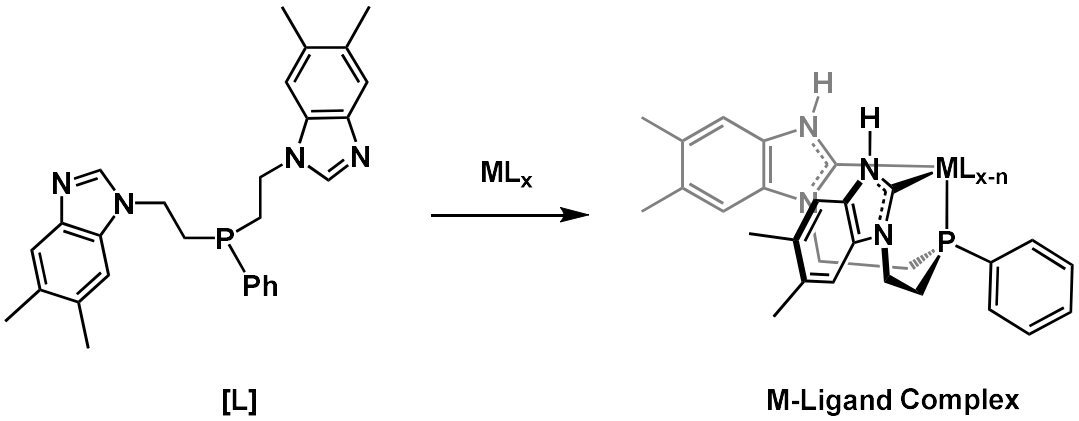


[L] M-Ligand Complex

## 1.6 NOTES TO THE CHAPTER


1. Annual Energy Review 2009; U.S. Energy Information Administration: Washington, DC, **2010**; Tables 12.2–12.4, pp 349– 353.
2. E. W. Team, "ESRL Global Monitoring Division - Global Greenhouse Gas Reference Network.", web.archive.org/web/20170918142645/http://www.esrl.noaa.gov/gmd/ccgg/trends/full.html, (accessed 26 Nov. 2017).
3. N. S. Lewis and D. G. Nocera, *Proc. Natl. Acad. Sci.*, 2006, **103**, 15729-15735.
4. J. D. Figueroa, T. Fout, S. Plasynski, H. McIlvried and R. D. Srivastava, *Int. J. Greenhouse Gas Control*, 2008, **2**, 9-20.
5. N. MacDowell, N. Florin, A. Buchard, J. Hallett, A. Galindo, G. Jackson, C. S. Adjiman, C. K. Williams, N. Shah and P. Fennell, *Energy Environ. Sci.*, 2010, **3**, 1645-1669.
6. W.-H. Wang, Y. Himeda, J. T. Muckerman, G. F. Manbeck and E. Fujita, *Chem. Rev.*, 2015, **115**, 12936-12973.
7. Y. Inoue, H. Izumida, Y. Sasaki and H. Hashimoto, *Chem. Lett.*, 1976, **5**, 863-864.
8. A. F. Dalebrook, W. Gan, M. Grasemann, S. Moret and G. Laurenczy, *Chem. Commun.*, 2013, **49**, 8735-8751.
9. A. K. Singh, S. Singh and A. Kumar, *Catal. Sci. Technol.*, 2016, **6**, 12-40.
10. D. Mellmann, P. Sponholz, H. Junge and M. Beller, *Chem. Soc. Rev.*, 2016, **45**, 3954-3988.
11. M. S. Jeletic, E. B. Hulley, M. L. Helm, M. T. Mock, A. M. Appel, E. S. Wiedner and J. C. Linehan, *ACS Catal.*, 2017, **7**, 6008-6017.
12. C. A. Huff and M. S. Sanford, *ACS Catal.*, 2013, **3**, 2412-2416.
13. R. Tanaka, M. Yamashita and K. Nozaki, *J. Am. Chem. Soc.*, 2009, **131**, 14168-14169.
14. S. Sanz, M. Benítez and E. Peris, *Organometallics*, 2010, **29**, 275-277.
15. G. Zassinovich, G. Mestroni and S. Gladiali, *Chem. Rev.*, 1992, **92**, 1051-1069.

16. J. S. M. Samec, J.-E. Backvall, P. G. Andersson and P. Brandt, *Chem. Soc. Rev.*, 2006, **35**, 237-248.
17. F. E. Hahn and M. C. Jahnke, *Angew. Chem., Int. Ed.*, 2008, **47**, 3122-3172.
18. M. N. Hopkinson, C. Richter, M. Schedler and F. Glorius, *Nature*, 2014, **510**, 485-496.
19. S. Díez-González and S. P. Nolan, *Coord. Chem. Rev.*, 2007, **251**, 874-883.
20. H. Jacobsen, A. Correa, A. Poater, C. Costabile and L. Cavallo, *Coord. Chem. Rev.*, 2009, **253**, 687-703.
21. C. Heinemann, T. Müller, Y. Apeloig and H. Schwarz, *J. Am. Chem. Soc.*, 1996, **118**, 2023-2038.
22. T. L. Amyes, S. T. Diver, J. P. Richard, F. M. Rivas and K. Toth, *J. Am. Chem. Soc.*, 2004, **126**, 4366-4374.
23. A. M. Magill, K. J. Cavell and B. F. Yates, *J. Am. Chem. Soc.*, 2004, **126**, 8717-8724.
24. A. J. Arduengo, H. V. R. Dias, J. C. Calabrese and F. Davidson, *Organometallics*, 1993, **12**, 3405-3409.
25. E. Mas-Marzá, M. Sanaú and E. Peris, *Inorg. Chem.*, 2005, **44**, 9961-9967.
26. F. E. Hahn, *ChemCatChem*, 2013, **5**, 419-430.
27. S. Kuwata and T. Ikariya, *Chem. Commun.*, 2014, **50**, 14290-14300.
28. F. E. Hahn, in *Advances in Organometallic Chemistry and Catalysis*, John Wiley & Sons, Inc., 2013, DOI: 10.1002/9781118742952.ch9, pp. 111-132.
29. M. C. Jahnke and F. E. Hahn, *Coord. Chem. Rev.*, 2015, **293**, 95-115.
30. J. M. C. and H. F. Ekkehardt, *Chem. Lett.*, 2015, **44**, 226-237.
31. J. Ruiz, D. Sol, J. F. Van der Maelen and M. Vivanco, *Organometallics*, 2017, **36**, 1035-1041.
32. R. J. Sundberg, R. F. Bryan, I. F. Taylor and H. Taube, *J. Am. Chem. Soc.*, 1974, **96**, 381-392.
33. R. Sundburg, R. Shepherd and H. Taube, *J. Am. Chem. Soc.*, 1972, **94**, 6558-6559.
34. F. Bonati, A. Burini, B. R. Pietroni and B. Bovio, *J. Organomet. Chem.*, 1989, **375**, 147-160.
35. N. Meier, F. E. Hahn, T. Pape, C. Siering and S. R. Waldvogel, *Eur. J. Inorg. Chem.*, 2007, **2007**, 1210-1214.
36. G. E. Dobereiner, C. A. Chamberlin, N. D. Schley and R. H. Crabtree, *Organometallics*, 2010, **29**, 5728-5731.
37. K. J. Cavell and D. S. McGuinness, *Coord. Chem. Rev.*, 2004, **248**, 671-681.
38. T. Kösterke, T. Pape and F. E. Hahn, *J. Am. Chem. Soc.*, 2011, **133**, 2112-2115.
39. J. T. Chantson and S. Lotz, *J. Organomet. Chem.*, 2004, **689**, 1315-1324.
40. S. H. Wiedemann, J. C. Lewis, J. A. Ellman and R. G. Bergman, *J. Am. Chem. Soc.*, 2006, **128**, 2452-2462.
41. J. C. Lewis, S. H. Wiedemann, R. G. Bergman and J. A. Ellman, *Org. Lett.*, 2004, **6**, 35-38.
42. S. E. Flowers and B. M. Cossairt, *Organometallics*, 2014, **33**, 4341-4344.
43. K. L. Tan, R. G. Bergman and J. A. Ellman, *J. Am. Chem. Soc.*, 2002, **124**, 3202-3203.
44. K. Araki, S. Kuwata and T. Ikariya, *Organometallics*, 2008, **27**, 2176-2178.
45. V. Miranda-Soto, D. B. Grotjahn, A. L. Cooksy, J. A. Golen, C. E. Moore and A. L. Rheingold, *Angew. Chem., Int. Ed.*, 2011, **50**, 631-635.

46. V. n. Miranda-Soto, D. B. Grotjahn, A. G. DiPasquale and A. L. Rheingold, *J. Am. Chem. Soc.*, 2008, **130**, 13200-13201.
47. F. E. Hahn, A. R. Naziruddin, A. Hepp and T. Pape, *Organometallics*, 2010, **29**, 5283-5288.
48. A. R. Naziruddin, A. Hepp, T. Pape and F. E. Hahn, *Organometallics*, 2011, **30**, 5859-5866.
49. T. Toda, S. Kuwata and T. Ikariya, *Chem. Eur. J.*, 2014, **20**, 9539-9542.
50. M. C. Jahnke and F. E. Hahn, *Coord. Chem. Rev.*, 2015, **293-294**, 95-115.

# Chapter 2. MONO- AND DI-METALATION OF IMIDAZOLE-PHOSPHINE LIGANDS WITH $[RUCP^*(\mu^3\text{-}CL)]_4$

*Significant portions of the following have been previous published.*[1]

## 2.1 INTRODUCTION

N-heterocyclic carbenes (NHCs) and their complexes with transition metals enable a variety of important transformations, such as the activation of white phosphorus, [2] olefin metathesis, [3] and substrate oxidation.[4] Often compared with electron-rich organophosphines,[5, 6] NHCs are considered strong σ-donors with weak back-bonding character.[6] The NHC framework can be functionalized at both the C–C backbone and at the nitrogen positions (wingtips), allowing the steric and electronic properties of these ligands to be easily tuned. Although transition-metal NHC complexes containing one metal center have been thoroughly studied, there are limited reports of NHCs acting as bridging ligands in heterometallic complexes, with a geometry where one metal is bound at the C1 position and the second metal is bound at one of the wingtip nitrogen atoms. [7-13] With this in mind, we envision using a tridentate ligand bearing two NHCs to create a macrocyclic framework supporting two different metal centers, as shown in Figure 2.1. Our approach builds upon the flourishing field of "protic" NHC complexes. [12, 14-18] With an appropriate choice of ancillary ligands, such structures could be poised to carry out a variety of unique transformations through cooperation between the two metal centers. This report details our preparation of a new bisimidazole-phosphine ligand that supports this type of binding motif, as well as mono- and dimetalation of this ligand.

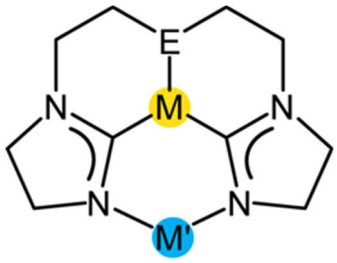


Figure 2.1 Motivating structural motif for a bimetallic tridentate biscarbene phosphine complex

## 2.2 RESULTS AND DISCUSSION

### 2.2.1 *Mono- and Di-metalation of a bisimidazole phosphine ligand*

The bisimidazole-phosphine ligand [(Me$_2$benzimid)Et]$_2$P$^{Ph}$ (**L**) was prepared using a three step synthesis from commercially available 5,6-dimethylbenzimidazole using methods derived from the literature.[12, 19] In the final step, vinyl-substituted benzimidazole (2 equiv.) was added to a –35 °C solution of phenylphosphine (1 equiv.) and KO$^t$Bu (0.8 equiv.) in THF (Scheme 2.1).[20] Monitoring the reaction by $^{31}$P{$^1$H} NMR spectroscopy showed conversion to **L**, with a characteristic singlet at –35 ppm, a downfield shift from the starting phenylphosphine singlet at –120 ppm.

**Scheme 2.1 Synthesis and metalation of a tridentate bisimidazole phosphine ligand.**

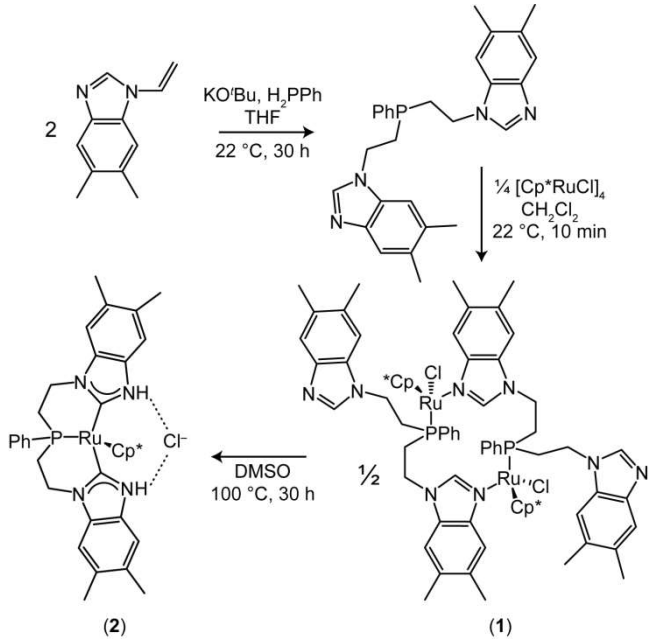


Addition of [RuCp*($\mu^3$-Cl)]$_4$ (0.25 equiv) to a –35 °C solution of **L** in $CH_2Cl_2$ rapidly produces orange, homobimetallic complex **1** (Scheme 2.1) as seen by *in situ* monitoring by $^{31}$P{$^1$H} NMR and $^1$H NMR spectroscopy. The appearance of a $^{31}$P{$^1$H} NMR resonance at 22 ppm, along with the concomitant disappearance of the $^{31}$P{$^1$H} NMR signal for the starting ligand at –35 ppm, suggests complete conversion to **1**. The $^1$H NMR spectrum of **1** displays four

methyl singlets as well as six singlets in the aromatic region that correspond to two electronically different imidazole groups within the complex (Figure 2.2). The X-ray structure (2.3) reveals that **1** is a dimeric species related in symmetry by a crystallographically imposed C2 proper rotation axis. Complex **1** has an inner sphere chloride with a Ru-Cl interatomic distance of 2.464(2) Å. A related example of a Cp*Ru dimer species with bridging phosphine-N-bound ligands has been reported in the literature.[21]

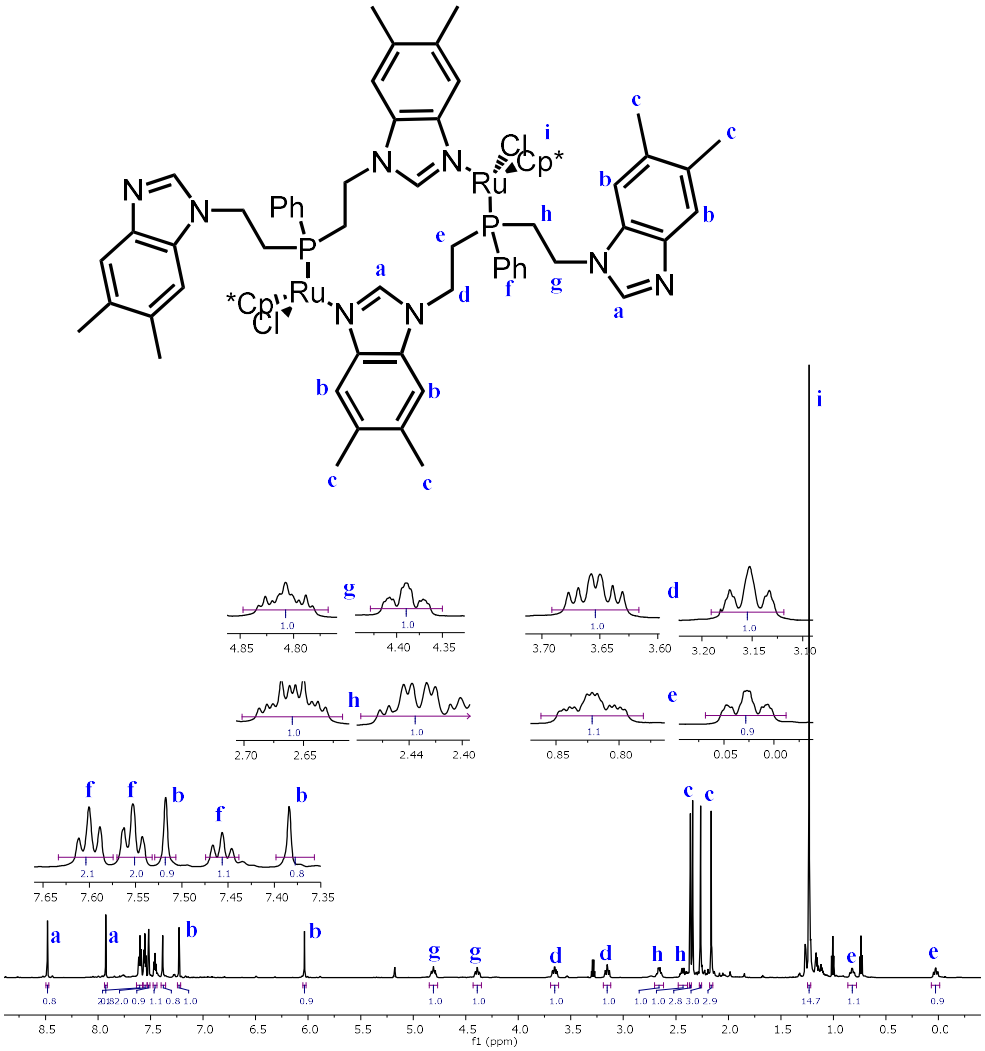


Figure 2.2. $^{1}$H NMR(700 MHz, $CD_2Cl_2$, 298 K) of **1** in $CD_2Cl_2$.

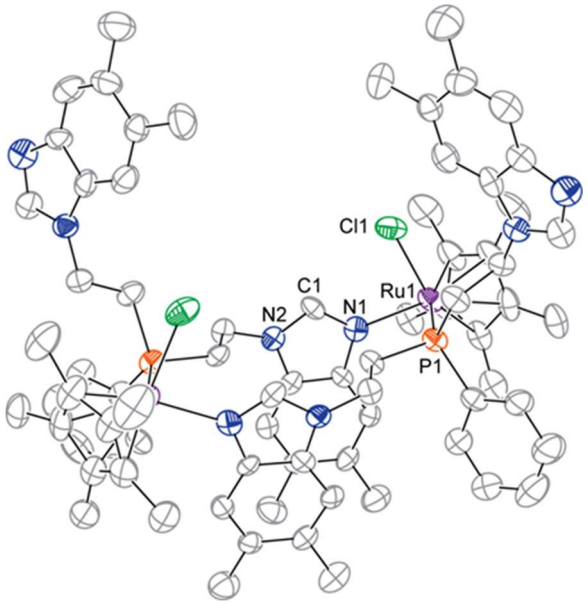


Figure 2.3. Single crystal X-ray diffraction structure of **1** with thermal ellipsoids shown at the 50% probability level. Hydrogen atoms are omitted for clarity.

When **1** is heated at 100 °C for 30 h in DMSO, tautomerization of the imidazole units and complete conversion to monometallic ruthenium biscarbene complex **2** is observed *in situ* by $^{1}$H and $^{31}$P{$^{1}$H} NMR spectroscopy. Complex **2** was isolated in 71 % yield as a pale-yellow powder. It should be noted that tautomerization of the proton at C1 also occurs in $CH_2Cl_2$ at room temperature over the course of a week as observed by $^{1}$H and $^{31}$P{$^{1}$H} NMR studies. This observation suggests that **2** is more thermodynamically stable than **1** and that base assistance is not strictly required for tautomerization,[11] however we postulate that halide dissociation is required in this case. The $^{31}$P{$^{1}$H} NMR spectrum of **2** displays a characteristic singlet at 38 ppm in THF-d$^{8}$. The presence of a broad N-H singlet in the $^{1}$H NMR spectrum of **2** at 14.5 ppm along with the appearance of a doublet centered at 198.5 ppm with a 17.5 Hz $^{2}J_{CP}$ in the $^{13}$C{$^{1}$H} NMR spectrum are consistent with a bis-carbene ruthenium complex where the NHC moieties are magnetically equivalent.

High-quality, yellow crystals of **2** were obtained via vapor diffusion of $Et_2O$ into a saturated THF solution of **2** at 22 ℃. The X-ray crystal structure shows that **2** contains a pseudo mirror plane through P1 and Ru1, as well as an outer-sphere chloride with hydrogen bonding interactions to the N-H imidazole wingtips (Figure 2.4). This structure is the first reported tridentate ligand with an NHC-phosphine-NHC backbone (CPC ligand) bound to a metal center, though related PCPC

tetradentate macrocycles and bidentate CP complexes have been reported.[22-25] Importantly, complex **2** contains an unprecedented NHC-donor-NHC motif with two N-H wingtips poised for further functionalization.

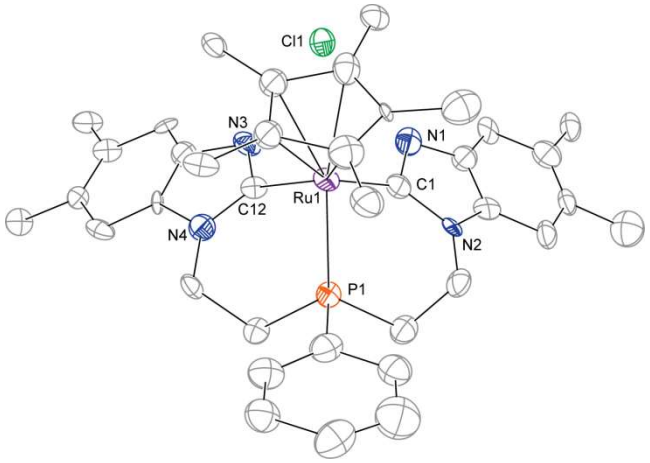


Figure 2.4. Single crystal X-ray diffraction structure of 2 with thermal ellipsoids shown at the 50% probability level. Hydrogen atoms are omitted for clarity.

The N-H wingtips of **2** are cleanly deprotonated with 2 equivalents of *n*-BuLi in THF at −78 °C to form **3** (**Scheme 2.2**). Complex **3** was isolated as a bright "highlighter-yellow" colored powder in 53 % yield. A downfield shift in the $^{31}P\{^{1}H\}$ NMR spectrum, with respect to **2,** in THF-$d^8$ from 38 ppm to 46 ppm indicated the formation of a new species. A doublet at 195.8 ppm ($^{2}J_{cp}$= 20 Hz) in the $^{13}C\{^{1}H\}$ NMR spectrum along with the absence of any N-H peaks in the $^{1}H$ NMR spectrum are consistent with the ruthenium carbene bond remaining intact and complete deprotonation of the N-H wingtips.

**Scheme 2.2. Insertion of a second metal center into the biscarbene ligand framework**

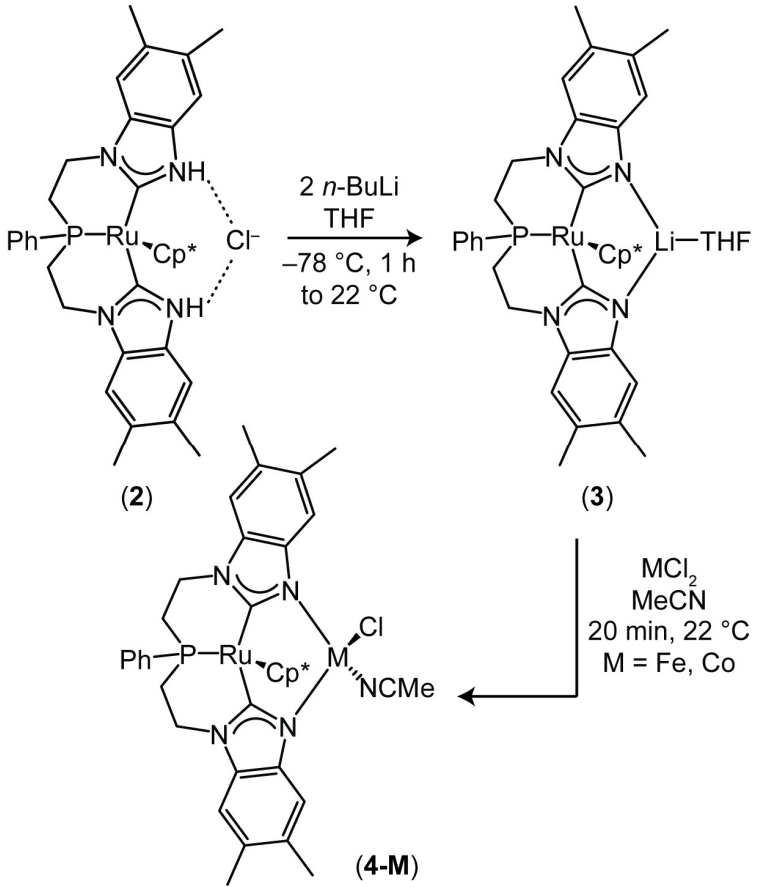


X-ray quality crystals of **3** were grown via slow evaporation of THF at 22 °C. The X-ray crystal structure of **3** reveals Li ion coordination between the deprotonated imidazole wingtips with a N1-Li1 distance of 1.925(17) Å and a N3-Li1 distance of 1.916(18) Å, (Figure 2.5) along with the coordination of one THF molecule to the lithium ion. The structure and synthesis of **3** are related to recently reported transition metal and rare earth metal complexes linked to lithium through a bridging imidazole or through a "protic" carbene ligand.[12, 13]

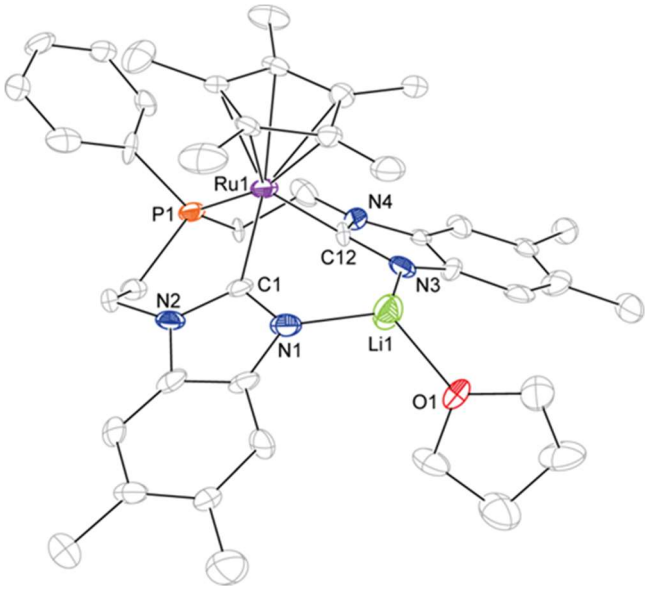


Figure 2.5. Single crystal X-ray diffraction structure of 3 with thermal ellipsoids shown at the 50% probability level. Hydrogen atoms are omitted for clarity.

Complex **3** is a useful precursor for the synthesis of heterobimetallic complexes **4-Fe** and **4-Co** (Scheme 2.2). The addition of a metal dichloride salt, either $FeCl_2$ or $CoCl_2$, to an equimolar amount of **3** in acetonitrile at room temperature immediately evokes a color change, from light yellow to emerald green in the case of $CoCl_2$ and from light yellow to a darker yellow in the case of $FeCl_2$. The $^1H$ NMR spectra of both **4-Fe** and **4-Co** display broad and contact shifted resonances, consistent with paramagnetic complexes. This observation, combined with an understanding of the electron localization in **3,** and Evans method analysis of **4-Fe** and **4-Co** is consistent with a preliminary assignment of Ru(II)-Fe(II) and Ru(II)-Co(II), respectively. High quality crystals suitable for X-ray diffraction precipitated out of the NMR solutions after 24 hours in sealed J-Young tubes. Complexes **4-Fe** (Figure 2.66) and **4-Co** (Figure 2.7) are isostructural. Both complexes have M-Cl bonds with the chloride ligand pointing in the same direction as the Cp*-ring and both Fe and Co centers are bound to one molecule of acetonitrile. The M-N1 and M-N3 bond lengths of 1.9601(16) and 1.9697(16) Å (M = Co) and 2.0017(17) and 2.0006(17) Å (M = Fe) are consistent with a symmetric electronic structure with both nitrogen atoms assigned as anionic.[26] There is no significant variation in the Ru-C1 or Ru-C12 interatomic distances from **2** (2.029(8) and 2.029(10) Å) to **3** (2.073(9) and 2.024(9) Å) to **4-Fe** (2.0355(19) and 2.0407(19) Å)

and **4-Co** (2.029(19) and 2.0348(19) Å). Both **4-Fe** and **4-Co** have a Ru-M interatomic distance of roughly 3.6 Å.

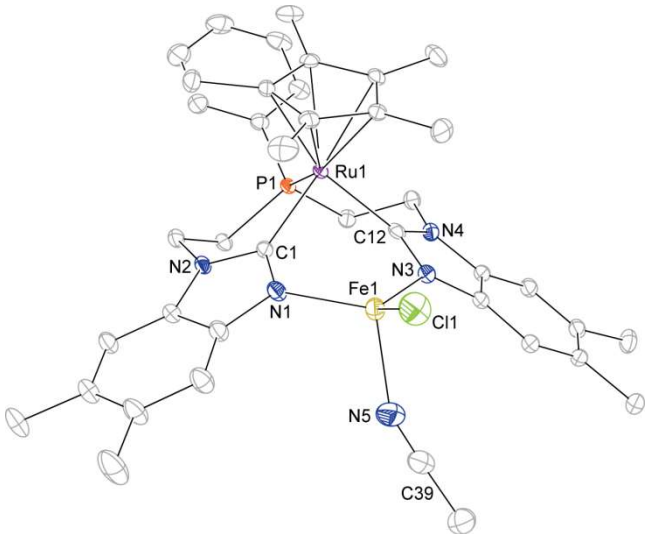


Figure 2.6. Single crystal X-ray diffraction structure of **4-Fe** with thermal ellipsoids shown at the 50% probability level. Hydrogen atoms are omitted for clarity.

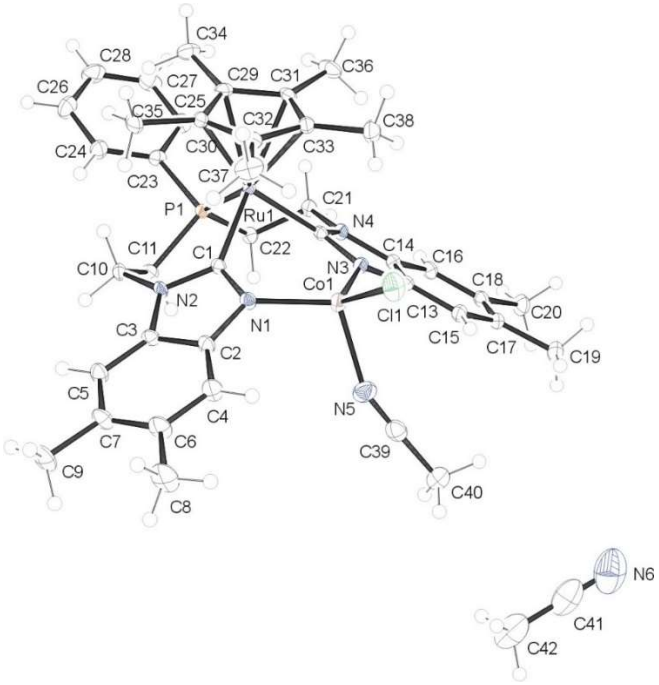


Figure 2.7. Crystal Structure Complex 4-Co. ORTEP of the structure with thermal ellipsoids at the 50% probability level.

### 2.2.2 *Metalation of a mono-imidazole phosphine ligand*

*Contributions to this project were made by Yuting F. Lin*

We have also have studied metalation of a mono-imidazole phosphine ligand (**L-Yuting**). Ligand species **L-Yuting** was prepared by the addition of vinyl imidazole to an equimolar amount of diphenylphosphine followed by addition of a catalytic amount of KOtBu in THF at room temperature.[27] Stirring the reaction overnight resulted in a color change from a vibrant orange to a pale yellow. Ligand **L-Yuting** can be isolated as a white powder in 73% yield. Monitoring of the reaction with $^{31}$P-NMR spectroscopy showed complete conversion to ligand **L-Yuting** with a characteristic singlet at -23 ppm, a downfield shift from the starting diphenylphosphine singlet at -40 ppm.

The addition of 0.25 equivalents of [RuCp*($\mu^3$-Cl)]$_4$ to a room temperature solution of complex **L-Yuting** in $CH_2Cl_2$ rapidly produced the dark-yellow, homobimetallic complex **5** (Scheme 2.4). The $^{31}$P-NMR shows a downfield shift of the singlet to 28 ppm. High quality crystals were obtained by cooling a supersaturated solution of complex **5** in THF from 100 °C to 22 °C in a sealed J-Young tube. Single crystal X-ray analysis revealed that complex **5** crystalized in a triclinic P-1 space group (Figure 2.8). The molecular structure contains a 180-degree improper inversion center.

**Scheme 2.3. Synthesis of an ethyl linked mono-imidazole phosphine chelate complex 5 followed by the synthesis of complex 6.**

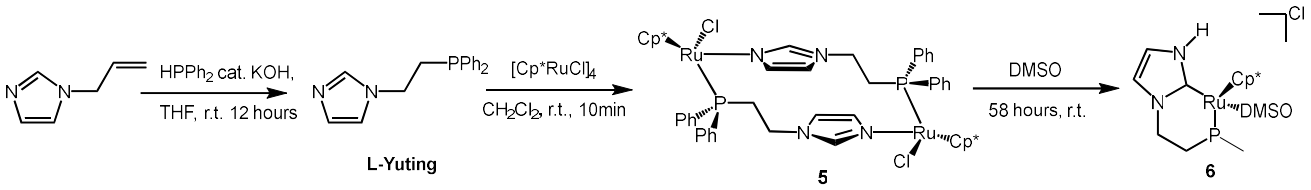

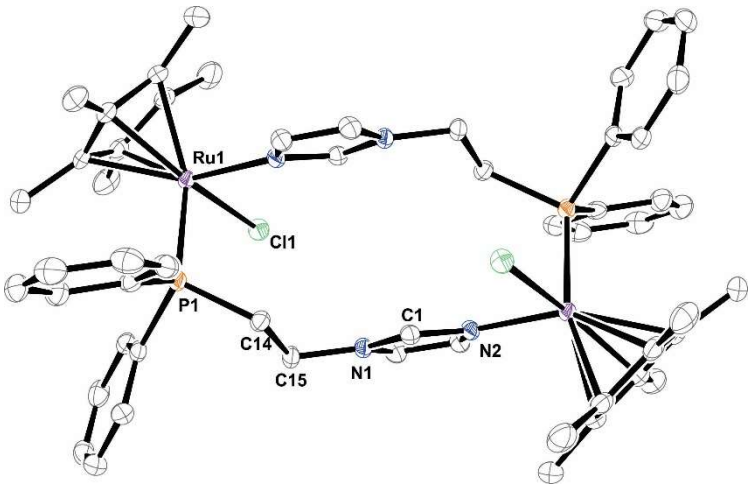


Figure 2.8 X-ray crystal structure of Complex 5. Showing 50% probability ellipsoids. Hydrogen atoms and solvent omitted for clarity. Select bond lengths

Base promoted tautomerization from imidazole bound metal complexes to NHC complexes is a well-studied transformation.[28] However, complete tautomerization of complex **5** occurs in DMSO at room temperature after 58 hours to form the N-heterocyclic carbene complex **6** without the use of a exogenous base (Scheme 2.3). Heating complex **5** at 100 °C for 17 hours also affords complex **6**. The $^{1}$H-NMR spectrum of complex **6** shows a broad N-H singlet at 11.20 ppm. This proton resonance, in conjunction with the doublet in the $^{13}$C-NMR spectrum at 170.0 ppm ($^{2}J_{CP}$ value of 19.7 Hz), strongly support the existence of a ruthenium carbene moiety in this complex. The $^{1}$H-NMR spectrum also shows two sets of diastereotopic protons that are consistent with this six-membered ring system consisting of Ru1, P1, C1, N2, and the ethane backbone. Monitoring the reaction via $^{31}$P-NMR spectroscopy (Figure 2.09) shows the formation of an intermediate at 32 ppm, which we hypothesize is the DMSO adduct of complex 2 that results from breakup of the dimer species. The single product, complex **6**, is seen in the phosphorus NMR at 36 ppm.

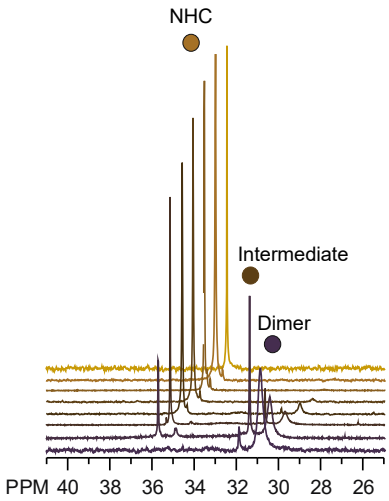


Figure 2.9. Stacked 1H-NMR plot displaying the reaction from dimer complex **5** to NHC complex **6**.

Our investigations into the synthesis of the complex **6** revealed several features of the metalation of this type of imidazole linked phosphine ligand that were previously unreported.[29, 30] First, the clean isolation of the homo-bimetallic intermediate complex **5** highlights that pre-coordination to two ligand units precedes carbene formation. Secondly, through careful solvent screening, we have revealed the importance of using a polar, hydrogen bond forming solvent in the formation of the desired NHC complex.

## 2.3 CONCLUSIONS

In this Chapter, we have reported the synthesis of heterobimetallic complexes **4-Fe** and **4-Co** supported by a new CPC tridentate ligand. These complexes have been prepared by initial coordination of the bisimidazole-phosphine ligand to $[RuCp^*(\mu^3\text{-}Cl)]_4$ to form **1**, followed by tautomerization in DMSO to form **2**. Deprotonation of the N-H wingtips of **2** leads to the formation of **3**, which can then be converted to **4-Fe** and **4-Co** by salt metathesis with the respective metal chlorides. We hypothesize that this strategy for the synthesis of bimetallic complexes supported by this type of bisimidazole-phosphine ligand could be generalized to many other metal centers. We are currently targeting other bimetallic complexes supported by **L** that will allow for

cooperative reactivity between the two adjacent metal centers to study the influence of metal identity on the electronic structure and reactivity of these complexes.

## 2.4 EXPERIMENTAL

Unless otherwise noted, all experiments were carried out under an inert-atmosphere of nitrogen using either Schlenk line or glove box techniques. The NMR spectra were obtained on a Bruker AV301, a Bruker DRX500, a Bruker AV300, or Bruker AV700 spectrometers. All solvents were dried over calcium hydride, distilled before use, and stored over molecular sieves under $N_2$. Anhydrous $FeCl_2$ and $CoCl_2$ were purchased from Strem Chemicals and were used without further purification. Superhydride, 5,6-dimethylbenzimidazole, phenylphosphine, $[Cp^*RuCl_2]_x$, were purchased from Sigma Aldrich and used without further purification. All deuterated solvents were purchased from Cambridge Isotope Laboratories, Inc., were dried over calcium hydride, distilled before use, and stored over molecular sieves under $N_2$. All glassware was dried in an oven at 160 °C for at least 3 hours before use. $[RuCp^*Cl]_4$ was prepared according to the published procedure.[31] Evan's method analysis was performed with 4-Co and 4-Fe separately in sealed J-Young tubes using $d^6$-DMSO as a solvent and ferrocene as an internal standard or additionally using $d^6$-benzene as both the solvent and internal standard. Crystallographic details and supplementary information and figures, including all spectra discussed in this chapter, can be found in section 2.5.

*Chloroethyl-substituted 5,6-dimethylbenzimidazole.* This complex was prepared via modification of a procedure reported by Hahn *et al*.[27] This reaction is not air sensitive and was conducted outside the glove box. A 1 L round bottom flask equipped with a stir bar was charged with 5,6-dimethylbenzimidazole (15.788 g, 108 mmol, 1 eq), KOH (33.528 g, 5.98 mmol, 5.5 eq), $K_2CO_3$ (29.60 g, 214 mmol, 2 eq), $Bu_4NBr$ (2.310 g, 7.17 mmol, 0.06 eq) a stir bar, and dichloroethane (300 ml). The mixture was refluxed at 60 °C for 4 hours and a brown solution with an off-white suspension was observed. The solution was allowed to cool to room temperature, then the solids were collected on a frit, and the remaining product was extracted with DCM (2 x 100 ml). The solvent was removed via rotary evaporation and the resulting solids were carried on to the synthesis of vinyl-substituted 5,6-dimethylbenzimidazole. Our characterizations of the products of this

reaction revealed that the organic extract is a mixture of chloroethyl-substitituted 5,6-dimethylbenzimidazole and vinyl-substituted 5,6-dimethylbenzimidazole.

*Vinyl-substituted 5,6-dimethylbenzimidazole.* This reaction is not air sensitive and was conducted outside of the glove box. Assuming full conversion from the previous reaction, a 1 L round bottom flask equipped with a stir bar was charged with chloroethyl-substituted 5,6-dimethylbenzimidazole (22.537 g, 108 mmol, 1 eq ), hydroquinone (0.595 g, 5.40 mmol, 0.05 eq), and KOH (25.516 g, 455 mmol, 4 eq), and isopropanol (300 ml) The reaction mixture was refluxed under nitrogen for 2 hours. The volatiles were removed via rotary evaporation, and the resulting solids were dissolved in 1 L of water. The solution was separated into 5 fractions of 200 ml. The organic product was extracted from each 200 ml portion of aqueous solution with DCM (3 x 100 ml). The DCM fractions were collected and combined, washed with 200 ml of saturated NaCl solution, dried over $MgSO_4$, filtered, and the solvent was removed via rotary evaporation. The apricot-beige crystalline product was isolated by recrystallization from hexanes, and dried under vacuum giving 11.305 g (61% yield from 5,6-dimethylbenzimidazole). $^1$H NMR (300 MHz, Chloroform-*d*) δ 7.95 (s, 1H, Ar-H), 7.50 (s, 1H, Ar-H), 7.19 (s, 1H, Ar-H), 7.02 (dd, *J* = 15.9, 9.0 Hz, 1H, C-H), 5.42 (dd, *J* = 15.9, 1.6 Hz, 1H, C-H), 4.96 (dd, *J* = 9.0, 1.6 Hz, 1H, C-H), 2.33 (s, 3H, $CH_3$), 2.31 (s, 3H, $CH_3$). $^{13}$C NMR (75 MHz, $CD_2Cl2$) δ 143.04, 140.29, 133.31, 132.13, 131.33, 128.68, 120.57, 110.98, 101.19, 20.66, 20.34.

*[(Me$_2$benzimid)Et]$_2$P$^{Ph}$* ***(L).*** A −35°C solution of phenylphosphine (18.662 g, 10 % weight in hexanes, 17.0 mmol, 2 eq) and a –35°C solution of KO$^t$Bu (0.8336 g, 7.4289 mmol, 0.8 eq), in THF (15 ml) were added to a 100 ml round bottom flask equipped with a stir bar. A color change was observed from colorless to bright yellow. The resulting solution was added in several portions to a 250 ml round bottom Schlenk bomb, equipped with a stir bar, containing a –35°C solution of vinyl-substituted 5,6-dimethylbenzimidazole (3.205 g, 18.6 mmol, 2 eq) in THF (15 ml). The resulting mixture was allowed to warm to room temperature, was monitored via $^{31}$P{$^1$H}-NMR spectroscopy, and was determined to be complete after 24 hours. The resulting solution was dried under vacuum on the Schlenk line. A white powder, 1.483 g (39% yield), was collected upon recrystallization from toluene. $^1$H NMR (500 MHz, Benzene-$d_6$) δ 7.96 (s, 2H, Ar-H), 7.43 (s, 2H, Ar-H), 7.28 (dt, *J* = 6.3, 3.6 Hz, 1H, Ph-H), 7.24-7.10 (m, 1H, Ph-H), 6.86 (s, 2H, Ar-H), 3.60-3.40

(m, 5H, $CH_2$), 2.35 (s, 6H, $CH_3$), 2.28 (s, 6H, $CH_3$), 1.69-1.59 (m, 2H, $CH_2$), 1.69-1.49 (m, 2H, $CH_2$). $^{13}C$ NMR (126 MHz, $CDCl_3$) δ 142.56, 141.75, 134.83 (d, $J_{CP}$= 13.6 Hz), 132.82, 132.65, 132.03, 131.81, 131.02, 130.35, 129.08 (d, $J_{CP}$ = 7.7 Hz), 120.48, 109.56, 41.96 (d, $J_{CP}$ = 22.4 Hz), 29.12 (d, $J_{CP}$ = 14.4 Hz), 20.56, 20.22. $^{31}P\{^1H\}$ NMR (202 MHz, $CDCl_3$) δ −34.9 Elemental analysis: C 73.723, H 6.660, N 11.745; predicted $C_{28}H_{31}N_4P$ – C 73.99, H 6.87, N 12.33.

*Complex **1**.* In an $N_2$ glove box, a –35 °C solution of $[RuCp^*Cl]_4$ (0.303 g, 0.303 mmol, 0.25 eq) in DCM (15 ml) was added dropwise to a 100 ml Schlenk bomb a stirring containing a –35 °C solution of **L** (0.550 g, 1.21 mmol, 1 eq) in DCM (15 ml). The reaction mixture was allowed to warm to room temperature over the course of 45 minutes. The volatiles were removed under reduced pressure, and the resulting solids were directly dissolved in DMSO and used for the synthesis of complex **2**. Complex **1** was recrystallized for single-crystal X-ray diffraction analysis using slow evaporation of DCM. $^1H$ NMR (700 MHz, Methylene Chloride-d2) δ 8.48 (s, 1H), 7.92 (s, 1H), 7.60 (t, J = 7.8 Hz, 2H, Ph-H), 7.55 (td, J = 7.6, 1.7 Hz, 2H, Ar-H), 7.52 (s, 2H, Ar-H), 7.46 (t, J = 7.2 Hz, 1H, Ph-H), 7.38 (s, 1H, Ph-H), 7.23 (s, 1H, Ar-H), 6.03 (s, 1H, Ar-H), 4.81 (tt, J = 13.3, 4.4 Hz, 1H, $CH_2$), 4.39 (tdd, J = 13.6, 4.9, 2.6 Hz, 1H, $CH_2$), 3.65 (ddd, J = 14.3, 12.5, 6.0 Hz, 1H, $CH_2$), 3.15 (tt, J= 13.5, 3.2 Hz, 1H, $CH_2$), 2.66 (tdd, J = 13.1, 8.1, 4.6 Hz, 1H, $CH_2$), 2.43 (qd, J = 12.6, 4.9 Hz, 1H, $CH_2$), 2.36 (s, 3H, $CH_3$), 2.34 (s, 3H, $CH_3$), 2.27 (s, 3H, $CH_3$), 2.16 (s, 3H, $CH_3$), 1.23 (d, J = 1.5 Hz, 15H, $CH_2$), 0.82 (dddd, J = 15.6, 13.0, 6.1, 2.8 Hz, 1H, $CH_2$), 0.03 (dddd, J = 15.2, 12.4, 4.6, 2.6 Hz, 1H, $CH_2$). $^{13}C\{^1H\}$ NMR (75.47 Hz) $d^8$-THF δ147.3, 144.2, 143.2, 143.1, 139.3 (d, 26.4 Hz), 133.6, 132.7 (d, 15.8 Hz), 131.9, 131.8, 131.3, 130.4, 130.0, 129.8, 129.2 (d, 7.5 Hz), 121.6, 120.6, 111.8, 110.5, 81.4 (d, 2.3 Hz), 43.7 (d, 14.3 Hz), 40.9 (d, 9.1 Hz), 29.1 (d, 10.6 Hz), 26.9 (d, 21.9 Hz), 20.6, 20.4, 20.2, 20.1, 10.1. $^{31}P\{^1H\}$ NMR (202 MHz, THF) δ 22.3. Elemental analysis: C62.629, H6.262, N 7.521; predicted $C_{38}H_{46}N_4PRuCl$ – C 62.84, H 6.38, N 7.71.

*Complex **2**.* In an $N_2$ glove box, compound **1** was dissolved in 5 ml of DMSO in a Schlenk bomb, was sealed, removed from the glove box, and was heated on a Schlenk line at 100 °C for 30 hours. DMSO was removed under reduced pressure at 100 °C. The resulting solids were recrystallized from THF and pentane, washed 3 times with 2 ml of cold THF (−35 °C), washed 3 times with 2 ml pentane, and then dried under reduced pressure. The resulting pale yellow powder was

collected with a yield of 0.608 g, 71% yield (from $[RuCp^*Cl]_4$). $^1H$ NMR (700 MHz, Methylene Chloride-d2) δ 13.25 (s, 2H, N-H), 7.47 (s, 2H, Ar-H), 7.45 – 7.38 (m, 4H, Ph-H), 7.36 – 7.31 (m, 1H, Ph-H), 6.86 (s, 2H, Ar-H), 4.58 (ddt, J = 34.1, 13.1, 3.6 Hz, 2H, Ar-H), 3.92 (q, J = 13.3 Hz, 2H, CH3), 2.70 (ddd, J = 15.7, 12.4, 4.1 Hz, 2H, $CH_2$), 2.19 (s, 7H, $CH_3$), 2.17 (s, 6H, $CH_3$), 1.33 (d, J = 1.5 Hz, 15H, Cp*), 1.15 (ddt, J = 16.3, 13.7, 3.1 Hz, 2H, $CH_2$). $^{13}C$ NMR (176 MHz, $CD_2Cl2$) δ 194.7, 194.6, 134.3, 133.4, 131.2, 130.3, 129.9, 129.9, 129.5, 129.0, 128.9, 112.0, 108.3, 92.5, 68.1, 54.2, 54.0, 53.8, 53.7, 53.5, 44.0, 43.9, 31.0, 30.8, 26.0, 20.4, 19.9, 10.6. $^{31}P\{^1H\}$ NMR (121 MHz, THF) δ 38.3. Elemental analysis: C 62.925, H 6.078, N 6.819; predicted $C_{38}H_{46}N_4PRuCl$ – C 62.84, H 6.38, N 7.71.

*Complex* **3.** In the glove box, compound **2** (0.487 g, 0.692 mmol, 1 eq) was dissolved in 30 ml of THF and was cooled to −78 °C. A solution of 1.6 M *n*BuLi (0.865 ml, 1.38 mmol, 2 eq) in THF was added to the cold stirring solution of complex **2** via syringe. The reaction mixture immediately turned a dark-yellow color and was allowed to stir at −78 °C for 1 hour before being allowed to warm to room temperature. The resulting solution was filtered through celite and the product was precipitated out of solution by the addition of $Et_2O$. The highlighter-yellow solid was collected in a 53% yield (0.2731 g). $^1H$ NMR (700 MHz, THF-$d_8$) δ 7.71 (t, *J* = 7.8 Hz, 2H, Ph-H), 7.51 (t, *J* = 7.4 Hz, 2H, Ph-H), 7.39 (t, *J* = 7.3 Hz, 1H, Ph-H), 7.04 (s, 2H, Ar-H), 6.79 (s, 2H, Ar-H), 4.61 (ddt, *J* = 33.8, 12.5, 3.6 Hz, 2H, $CH_2$), 4.17 (q, *J* = 13.0 Hz, 2H, $CH_2$), 2.77 (ddd, *J* = 15.2, 11.6, 4.1 Hz, 2H, $CH_2$), 2.29 (s, 6H, $CH_3$), 2.28 (s, 6H, $CH_3$), 1.41 (s, 15H, Cp*), 1.09 (tt, *J* = 13.7, 2.8 Hz, 2H, $CH_2$). $^{13}C$ NMR (176 MHz, THF) δ 198.50, 198.39, 146.29, 137.15, 130.43, 128.44, 128.28, 125.42, 124.18, 114.15, 106.62, 90.67, 43.18, 32.56, 32.41, 26.19, 25.57, 25.46, 20.22, 20.19, 10.32, 10.30. $^{31}P\{^1H\}$ NMR (202 MHz, THF) δ 45.89. Elemental analysis: C 65.237, H 6.276, N 7.078 ; predicted $C_{42}H_{52}N_4PORuLi$ – C 65.69, H 6.82, N 7.29.

*Complex* **4-Fe.** $FeCl_2$ (2.9 mg, 0.0187 mmol, 1eq) was added to a stirring solution of complex **3** (14.0 mg, 0.0187mmol, 1eq) in 1 ml of acetonitrile for 30 minutes at room temperature. The solution was filtered through celite then dried under reduced pressure to give a goldenrod colored powder 6.2 mg (48% yield). $^1H$ NMR (500 MHz, $CD_3CN$) δ 29.18, 25.87, 16.13, 9.37, 8.13, 7.97, 3.67, 1.94, 1.82, 1.32, 0.89, -1.87, -3.36, - 26.67. $\mu_{eff}$ = 4.2 BM. Elemental analysis: C 58.046, H 5.753, N 8.430; predicted $C_{40}H_{47}N_5PRuFeCl$ – C, 58.51, H 5.77, N 8.53.

*Complex **4-Co.*** $CoCl_2$ (3.1 mg, 0.238 mmol, 1 eq) was added to a stirring solution of complex **7** (0.1878 g, 0.238 mmol, 1 eq) in 5 ml of acetonitrile and was stirred for 30 minutes at room temperature. After 30 minutes at room temperature the solution became cloudy as LiCl precipitated out of solution. The solution was filtered through celite and dried under vacuum to give a dark green powder 0.112 g (62% yield). $^1$H NMR (500 MHz, Benzene-d$^6$) δ 42.29 (s, 2H), 31.55 (s, 2H), 28.01 (d, $J_{HP}$ = 34.0 Hz, 2H), 26.62 (s, 2H), 17.84 (s, 2H), 16.04 (s, 2H), 12.69 (s, 6H,$CH_3$), 10.93 (s, 2H), 10.07 (s, 1H), 6.16 (s, 3H, $NCCH_3$), 0.30 (s, 2H), -6.36 (s, 6H, $CH_3$), -19.09 (s, 15H, Cp*-$CH_3$). $\mu_{eff}$ =3.2 BM. Elemental analysis: C 56.456, H 5.271, N 7.817; predicted $C_{40}H_{47}N_5PRuCoCl$ – C, 58.29, H 5.75, N 8.49.

*Ligand **L-Yuting.*** 20 ml vials were charged with KOtBu (0.249 mg, 21.3 mmol, 0.1 eq) and $Ph_2PH$ (3.978 g, 21.4 mmol, 1 eq) were weighed out and dissolved in THF. The KOtBu-THF mixture was added portion-wise to the stirring $Ph_2PH$-THF solution. Upon addition of KOtBu, the reaction mixture turned vibrant orange. The orange solution was transferred to a 100 ml Schlenck bomb equipped with a stir bar. Vinyl-imidazole (1.995 g, 21.3 mmol, 1 eq) was weighed out and then added via pipette to the stirring mixture in the Schlenk bomb. The reaction mixture was stirred overnight and a color change from bright orange to yellow occurred. The volatiles were removed via vacuum and remaining solids were dissolved in toluene and filtered through celite. The extracts were collected and the toluene was removed via vacuum. The product was recrystallized using diethyl ether and pentane to give a white solid, which was collected and dried on a frit. Yield: 3.183 g (11.6 mmol, 54.5%). $^1$H NMR (500 MHz, $CDCl_3$): δ7.40 (m, 11H, Ar-H), 7.04 (m, 1H, Ar-H), 6.89 (m, 1H, Ar-H), 4.02 (m, 2H, -$CH_2$), 2.53 (m, 2H, -$CH_2$). $^1$P{$^1$H} NMR (300 MHz, DMSO-d$^6$): δ-22.61.

*Complex **5.** [RuCp*Cl]$_4$* (0.417 g, 0.383 mmol, 1 eq) and **L-Yuting** (0.451 g, 1.76 mmol, 4 eq) were dissolved in THF and were mixed together in a 50 ml Schlenck bomb for 10 minutes at room temperature. Next, the volatiles were removed via vacuum under 100 °C to give an orange color solid. The orange precipitate was washed three times with 5 ml diethyl ether and then three times 5 ml THF. After decanting, the remaining precipitate was dried on the frit. An orange-yellow solid was collected with a yield of 0.652 g (0.590 mmol, 76.1%). $^1$H NMR (500 MHz, dDMSO):

δ 7.73-7.82 (m, 8 H, Ar-H), 7.48 (m, 17H, Ar-H), 6.97 (d, 3H, Ar-H), 3.99 (m, 4H, -$CH_2$), 3.04 (m, 4H, -$CH_2$), 1.29 (s, 30H, -$CH_3$). $^{31}P\{^1H\}$ NMR (202 MHz, DMSO-$d^6$): δ 30.57. $^{13}C\{^1H\}$ NMR (75.4 MHz, THF-$d^8$): δ 144.52 (d, $J_{CP}$ = 32.30 Hz), 141.23, 137.60 (d, $J_{CP}$ = 14.21 Hz), 133.96, 132.28 (d, $J_{CP}$ = 29.72 Hz), 131.56 (d, $J_{CP}$ = 8.09 Hz), 130.41, 128.47, 128.28, 128.16, 119.12, 82.11 (s, $J_{CP}$ = 2.53 Hz), 43.32 (d, $J_{CP}$ = 7.71 Hz), 32.39 (d, $J_{CP}$ = 12.12 Hz), 9.55.

*Complex **6**.* Species **5**, from the previous synthesis, was dissolved in $d^6$-DMSO and heated at 100 °C for 17 hours. The mixture is then pumped down at 100 °C and washed three times 5 ml of diethyl ether and then three times 5 ml of THF. The pale yellow solid was collected and was dried on a frit with a yield of 284.6mg (50.9 mmol, 64%). $^1H$ NMR (300 MHz, DMSO-$d^6$): δ 11.20 (s, 1H, -NH), 7.38 (m, 14H, *Ar-H*), 4.65 (m, 1H, -$CH_2$), 4.25 (m, 1H, -$CH_2$), 2.72 (m, 1H, -$CH_2$), 2.62 (m, 1H, -$CH_2$), 1.49 (s, 17H, -$CH_3$). $^{31}P\{^1H\}$ NMR (202 MHz, dDMSO): δ35.68. $^{13}C\{^1H\}$ NMR (125.7 MHz, DMSO-$d^6$): δ170.03 (d, $J_{CP}$ = 18.76 Hz), 136.32 (d, $J_{CP}$ = 38.59 Hz), 135.32 (d, $J_{CP}$ = 42.13 Hz), 132.10, 130.21, 129.94, 128.68 (d, $J_{CP}$ = 8.961 Hz), 128.17 (d, $J_{CP}$ = 9.22 Hz), 124.39, 119.97, 93.59, 45.26, 24.66 (d, $J_{CP}$ = 28.68Hz), 10.10.

## 2.5 SUPPORTING INFORMATION

Table 2.01. Crystallographic details for Complexes **L**, **1** and **2**.

| Molecule | ligand **L** | Complex **1** | Complex **2** |
|---|---|---|---|
| Empirical formula | C28 H31 N4 P | C76 H92 Cl2 N8 P2 Ru2 | C42 H54.63 Cl N4 O P Ru |
| Formula weight | 454.54 | 1452.56 | 799.02 |
| Temperature | 100(2) K | 100(2) K | 100(2) K |
| Wavelength | 0.71073 Å | 0.71073 Å | 0.71073 Å |
| Crystal system | Triclinic | Monoclinic | Monoclinic |
| Space group | P -1 | C 2/c | P 21 |
| Unit cell dimensions | a = 6.203(2) Å | a = 27.312(3) Å | a = 16.1738(18) Å |
| | b = 7.722(2) Å | b = 16.392(3) Å | b = 13.9542(15) Å |
| | c = 24.580(9) Å | c = 23.012(3) Å | c = 17.0592(18) Å |
| | α= 93.16(2)°. | α = 90°. | α = 90°. |
| | β= 93.29(2)°. | β = 125.993(15)°. | β = 92.634(7)°. |
| | γ = 96.47(2)°. | γ = 90°. | γ = 90°. |
| Volume | 1165.7(7) Å3 | 8336(2) Å3 | 3846.1(7) Å3 |
| Z | 2 | 4 | 4 |
| Density (calculated) | 1.295 Mg/m3 | 1.157 Mg/m3 | 1.380 Mg/m3 |
| Absorption coefficient | 0.142 mm-1 | 0.506 mm-1 | 0.557 mm-1 |
| F(000) | 484 | 3024 | 1675 |
| Crystal size | 0.15 x 0.15 x 0.05 mm3 | 0.05 x 0.04 x 0.03 mm3 | 0.10 x 0.07 x 0.05 mm3 |
| Theta range for data collection | 1.66 to 26.45°. | 1.84 to 26.62°. | 1.89 to 26.70°. |
| Index ranges | -7<=h<=7, -9<=k<=9, 0<=l<=30 | -34<=h<=34, -20<=k<=20, -28<=l<=28 | -20<=h<=20, -17<=k<=17, -21<=l<=21 |
| Reflections collected | 22245 | 73880 | 16464 |
| Independent reflections | 4827 [R(int) = 0.1968] | 8588 [R(int) = 0.1661] | 15795 [R(int) = 0.0925] |
| Completeness to theta = 25.00° | 99.00% | 99.60% | 99.30% |
| Max. and min. transmission | 0.9929 and 0.9790 | 0.9850 and 0.9751 | 0.9727 and 0.9464 |
| Refinement method | Full-matrix least-squares on F2 | Full-matrix least-squares on F2 | Full-matrix least-squares on F2 |
| Data / restraints / parameters | 4827 / 249 / 398 | 8588 / 0 / 415 | 15795 / 150 / 911 |
| Goodness-of-fit on F2 | 1.071 | 0.969 | 1.038 |
| Final R indices [I>2sigma(I)] | R1 = 0.1225, wR2 = 0.2276 | R1 = 0.0742, wR2 = 0.1560 | R1 = 0.0876, wR2 = 0.1593 |
| R indices (all data) | R1 = 0.2379, wR2 = 0.2799 | R1 = 0.1541, wR2 = 0.1805 | R1 = 0.1423, wR2 = 0.1764 |
| Largest diff. peak and hole | 0.884 and -0.543 e.Å-3 | 0.558 and -0.712 e.Å-3 | 1.153 and -0.902 e.Å-3 |

Table 2.02. Crystallographic details for complexes **3**, **4-Co** and **4-Fe**.

| Molecule | Complex **3** | Complex **4-Co** | Complex **4-Fe** |
|---|---|---|---|
| Empirical formula | C42 H52 Li N4 O P Ru | C42 H50 Cl Co N6 P Ru | C42 H50 Cl Fe N6 P Ru |
| Formula weight | 767.86 | 865.3 | 862.22 |
| Temperature | 100(2) K | 100(2) K | 100(2) K |
| Wavelength | 0.71073 Å | 0.71073 Å | 0.71073 Å |
| Crystal system | Triclinic | Triclinic | triclinic |
| Space group | P -1 | P -1 | P`1 |
| Unit cell dimensions | a = 11.927(5) Å | a = 7.9318(4) Å | a = 7.9435(4) Å |
| | b = 13.386(6) Å | b = 13.6965(6) Å | b = 13.7706(7) Å |
| | c = 13.735(7) Å | c = 19.1742(9) Å | c = 19.1235(10) Å |
| Volume | 1856.0(15) Å3 | 2006.40(16) Å3 | 2015.63(18) Å3 |
| | α = 62.884(9)°. | α = 97.261(2)°. | α= 97.024(3)°. |
| | β = 75.794(9)°. | β = 97.275(2)°. | β= 98.273(3)°. |
| | γ = 73.748(13)°. | γ = 100.672(2)°. | γ = 99.943(3)°. |
| | | | |
| Z | 2 | 2 | 2 |
| Density (calculated) | 1.374 Mg/m3 | 1.432 Mg/m3 | 1.421 Mg/m3 |
| Absorption coefficient | 0.504 mm-1 | 0.934 mm-1 | 0.878 mm-1 |
| F(000) | 804 | 894 | 892 |
| Crystal size | 0.05 x 0.02 x 0.02 mm3 | 0.15 x 0.15 x 0.08 mm3 | 0.45 x 0.15 x 0.15 mm3 |
| Theta range for data collection | 2.14 to 26.44°. | 2.17 to 28.51°. | 2.18 to 30.70°. |
| Index ranges | -12<=h<=14, -16<=k<=16, -17<=l<=17 | -10<=h<=10, -18<=k<=18, -25<=l<=25 | -11<=h<=11, -19<=k<=19, -27<=l<=27 |
| Reflections collected | 13902 | 70827 | 82800 |
| Independent reflections | 7222 [R(int) = 0.1789] | 10133 [R(int) = 0.0549] | 12328 [R(int) = 0.0901] |
| Completeness to theta = 25.00° | 96.20% | 99.90% | 98.40% |
| Max. and min. transmission | 0.9900 and 0.9752 | 0.9290 and 0.8726 | 0.8796 and 0.6934 |
| Refinement method | Full-matrix least-squares on F2 | Full-matrix least-squares on F2 | Full-matrix least-squares on F2 |
| Data / restraints / parameters | 7222 / 58 / 460 | 10133 / 0 / 480 | 12328 / 0 / 480 |
| Goodness-of-fit on F2 | 0.923 | 1.035 | 1.062 |
| Final R indices [I>2sigma(I)] | R1 = 0.0894, wR2 = 0.1098 | R1 = 0.0301, wR2 = 0.0668 | R1 = 0.0360, wR2 = 0.0906 |
| R indices (all data) | R1 = 0.2699, wR2 = 0.1590 | R1 = 0.0449, wR2 = 0.0728 | R1 = 0.0467, wR2 = 0.1008 |
| Largest diff. peak and hole | 0.974 and -1.017 e.Å-3 | 0.826 and -0.624 e.Å-3 | 1.350 and -1.062 e.Å-3 |

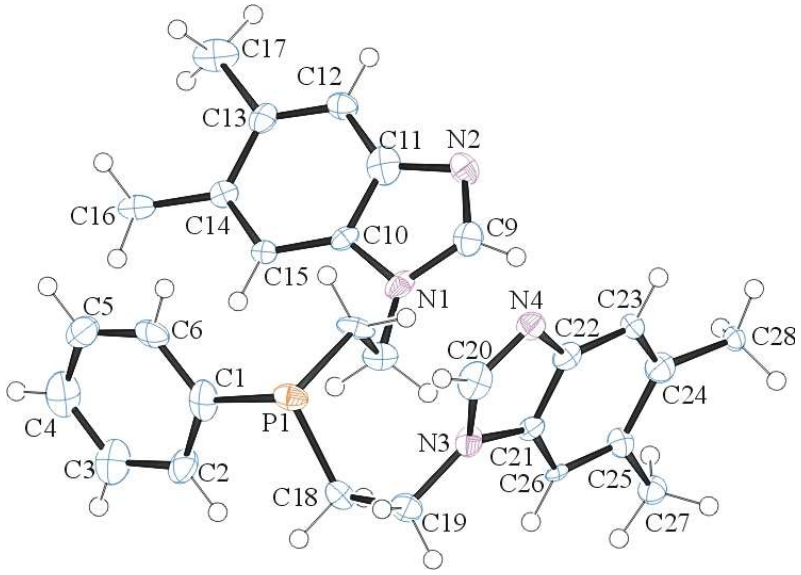


Figure 2.10 Crystal structure of ligand **L**. ORTEP of the structure with thermal ellipsoids at the 50% probability level, disorder omitted for clarity

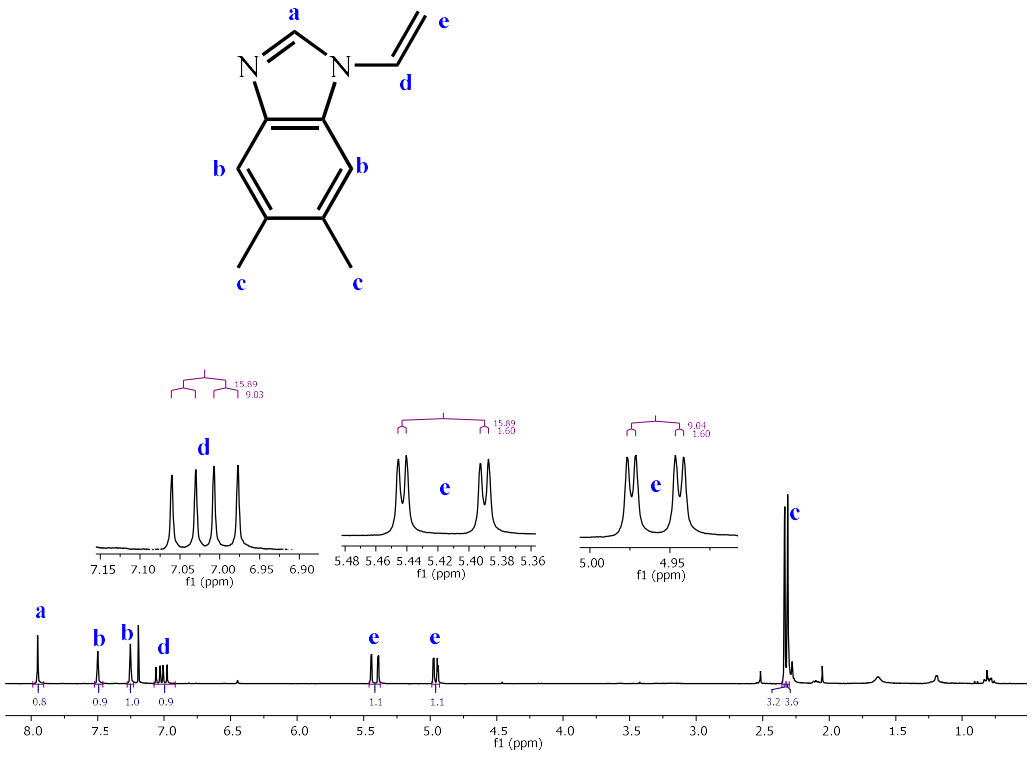


Figure 2.11. $^{1}$H NMR spectrum of vinyl-substituted 5,6-dimethylbenzimidazole in $C_6D_6$.

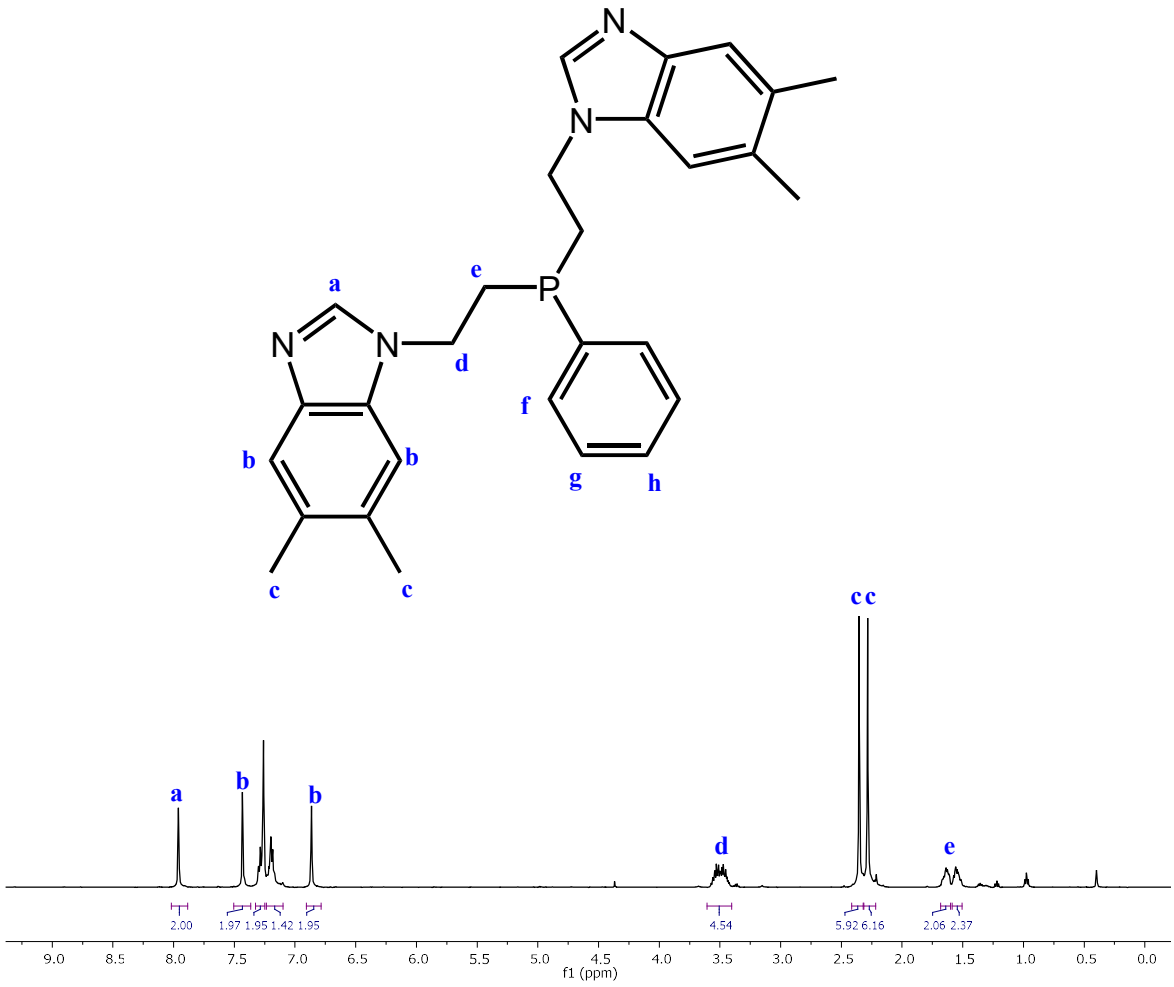


Figure 2.12. $^{1}$H NMR of **L** in $CDCl_3$.

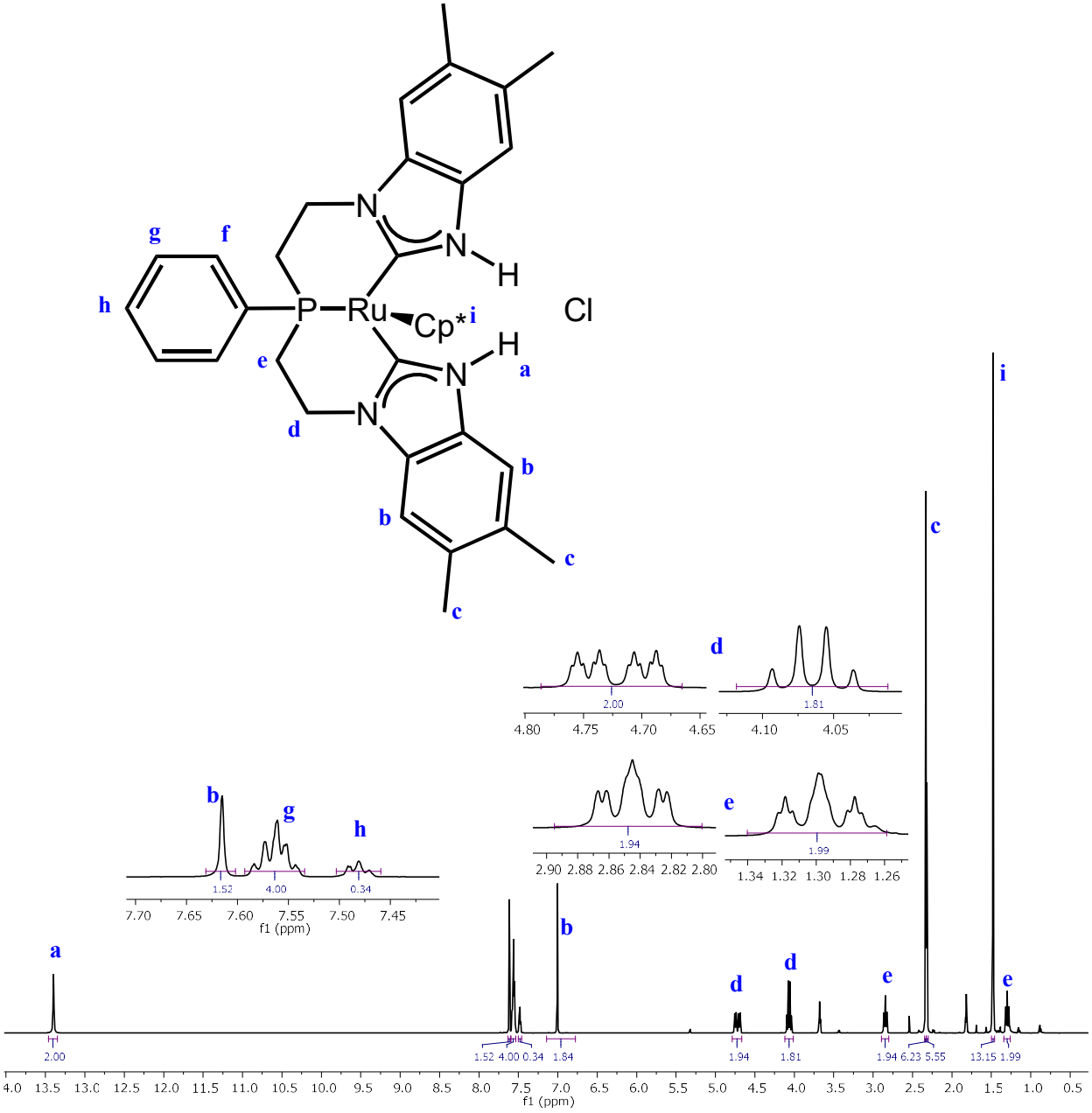


Figure 2.13. $^{1}H$ NMR of **2** in $CD_2Cl_2$.

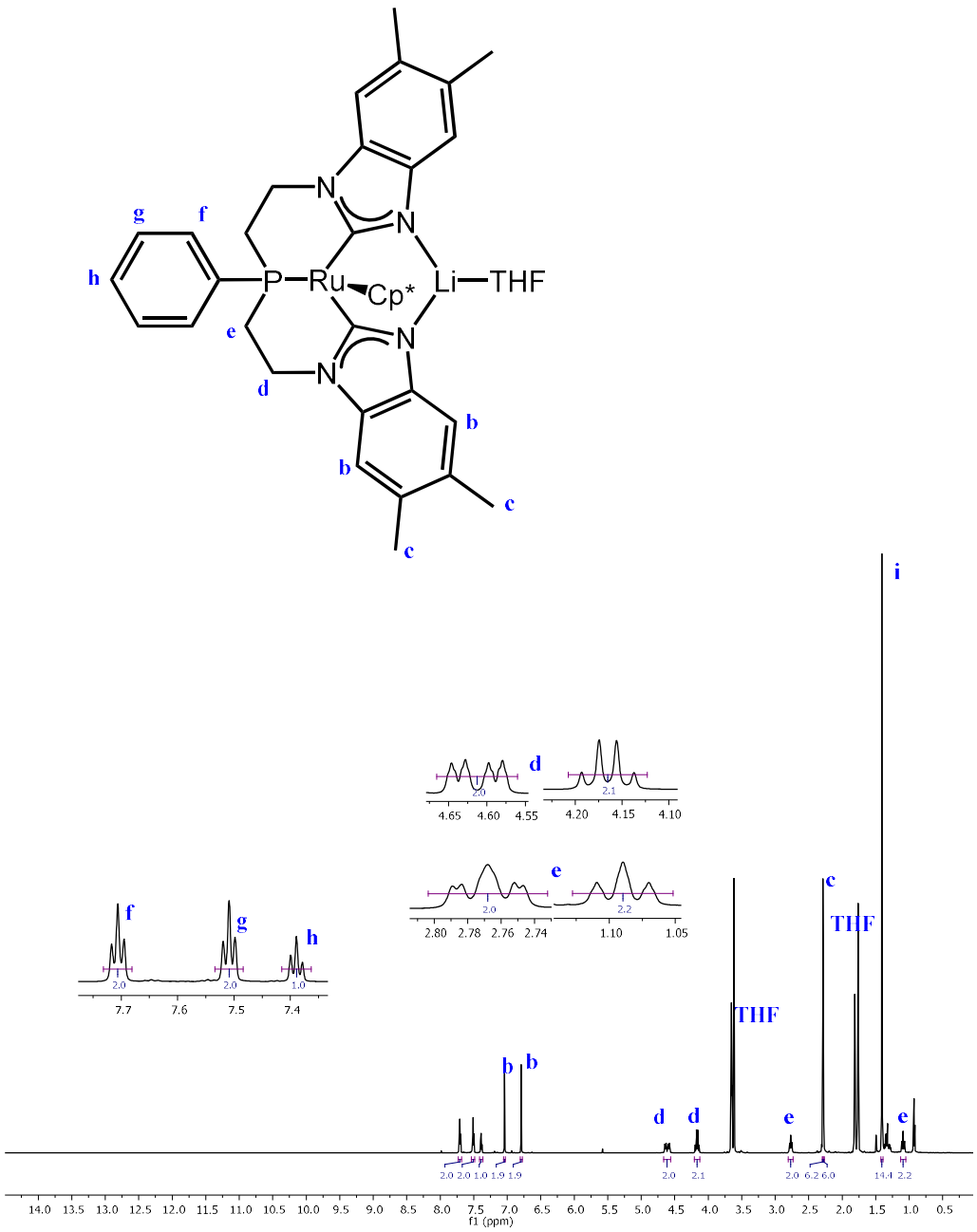


Figure 2.14. $^{1}H$ NMR of **3** in $CD_2Cl_2$.

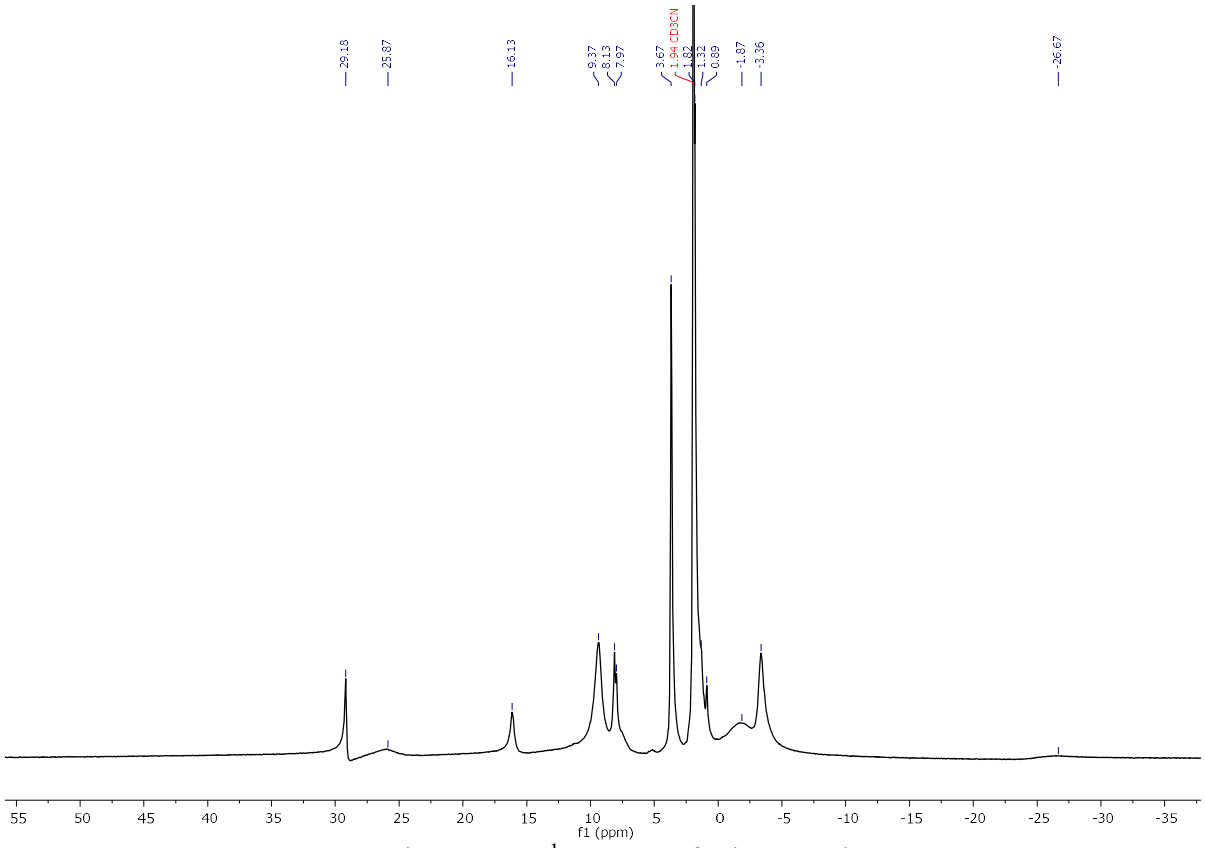


Figure 2.15. $^{1}$H NMR of **2** in $CD_2Cl_2$.

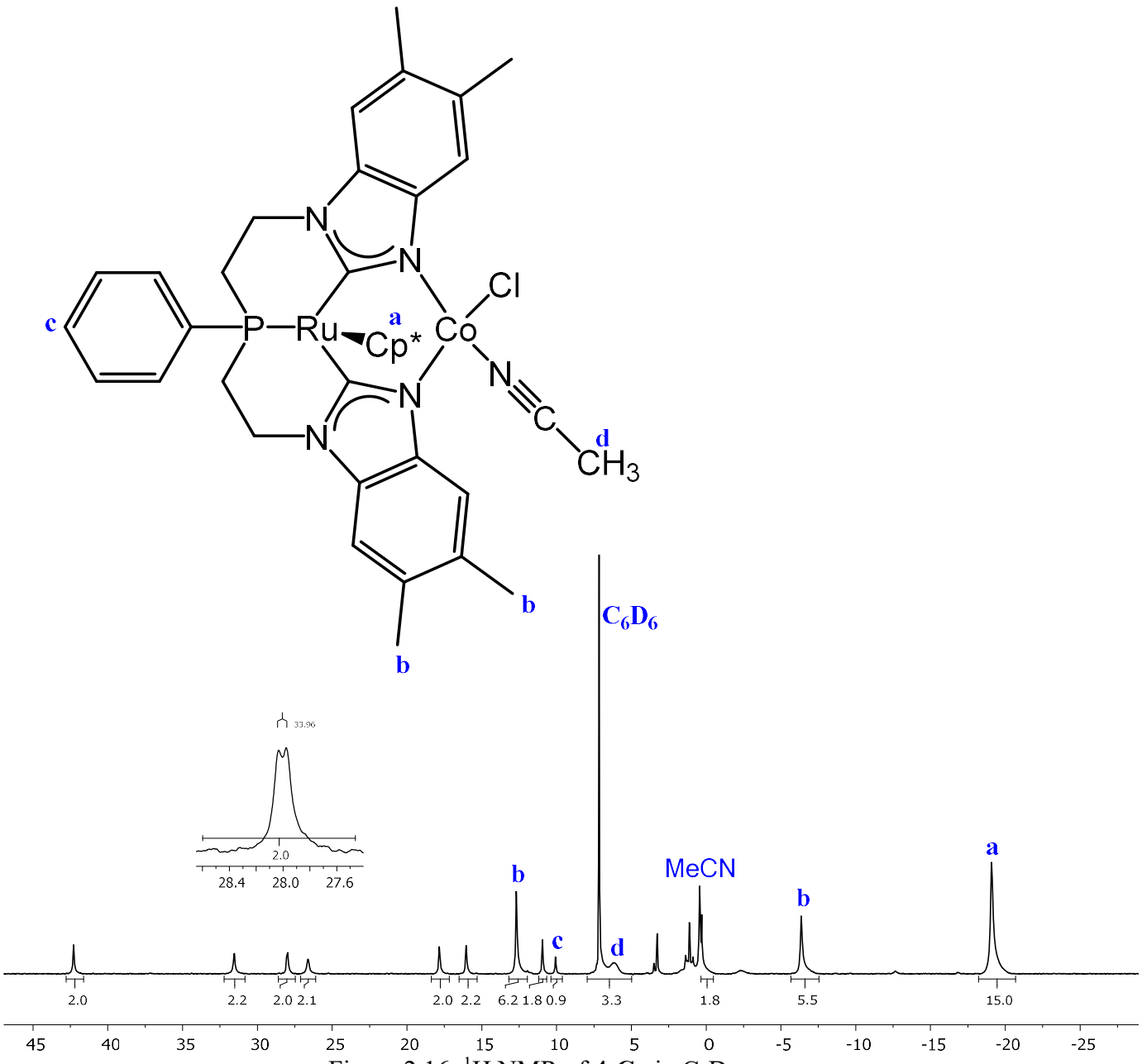


Figure 2.16. $^{1}$H NMR of **4-Co** in $C_6D_6$.

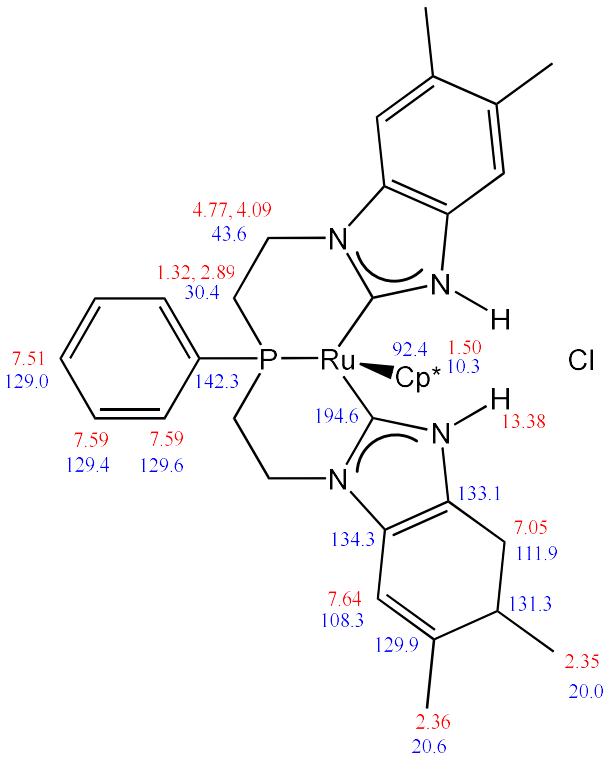


**HSQC**

| $^{1}H$ | $^{13}C$ |
|---|---|
| Methyl groups | |
| 2.36 | 19.9 |
| 2.35 | 20.4 |
| Cp* Methyl group | |
| 1.50 | 10.3 |
| $CH_2$ groups | |
| 1.33, 2.89 | 30.4 |
| 4.09, 4.77 | 43.6 |
| CH groups (aromatic) | |
| 7.05 | 107.9 |
| 7.64 | 111.5 |
| CH groups (phenyl) | |
| 7.59 | 129.0 |

**$^{1}H$-$^{13}C$ HMBC**

| | | |
|---|---|---|
| 1.32 | 3 | 142.3 |
| | 2 | 44.1 |
| 1.50 | 4 | 194.4 |
| | 2 | 92.4 |
| 2.35 | 2 | 131.3 |
| | 3 | 111.9 |
| 2.36 | 2 | 129.9 |
| | 3 | 108.3 |
| 4.09 | 3 | 133.1 |
| | 2 | 30.9 |
| 7.05 | 2 | 133.5 |
| | 4 | 111.8 |
| | 3 | 20.6 |
| 7.51 | 2 | 129.6 |
| 7.59 | 2 | 142.3 |
| | 2 | 129.4 |
| 7.64 | 2 | 131.7 |
| | 3 | 20.0 |
| 13.38 | 2 | 194.6 |
| | 2 | 133.1 |

Figure 2.17. HSQC, and HMBC assignments of **2**.

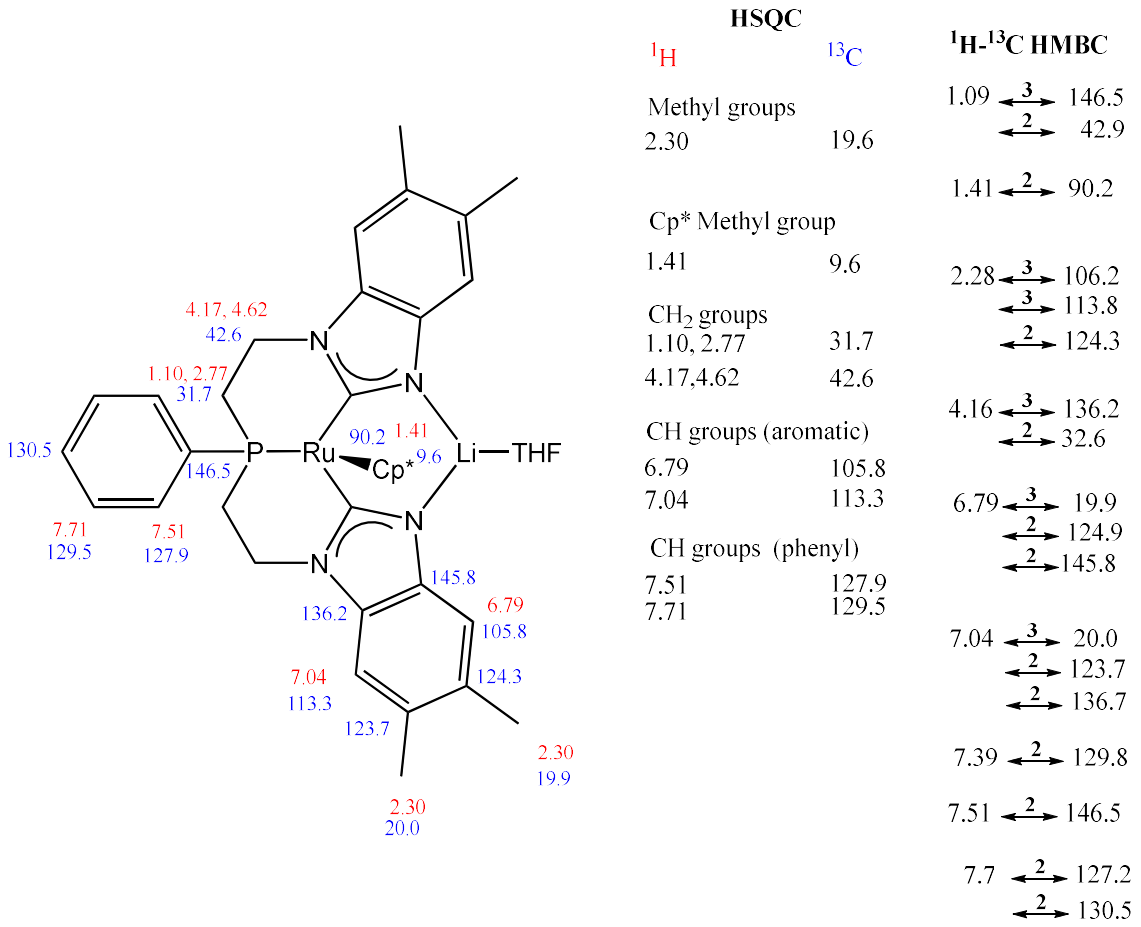


Figure 2.18. HSQC, and HMBC assignments of **3**.

## 2.6 NOTES TO THE CHAPTER


1. Adapted with permission from (S. E. Flowers and B. M. Cossairt, *Organometallics*, 2014, **33**, 4341-4344.). Copyright (2014) American Chemical Society.
2. J. Masuda, W. Schoeller, B. Donnadieu and G. Bertrand, *J. Am. Chem. Soc.*, 2007, **129**, 14180-14181.
3. T. M. Trnka and R. H. Grubbs, *Acc. Chem. Res.*, 2001, **34**, 18-29.
4. V. Dragutan, I. Dragutan, L. Delaude and A. Demonceau, *Coord. Chem. Rev.*, 2007, **251**, 765-794.
5. D. Pugh and A. A. Danopoulos, *Coord. Chem. Rev.*, 2007, **251**, 610-641.
6. W. A. Herrmann, *Angew. Chem., Int. Ed.*, 2002, **41**, 1290-1309.
7. M. A. Huertos, J. Pérez, L. Riera, J. Díaz and R. López, *Chem. Eur. J.*, 2010, **16**, 8495-8507.
8. M. Brill, J. Díaz, M. A. Huertos, R. López, J. Pérez and L. Riera, *Chem. Eur. J.*, 2011, **17**, 8584-8595.
9. J. Ruiz, A. Berros, B. F. Perandones and M. Vivanco, *Dalton Trans.*, 2009, 6999-7007.
10. L. Xiang, J. Xiao and L. Deng, *Organometallics*, 2011, **30**, 2018-2025.

11. J. Ruiz and B. F. Perandones, *J. Am. Chem. Soc.*, 2007, **129**, 9298-9299.
12. V. Miranda-Soto, D. B. Grotjahn, A. L. Cooksy, J. A. Golen, C. E. Moore and A. L. Rheingold, *Angew. Chem., Int. Ed.*, 2011, **50**, 631-635.
13. M. F. Schettini, G. Wu and T. W. Hayton, *Chem. Commun.*, 2012, **48**, 1484-1486.
14. F. E. Hahn, *ChemCatChem*, 2013, **5**, 419-430.
15. V. Miranda-Soto, D. B. Grotjahn, A. G. DiPasquale and A. L. Rheingold, *J. Am. Chem. Soc.*, 2008, **130**, 13200-13201.
16. K. Araki, S. Kuwata and T. Ikariya, *Organometallics*, 2008, **27**, 2176-2178.
17. T. Toda, S. Kuwata and T. Ikariya, *Chem. Eur. J.*, 2014, **20**, 9539-9542.
18. F. E. Hahn, V. Langenhahn, T. Lugger, T. Pape and D. Le Van, *Angew. Chem., Int. Ed.*, 2005, **44**, 3759-3763.
19. F. E. Hahn, A. R. Naziruddin, A. Hepp and T. Pape, *Organometallics*, 2010, **29**, 5283-5288.
20. K. Kottsieper, O. Stelzer and P. Wasserscheid, *J. Mol. Catal. A*, 2001, **175**, 285-288.
21. V. T. Annibale, R. Batcup, T. Bai, S. J. Hughes and D. Song, *Organometallics*, 2013, **32**, 6511-6521.
22. A. Flores-Figueroa, T. Pape, K.-O. Feldmann and F. E. Hahn, *Chem. Commun.*, 2010, **46**, 324-326.
23. P. G. Edwards and F. E. Hahn, *Dalton Trans.*, 2011, **40**, 10278-10288.
24. S. Gaillard and J.-L. Renaud, *Dalton Trans.*, 2013, **42**, 7255-7270.
25. A. R. Naziruddin, A. Hepp, T. Pape and F. E. Hahn, *Organometallics*, 2011, **30**, 5859-5866.
26. F. H. Allen, *Acta. Cryst.*, 2002, **B58**, 380-388.
27. F. E. Hahn, A. R. Naziruddin, A. Hepp and T. Pape, *Organometallics*, 2010, **29**, 5283-5288.
28. J. Ruiz and B. F. Perandones, *J. Am. Chem. Soc.*, 2007, **129**, 9298-9299.
29. V. n. Miranda-Soto, D. B. Grotjahn, A. G. DiPasquale and A. L. Rheingold, *J. Am. Chem. Soc.*, 2008, **130**, 13200-13201.
30. V. Miranda-Soto, D. B. Grotjahn, A. L. Cooksy, J. A. Golen, C. E. Moore and A. L. Rheingold, *Angew. Chem., Int. Ed.*, 2011, **50**, 631-635.
31. P. J. Fagan, M. D. Ward and J. C. Calabrese, *J. Am. Chem. Soc.*, 1989, **111**, 1698-1719.

# Chapter 3. SYNTHESIS OF RUTHENIUM COMPLEXES SUPPORTED BY A TRIPODAL, PROTIC BIS(N-HETEROCYCLIC CARBENE) PHOSPHINE LIGAND FROM RUTHENIUM(II) ARENE PRECURSORS

*Significant portions of the following have been previous published.*[1]
*Contributions to this project were made by M. Cecilia Johnson and Michael R. Norris.*

## 3.1 INTRODUCTION

First introduced in 1968,[2, 3] N-heterocyclic carbenes (NHCs) are of interest to the organometallic community as useful ligands for their tunable steric profiles and strongly electron donating properties.[4-6] Although methods of metalating traditional NHCs with substituted NR wingtips have been known for decades,[7] the synthesis of protic NHCs (PNHCs) has been far less studied. Protic NHCs are attractive because of their tunable protonation state, which allows them to serve as a proton relay, participate in substrate insertion reactions, and ligate Lewis acids. Methods for metalation of PNHCs have been developed and are covered in several reviews,[8-12] and early metalation studies reveal thermodynamically controlled formation of the desired carbene complexes for certain metal fragments including Ru(II).[13, 14] However, there are still very few examples in the literature of chelating ligands containing two PNHCs.[1, 15-18]

Separately, organometallic complexes supported by facially coordinating tripodal ligands have proven to be versatile and effective catalysts for a variety of chemical transformations. One of the most widely utilized, reviewed, and recognized members of this family of ligands is bis(diphenylphosphinoethyl)phenylphosphine (Triphos) and its synthetic variants. This ligand is characterized by its strong sigma donor character, neutral charge, and chemically tunable backbone, which has led to its utilization as a ligand in many different catalytic reactions including hydrogenation,[19-22] alcohol amination,[23] methylation of amines,[24] and formic acid dehydrogenation.[25] Another well-established class of tripodal ligands are tris(pyrazolyl)borate (Tp) and its synthetic variants. Tp ligands are monoanionic, facially coordinating ligands, and like Triphos are good sigma donors. Focusing solely on ruthenium complexes supported by Tp ligands,

these complexes are effective catalysts for hydrogenation,[26] coupling chemistry,[27] hydration of nitriles,[28] hydroarylation,[29] and isomerization and cyclization reactions[30].

Motivated by the exemplary catalytic performance of catalysts ligated by tripodal ligands like Triphos and Tp, and the attractive qualities of PNHCs, our group became interested in developing a general strategy for the direct metalation of a bis(imidazole)phosphine ligand to create novel catalyst structures bearing tripodal PNHC ligands. In this chapter we will discuss the metalation of bisimidazole phosphine ligands with $[(arene)RuCl_2]_2$ and [Ru(Bz)(bpy)(OTf)](OTf) (Bz = benzene, bpy = 2,2′-bipyridine, OTf = trifluoromethanesulfonate).

## 3.2 Results and Discussion

### 3.2.1 *Metalation with [Ru(Bz)(bpy)(OTf)](OTf)*

Synthesis of the phosphine ligand $PhP(Etbim)_2$ was carried out using a modified procedure with benzimidazole as the NHC precursor.[18] Protonation of the benzimidazole moieties in $PhP(bim)_2$ followed by reaction with [Ru(Bz)(bpy)(OTf)](OTf) leads to a precursor **7** where only the Phosphorus atom binds to the Ruthenium center. This complex is then cleanly converted to **8-OH₂** at 175 °C in ethylene glycol (**Scheme 3.1**). Interestingly, the $^1H$ NMR and $^{31}P\{^1H\}$ NMR spectra of **8-OH₂** in $CD_2Cl_2$ or DMSO-$d^6$ show multiple products with broad resonances (Figure 3.1). However, addition of a $Cl^-$ source to a solution of **8-OH₂** in either solvent leads immediately to clean and interpretable $^1H$, $^{31}P\{^1H\}$, and $^{13}C\{^1H\}$ NMR spectra (Figure 3.2).

**Scheme 3.1. Reaction of ligand $PhP(Etbim)_2$ with [Ru(Bz)(bpy)(OTf)](OTf) to $[8\text{-}C]^{2+}$**

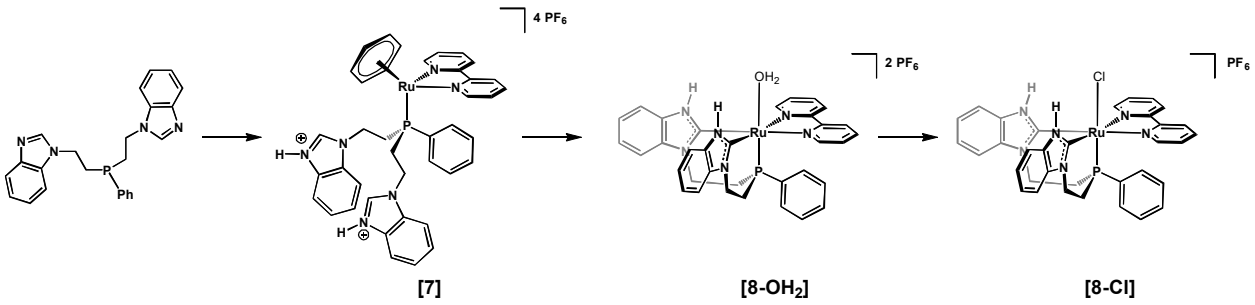

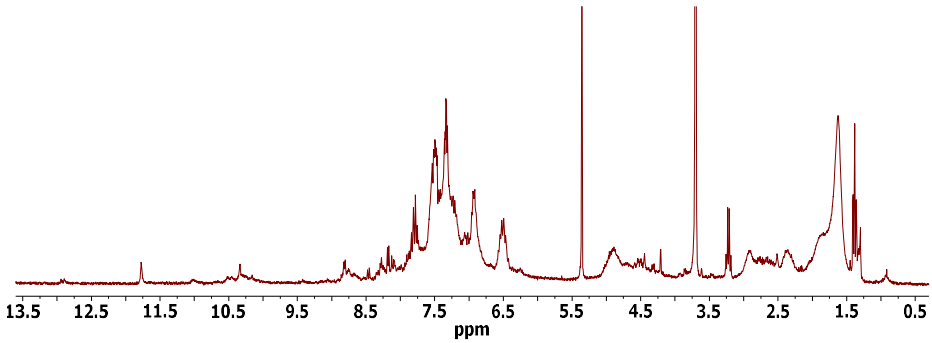


Figure 3.1. $^{1}$H NMR spectrum (300 MHz, $CD_2Cl_2$) of $[Ru(bpy)(PhP(Etbim)_2)(OH_2)](PF_6)_2$, (**8-OH$_2$**), from crude reaction in $CD_2Cl_2$.

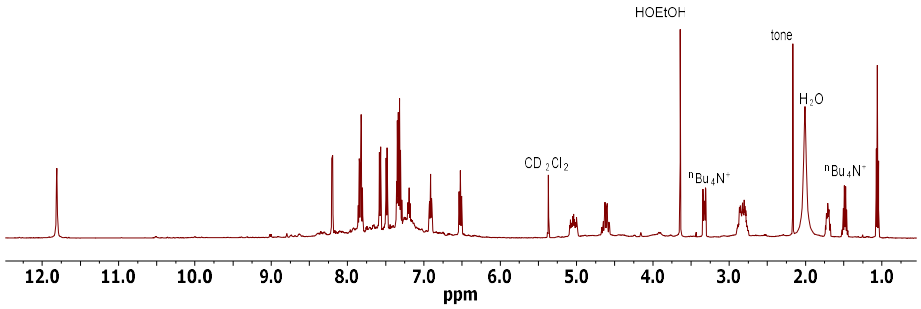


Figure 3.2. $^{1}$H NMR spectrum (500 MHz, $CD_2Cl_2$) of **8-Cl** from addition of $nBu_4NCl$ to a sample of **8-OH$_2$** in $CD_2Cl_2$.

Crystals suitable for X-ray diffraction were grown of **8-Cl** by slow diffusion of $Et_2O$ into an acetone solution (Figure 3.3). The $Cl^-$ acts to lock the N–H protons into a symmetric geometry due to Hydrogen bonding interactions, which may also explain why the $^{1}$H NMR spectrum of **8-OH$_2$** shows multiple resonances when $H_2O$ is bound if a variety of H-bonding interactions cause multiple conformers to exist in solution. The $^{1}$H NMR spectrum of **8-OH$_2$** is also sharp and well-defined in $CD_3OD$ (Figure 3.4), similar to the spectrum of **8-Cl**, although the N–H protons cannot be located in $CD_3OD$, likely due to H/D exchange.

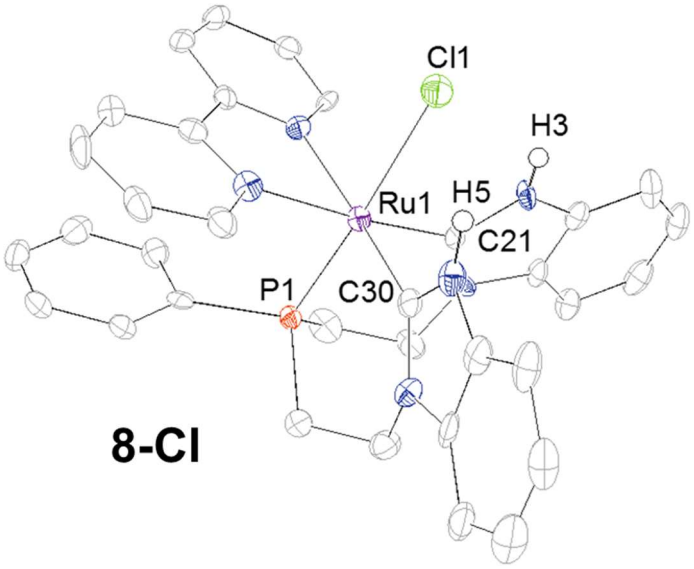


Figure 3.3. Molecular structures of **8-Cl**, with thermal ellipsoids shown at 50% probability. **8-Cl** displays H-bonding interactions between N-H groups and bound Cl with one $Cl^-$ counter-ion omitted for clarity. Selected interatomic distances (Å) for (**8-Cl**): Ru1–Cl1 2.534(2), Ru1–C21 2.011(6), Ru1–C30 2.024(6), H3–Cl1 2.475, H5–Cl1 2.509.

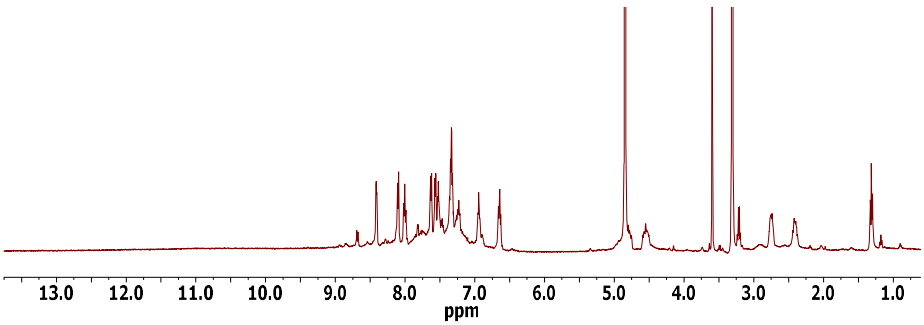


Figure 3.4. $^1$H NMR spectrum (500 MHz, $CD_3OD$) of **8-OH$_2$** showing distinct aromatic and $CH_2$ peaks as well as a lack of N-H peaks in the 10–13 ppm range presumably from H/D scrambling.

### 3.2.2 *Metalation with [(Arene)RuCl$_2$]$_2$*

Complex **9** can be prepared in one pot in 93% yield. A 2:1 mixture of **L** and $[(C_6H_6)RuCl_2]_2$ is stirred at 170 °C in N-methyl-2-pyrrolidone (NMP) for one hour, and the volatiles are removed

under reduced pressure. The resulting dark yellow solids are dissolved in acetonitrile, four equivalents of $AgBF_4$ are added, and the mixture is stirred for one hour at ambient temperature. Upon further purification, **9** can be isolated as an off-white powder (Scheme 3.2). Complex **9** is characterized by a $^{31}P\{^1H\}$ NMR singlet at 44 ppm in $CD_2Cl_2$ and by several, distinctive $^1H$ NMR signals: one N-H singlet at 10.8 ppm, three phenyl group proton multiplets at 7.8, 7.7, and 7.6 ppm; four multiplets for the diastereotopic protons on the ethylene linker; two singlets for the protons on the bound acetonitrile ligands *trans* to the NHCs at 2.2 ppm, and one singlet corresponding to the acetonitrile unit *trans* to the phosphorus at 2.6 ppm.

**Scheme 3.2. One-pot and step-wise synthesis of $[(MeCN)_3Ru(PNHC)_2P^{Ph}][BF_4]_2$, complex 9. Note, the structure of complex 11 is solvent (S) dependent, with evidence for dimerization in non-coordinating solvent.**

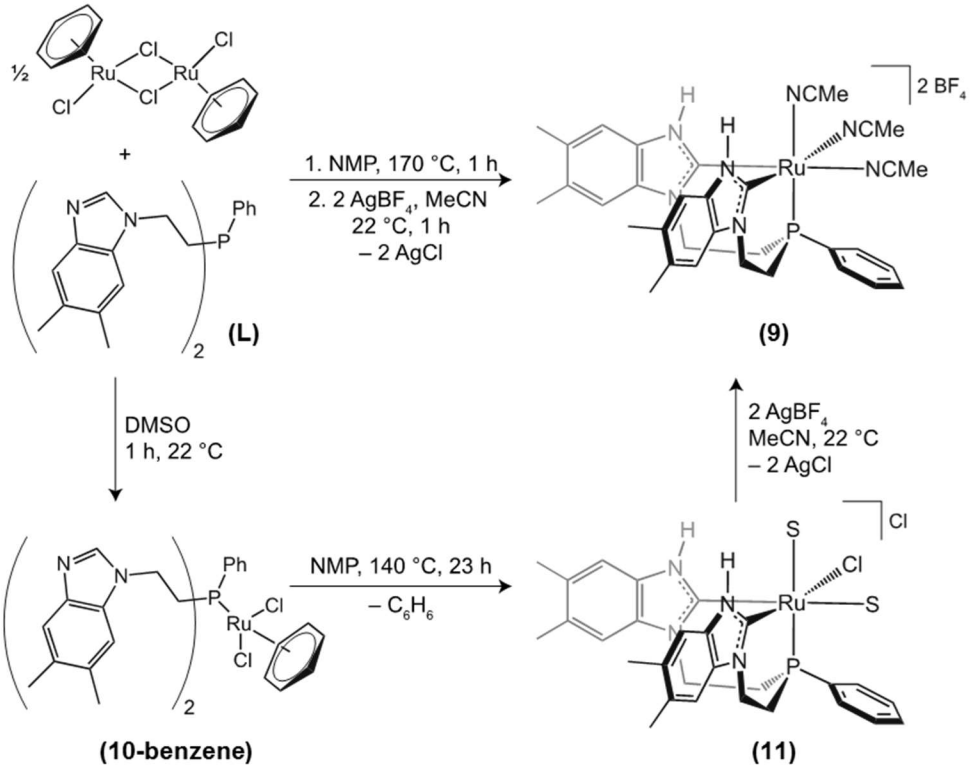


Colorless crystals suitable for single crystal X-ray diffraction were grown via slow diffusion of diethyl ether into a supersaturated solution of **9** in acetonitrile at -35°C. The structure of **9** (Figure 3.5) shows that the PNHC binds facially to the ruthenium center. The bond lengths of

the PNHCs in the crystal structure of **CCC** are within the range of structures we have previously characterized.[1, 18] The Ru-N(nitrile) bond lengths are similar for all three positions, ranging from 2.104(2) Å for Ru1-N6 to 2.115(2) Å for Ru1-N5.

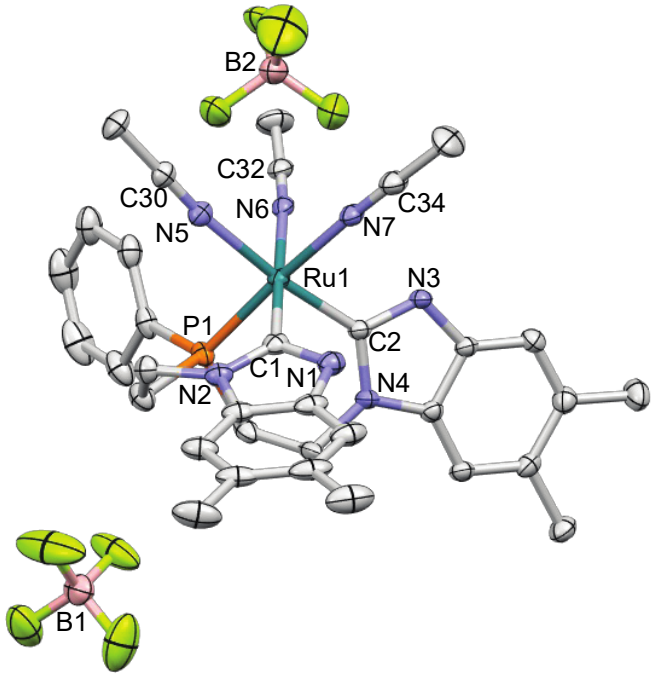


Figure 3.5. Single crystal X-ray diffraction structure of **9** with thermal ellipsoids shown at the 50% probability level. Hydrogen atoms are omitted for clarity. Selected interatomic distances (Å): Ru1-N5 2.115(2), N5-C30 1.133(4), Ru1-N6 2.104(2), N6-C32 1.139(4), Ru1-N7 2.114(2), N7-C34 1.133(4), Ru1-P1 2.2680(7), Ru1-C1 2.0063, Ru1-C2 2.003(3), C1-N1 1.355(4), C1-N2 1.360(4), C2-N3 1.355(3), C2-N4 1.360(3).

To understand the detailed coordination chemistry that precedes the formation of **9**, we investigated the metalation of **L** under more mild conditions. Sonication of a 2:1 mixture of **L** and $[(C_6H_6)RuCl_2]_2$ at room temperature in DMSO, dichloromethane, or NMP leads to complete conversion to the phosphine-ligated complex, $(C_6H_6)Ru(L)Cl_2$ (**10-benzene**), within one hour, as observed *in situ* by $^1H$ NMR and $^{31}P\{^1H\}$ NMR spectroscopy (Scheme 3.02). Complex **10-benzene** is characterized in DMSO-$d_6$ by a $^{31}P\{^1H\}$ NMR singlet at 14 ppm, a downfield shift from $^{31}P\{^1H\}$ NMR signal for **L** at -34 ppm, and by several distinctive $^1H$ NMR signals including three aromatic singlets corresponding to the aromatic protons on the imidazole units at 8.1, 7.4,

and 7.2 ppm respectively; two singlets corresponding to the methyl groups on the benzimidazole at 3.0 and 2.3 ppm; and one singlet at 5.7 ppm corresponding to the six equivalent protons on the $\eta^6$-benzene ring suggesting that benzene remains bound to the ruthenium center. Similarly, the addition of $[(p\text{-cymene})RuCl_2]_2$ (0.5 equiv) to a 22 °C solution of **L** in dichloromethane produces the bright orange phosphine adduct, **10-cymene**. The appearance of a singlet at 11 ppm along with the simultaneous disappearance of the free ligand resonance at -34 ppm in the $^{31}P\{^1H\}$ NMR spectra in $CD_2Cl_2$, suggests complete conversion to **10-cymene** within one hour.

High quality orange hexagonal prisms suitable for single crystal X-ray diffraction were grown via slow evaporation from a super-saturated solution of **10-benzene** in dichloromethane and diethyl ether at -35°C. The crystal structure of **10-benzene** shows a three-legged piano-stool geometry around the ruthenium center, with an $\eta^6$-benzene ligand and with legs consisting of two chlorine atoms and **L** bound to the ruthenium center by the phosphorus atom only (Figure 3.6). Coordination of $[(arene)RuCl_2]_2$ complexes with phosphine ligands to give $(arene)Ru(PR_3)Cl_2$ complexes have been well reported in the literature.[31-33]

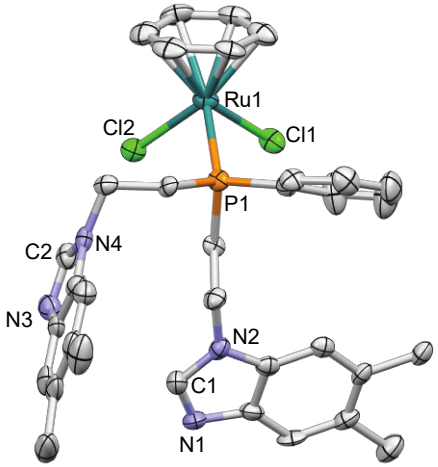


Figure 3.6. Single crystal X-ray diffraction structure of **10-benzene** with thermal ellipsoids shown at the 50% probability level. Hydrogen atoms are omitted for clarity. Selected interatomic distances (Å): Ru1-P1 2.3254(17), Ru1-Cl1 2.4061(15), Ru1- Cl2 2.4192(16), C2-N3 1.298(8), C2-N4 1.368(7), C1-N1 1.306(7), C1-N2 1.369(8).

Heating **10-benzene** at 170 °C for forty-five minutes in NMP and monitoring the reaction by $^{31}P\{^{1}H\}$ NMR spectroscopy demonstrates the disappearance of the **10-benzene** singlet at 13 ppm and the appearance of a new singlet corresponding to a new species **11** at 55 ppm. Analysis with an internal standard in NMP supported *in situ* conversion of **10-benzene** to **11** in >60% yield (Figure 3.7).

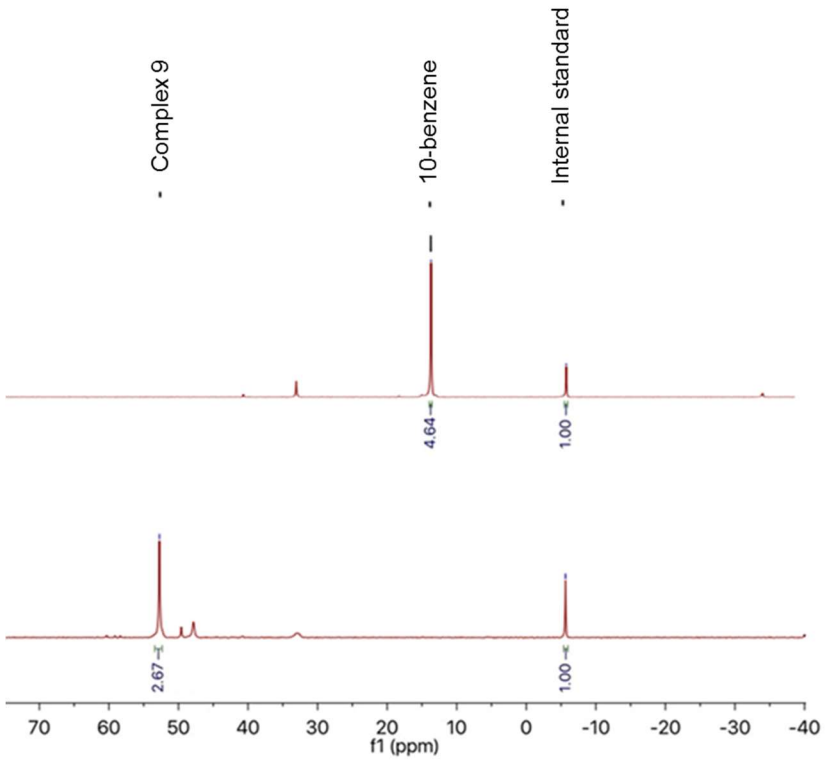


Figure 3.7. $^{31}P\{^{1}H\}$ NMR (299 K, 121.49 MHz) of **10-benzene** in NMP with a triphenyl phosphine internal standard in a capillary (top), heated at 170 °C for 45 minutes yielding complex **11** (bottom).

To further investigate this metalation reaction, **10-benzene** was heated at 140 °C in NMP and the reaction mixture was monitored over time by $^{31}P\{^{1}H\}$ NMR spectroscopy. After five hours at 140 °C the singlet for **10-benzene** at 13 ppm decreased and many new signals appeared in the $^{31}P\{^{1}H\}$ NMR spectrum. Continued heating led to the disappearance of these peaks and to the appearance of a single species, **11**, at 55 ppm after twenty-three hours at 140 °C (Scheme 3.2, Figure 3.8). These results suggest that there may be multiple intermediates that form between **10-**

**benzene** and **11**. Compound **11** can also be synthesized from $[(p\text{-cymene})RuCl_2]_2$ in a similar manner but requires 43 hours of heating at 140 °C, consistent with the expected relative lability of the arenes.[34] Compound **11** can be cleanly isolated from this reaction as a yellow-orange powder.

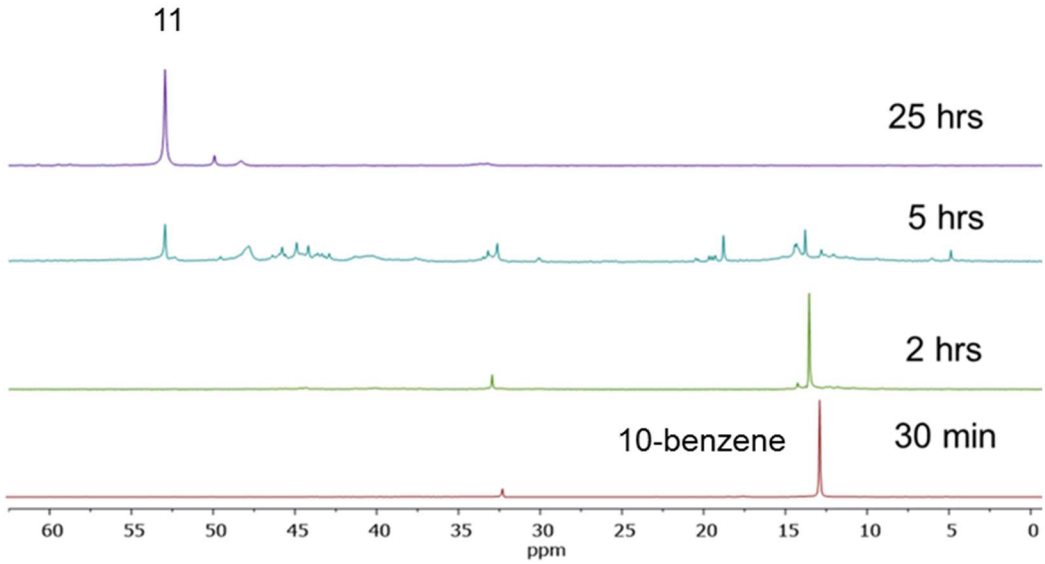


Figure 3.8. $^{31}P\{^1H\}$ NMR (298 K, 700 MHz) of **10-benzene** heated at 140 °C over time in NMP.

In $CD_2Cl_2$, the $^{31}P\{^1H\}$ NMR spectrum of **11** reveals one singlet peak at 53 ppm, suggesting there is one phosphorus environment in the isolated molecule. The $^1H$ NMR spectrum in $CD_2Cl_2$ displays a single set of peaks for the phenyl group attached to the phosphorus atom with multiplets at 8.12, 7.43, and 7.29 ppm. Although there is only one set of peaks corresponding to the phenyl group, the $^1H$ NMR spectrum shows two inequivalent ethylene imidazole arms in this complex. In a symmetric PNHC complex we would expect one singlet N-H peak (2H), two aromatic C-H singlets (2H each), four multiplets corresponding to the two sets of diastereotopic protons on the ethylene linker (2H each), and two methyl singlets (6H each).[1] The $^1H$ NMR spectrum of **11** in $CD_2Cl_2$ contains two singlet N-H peaks at 11.0 ppm and 10.9 ppm (1H each); four aromatic singlets at 7.3ppm, 7.1 ppm, 7.0 ppm, and 6.9 ppm (1H each); eight multiplets corresponding to the diastereotopic ethylene linker protons (1H each), and 4 methyl singlets at 2.5, 2.4, 2.3, and 2.2 ppm (3H each). These results indicate that the structure of **11** has two chemically distinct ethylene

imidazole linkers, suggesting possible dimer formation in non-coordinating solvent. Compound **11** is soluble in dichloromethane, acetonitrile and DMSO. When dissolved in a coordinating solvent, the spectral features of **11** drastically change. For example, when **11** is dissolved in $CD_3CN$ the $^{31}P\{^1H\}$ NMR displays two separate peaks at 45 and 43 ppm, and a distinct $^1H$ NMR spectrum compared to the same complex in $CD_2Cl_2$ (Figure 3.9).

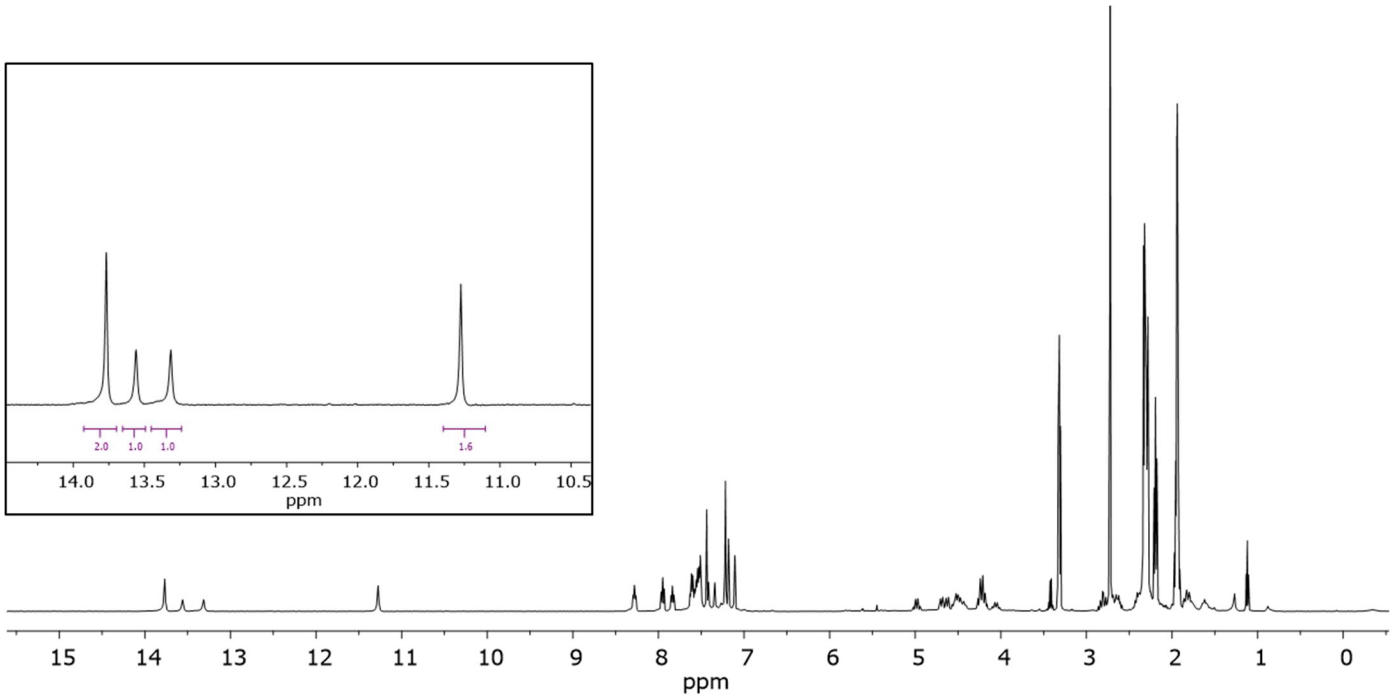


Figure 3.9. $^1H$ NMR (298 K, 499.72 MHz) of **11** in $CD_3CN$.

Similarly, when **11** is dissolved in DMSO a new species, $[(DMSO)_2ClRu(PNHC)_2P^{Ph}][Cl]$ (**11-DMSO),** is observed. High quality crystals suitable for X-ray diffraction were grown in air with a super saturated solution of **11-DMSO** in a 1:1 mixture of DMSO and $CD_2Cl_2$ (Figure 3.10). The crystal structure shows a facially bound bis-PNHC ligand. The PNHCs are chemically inequivalent in this structure because one is bound to the ruthenium *trans* to chloride, while the other is bound *trans* to a sulfur-coordinated DMSO molecule. In addition, there is a second molecule of DMSO coordinated through an oxygen atom to the ruthenium center *trans* to the phosphorus. The carbene *trans* to the sulfur atom of DMSO shows a Ru-C bond distance of 2.049(7) Å and the carbene *trans* to the chloride has a Ru-carbon distance of 2.007(7) Å. There is one outer sphere chloride that shows hydrogen bonding interactions with the N-H moieties.

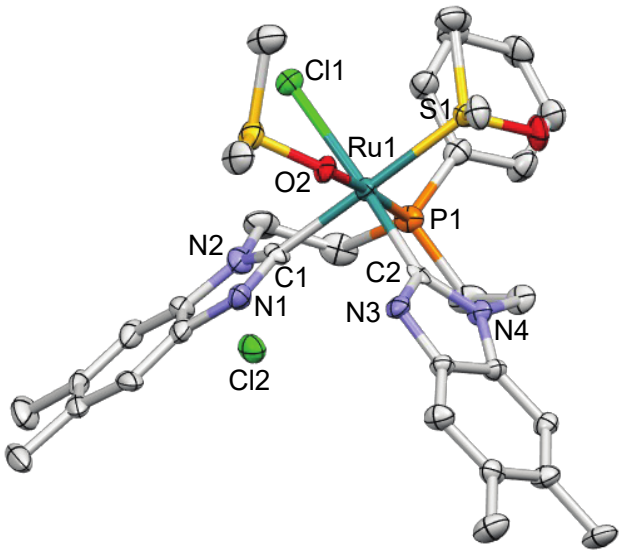


Figure 3.10. Single crystal X-ray diffraction structure of **11-DMSO** with thermal ellipsoids shown at the 50% probability level. Hydrogen atoms and DMSO solvent molecule are omitted for clarity. Selected interatomic distances (Å): Ru1-Cl1 2.508(2), Ru1-O2 2.229(4), Ru1-S1 2.332(2), Ru1-C1 2.049(7), C1-N1 1.365(8), C1-N2 1.376(9), Ru1-C2 2.007(7), C2-N3 1.359(8), C2-N4 1.370(8).

When two equivalents of $AgBF_4$ are added to **11** in acetonitrile and the resulting mixture is sonicated for 10 minutes, complex **9** is produced as evidenced by NMR spectroscopy and crystallographic analysis (Scheme 3.2).

In previous reports, tautomerization or activation of the C-H protons in **L** was achieved by heating **L** and $[Cp^*RuCl]_4$ at 100 °C.[18] To see if these conditions would be applicable for the synthesis of **9**, **10-benzene** was heated at 100 °C for 17 hours in DMSO. The PNHC species was not observed, but conversion to a DMSO adduct, $(DMSO)_3Ru(L)Cl_2$ (**10-DMSO**), is proposed based on the *in situ* $^1H$ NMR and $^{31}P\{^1H\}$ NMR spectra (Scheme 3.3). The time resolved $^{31}P\{^1H\}$ NMR spectra reveal that the singlet associated with **10-DMSO,** at 31 ppm, increases over time while the $^{31}P\{^1H\}$ NMR resonance at 14 ppm associated with **10-benzene** disappears. In the $^1H$ NMR spectrum, the $\eta^6$-benzene singlet at 5.7 ppm decreases in intensity over time, indicating that benzene dissociates from the ruthenium center. Also, the $^1H$ NMR spectrum of species **10-DMSO** has three singlets in the aromatic region with chemical shifts of 8.2 ppm, 7.4 ppm, and 7.2 ppm,

indicating that tautomerization or activation of the C(1) proton has not occurred. The most dramatic shift in the $^{1}$H NMR spectrum of **10-DMSO** is the methylene region between 3-5 ppm which maintain four distinct signals corresponding to the diasteriotopic protons on the ethylene linker. Similar results are obtained when heating complex **10-cymene** in DMSO, however the reaction proceeds at a slower rate.

**Scheme 3.3. Synthesis of 10-DMSO, 12 a/b, and 13a/b from complex 10-arene.**

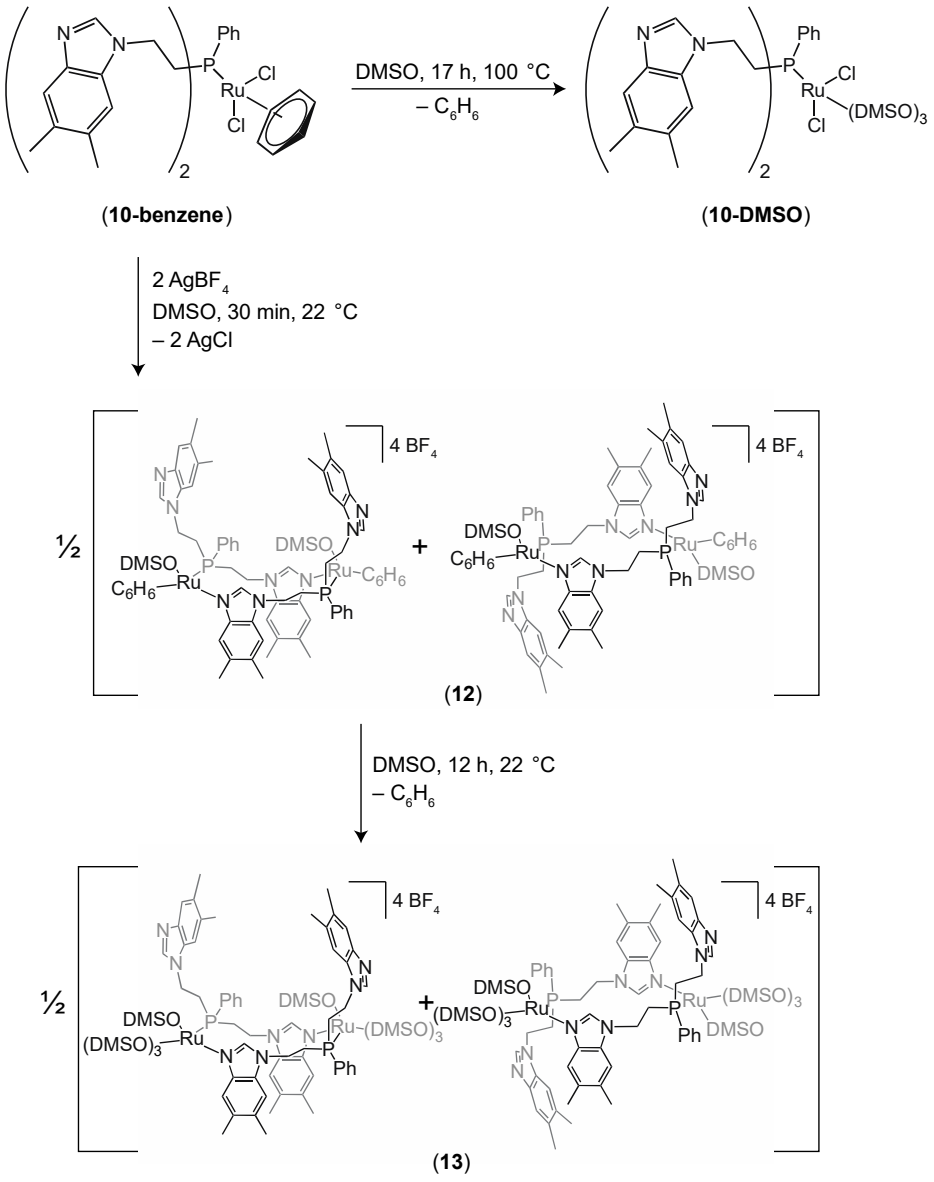

Another method for formation of PNHCs is base promoted tautomerization. For example, in the presence of a suitable metal precursor, the addition of a slight excess of KOtBu to deprotonate the imidazole at the C1 position, followed by addition of $NH_4PF_6$ to protonate the N-H wingtips generates the desired PNHC complex.[35, 36] When KOtBu was added to **10-benzene** in $CD_2Cl_2$, the appearance of multiple aromatic peaks in the $^1H$ NMR spectrum between 7.1 and 8.0 ppm and at least five peaks between 2.3 and 2.5 ppm, corresponding to the benzimidazole methyl substituents, suggest that the two imidazole arms have become inequivalent. Additionally, deprotonation of the ethylene linkers is probable as evidence by the appearance of new multiplets in the olefinic region between 6.0 and 6.3 ppm (Figure 3.11).

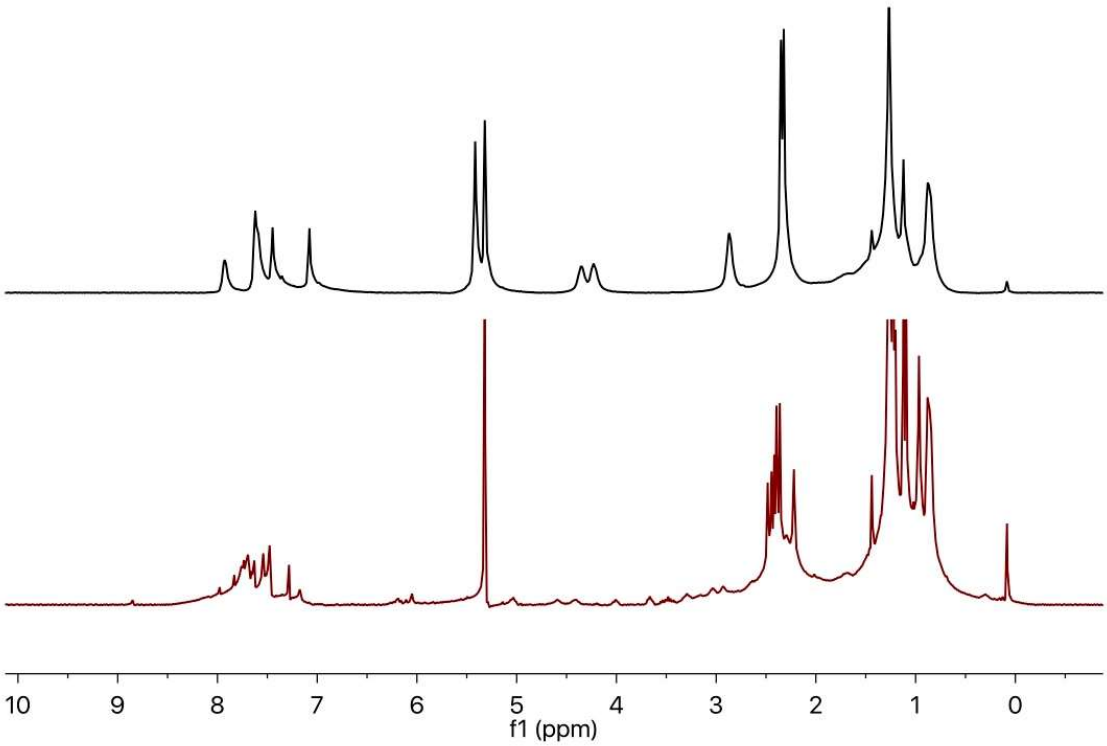


Figure 3.11. $^1H$ NMR (298 K, 499.7 MHz) in $CD_2Cl_2$ of **10-benzene** (top) and **10-benzene** with the addition of KOtBu after filtering (bottom).

With the addition of $NH_4PF_6$, the $^1H$ NMR spectrum simplifies to reveal a major product similar to the starting material, **10-benzene**. The absence of the distinctive PNHC peak(s), as well as the persistence of the C(1) imidazole peaks between 6.0 and 6.25 ppm, indicate that the base

promoted tautomerization is not a feasible method for achieving the desired PNHC complex in this particular case (Figure 3.12).

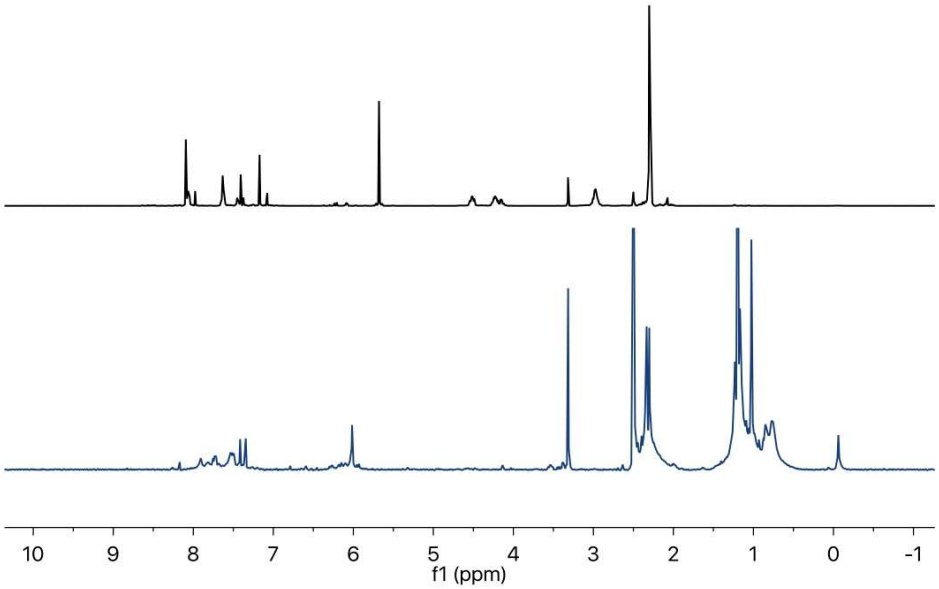


Figure 3.12. $^{1}$H NMR (298 K, 499.7 MHz) in DMSO-d$^{6}$ of **10-benzene** (top) and **10-benzene** with the addition of KOtBu, followed by the addition of $NH_4PF_6$, filtered, concentrated, and re-dissolved in DMSO-d$^{6}$ (bottom).

Yet another method in the literature for synthesizing metal complexes containing PNHC complexes is through the transmetalation of a lithiated azole unit.[37] The general synthesis involves initial deprotonation of the azole at the C(1) position using a strong base, such as nBuLi to make the lithiated azole complex. Next a metal chloride complex is added to the solution to form the metal NHC complex, then the NHC is protonated using an acid, in most cases HCl (Scheme 2).[38-40] For this transmetalation to be successful the proton at the C(1) position of the azole must be the most acidic proton in solution, otherwise a mixture of products will be observed.

**Scheme 3.4. Generalized synthetic method for the formation of metal complexes containing protic NHCs via transmetalation of lithium azoles.**

The addition of nBuLi (1.6 M in THF, 2 equiv) to a -78 °C solution of **L** in THF leads to a slight color change from colorless to pale yellow. The $^{31}P\{^{1}H\}$ NMR spectrum of the crude reaction mixture has three discernable peaks, one at -10 ppm, one at -20 ppm and one at -30 ppm. After 24 hours at room temperature only one peak is observed at -30 ppm. The $^{1}H$ NMR spectrum showed broad signals which were unable to be resolved or assigned. Clear, colorless crystals precipitated from solution after days of sitting at 22 °C under nitrogen.

The X-ray structure of these crystals revealed a rhombohedral unit cell with the space group R -3, consisting of lithium imidazole hexamers (Figure 3.13). We hypothesize that **14** is formed via the deprotonation of one of the protons at C(11). This ligand decomposition pathway competes with the deprotonation at the C(1) position of L (Scheme 11). This observed reactivity leads to the conclusion that the transmetalation of a lithium imidazole complex will not produce the desired NH, NHC metal complex.

**Scheme 3.5. Proposed reaction to form compound 14.**

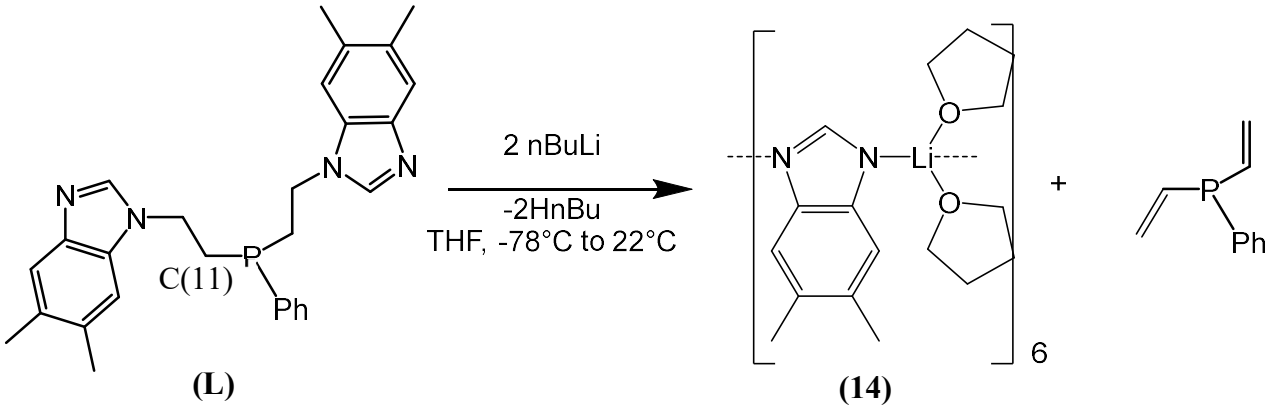


**(L)** **(14)**

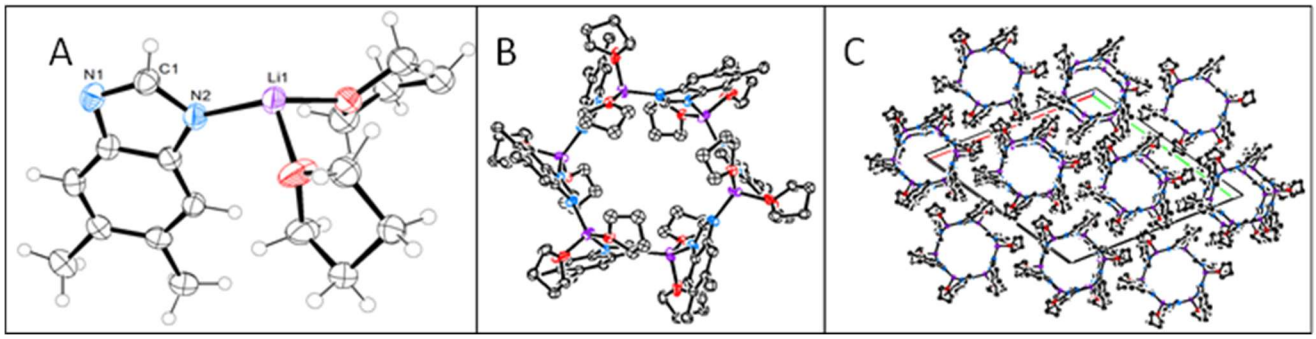


Figure 3.13. A) The asymmetric unit of the x-ray crystal structure of **11**, the six fold disorder in the THF is omitted for clarity. B) The molecular hexamer of **11** in the solid state. C) The unit cell of the crystal structure of **11** displaying the solvent voids that run through of the hexamer units.

Since heating **10-benzene** at 100 °C, lithiated azoles, and base promoted tautomerization did not lead to formation of the desired PNHC complex, we were curious to see if different reactivity would be observed with **10-benzene** following replacement of the coordinated chlorides with non-coordinating counter anions. The addition of two equivalents $AgBF_4$ to a solution of **10-benzene** in DMSO at 22 °C followed by five minutes of sonication led to a change in the appearance of the solution from transparent orange to cloudy yellow. After 30 minutes $^{31}P\{^1H\}$ NMR spectral analysis reveals complete conversion to two new species, a major product **12a** and minor product **12b** with $^{31}P\{^1H\}$ NMR resonances at 17 ppm and 15 ppm, respectively, which are present in a 100:33 ratio. Two singlets in the $^1H$ NMR spectrum located at 6.5 ppm and 5.9 ppm are associated with the $\eta^6$-benzene proton signals, and are also present in a 100:33 ratio (Figure 3.14). These data suggested the likely formation of a mixture of dimerized diastereomers, $[(C_6H_6)(DMSO)Ru(L)]_2[BF_4]_4$, under these conditions as shown in Scheme 3.3. We had encountered both of the anticipated coordination environments separately in earlier experiments with $[RuCp^*Cl]_4$ and related ligands,[18] but only a single diastereomer is formed in each of these cases as evidenced by NMR spectroscopy and single crystal X-ray diffraction studies (Figure 3.15). In the case of Cp* coordination to ruthenium, steric effects may preclude observation of the other diastereomer.

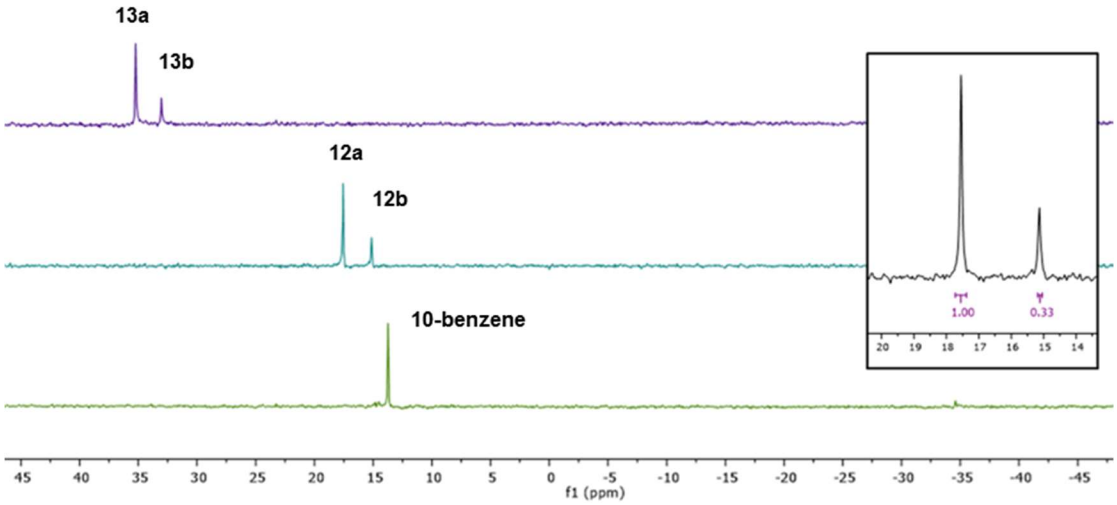


Figure 3.14. $^{31}P\{^{1}H\}$ NMR (298 K, 700 MHz) spectra of **10**, **12a**, **12b**, **13a**, and **13b** DMSO-$d^6$.

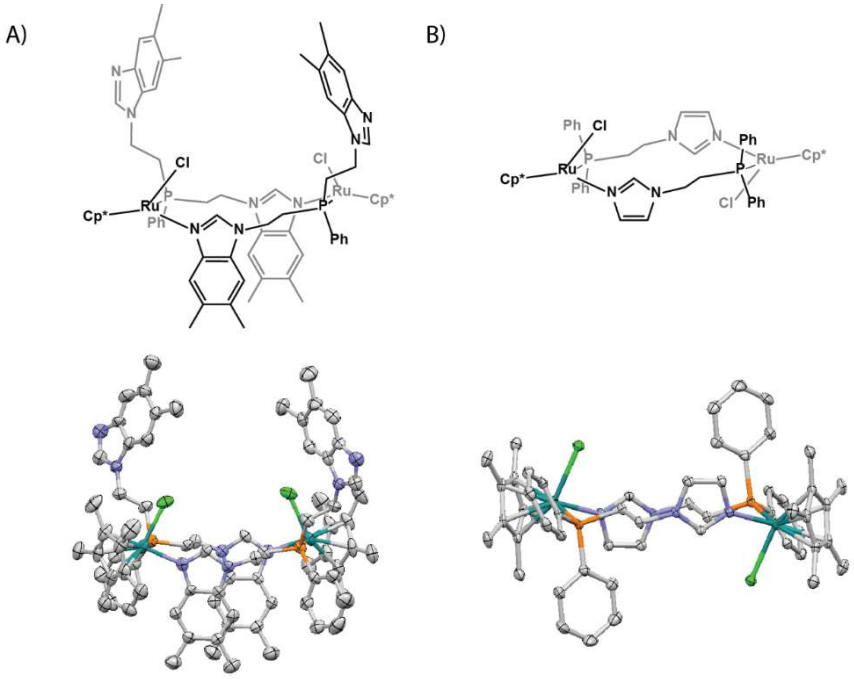


Figure 3.15. a) Crystal structure and ChemDraw model of $[Cp^*Ru(PNHC_2P^{Ph})Cl]_2$, which shows $C_2$ symmetry around the center of the molecule. b) Crystal structure and ChemDraw model of $[Cp^*Ru(PNHCP^{Ph2})Cl]_2$ from unpublished work by Flowers and Lin, this molecule contains only a twofold improper inversion axis.

When the mixture of **12a** and **12b** is sonicated for one hour or left at room temperature overnight, complete conversion to **13a** and **13b** is observed by $^{1}H$ NMR and $^{31}P\{^{1}H\}$ NMR spectroscopy along with a colour change from yellow-orange to pale yellow (Scheme 3.3). The $^{31}P\{^{1}H\}$ spectrum of **13a** and **13b** displays two singlets, one at 35 ppm and the other at 33 ppm, a downfield shift from the resonances of **12a** and **12b**, indicating the formation of two new species, which we propose to be the result of ligand substitution with loss of the arene, resulting in dimers of the general formulation $[(DMSO)_4Ru(L)]_2[BF_4]_4$ (Scheme 3.3). These new species also appear at a ratio of 100:33 by integration of the $^{31}P\{^{1}H\}$ NMR spectrum, supporting the hypothesis that the dimers **13a** and **13b** remain intact during the ligand substitution reaction. The $^{1}H$ NMR spectrum, along with COSY NMR studies, also supports the existence of diastereomers **13a** and **13b**. A close examination of the methylene region of both the 2D COSY spectrum and the 1D $^{1}H$ NMR spectrum reveal that there are four inequivalent types of methylene environments present in solution. These diastereotopic ethylene linker resonances integrate to 1:1:0.3:0.3, consistent with both the $^{31}P\{^{1}H\}$ NMR spectrum ratios and the proposed structures of **13a** and **13b** (Figure 3.16). The aromatic region of the COSY spectrum also reveals that there are only two distinct types of phenyl groups in solution. This supports our conclusion that the solution consists of a mixture of diastereomers.

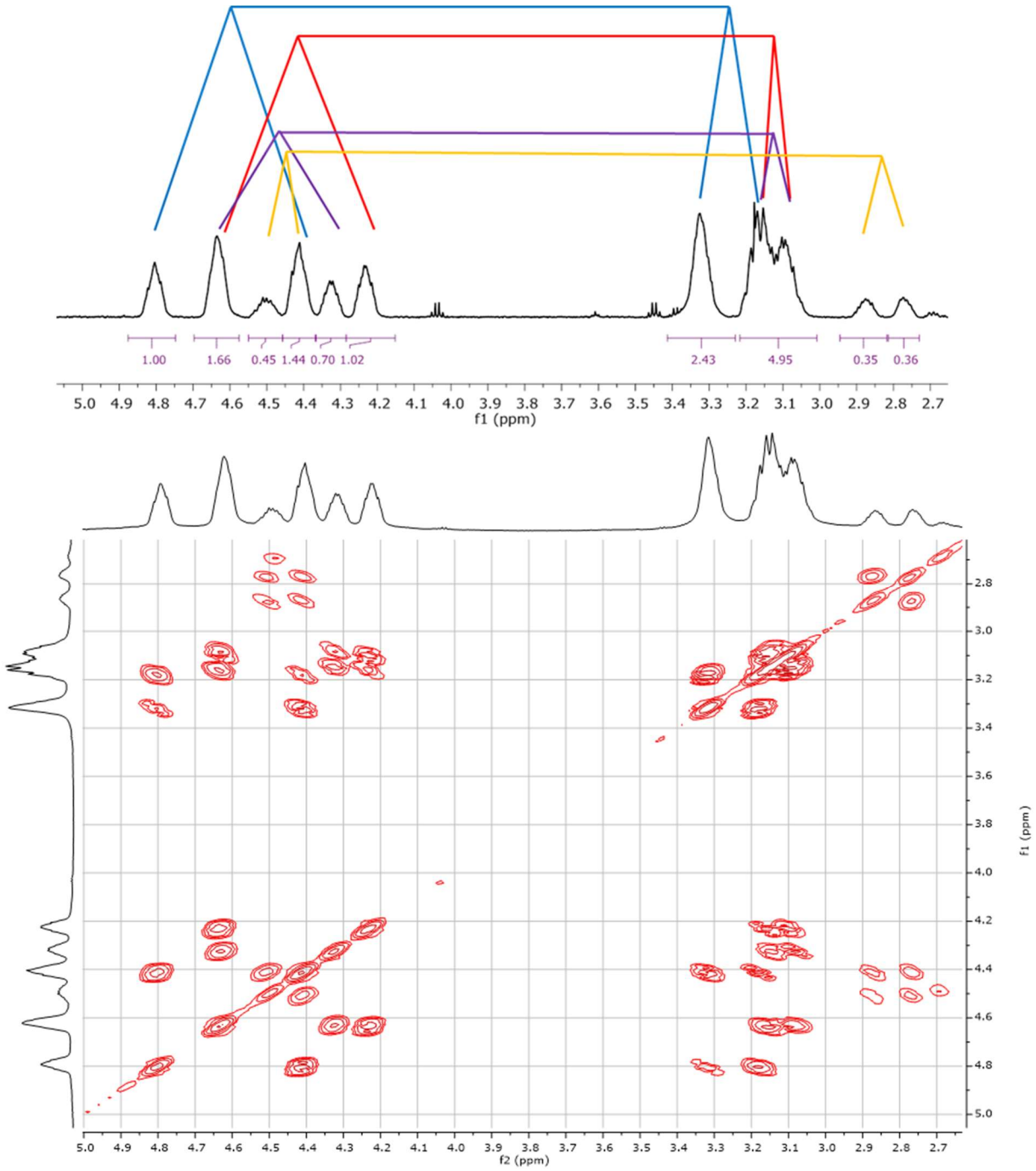


Figure 3.16. Top) $^{1}$H NMR (DMSO-$d_6$, 298 K, 700 MHz) spectrum of the ethylene linker region of **13a** and **13b**. Bottom) COSY NMR spectrum of the ethyl linker region of **13a** and **13b**.

Similar to what is observed for the **10-benzene**, when two equivalents $AgBF_4$ are added to a solution of **10-cymene** in DMSO or in acetonitrile, complete conversion to **12a-cymene** and **12b-cymene** is observed after 30 minutes. The ratio of major to minor product is 100:16 in DMSO

and 100:30 in acetonitrile and the p-cymene remains bound to the ruthenium center after more than 24 hours. Heating the DMSO reaction at 50 °C for 38 hours shows incomplete conversion to **13a** and **13b**, which increase simultaneously at a ratio of 100:36 suggesting that the dimer breaks apart in the presence of heat and DMSO before p-cymene dissociates. The ratio of the major to minor diastereomer changes based on the identity of the coordinating solvent and the structure of the coordinated aromatic ligand (p-cymene or benzene). We hypothesize that the steric interactions of ligands around the metal center alter the equilibrium between the two diastereomers in solution.

Continuous heating of **13a** and **13b** in DMSO lead to decomposition of these complexes into multiple products as seen by $^{31}$P-NMR spectroscopy (Figure 3.17).

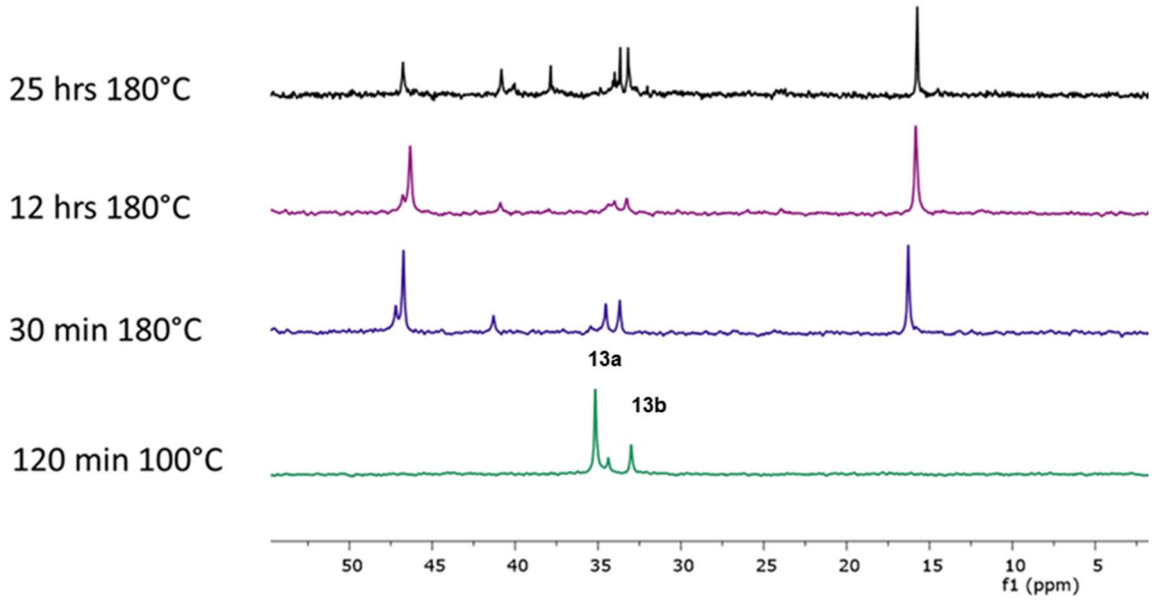


Figure 3.17. $^{1}$H NMR (DMSO-$d_6$, 500 MHz) heating a mixture of **13a** and **13b** at 100 °C followed by 180 °C at different time points.

In an attempt to isolate a single product, similar reaction conditions to those used for the previously reported base catalysed tautomerization of imidazole ligands to PNHCs were tested with **13a** and **13b**.[35, 36] When **13a** and **13b** are heated at 60 °C for five days with excess triethylamine minimal change is seen by $^{31}$P{$^{1}$H} NMR or by $^{1}$H NMR spectroscopy (Figure 3.18).

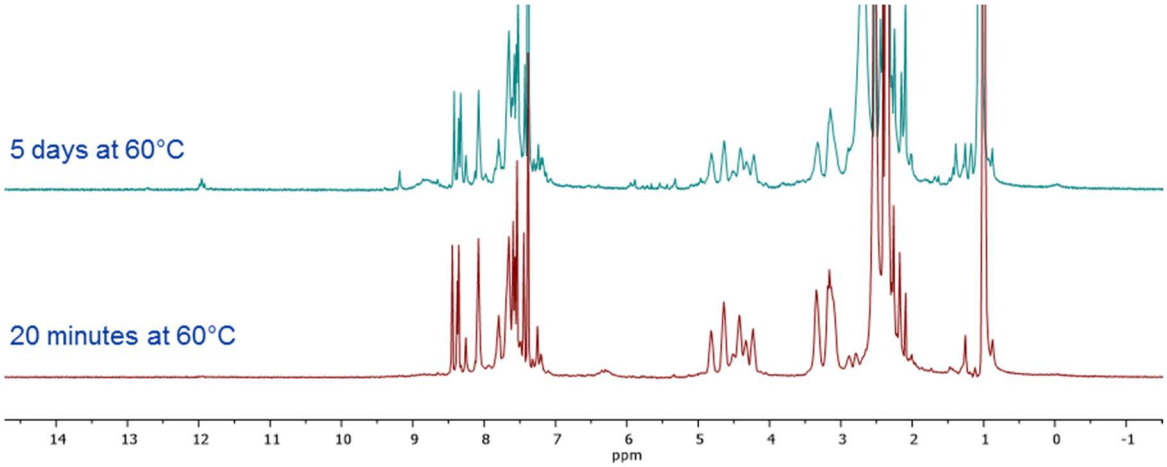


Figure 3.18. $^{1}$H NMR (DMSO-d$^{6}$, 700 MHz, 298 K) of complexes **13a** and **13b** heated with triethyamine at 60 °C for 20 minutes (bottom) and 5 days (top).

Furthermore, addition of two equivalents of KOtBu to a DMSO solution of **13a** and **13b** led to the formation of multiple species by $^{31}$P{$^{1}$H} NMR and $^{1}$H NMR spectroscopy, similar to what we saw previously in attempts to promote tautomerization using this base (Figure 3.19).

Overall, the success of the one pot synthesis of **9** relies upon the use of NMP as a solvent to access sufficient temperature needed to overcome the activation barrier associated with the demanding redox tautomerization reaction. The addition of $AgBF_4$ allows for chloride displacement and the clean formation of a single conformer of the desired tris-solvento platform.

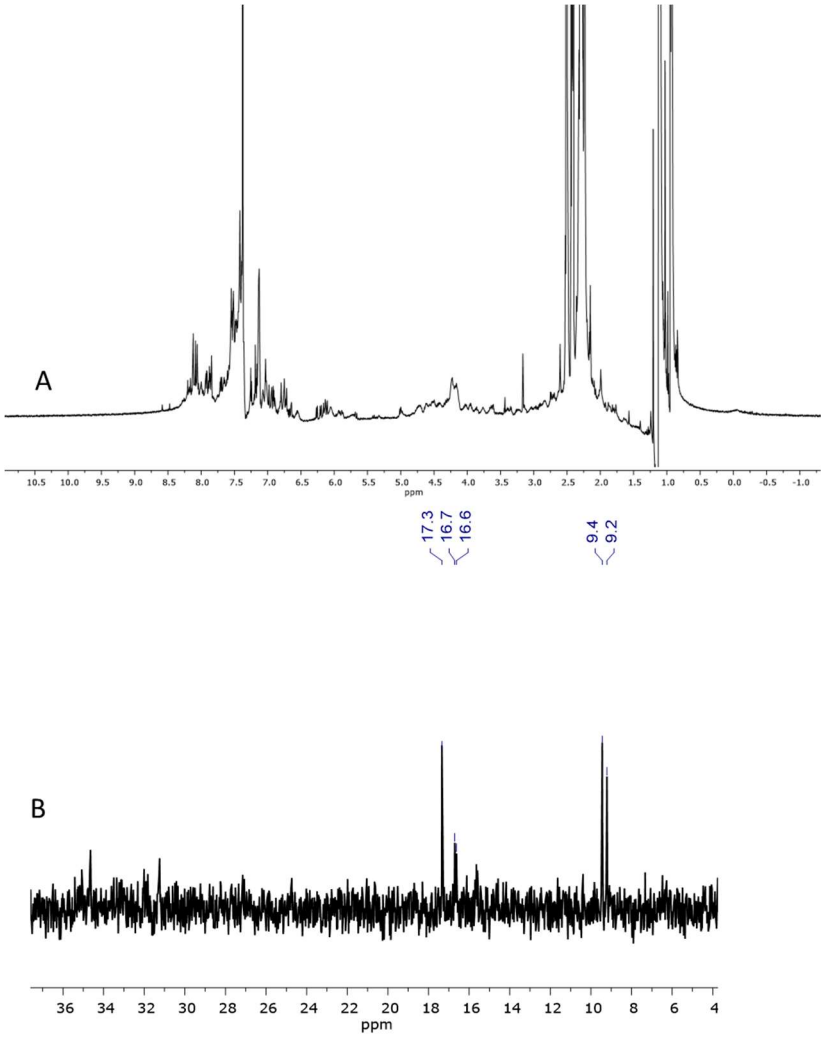


Figure 3.19. $^{1}$H NMR (**A**, 700 MHz) and $^{31}$P{$^{1}$H} NMR (**B,** 283.4 MHz) of **13a** and **13b** with addition of two equivalents of KOtBu to in DMSO-$d_6$ at 298 K.

## 3.3 CONCLUSIONS

We have explored the coordination chemistry and reactivity of a facially coordinating tripodal bis(PNHC) ligand and the arene dimer precursors $[(C_6H_6)RuCl_2]_2$ and $[(p\text{-cymene})RuCl_2]_2$. Ultimately, the tris-solvento complex $[(MeCN)_3Ru(PNHC)_2P^{Ph}]^{2+}$ (**9**) can be synthesized in a one pot procedure using NMP as a solvent. We hypothesize that the one pot synthesis of **9** can be adapted for use as a general strategy to access a range of other transition metal complexes ligated by the bis(PNHC) ligand. The use of NMP appears critical for generating these bis-PNHC complexes due to its polarity, hydrogen bonding ability, and high boiling point.

Using other solvents, such as DMSO, dichloromethane, and acetonitrile we can access a series of phosphine-bound monomer and dimer species with non-activated imidazole units.

## 3.4 EXPERIMENTAL

### I. General Information

Unless otherwise noted, all manipulations were carried out under a $N_2$ atmosphere using standard Schlenk technique. All solvents were purchased from Fisher Scientific. Benzimidazole (98%), sodium hydride (60% dispersion in mineral oil), phenylphosphine (10% wt. in hexanes), nbutyllithium solution (1.6 M in hexanes), 1,4-cyclohexadiene (97%), 2,2'-bipyridyl, trimethylamine (≥99%), tetrabutylammonium hexafluorophosphate, and sodium formate-13C (99 atom %) were purchased from Sigma-Aldrich. 1,2-dichloroethane (certified ACS) was purchased from Fisher Scientific. Trifluoromethanesulfonic acid (98+%) and 1,1,3,3- tetramethyldisiloxane (97%) were purchased from Alfa Aesar. Ruthenium (III) chloride hydrate was purchased from Pressure Chemical. Sodium bicarbonate ($^{13}C$, 99%) was purchased from Cambridge Isotope Labs. $[Ru(Bz)Cl_2]_2$[41] and $[Ru(Bz)(bpy)(OTf)](OTf)$[42] were synthesized according to previously published literature procedures. $^1H$, $^{31}P$, and $^{13}C$ NMR were taken on either a Bruker AV500, Bruker AV700, Bruker DRX500, or Bruker AV300 spectrometer. Anhydrous DMSO-d6 was purchased from Sigma-Aldrich, $CD_2Cl_2$ and $CD_3CN$ were purchased from Cambridge Isotope Labs, dried over calcium hydride, distilled before use, and stored over molecular sieves under $N_2$. Dichloromethane, acetonitrile and diethyl ether were dried through columns of activated alumina and molecular sieves under $N_2$ gas. NMP, DMSO, DMSO-$d_6$, dichloro(p-cymene)ruthenium(II) dimer, and $AgBF_4$ were purchased anhydrous from Sigma Aldrich and were used without further purification. Dichloro(benzene)ruthenium(II) dimer was prepared according to a published literature procedure.[43] **L** was prepared using a modified procedure from published in the literature.[1] All NMR spectra were taken on either a Bruker AV500, AV700, DRX500, or AV300 spectrometer at 298 K.

*1-(N-chloroethyl)-1,3-benzimidazole* (bimEtCl). In a typical reaction, benzimidazole (5.0 g, 42.5 mmol, 1eq) and sodium hydride (2.04 g, 51 mmol, 1.2 eq) were added to a flask with dichloroethane (100 mL) and placed under $N_2$. The reaction mixture was then heated at reflux

overnight, whereupon the reaction mixture was cooled and quenched with $H_2O$ (100 mL). The organic phase was then separated, and the aqueous phase was extracted with dichloromethane (50 mL). The combined organics were then washed with aqueous NaOH (2 x 100 mL), $H_2O$ (100 mL), and brine (100 mL). The combined organics were then dried with $MgSO_4$, filtered through celite, and the solvent was removed on a rotovap. Pentane (100 mL) was added to the resulting yellow oil and the product was sonicated for 30 minutes, which resulted in a white solid that was collected on a medium porosity frit and washed with pentane. Yield: 5.65 g (74%). 1H NMR (300 MHz, CDCl3) δ 7.99 (s, 1H), 7.84 (m, 2H), 7.50 – 7.24 (m, 2H), 4.54 (t, J = 6.0 Hz, 2H), 3.88 (t, J = 6.0 Hz, 2H).

*PhP(Etbim)$_2$ (**L-Norris**, updated synthesis)*. In a $N_2$ glovebox, a Schlenk flask equipped with a stir bar was charged with phenylphosphine (0.61 g, 5.5 mmol, 1 eq) and anhydrous THF (30 mL). The reaction flask was sealed and removed from the glove box, was connected to a $N_2$ Schlenk line, and was cooled to - 78 °C before n-butyllithium (0.78 g, 12.2 mmol, 2.2 eq) was slowly added via syringe. The reaction mixture turned a bright orange-red color and was allowed to warm to room temperature with vigorous stirring. After sitting at room temperature for 30 min, the reaction mixture was again cooled to -78 °C and a solution of bimEtCl (2.0 g, 11 mmol, 2 eq) in THF (20 mL) was added via cannula. The reaction mixture was warmed to room temperature and then heated at 55 °C overnight. After allowing the reaction mixture to cool, H2O (100 mL) was added to the reaction vessel to quench the reaction and the organic phase was separated. The aqueous phase was washed with dichloromethane (2 x 80 mL). The organic layers were combined and washed with $H_2O$ (2 x 100 mL) and brine (100 mL), then dried over $MgSO_4$, filtered through celite, and the solvent removed on a rotovap to give a cloudy yellow oil. Diethylether (200 mL) was added and the flask was sonicated for 30 min. The resulting white powder was collected on a medium porosity frit and was washed with diethylether. Yield: 1.47 g (67%). $^1$H NMR (500 MHz, $CDCl_3$) δ 7.76 (m, 4H), 7.53 – 7.43 (m, 5H), 7.31 – 7.18 (m, 6H), 4.15 (tdd, J = 14.7, 12.1, 6.5 Hz, 4H), 2.23 (d, J = 29.3 Hz, 4H) $^{31}P\{^1H\}$ NMR (202 MHz, $CDCl_3$) δ –32.9.

*[Ru(Bz)(bpy)(PhP(EtbimH$^+$)$_2$)](PF$_6$)$_4$ **(7)***. A three-necked round bottom flask equipped with a stir bar was charged with PhP(Etbim)$_2$ (818 mg, 2.1 mmol, 1 eq) and ethanol (50 ml). The mixture was degassed with $N_2$. Trifluoromethanesulfonic acid (7.6 g, 5.0 mmol, 2.4 eq) was then carefully

added to the reaction mixture via syringe and the mixture was stirred at room temperature for 10 min with $N_2$ flowing over the reaction solution and venting through a needle. A solution of [Ru(Bz)(bpy)(OTf)](OTf) (1.30 g, 2.1 mmol, 1 eq) in ethanol (20 mL) was then added via syringe and the reaction was heated at reflux for 45 min. The reaction solution was then added to an aqueous solution of $NH_4PF_6$ (30 mL) and the ethanol was removed on the rotovap. A light yellow solid precipitated and was collected on a medium porosity frit. The solid was washed with water and diethylether. Yield: 1.80 g (65%). 1H NMR (500 MHz, Acetonitrile-d3) δ 9.13 (s, 2H), 8.91 (d, J = 5.7 Hz, 2H), 8.09 (td, J = 7.9, 1.3 Hz, 2H), 7.99 – 7.94 (m, 2H), 7.90 (dd, J = 8.3, 1.3 Hz, 2H), 7.87 – 7.82 (m, 2H), 7.77 – 7.69 (m, 4H), 7.61 (ddd, J = 7.4, 5.6, 1.4 Hz, 2H), 7.40 (t, J = 7.4 Hz, 1H), 7.03 (td, J = 7.8, 2.8 Hz, 2H), 6.42 (s, 6H), 6.39 – 6.33 (m, 2H), 4.76 (dddd, J = 14.9, 12.0, 5.6, 3.5 Hz, 2H), 4.53 (tt, J = 14.3, 12.2, 6.2, 3.5 Hz, 2H), 3.64 (ddt, J = 15.4, 12.3, 6.1 Hz, 2H), 3.25 (dddd, J = 15.3, 12.5, 10.2, 3.5 Hz, 2H). 31P{1H} NMR (202 MHz, $CD_3CN$) δ 23.9 Elemental Analysis – Predicted (Actual): C, 36.52(36.60); H, 2.99(2.98); N, 6.39(6.20).

*[Ru(bpy)(PhP(Etbim)$_2$)(OH$_2$)](PF$_6$)$_2$,* ***(8-OH$_2$).*** A three-necked flask was charged with **7** (1.8 g, 1.4 mmol, 1 eq), trimethylamine (0.83 g, 8.2 mmol, 5.9 eq), and ethylene glycol (22 mL). The reaction solution was degassed with $N_2$ and then heated at 155 °C for 1h. After allowing the reaction mixture to cool, it was added to an aqueous $NH_4PF_6$ solution (100 mL). An orange solid precipitated, which was collected on medium porosity frit and was washed with water and diethylether. Yield 1.13 g (84%). Elemental Analysis−Predicted (Actual): C, 42.38(41.76); H, 3.45(3.40); N, 8.72(8.27).

*[Ru(bpy)(PhP(Etbim)$_2$)(Cl)](PF$_6$),* ***(8-Cl)****.* A vial equipped with a stir bar was charged with 1 (274 mg, 0.284 mmol, 1 eq) and NaCl (303 mg, 5.18, mmol, 18 eq) and methanol (20 ml) and was stirred for 1 hour at room temperature. The solution was transferred to a Schlenk bomb and all volatiles were removed under vacuum at 100 °C over the course of 1 hour. The evacuated Schlenk bomb and solids were brought into the glove box and the solids were dissolved in DCM and filtered through celite. The volatiles were removed via vacuum overnight giving 150 mg of a dark red powder (63.6% yield). $^1$H NMR (500 MHz, $CD_2Cl_2$) δ 11.81 (s, 2H), 8.26 – 8.15 (m, 2H), 7.89 – 7.80 (m, 4H), 7.57 (d, *J* = 7.8 Hz, 2H), 7.49 (dd, *J* = 7.0, 1.7 Hz, 2H), 7.38 – 7.30 (m, 4H), 7.22 – 7.17 (m, 1H), 6.91 (td, *J* = 7.8, 2.2 Hz, 2H), 6.56 – 6.50 (m, 2H), 5.04 (dddd, *J* = 25.3, 14.5, 6.4,

4.4 Hz, 2H), 4.61 (tdd, $J$ = 14.5, 10.5, 3.2 Hz, 2H), 2.83 (ddddd, $J$ = 31.7, 14.6, 10.6, 7.9, 2.8 Hz, 4H). $^{13}C\{^{1}H\}$ NMR (126 MHz, $CD_2Cl_2$) δ 195.89 (d, $J_{CP}$ = 15.1 Hz), 155.84, 151.77, 137.30, 136.14, 133.82, 132.34, 131.99, 129.93, 129.10, 129.02, 127.98, 127.92, 126.72, 123.68, 123.23, 122.81, 111.00, 109.43, 43.51, 23.92. $^{31}P\{^{1}H\}$ NMR (202 MHz, $CD_2Cl_2$) δ 45.70. Elemental Analysis − Predicted (Actual): C, 48.84(48.51); H, 3.74(4.53); N, 10.05(9.84).

*$((MeCN)_3Ru(PNHC)_2P^{Ph})(BF_4)_2$* ***(9).*** One pot synthesis: In a $N_2$ glovebox, a 100 ml thick-walled Schlenk tube equipped with a stir bar was charged with dichloro(benzene)ruthenium(II) dimer (0.182 g, 0.363 mmol, 1 eq) and **L** (0.334 mg, 0.734 mmol, 2 eq), and NMP (10 ml). The reaction mixture was allowed to stir at room temperature for at least an hour. The Schlenk tube was sealed, removed from the glove box, connected to the Schlenk line, and heated outside the box at 170 °C for one hour. The volatiles were then removed under reduced pressure, at 100 °C on the Schlenk line, over the course of four hours. The Schlenk tube was brought into the glove box and acetonitrile (10 ml) and $AgBF_4$ (0.284 g, 1.45 mmol, 4 eq) were added to the reaction mixture. The solution immediately became gray and cloudy. The resultant mixture was stirred for 1 hr before being filtered through celite and the captured solids were washed with acetonitrile (3 x 5 ml). The volume of the extracts was reduced by half under reduced pressure, and the product was precipitated from solution with diethyl ether (30 ml). The resulting precipitate was collected on a frit and was washed with diethyl ether (3 x 15 ml), and dried overnight under reduced pressure. The product was collected as a white powder (0.583 g, 93% yield).

From Complex **11**: Complex **11** (55.9 mg, 0.08374 mmol, 1 eq) was suspended in $CD_3CN$ (1.5 ml) in a 20 ml vial and transferred to a vial containing $AgBF_4$ (19.5 mg, 0.101 mmol, 2 eq) via pipette. The mixture immediately turned purple**.** After stirring for an hour, the solution was filtered via syringe filter, washed two times with 2 ml of acetonitrile and the product was precipitated out of solution with 35 ml of diethyl ether. The precipitate was collected on a medium porosity frit and washed three times with 15 ml of diethyl ether, dried under reduced pressure overnight, and was collected as a white powder (56.9 mg, 80% yield). High quality crystals suitable for X-ray diffraction were grown by slow diffusion of diethyl ether into the $CD_3CN$ solution at -35°C. $^{1}H$ NMR (700 MHz, Methylene Chloride-$d_2$) δ 10.78 (s, 2H, N-H), 7.85 (dd, $J$ = 10.2, 7.7 Hz, 2H, Ph-H), 7.64 (td, $J$ = 7.8, 2.1 Hz, 2H, Ph-H), 7.61 – 7.56 (m, 1H, Ph-H), 7.39 (s, 2H, Ar-H), 7.11 (s, 2H, Ar-H), 4.39 (dddd, $J$ = 19.3, 13.2, 10.0, 2.5 Hz, 2H, -$CH_2$), 4.25 (dddd, $J$ = 26.2, 14.2, 7.3,

3.2 Hz, 2H, -$CH_2$), 2.71 (tdd, *J* = 12.9, 7.1, 3.7 Hz, 2H, -$CH_2$), 2.62 (s, 3H, $NCCH_3$), 2.35 (s, 6H, -$CH_3$), 2.33 (s, 6H, -$CH_3$), 2.22 (s, 6H $NCCH_3$), 2.14 (tdd, *J* = 13.0, 9.6, 6.0 Hz, 2H, -$CH_2$). $^{31}P\{^1H\}$ NMR (202 MHz, Acetonitrile-$d_3$) δ 44.73 . $^{13}C$ NMR (176 MHz, $CD_3CN$) δ 189.05, 188.95, 134.87, 134.63, 134.07, 133.39, 133.11, 132.41, 131.90, 131.85, 131.44, 129.79, 129.74, 124.69, 118.31, 111.88, 110.58, 26.73, 26.53, 20.29, 20.04. Anal. Calc. for $B_2C_{34}F_8H_{40}N_4PRu$: C, 47.91; H, 4.73; N, 11.5. Found: C, 47.09; H, 4.65; N, 11.35 %.

*$(C_6H_6)Ru(L)Cl_2$* ***(10-benzene)***. Ligand **L** (232 mg, 0.466 mmol, 1 eq) was dissolved in dichloromethane (15 ml) and the resulting solution was transferred to a 20 ml vial charged with dichloro(benzene)ruthenium(II) dimer and a stir bar. The solution turned dark red and was allowed to stir for an hour at room temperature. The solution was filtered through celite and the celite was washed with dichloromethane (5 ml). The volatiles were removed under vacuum until less than 1 ml of liquid remained. The product was precipitated with 40 ml of filtered diethyl ether, collected on a medium porosity frit, washed with diethyl ether (3 x 15 ml), and dried under vacuum overnight, producing a dark orange powder (222 mg, 68% yield). High quality orange hexagonal prisms suitable for single crystal X-ray diffraction were grown via slow evaporation of solvent from a super-saturated solution in dichloromethane and diethyl ether at -35°C. $^1H$ NMR (500 MHz, Methylene Chloride-$d_2$) δ 7.95 – 7.83 (m, 2H, Ar-H), 7.68 – 7.58 (m, 3H, Ar-H), 7.55 (s, 2H, Ar-H), 7.45 (s, 2H, Ar-H), 7.07 (s, 2H, Ar-H), 5.42 (s, 6H, Ru-Benzene), 4.34 (dt, *J* = 15.9, 7.9 Hz, 2H, -$CH_2$), 4.21 (dq, *J* = 15.8, 8.2 Hz, 2H, -$CH_2$), 2.83 (q, *J* = 8.9 Hz, 4H, -$CH_2$), 2.35 (s, 6H, -$CH_3$), 2.32 (s, 6H, -$CH_3$). $^{31}P\{^1H\}$ NMR (202 MHz, DMSO-$d_6$) δ 13.7. $^{13}C$ NMR (126 MHz, Benzene-$d_6$) δ 142.9, 142.3, 134.3 , 132.8 , 132.2 , 131.9 , 131.6 , 130.7 (d, *J* = 8.2 Hz), 129.9 (d, *J* = 9.5 Hz), 120.7 , 110.06 , 89.00 (d, *J* = 3.4 Hz), 40.6 , 26.3 (d, *J* = 25.4 Hz), 20.7 , 20.3. Anal. Calc. for $C_{34}H_{37}Cl_2N_4PRu$: C, 57.95; H, 5.29; N, 7.95. Found: C, 56.92; H, 5.43; N, 7.69 %.

*(p-cymene)Ru(L)Cl₂* ***(10-cymene)***. Ligand **L** (41.3 mg, 0.0909 mmol, 1 eq) was dissolved in dichloromethane (4 ml), and the resulting solution was transferred to 20 ml vial charged with dichloro(p-cymene)ruthenium(II) dimer (29 mg, 0.0468 mmol, 0.515 eq) and a stir bar. The solution immediately turned clear vibrant orange. The solution was allowed to stir at room temperature for 90 min before the volatiles were removed via reduced pressure. The product was isolated as a bright orange precipitate from a 1:10 mixture of dichloromethane and diethyl ether.

The orange powder was collected on a medium porosity frit and was dried overnight under vacuum (30.8 mg, 45% yield). $^{1}$H NMR (500 MHz, Methylene Chloride-$d_2$) δ 7.88 (tt, $J$ = 6.9, 2.3 Hz, 2H, Ph-H), 7.66 (dt, $J$ = 4.4, 2.2 Hz, 3H, Ph-H), 7.60 (s, 2H, Ar-H), 7.51 (s, 1H, Ar-H), 7.11 (s, 2H, Ar-H), 5.29 – 5.18 (m, 4H, -$CH_2$, Ar-H p-cymene), 4.42 – 4.22 (m, 4H, -$CH_2$), 3.08 (ddt, $J$ = 13.7, 9.7, 6.7 Hz, 2H, -$CH_2$), 2.83 (dddd, $J$ = 14.8, 12.7, 9.4, 5.3 Hz, 2H, -$CH_2$), 2.40 (s, 6H, -$CH_3$), 2.37 (s, 6H, -$CH_3$), 1.82 (s, 3H, -$CH_3$), 1.11 (d, $J$ = 6.9 Hz, 6H**,** -$CH_3$). $^{31}$P{$^{1}$H} NMR (283 MHz, $CD_2Cl_2$) δ 10.8. $^{13}$C NMR (176 MHz, $CD_2Cl_2$) δ 142.9, 142.4, 134.3 (d, $J$ = 40.0 Hz), 132.7, 132.3, 131.6 131.6 , 130.4 (d, $J$ = 7.5 Hz), 129.9 (d, $J$ = 9.2 Hz), 120.7 , 110.0 , 109.1 , 97.4 , 89.3 , 86.2 , 40.4 , 30.7 , 25.5 (d, $J$ = 23.8 Hz), 22.1 , 20.7 , 20.3 , 18.0.

*Synthesis of [(PNHC)$_2$P$^{Ph}$RuCl]Cl* ***(11)***. In a 20 ml scintillation vial ($C_6H_6$)$RuCl_2$ (64 mg, 0.217 mmol, 1 eq) was dissolved in NMP (2 ml) and was transferred via pipette to a vial equipped with a stir bar and the free **L** (123 mg, 0.433 mmol, 2 eq). The solution was allowed to stir for 30 min at room temperature before being transferred to a sealed tube. The sealed tube was heated for 23 hours at 140 °C. The sealed tube was brought back into the glove box and the product was precipitated with 15 ml of diethyl ether, collected on a medium porosity frit, washed 3 times with 10 ml of diethyl ether and dried overnight under vacuum, and was collected as an off-white powder (98.0 mg, 36% yield). $^{1}$H NMR (300 MHz, Methylene Chloride-$d_2$) δ 10.96 (s, 1H, N-H), 10.88 (s, 1H, N-H), 8.08 (dd, $J$ = 9.9, 7.7 Hz, 2H, Ph-H), 7.39 (t, $J$ = 7.4 Hz, 1H, Ph-H), 7.31 – 7.19 (m, 3H, Ar-H), 7.10 (s, 1H, Ar-H), 6.95 (d, $J$ = 3.4 Hz, 2H, Ar-H), 4.92 – 4.71 (m, 1H, -$CH_2$), 4.63 – 4.40 (m, 1H, -$CH_2$), 4.30 (dddt, $J$ = 87.5, 27.6, 14.1, 6.3, 3.6 Hz, 1H, -$CH_2$), 3.89 – 3.71 (m, 1H, -$CH_2$), 2.76 – 2.61 (m, 1H, -$CH_2$), 2.37 (s, 3H, -$CH_3$), 2.33 (s, 3H, -$CH_3$), 2.28 (s, 3H, -$CH_3$), 2.21 (s, 12H, -$CH_3$). $^{31}$P{$^{1}$H} NMR (121 MHz, $CD_2Cl_2$) δ 52.9.

*[(PNHC)$_2$P$^{Ph}$RuCl(DMSO)$_2$]Cl* ***(11-DMSO)***. Complex **11** was dissolved in DMSO. High quality crystals suitable for X-ray diffraction were grown in air with a super saturated solution in a 1:1 mixture of DMSO and dichloromethane.

*[(p-cymene)(DMSO)Ru(L)]$_2$(BF$_4$)$_4$* ***(12a-cymene and 12b-cymene)***. In a $N_2$ glovebox, a J-Young tube was charged with dichloro(p-cymene)ruthenium(II) dimer (9 mg, 0.014 mmol, 0.5 eq), **L** (16 mg, 0.0291 mmol, 1 eq), and DMSO-$d_6$ (1.4 ml). The J-Young tube was sealed and the reaction

vessel was sonicated for 28 min. The J-Young tube was returned to the glove box and $AgBF_4$ (11 mg, 0.583 mmol, 2 eq) was added to the reaction mixture. The tube was again sealed and the mixture was sonicated. After five minutes of sonication the orange solution turned cloudy and the color changed from orange to yellow-orange. The reaction was judged complete after 90 minutes of sonication.

Major Diastereomer: $^1$H NMR (500 MHz, Acetonitrile-$d_3$) δ 9.21 (s, 1H, Ar-H), 8.65 (s, 1H, Ar-H), 7.98 (t, $J$ = 8.9 Hz, 2H, Ph-H), 7.75 – 7.59 (m, 5H, Ar-H), 6.94 (s, 1H, Ar-H), 6.72 (s, 1H, Ar-H), 5.37 (d, $J$ = 6.0 Hz, 1H, p-cymene Ar-H), 5.09 – 4.95 (m, 1H, -$CH_2$), 4.94 (d, $J$ = 6.4 Hz, 1H, p-cymene Ar-H), 4.45 (m, 1H, -$CH_2$), 4.08 (d, $J$ = 5.9 Hz, 1H, p-cymene Ar-H), 3.98 (q, $J$ = 14.9 Hz, 1H, -$CH_2$), 3.83 (d, $J$ = 6.4 Hz, 1H, p-cymene Ar-H), 3.74 (dq, $J$ = 15.0, 7.7, 7.0 Hz, 1H, -$CH_2$), 3.50 (d, $J$ = 15.9 Hz, 1H, -$CH_2$), 3.36 (td, $J$ = 13.5, 6.4 Hz, 1H, -$CH_2$), 3.18 – 3.07 (m, 1H, -$CH_2$), 2.36 (s, 6H, -$CH_3$), 2.34 (s, 3H, -$CH_3$), 2.34 (s, 3H, -$CH_3$), 1.62 (s, 3H, -$CH_3$), 1.30 – 0.94 (m, 1H, -CH), 0.86 (d, $J$ = 6.9 Hz, 3H, -$CH_3$), 0.43 (d, $J$ = 6.9 Hz, 3H, -$CH_3$). $^{31}$P{$^1$H } NMR (202 MHz, $CD_3CN$) δ 13.2.

Minor Diastereomer: $^1$H NMR (500 MHz, Acetonitrile-$d_3$) δ 8.27 (s, 1H, Ar-H), 8.10 (s, 1H, Ar-H), 8.00 (s, 1H, Ar-H), 7.89 – 7.81 (m, 3H, Ph-H), 7.45 (s, 1H, Ar-H), 7.31 (s, 1H, Ar-H), 7.27 (s, 1H, Ar-H), 7.16 (s, 1H, Ar-H), 6.99 (s, 1H, Ar-H), 5.88 (d, $J$ = 6.6 Hz, 1H, p-cymene Ar-H), 5.81 (d, $J$ = 6.5 Hz, 1H, p-cymene Ar-H), 5.69 (d, $J$ = 6.3 Hz, 1H, p-cymene Ar-H), 5.59 (d, $J$ = 6.4 Hz, 1H, p-cymene Ar-H), 5.16 – 5.08 (m, 1H, -$CH_2$), 4.18 (td, $J$ = 16.9, 9.4 Hz, 1H, -$CH_2$), 3.33 – 3.25 (m, 1H, -$CH_2$), 3.24 – 3.18 (m, 1H, -$CH_2$), 3.02 (tt, $J$ = 15.5, 8.0 Hz, 1H, -$CH_2$), 2.87 – 2.73 (m, 2H, -$CH_2$), 2.38 (s, 3H, -$CH_3$), 2.32 (s, 3H, -$CH_3$), 2.27 (s, 3H, -$CH_3$), 2.24 (s, 3H, -$CH_3$), 1.84 (s, 3H, -$CH_3$), 1.30 – 0.94 (m, 1H, -CH), 1.08 (d, $J$ = 7.1 Hz, 3H, -$CH_3$), 1.02 (d, $J$ = 6.9 Hz, 3H, -$CH_3$). $^{31}$P{$^1$H} NMR (202 MHz, $CD_3CN$) δ 19.49.

*$[(DMSO)_4Ru(L)]_2(BF_4)_4$* ***(13a and 13b)***. The benzene dissociates from **12a-benzene** and **12b-benzene** on prolonged exposure to DMSO with gentle heating.

Major Diastereomer: $^1$H NMR (700 MHz, DMSO-$d_6$) δ 8.46 (s, 1H, Ar-H), 8.37 (s, 1H, Ar-H), 8.08 – 8.03 (m, 2H), 7.63 (td, $J$ = 7.4, 2.3 Hz, 2H, Ph-H), 7.58 – 7.56 (m, 1H, Ph-H), 7.58 (s, 1H, Ar-H), 7.56 (s, 1H, Ar-H), 7.52 (s, 1H, Ar-H), 7.43 (s, 1H, Ar-H), 4.79 (ddt, $J$ = 15.4, 10.4, 5.3 Hz, 1H, -$CH_2$), 4.62 (m, 1H, -$CH_2$), 4.45 – 4.36 (m, 1H, -$CH_2$), 4.22 (ddt, $J$ = 15.4, 10.8, 5.5 Hz,

1H, -$CH_2$), 3.35 – 3.26 (m, 2H, -$CH_2$), 3.21 – 3.02 (m, 2H, -$CH_2$) 2.39 (s, 3H, -$CH_3$)m2.36 (s, 3H, -$CH_3$) 2.34 (s, 3H, -$CH_3$) 2.32 (s, 3H, -$CH_3$). $^{31}P\{^1H\}$ NMR (283 MHz, DMSO) δ 35.2.

Minor Diastereomer: $^1H$ NMR (700 MHz, DMSO-d6) δ8.39 (s, 1H, Ar-H), 8.25 (s, 1H, Ar-H), 7.79 – 7.75 (m, 2H, Ph-H), 7.69 – 7.66 (m, 2H, Ph-H), 7.52 (s, 1H, Ar-H), 4.67 – 4.57 (m, 1H, -$CH_2$), 4.45 – 4.36 (m, 1H, -$CH_2$), 4.50 (tq, J = 15.3, 7.9, 7.1 Hz, 1H, -$CH_2$), 4.32 (ddt, J = 15.3, 10.9, 5.8 Hz, 1H, -$CH_2$), 3.21 – 3.02 (m, 2H, -$CH_2$), 2.87 (tt, J = 13.0, 6.3 Hz, 1H, -$CH_2$), 2.76 (dq, J = 14.0, 6.8 Hz,1H, -$CH_2$), 2.32 (s, 3H, -$CH_3$), 2.17 (s, 3H, -$CH_3$). $^{31}P\{^1H\}$ NMR (283 MHz, DMSO) δ 32.9.

## 3.5 SUPPORTING INFORMATION

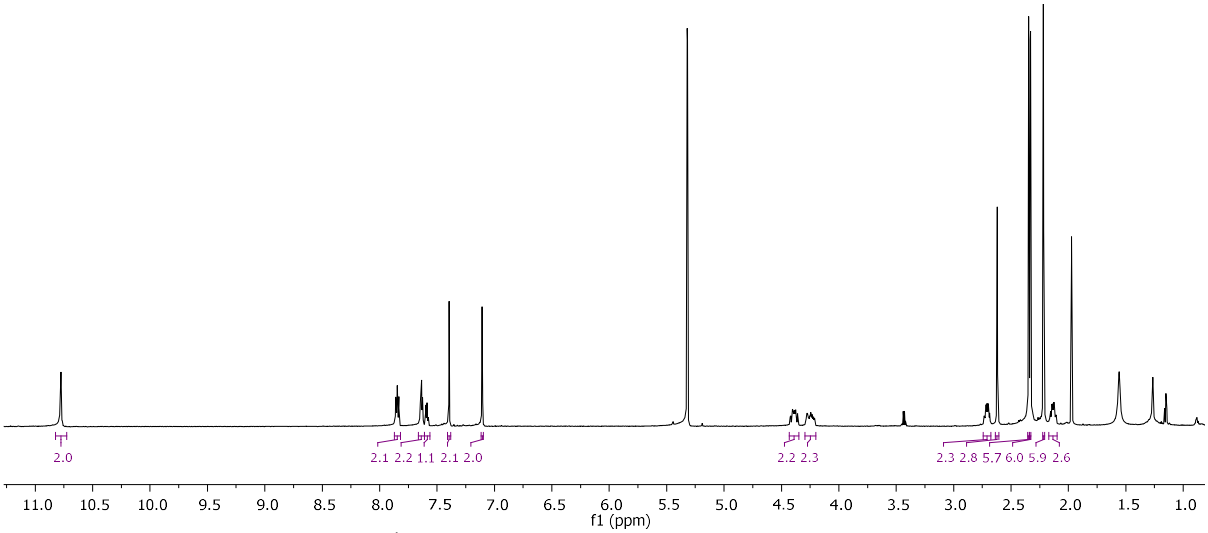


Figure 3.20. $^1H$ NMR (298 K, 499.7 MHz) of **9** in $CD_2Cl_2$.

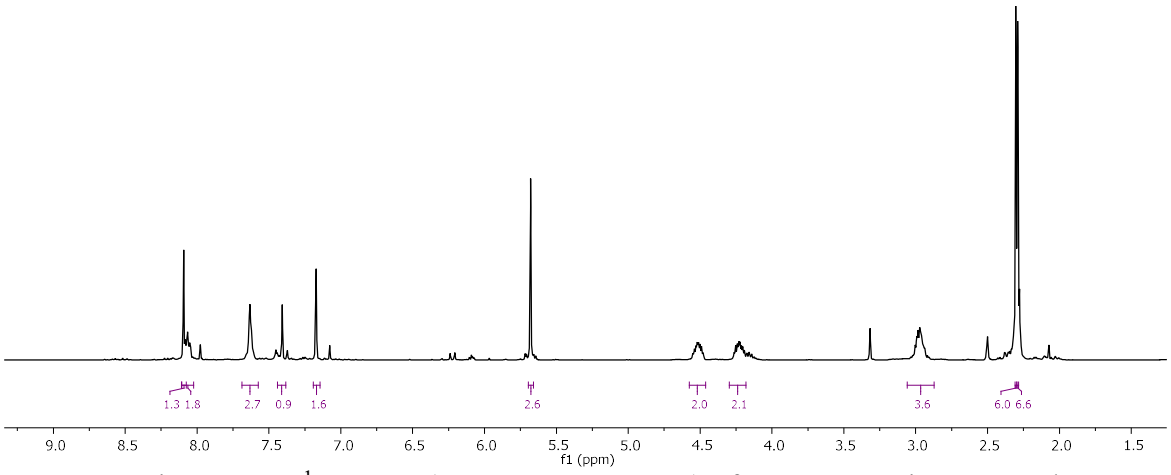


Figure 3.21. $^{1}$H NMR (298 K, 499.72 MHz) of **10-benzene** in DMSO-$d_6$.

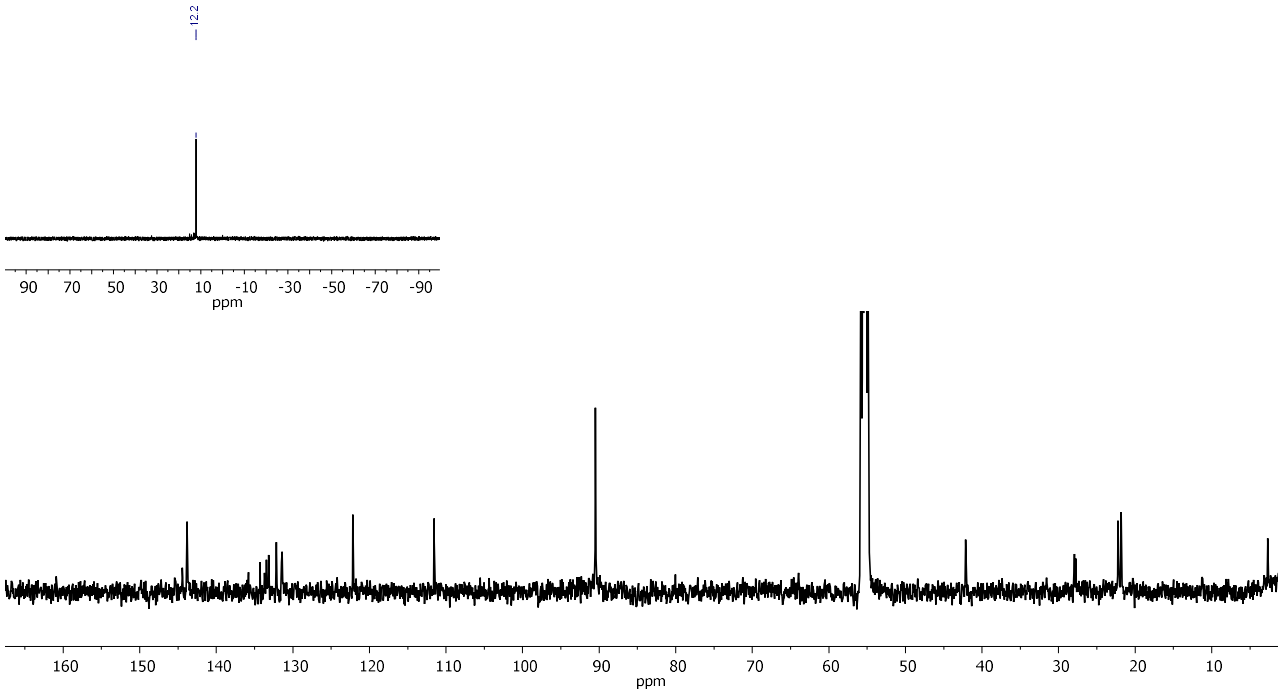


Figure 3.22 Top) $^{31}$P NMR (298 K, 202.29 MHz) of **10-benzene** in DMSO-$d_6$. Bottom) $^{13}$C NMR (298 K, 125.77 MHz) of **10-benzene** in DMSO-$d^6$.

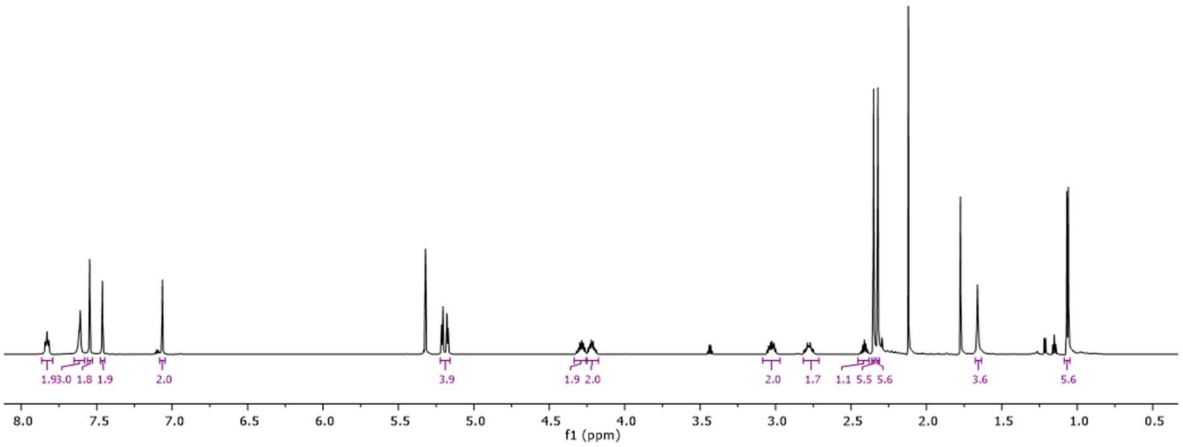


Figure 3.23. $^{1}$H NMR (298 K, 700.07 MHz) of **10-cymene** in DMSO-$d_6$.

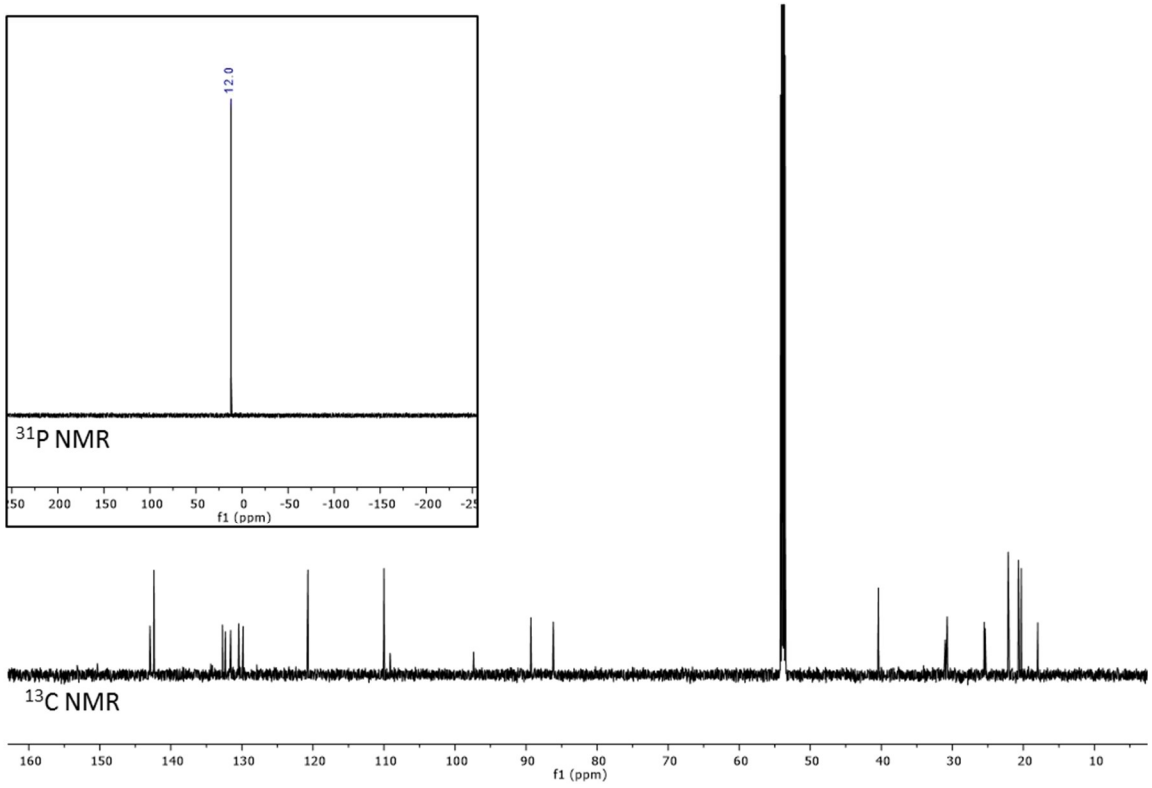


Figure 3.24. $^{31}$P NMR (298 K, 283.39 MHz) of **10-cymene** in DMSO-$d_6$, and $^{13}$C NMR (298 K , 176.05 MHz) of **10-cymene** in DMSO-$d_6$.

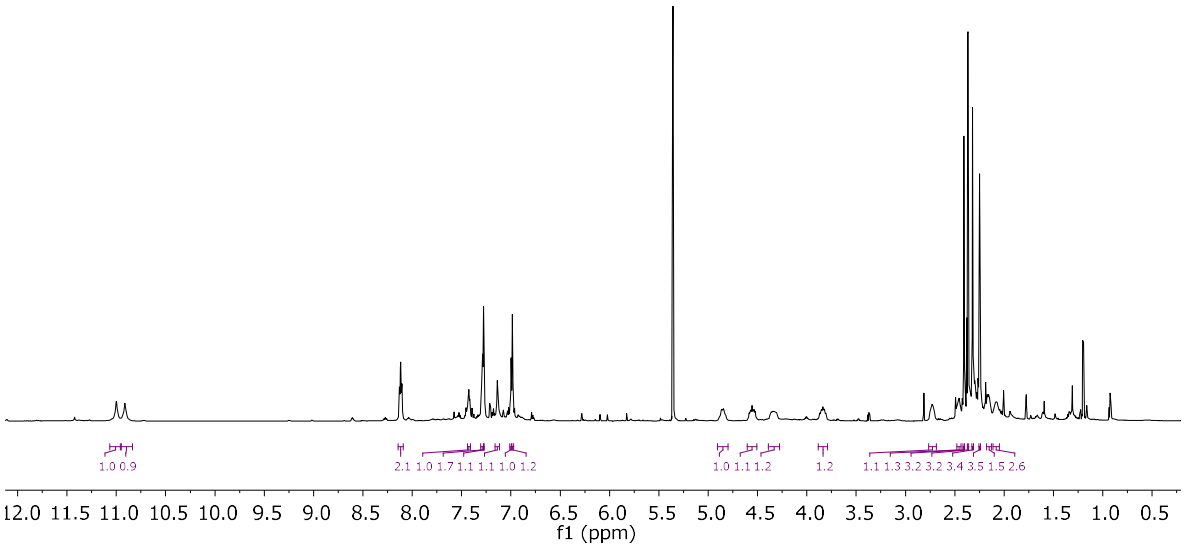


Figure 3.25. $^{1}$H NMR (298 K, 700 MHz) of **11** in $CD_2Cl_2$.

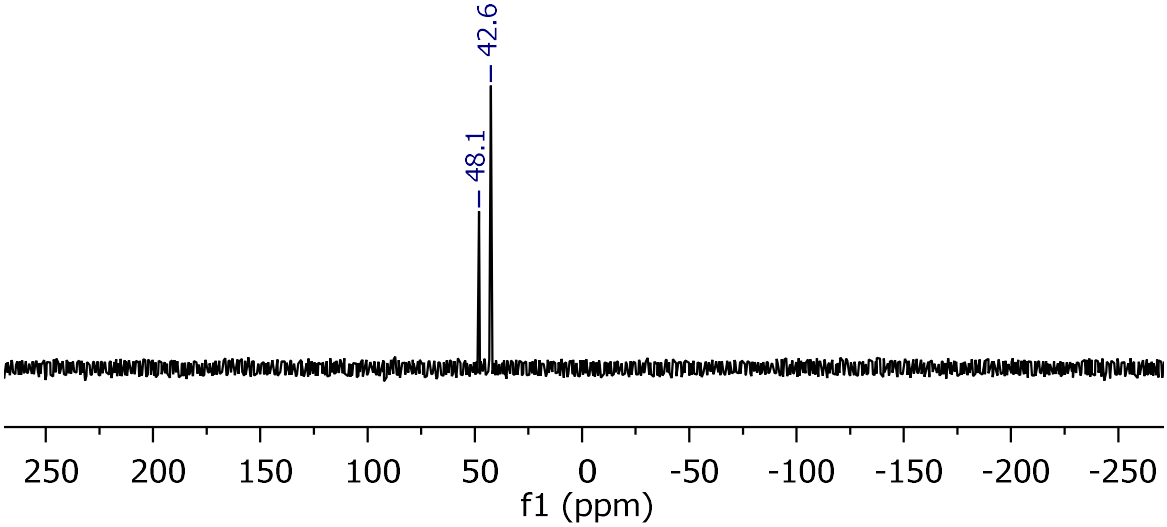


Figure 3.26. $^{31}$P NMR (298 K, 283.39 MHz) of **11** in $CD_3CN$.

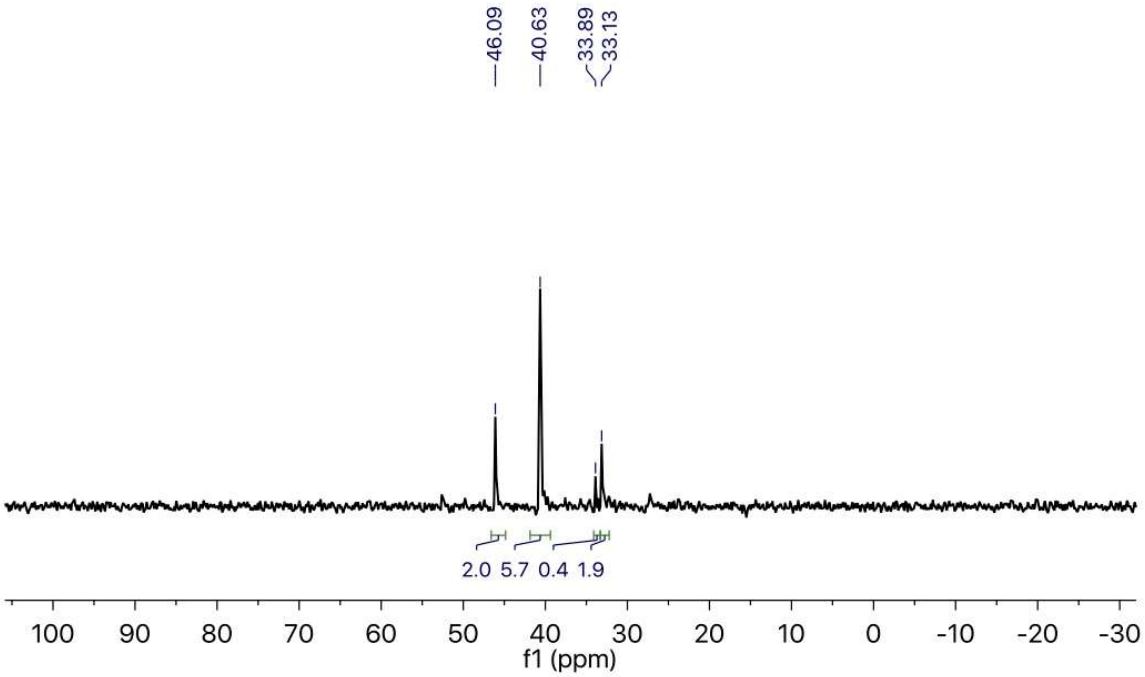


Figure 3.27. $^{31}P$ NMR (298 K, 202.29 MHz) of **11** in DMSO-$d^6$.

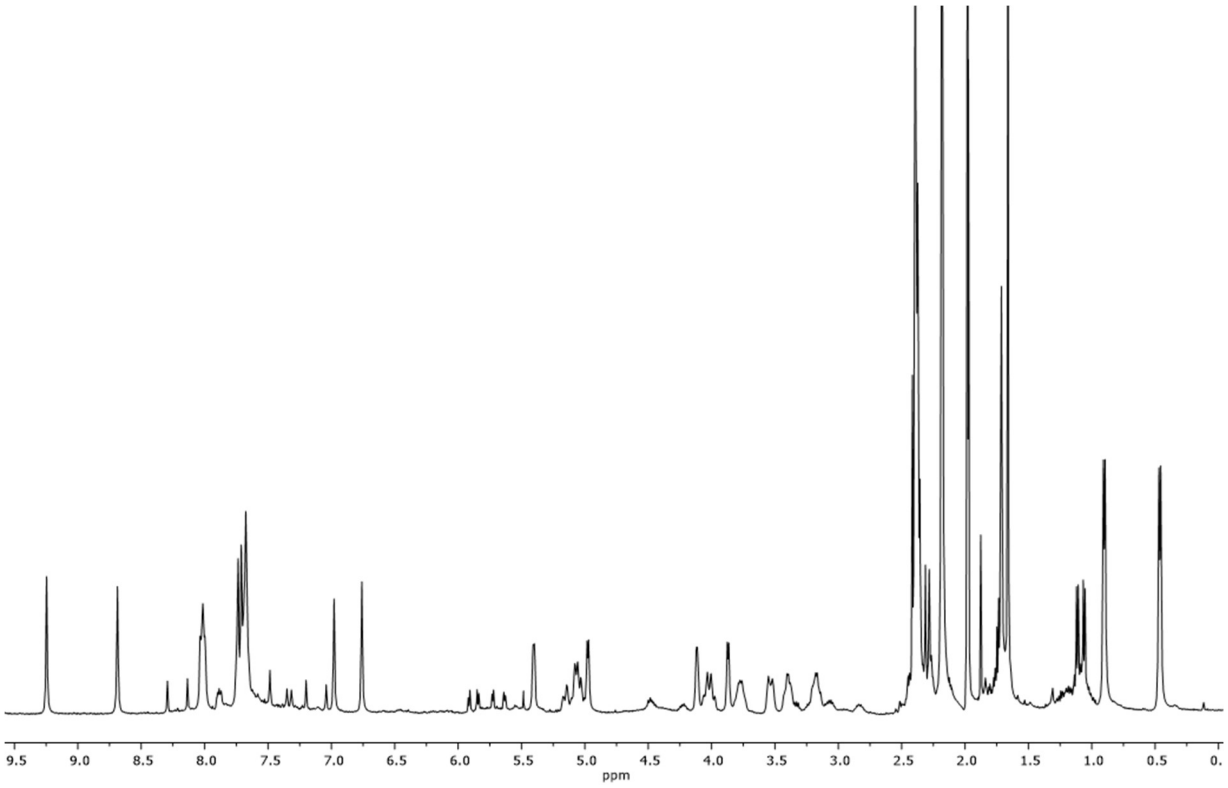


Figure 3.28. $^{1}H$ NMR (298 K, 500 MHz) in $CD_3CN$ **12a-cymene** and **12b-cymene**.

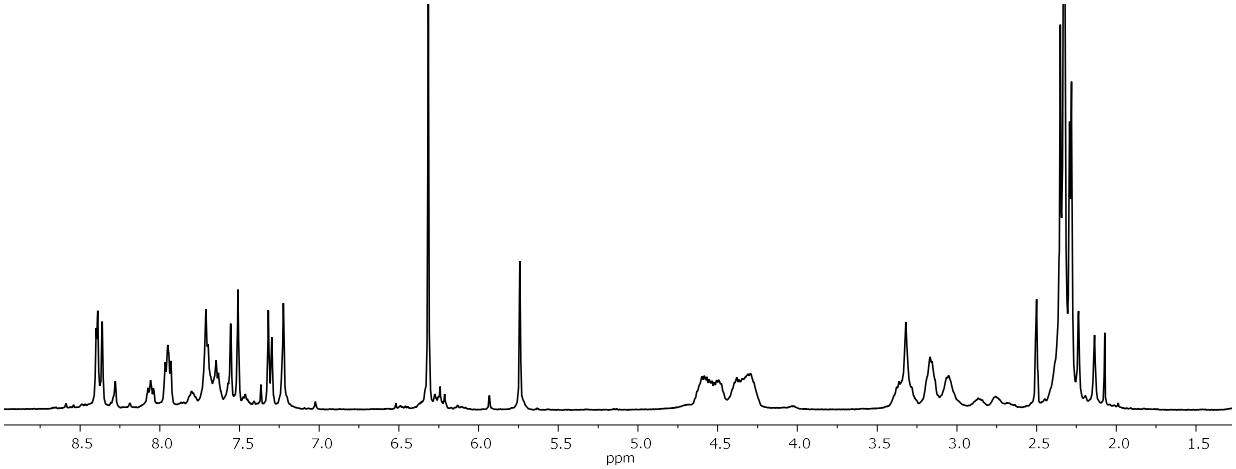


Figure 3.29. $^{1}$H NMR (298 K, 700 MHz) **12a-benzene** and **12b-benzene** DMSO-d$^{6}$.

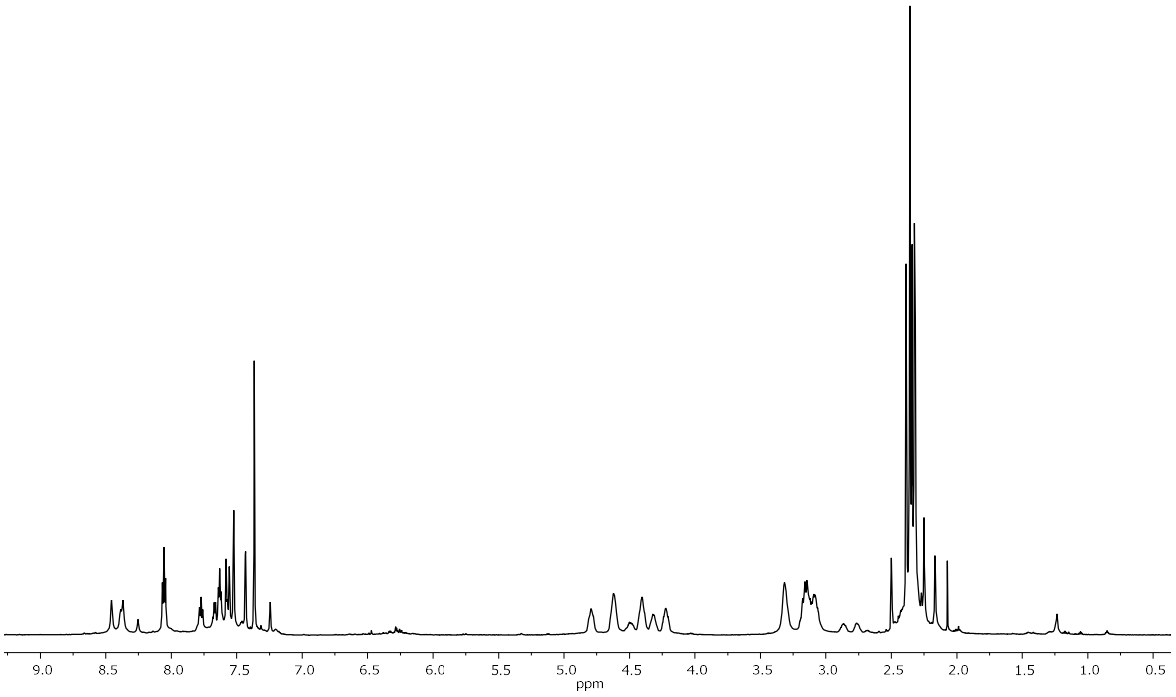


Figure 3.30. $^{1}$H NMR (298 K, 700 MHz) **13a** and **13b** in DMSO-d$^{6}$

Table 3.1 Crystallographic information for complexes **8-Cl**, **9**, **10-benzene**, and **11-DMSO**.

| Molecule | Compound **8-Cl** | Compound **9** | Compound **10-benzene** | Compound **11-DMSO** |
|---|---|---|---|---|
| Empirical formula | C48 H54 F18 N8 O P4 Ru | C40 H49 B2 F8 N10 P Ru | C34 H37 Cl2 N4 P Ru | C66 H92 Cl4 N8 O5 P2 Ru2 S5 |
| Formula weight | 1325.94 | 975.55 | 704.62 | 1643.65 |
| Temperature | 100(2) K | 100(2) K | 293(2) K | 293(2) K |
| Wavelength | 0.71073 Å | 0.71073 Å | 0.71073 Å | 0.71073 Å |
| Crystal system | Monoclinic | Monoclinic | Trigonal | Monoclinic |
| Space group | P $2_1$/c | P 1 21/c 1 | R -3 | P 2/n |
| Unit cell dimensions | a = 12.0184(12) Å | a = 13.1696(6) Å | a = 33.798(4) Å | a = 13.445(5) Å |
| | b = 44.108(5) Å | b = 17.1948(8) Å | b = 33.798(4) Å | b = 10.038(5) Å |
| | c = 11.7885(12) Å | c = 20.3695(10) Å | c = 19.6172(17) Å | c = 27.511(5) Å |
| | a= 90°. | a= 90°. | 19407(4) Å3 | 3695(2) Å3 |
| | b= 117.748(5)°. | b= 94.836(3)°. | a= 90°. | a= 90.000(5)°. |
| | g = 90°. | g = 90°. | b= 90°. | b= 95.679(5)°. |
| Volume | 5530.6(10) Å3 | 4596.2(4) Å3 | g = 120°. | g = 90.000(5)°. |
| Z | 4 | 4 | 18 | 2 |
| Density (calculated) | 1.592 Mg/m3 | 1.410 Mg/m3 | 1.085 Mg/m3 | 1.477 Mg/m3 |
| Absorption coefficient | 0.505 mm-1 | 0.449 mm-1 | 0.547 mm-1 | 0.791 mm-1 |
| F(000) | 2688 | 2000 | 6516 | 1700 |
| Crystal size | 0.30 x 0.15 x 0.09 mm3 | 0.28 x 0.24 x 0.06 mm3 | 0.09 x 0.05 x 0.03 mm3 | 0.05 x 0.09 x 0.105 mm3 |
| Theta range for data collection | 1.85 to 26.45°. | 1.55 to 26.50°. | 1.25 to 25.43°. | 1.488 to 27.752°. |
| Index ranges | -15<=h<=15, -55<=k<=55, -14<=l<=14 | -16<=h<=16, -21<=k<=21, -25<=l<=25 | -40<=h<=40, -40<=k<=40, -23<=l<=23 | -16<=h<=17, -12<=k<=12, -33<=l<=33 |
| Reflections collected | 163382 | 202195 | 71162 | 49234 |
| Independent reflections | 11297 [R(int) = 0.0807] | 9538 [R(int) = 0.0425] | 7953 [R(int) = 0.1708] | 7838 [R(int) = 0.1776] |
| Completeness to theta = 25.00° | 99.20% | 99.50% | 99.80% | 99.50% |
| Max. and min. transmission | 0.9560 and 0.8633 | 0.9735 and 0.8845 | 0.9838 and 0.9524 | |
| Refinement method | Full-matrix least-squares on F2 | Semi-empirical from equivalents | Semi-empirical from equivalents | Full-matrix least-squares on F2 |
| Data / restraints / parameters | 11297 / 548 / 826 | Full-matrix least-squares on F2 | Full-matrix least-squares on F2 | 7838 / 0 / 430 |
| Goodness-of-fit on F2 | 1.158 | 9485 / 0 / 569 | 7953 / 0 / 383 | 0.968 |
| Final R indices [I>2sigma(I)] | R1 = 0.0794, wR2 = 0.1666 | R1 = 0.0413, wR2 = 0.1043 | R1 = 0.0662, wR2 = 0.1379 | R1 = 0.0666, wR2 = 0.1420 |
| R indices (all data) | R1 = 0.0867, wR2 = 0.1698 | R1 = 0.0518, wR2 = 0.1135 | R1 = 0.1388, wR2 = 0.1581 | R1 = 0.1762, wR2 = 0.1904 |
| Largest diff. peak and hole | 1.760 and -1.566 e.Å-3 | 1.284 and -0.837 e.Å-3 | 0.470 and -0.463 e.Å-3 | 1.322 and -2.111 e.Å-3 |

## 3.6 NOTES TO THE CHAPTER

1. Adapted with permission from (M. R. Norris, S. E. Flowers, A. M. Mathews and B. M. Cossairt, *Organometallics*, 2016, **35**, 2778-2781.). Copyright (2016) American Chemical Society.
2. K. Öfele, *J. Organomet. Chem.*, 1968, **12**, P42-P43.
3. H. W. Wanzlick and H. J. Schönherr, *Angew. Chem., Int. Ed.*, 1968, **7**, 141-142.
4. M. N. Hopkinson, C. Richter, M. Schedler and F. Glorius, *Nature*, 2014, **510**, 485-496.
5. W. A. Herrmann, *Angew. Chem., Int. Ed.*, 2002, **41**, 1290-1309.
6. N. Marion, S. Díez-González and S. P. Nolan, *Angew. Chem., Int. Ed.*, 2007, **46**, 2988-3000.
7. F. E. Hahn and M. C. Jahnke, *Angew. Chem., Int. Ed.*, 2008, **47**, 3122-3172.
8. F. E. Hahn, in *Advances in Organometallic Chemistry and Catalysis*, John Wiley & Sons, Inc., 2013, DOI: 10.1002/9781118742952.ch9, pp. 111-132.
9. F. E. Hahn, *ChemCatChem*, 2013, **5**, 419-430.
10. M. C. Jahnke and F. E. Hahn, *Coord. Chem. Rev.*, 2015, **293**, 95-115.
11. J. M. C. and H. F. Ekkehardt, *Chem. Lett.*, 2015, **44**, 226-237.
12. S. Kuwata and T. Ikariya, *Chem. Commun.*, 2014, **50**, 14290-14300.
13. R. J. Sundberg, R. F. Bryan, I. F. Taylor and H. Taube, *J. Am. Chem. Soc.*, 1974, **96**, 381-392.
14. G. Sini, O. Eisenstein and R. H. Crabtree, *Inorg. Chem.*, 2002, **41**, 602-604.
15. A. S. El-Tabl, M. Mohamed Abd El-Waheed, M. A. Wahba and N. Abd El-Halim Abou El-Fadl, *Bioinorg. Chem. Appl.*, 2015, **2015**, 126023.
16. J. L. Gomez-Lopez, D. Chávez, M. Parra-Hake, A. T. Royappa, A. L. Rheingold, D. B. Grotjahn and V. Miranda-Soto, *Organometallics*, 2016, **35**, 3148-3153.
17. D. C. Marelius, E. H. Darrow, C. E. Moore, J. A. Golen, A. L. Rheingold and D. B. Grotjahn, *Chem. Eur. J.*, 2015, **21**, 10988-10992.
18. S. E. Flowers and B. M. Cossairt, *Organometallics*, 2014, **33**, 4341-4344.
19. G. A. Filonenko, M. J. B. Aguila, E. N. Schulpen, R. van Putten, J. Wiecko, C. Müller, L. Lefort, E. J. M. Hensen and E. A. Pidko, *J. Am. Chem. Soc.*, 2015, **137**, 7620-7623.
20. T. J. Korstanje, J. Ivar van der Vlugt, C. J. Elsevier and B. de Bruin, *Science*, 2015, **350**, 298-302.
21. J. Coetzee, D. L. Dodds, J. Klankermayer, S. Brosinski, W. Leitner, A. M. Z. Slawin and D. J. Cole-Hamilton, *Chem. Eur. J.*, 2013, **19**, 11039-11050.
22. A. A. N. Magro, G. R. Eastham and D. J. Cole-Hamilton, *Chem. Commun.*, 2007, 3154-3156.
23. N. Nakagawa, E. J. Derrah, M. Schelwies, F. Rominger, O. Trapp and T. Schaub, *Dalton Trans.*, 2016, **45**, 6856-6865.
24. Y. Li, I. Sorribes, T. Yan, K. Junge and M. Beller, *Angew. Chem., Int. Ed.*, 2013, **52**, 12156-12160.
25. I. Mellone, M. Peruzzini, L. Rosi, D. Mellmann, H. Junge, M. Beller and L. Gonsalvi, *Dalton Trans.*, 2013, **42**, 2495-2501.
26. C. Yin, Z. Xu, S.-Y. Yang, S. M. Ng, K. Y. Wong, Z. Lin and C. P. Lau, *Organometallics*, 2001, **20**, 1216-1222.
27. Y. Arikawa, T. Asayama, Y. Moriguchi, S. Agari and M. Onishi, *J. Am. Chem. Soc.*, 2007, **129**, 14160-14161.

28. C. W. Leung, W. Zheng, Z. Zhou, Z. Lin and C. P. Lau, *Organometallics*, 2008, **27**, 4957-4969.
29. N. A. Foley, M. Lail, J. P. Lee, T. B. Gunnoe, T. R. Cundari and J. L. Petersen, *J. Am. Chem. Soc.*, 2007, **129**, 6765-6781.
30. E. Becker, S. Pavlik and K. Kirchner, *Adv. Organomet. Chem.*, 2008, **56**, 155-197.
31. H. Horvath, G. Laurenczy and A. Katho, *J. Organomet. Chem.*, 2004, **689**, 1036-1045.
32. A. Demonceau, A. W. Stumpf, E. Saive and A. F. Noels, *Macromolecules*, 1997, **30**, 3127-3136.
33. I. Moldes, E. de la Encarnacion, J. Ros, A. Alvarez-Larena and J. F. Piniella, *J. Organomet. Chem.*, 1998, **566**, 165-174.
34. J. DePasquale, M. Kumar, M. Zeller and E. T. Papish, *Organometallics*, 2013, **32**, 966-979.
35. J. Ruiz and B. F. Perandones, *J. Am. Chem. Soc.*, 2007, **129**, 9298-9299.
36. J. Ruiz, D. Sol, J. F. Van der Maelen and M. Vivanco, *Organometallics*, 2017, **36**, 1035-1041.
37. M. C. Jahnke and F. E. Hahn, *Coord. Chem. Rev.*, 2015, **293-294**, 95-115.
38. N. Meier, F. E. Hahn, T. Pape, C. Siering and S. R. Waldvogel, *Eur. J. Inorg. Chem.*, 2007, **2007**, 1210-1214.
39. F. Bonati, A. Burini, B. R. Pietroni and B. Bovio, *J. Organomet. Chem.*, 1989, **375**, 147-160.
40. H. G. Raubenheimer, F. Scott, G. J. Kruger, J. G. Toerien, R. Otte, W. van Zyl, I. Taljaard, P. Olivier and L. Linford, *J. Chem. Soc., Dalton Trans.*, 1994, 2091-2097.
41. M. A. Bennett and A. K. Smith, *J. Chem. Soc., Dalton Trans.*, 1974, 233-241.
42. M. R. Norris, J. J. Concepcion, C. R. K. Glasson, Z. Fang, A. M. Lapides, D. L. Ashford, J. L. Templeton and T. J. Meyer, *Inorg. Chem.*, 2013, **52**, 12492-12501.
43. M. A. Bennett and A. K. Smith, *J. Chem. Soc., Dalton Trans.*, 1974, **0**, 233-241.

# Chapter 4. REACTIVITY OF RUTHENIUM COMPLEXES SUPPORTED BY A TRIPODAL, PROTIC BIS(N-HETEROCYCLIC CARBENE) PHOSPHINE LIGAND WITH CARBON DIOXIDE

*Significant portions of the following have been previous published.*[1]
*Contributions to this project were made by M. Cecilia Johnson and Michael R. Norris.*

## 4.1 INTRODUCTION

Increased global energy demand, along with concerns of $CO_2$ as a contributor to climate change, have spurred intense research into alternative energy sources that do not result in greenhouse gas emissions. Hydrogen gas is a clean fuel that does not produce $CO_2$ as a product of combustion; however, the main source of $H_2$ on an industrial scale is the re-forming of natural gas, which results in significant $CO_2$ generation.[2] Thus, if $H_2$ is to be used as an alternative fuel, its source must be water, and the need to pressurize and transport $H_2$ requires advances in storage. Alternatively, the $CO_2$ generated from burning fossil fuels could be captured and reduced back to a useful form.[2-4] A number of electrochemical and hydrogenation systems have been studied that reduce $CO_2$ to CO,[5-11] formate/formic acid,[4, 12, 13], and methanol.[14-16] The continued challenge is finding catalysts that operate under ambient conditions for these transformations. An interesting proposition that combines the use of $H_2$ as a clean-burning fuel with $CO_2$ reduction is the storage of $H_2$ in formic acid as a transportable liquid, followed by dehydrogenation to retrieve the $H_2$.[17, 18] This strategy still requires $H_2$ that is not produced by the re-forming of natural gas and also only remains carbon neutral if the $CO_2$ formed in the dehydrogenation reaction is recaptured and recycled.[19, 20]

In order to understand and exploit $CO_2$ chemistry, complexes that interact with $CO_2$ in unique or unconventional ways and that are capable of multifaceted $CO_2$ transformations are necessary. In biology, for example, [NiFe] CO dehydrogenase enzymes utilize a push–pull mechanism to activate $CO_2$, where Ni acts as a Lewis base and $Fe^{2+}$ serves as a Lewis acid.[21] Several studies have utilized multi-metallic complexes or metal–ligand cooperation to achieve new and unique reactivity with $CO_2$, including studies of bifunctional Co(salen-R)M

complexes,[22] Zr/Co heterobimetallic complexes where $CO_2$ oxidatively adds across the two metal centers,[23] a $Cu^I$dimer/tetramer that reduces $CO_2$ to oxalate,[24] and Ru(PNP),[25] and Ru(PNN)[26] complexes that involve cooperative activation of $CO_2$ between a redox-active ligand and metal center.

## 4.2 Results and Discussion

### 4.2.1 *Stoichiometric reactivity studies with complex **8***

Stoichiometric studies of **8-OH$_2$** and **8-Cl** were conducted with gaseous $CO_2$, sodium bicarbonate, and sodium formate (Figure 4.1).

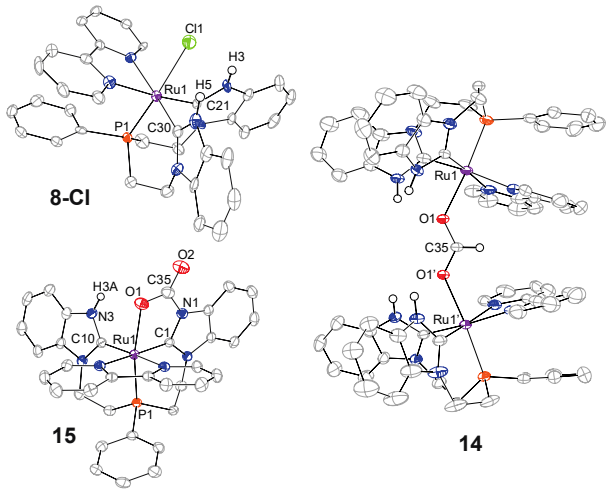


Figure 4.1. Chemical structures of **8-Cl**, synthesis described in Chapter 3, and $CO_2$ reaction products **14** and **15.** Molecular structures of **8-Cl**, **14**, and **15** with thermal ellipsoids shown at 50% probability. **8-Cl** displays H-bonding interactions between N–H groups and bound Cl with one $Cl^-$ counterion omitted for clarity. Complex **14** is a formate-bridged bimetallic Ru complex with three $PF_6^-$counterions removed for clarity. The same structure was determined for addition of $CO_2$, $HCO_3^-$, and $HCO_2^-$ to **8**. The structure of **15** shows a carbamate with the O atom bound to the Ru center with one $PF_6^-$ counterion removed for clarity. Selected interatomic distances (Å) and angles (deg): for **8-Cl**, Ru1–Cl1 2.534(2), Ru1–C21 2.011(6), Ru1–C30 2.024(6), H3–Cl1 2.475, H5–Cl1 2.509; for **14**, Ru1–O1 2.181, C35–O1 1.246, O1–C1–O1′ 125.3; for **15**, Ru1–O1 2.219, O1–C35 1.301, C35–O2 1.2229, C35–N1 1.457, H3A–O1 2.532, O1–C35–O2 127.29.

We studied the reaction of **8-OH$_2$** and $CO_2$ with the goal of exploring possible $CO_2$ reduction chemistry. Addition of $CO_2$ to solutions of **8-OH$_2$** in $CH_2Cl_2$ yielded orange crystals after standing at room temperature for several days. These crystals were analyzed by X-ray diffraction and were found to be a formate-bridged bimetallic complex (**14**, Figure 4.1, Scheme 4.1). The O–C–O bond angle in **14** is 125.3° with C–O bond lengths of 1.246 Å, consistent with reported formate-bridged metal complexes.[27] The IR spectrum of **14** displays a strong stretch at 1548 cm$^{-1}$ (Figure 4.2 ) and a peak in the $^{13}$C NMR at 170 ppm, both suggestive of a metal formate species.[27]

**Scheme 4.1. Orange crystals corresponding to 14 are produced when 8-OH$_2$ is combined in DCM with sodium bicarbonate or carbon dioxide.**

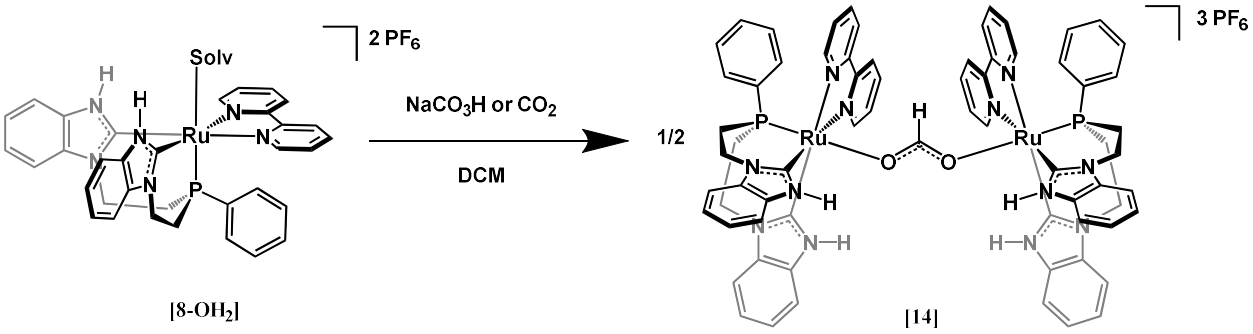


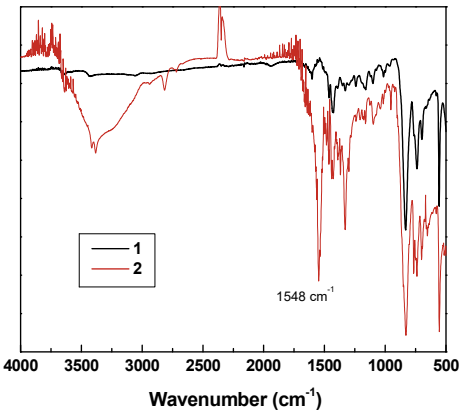


Figure 4.2 ATR-IR of powders of **8** and **14** showing a strong stretch at 1548 cm$^{-1}$ for the bridging formate in **14**.

It should be noted that while the Ru–formate complex (**14**) crystallizes in the bimetallic form in $CH_2Cl_2$, a solvent in which it is sparingly soluble, we believe that it readily converts to the monometallic form (**14-monomer**) and 1 equiv of Ru–solvent (**8-Solv**) complex in a coordinating solvent (Scheme 4.2, Figure 4.3, and Figure 4.4).

**Scheme 4.2. dimer 14 reaction in DMSO to give 14-monomer**

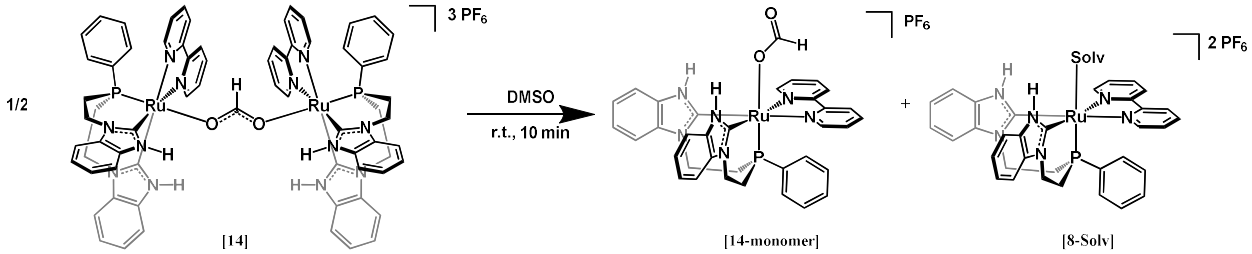


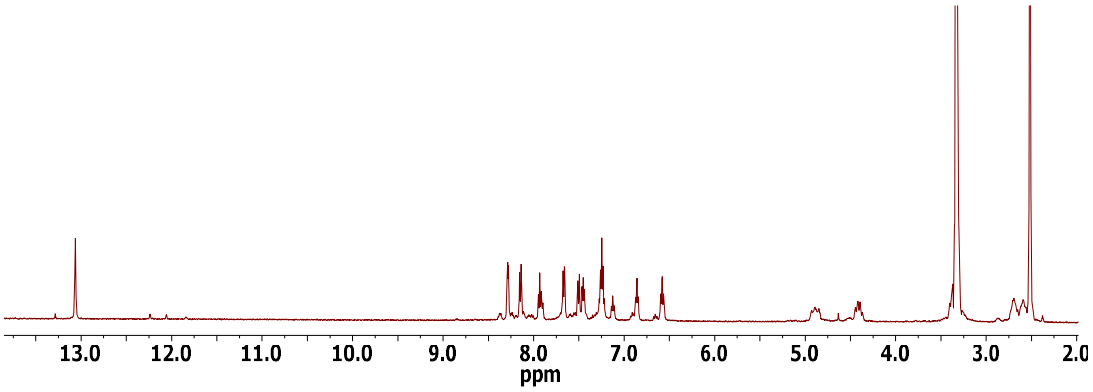


Figure 4.3. $^{1}H$ NMR spectrum (500 MHz, DMSO-$d_6$) of precipitate from reaction of $^{13}C$-formate and **8** in DCM.

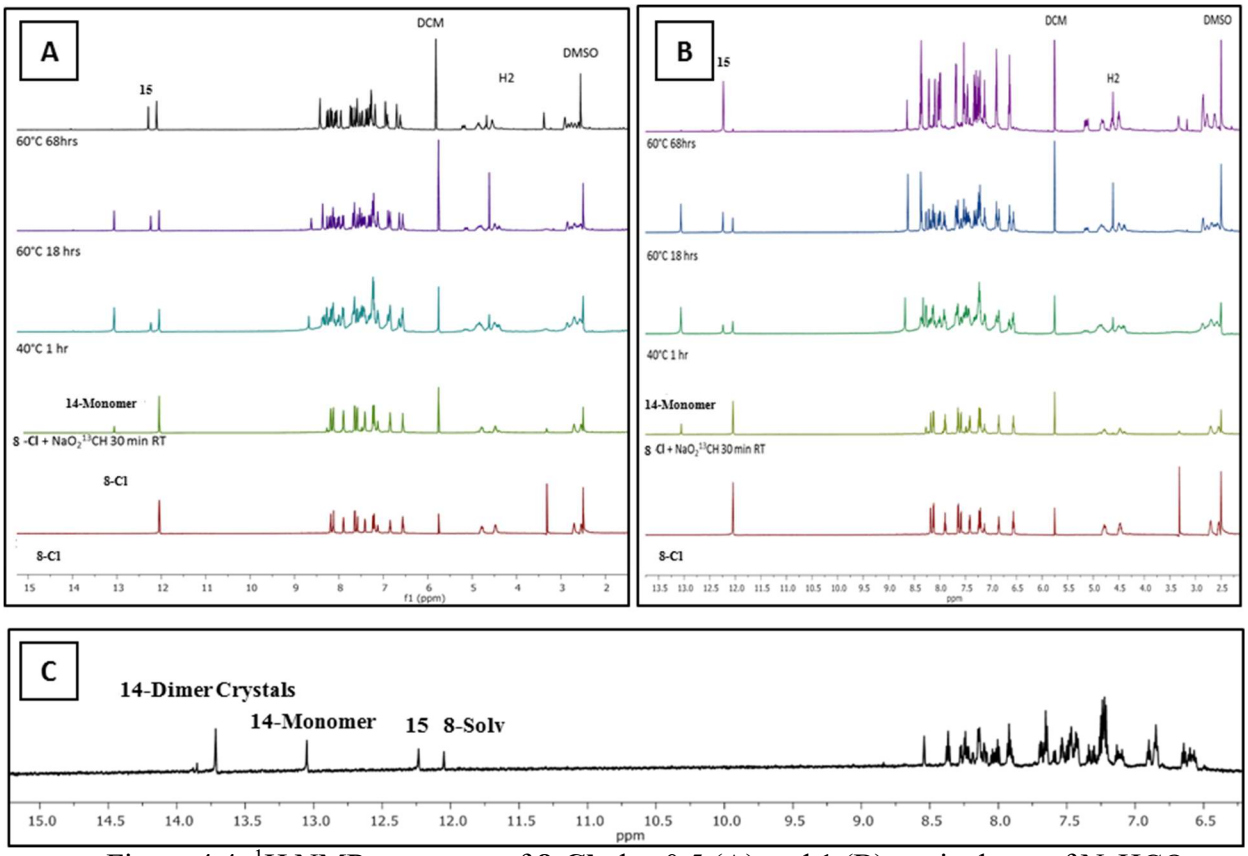


Figure 4.4. $^{1}$H NMR spectrum of **8-Cl** plus 0.5 (A) and 1 (B) equivalents of $NaHCO_2$ showing formation of 0.5 equivalent of **15** and 0.5 equivalents of **15**, respectively, supporting the identity of the species in Figure 4.3 as the monometallic Ru-formate. (C) $^{1}$H NMR of the N-H region of crystals of **14** dissolved in DMSO-$d_6$ after 10 minutes showing the spontaneous decomposition of **14** into **8-Solv** and the monometallic formate **(14-Monomer)** with partial conversion to **15**.

We hypothesized that the mechanism for reduction of $CO_2$ to formate could proceed via initial formation of a Ru–bicarbonate intermediate, as $CO_2$ can insert into M–OH and M–$OH_2$ bonds to equilibrate with bicarbonate.[28] This provides a plausible route for formation of a Ru–$HCO_3^-$ species which could undergo deoxygenation to form the reduced Ru–formate. Direct addition of $NaHCO_3$ to solutions of **8-OH$_2$** in $CH_2Cl_2$ also leads to complex **14-monomer** in low yield, consistent with the intermediacy of a Ru–$HCO_3^-$ species (Scheme 4.3). Although other examples exist of reduction of $HCO_3^-$ to formate, they require added energy by initial formation

of a M–H bond,[29] the use of high pressures of $H_2$, or the use of an applied electrochemical potential.[30]

**Scheme 4.3 Proposed Overall Transformation of Reduction of $H_2O$ to $H_2$.**

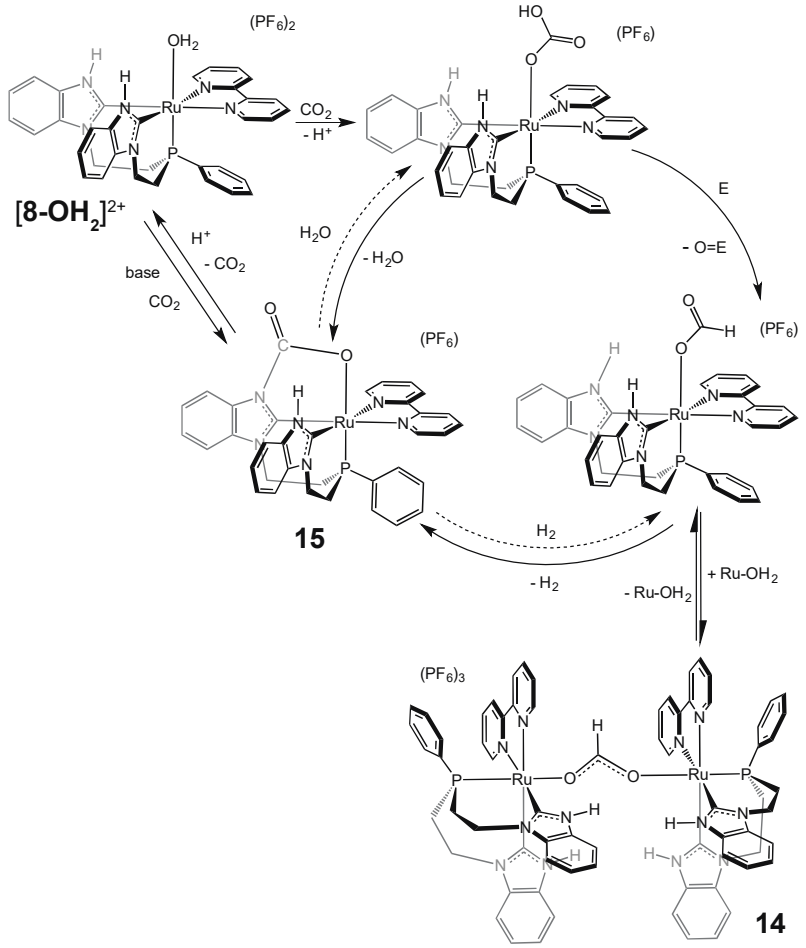


Importantly, the formation of **14** from $CO_2$ and $HCO_3^-$ represents a formal reduction of the added carbon species. A plausible explanation is that $HCO_3^-$ bound to the Ru center is deoxygenated by another species in solution, leading to the reduction of $HCO_3^-$ to formate (Scheme 4.1). Deoxygenation of a bound carbonate has at least one precedent in the literature where an O atom was transferred to a phosphine with concomitant production of $CO_2$ mediated by a $Rh^{III}$–$Rh^{I}$ cycle.[31] Addition of excess triphenylphosphine or trioctylphosphine, in the presence or absence of a nitrile, to **8-OH2** and $CO_2$ or $HCO_3^-$ also did not lead to the buildup of phosphine oxides, as evidenced by $^{31}P$ NMR spectroscopy. In reactions of complex **8-OH2** with $CO_2$ and

$HCO_3^-$, an oxidized product has not been identified; the fate of the O atom is the subject of continuing investigation.

To probe the deoxygenation reaction pathway further, 1,1,3,3-tetramethyldisiloxane (TMDS) was added to a solution of **8-OH$_2$** and $^{13}$C-labeled $NaHCO_3$ in DMSO-$d^6$. Since an oxygen atom must be removed from $HCO_3^-$ in order to make formate, it was hypothesized that the added silane reagent would offer an attractive acceptor for the O atom. After reacting at 50 °C overnight, the only observable species by $^{13}$C NMR is a new $^{13}$C-containing species, **15** ($^{13}C\{^1H\}$ peak at 155 ppm, Figure 4.5), in near 100% yield as determined by $^1$H NMR and $^{31}P\{^1H\}$ NMR spectroscopy (Figures 4.6 and 4.7). Running the same reaction with 10 equiv of $NaH^{13}CO_3$ in the absence of TMDS, however, also leads to clean conversion to **15** (Figure 4.8), albeit in lower (64%) yield, this lower yield, however could, perhaps be due to insufficient delay times or evaporation of dichloromethane. These experiments taken together suggest that the new species **15** may form independently of the formate-bridged bimetallic complex **14**.

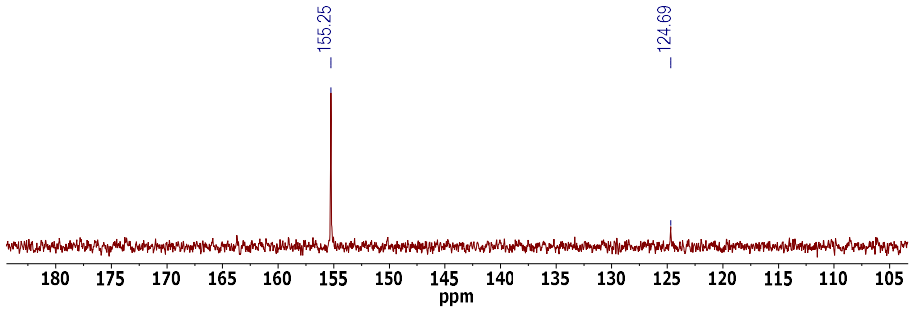


Figure 4.5. $^{13}C\{^1H\}$ NMR spectrum, (126 MHz, DMSO-$d_6$) of reaction of 1, *10* equiv. $NaH^{13}CO_3$, and 10 equiv. TMDS at 50 °C for 16h showing only **15**.

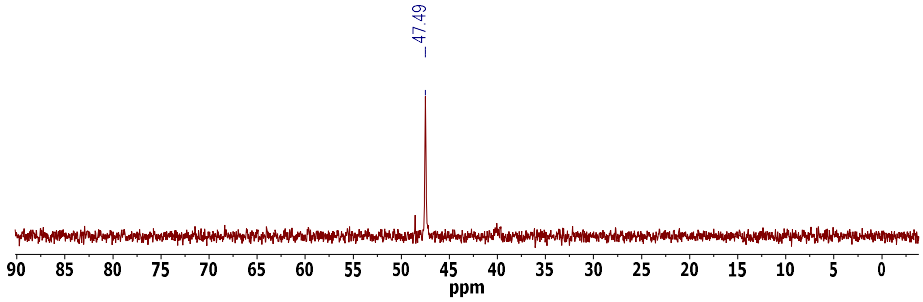


Figure 4.6. $^{31}P\{^1H\}$ NMR spectrum, (202 MHz, DMSO-$d_6$) of reaction of 1, *10* equiv. $NaH^{13}CO_3$, and 10 equiv. TMDS at 50 °C for 16h showing only **15**.

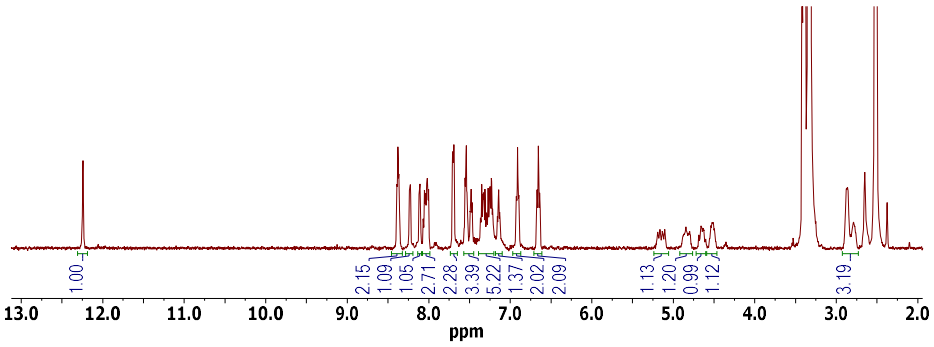


Figure 4.7. $^{1}$H NMR spectrum, (500 MHz, DMSO-$d_6$) of reaction of **8-OH$_2$**, *10* equiv. Na$H^{13}CO_3$, and 10 equiv. TMDS at 50 °C for 16h showing only **15**. Spectrum obtained by precipitation of product from DMSO by addition of water and re-dissolution of precipitate.

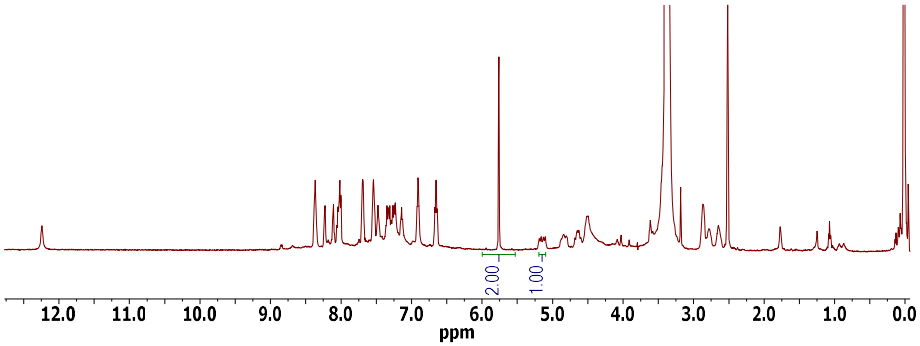


Figure 4.8. $^{1}$H NMR spectrum, (500 MHz, DMSO-$d_6$) of reaction of **8-OH$_2$**, 10 equiv. Na$H^{13}CO_3$, and 10 equiv. TMDS at 50 °C for 16h showing only **15**. Reaction mixture was spiked with 1 equiv. $CH_2Cl_2$ as an internal standard immediately prior to NMR.

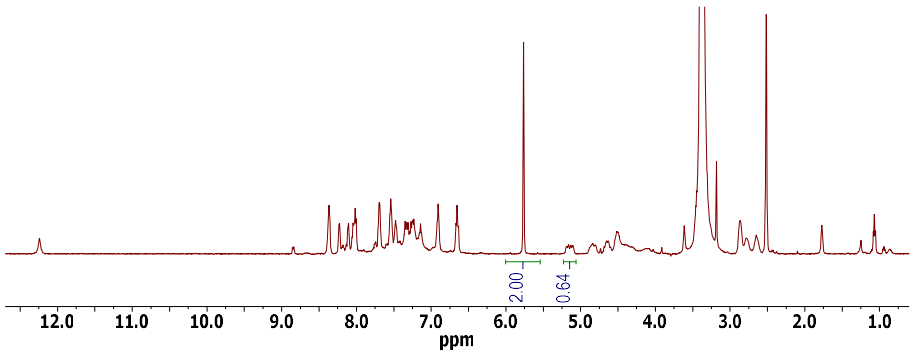


Figure 4.9. $^{1}$H NMR spectrum, (500 MHz, DMSO-$d_6$) of reaction of **8-OH$_2$** and 10 equiv. Na$H^{13}CO_3$ at 50 °C for 16h showing only **15**. Reaction mixture was spiked with 1 equiv. $CH_2Cl_2$ as an internal standard immediately prior to NMR.

To determine if **14** was relevant to the formation of **15**, the conversion of **8-Cl** in the presence of 1 equiv of $NaH^{13}CO_2$ in DMSO-$d_6$ was monitored by $^{31}P$, $^{13}C$, and $^{1}H$ NMR spectroscopy. Over the course of days at 68 °C, **8-Cl** cleanly converts to the formate-monomer **14-monomer** species, which goes on to give **15** with concomitant formation of $H_2$ (4.61 ppm in the $^{1}H$ NMR, Figure 4.10 and Scheme 4.4). The new species **15** shows a shift in the $^{31}P$ NMR from 52 ppm in **14-monomer** to 47 ppm for **15** and a shift in the $^{13}C$ NMR from 170 ppm for in **14-monomer** to 155 ppm for **15** (Figure 14.11).

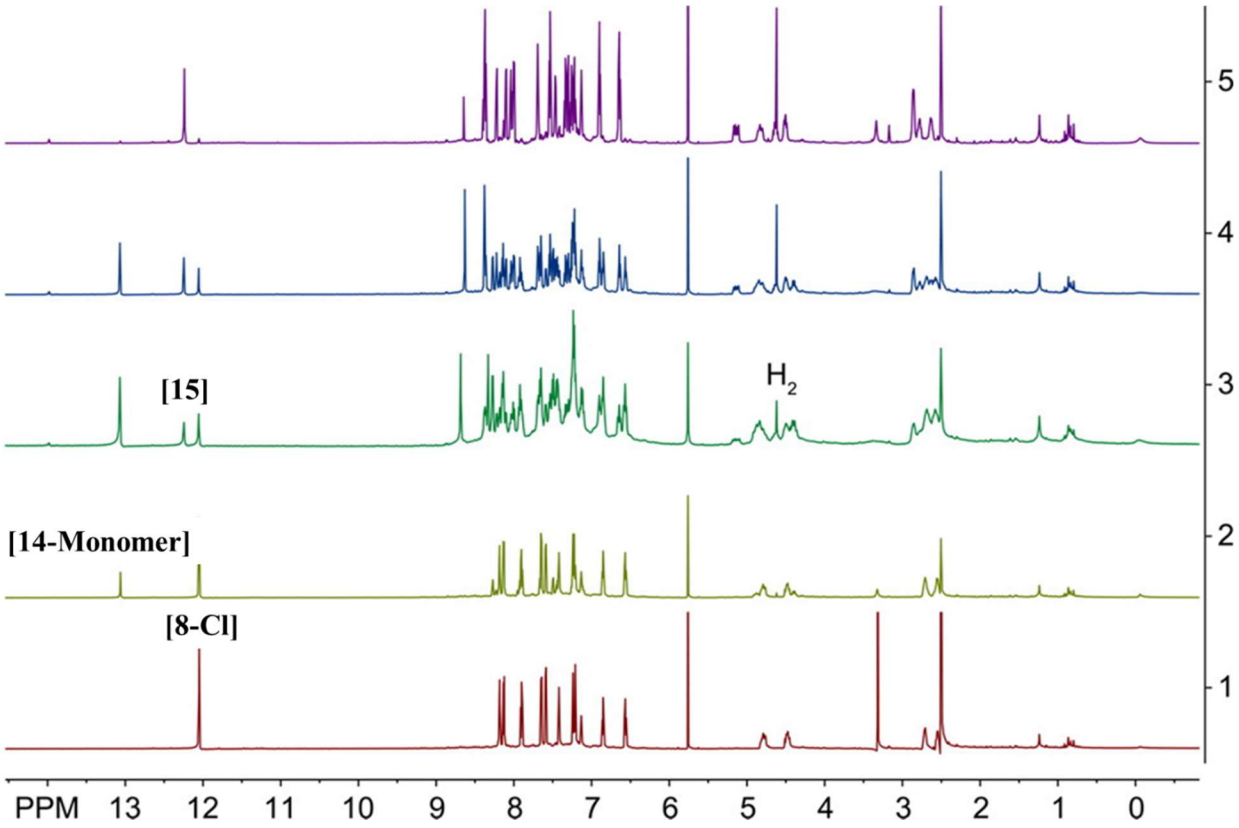


Figure 4.10. $^{1}H$ NMR (500 MHz, DMSO-$d_6$) spectra over time of the reaction of **8-Cl** with 1 equivalent of $NaH^{13}CO_2$ in DMSO at 60 °C, showing conversion to **14-monomer** followed by formation of **15** along with release of $H_2$, evidenced by the singlet at 4.6 ppm.

**Scheme 4.4 Conversion of 8-Cl to 15 in DMSO.**

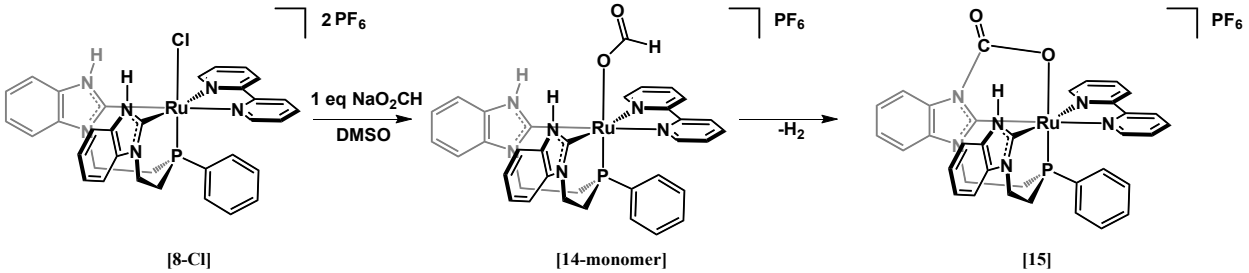


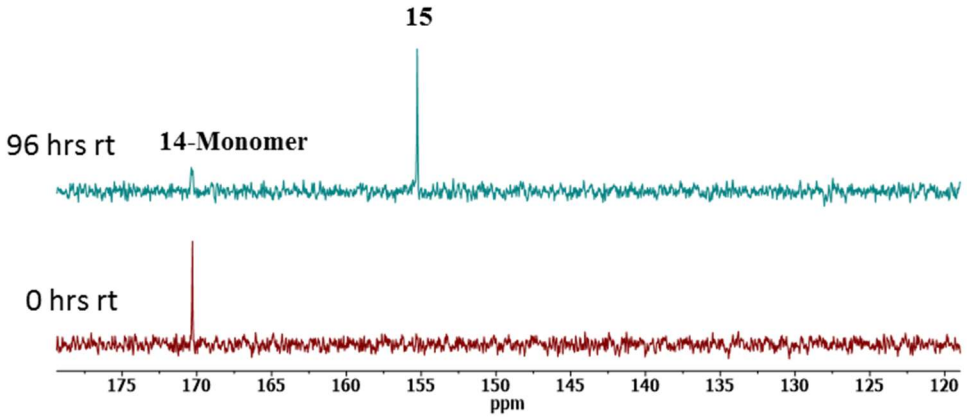


Figure 4.11 $^{13}C\{^{1}H\}$ NMR spectra (126 MHz, DMSO-$d_6$) of dehydrogenation reaction of **14-Monomer** in DMSO at room temperature over the course of 4 days showing conversion from **14-Monomer** to **15**.

The IR spectrum of **15** is also distinct from that of **14-Monomer** with two C–O stretches at 1634 and 1602 $cm^{-1}$, respectively. These data suggest that the formate C atom remains bound to the Ru complex in some fashion and is not released as $CO_2$ gas ($^{13}C$ NMR 124 ppm). Reaction of **8-OH₂** with $NaH^{13}CO_2$ in acetone also leads to **3**, with a $^{13}C$ signal at 155 ppm and release of $H_2$, as confirmed by GC analysis (Figure 4.12). Complex **15** can also be formed via deprotonation of a N–H moiety of **8-OH₂**, followed by reaction with $^{13}CO_2$, as confirmed by $^{1}H$ and $^{13}C$ NMR ($^{13}C$ 155 ppm, Figures 4.13 and 4.14).

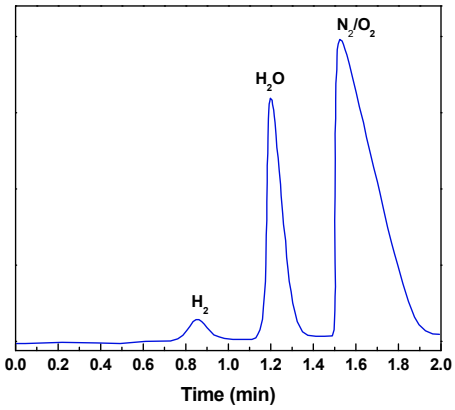


Figure 4.12. GC trace of 1 mL of headspace of reaction of **8-OH$_2$** and $NaHCO_2$ in acetone at room temperature for 1 h.

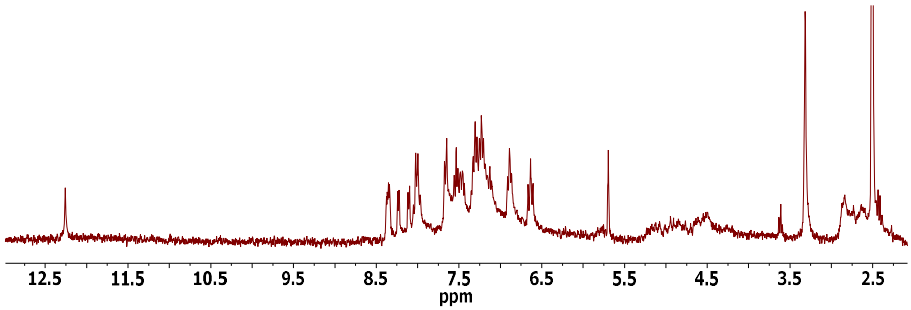


Figure 4.13. $^{1}H$ NMR spectrum (500 MHz, DMSO-$d_6$) of **15** formed by deprotonation of **8-OH$_2$** in DCM followed by reaction with $^{13}CO_2$.

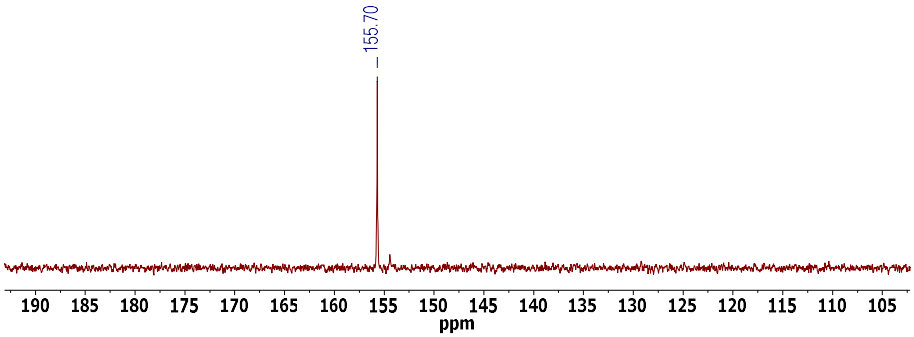


Figure 4.14. $^{13}C\{^{1}H\}$ NMR spectrum (126 MHz, DMSO-$d_6$) of **15** formed by deprotonation of **8-OH$_2$** in DCM followed by reaction with $^{13}CO_2$.

We hypothesized **15** to be a carbamate that formed through reaction of the C atom of $CO_2$ with the deprotonated N atom of the benzimidazole ligand backbone. This would be consistent with both the deprotonation followed by reaction with $CO_2$ and the dehydrogenation of formate where a proton from an N–H and a hydride from formate could form $H_2$ with simultaneous formation of the N–C bond to make a carbamate (Scheme 4.3). Additionally, the carbamate may form directly from reaction with bicarbonate via acid/base chemistry and formation of a N–C bond (Scheme 4.5). This pathway is consistent with observation of the facile formation of **15** when **8-OH₂** or **8-Cl** was heated in DMSO in the presence of $NaH^{13}CO_3$.

**Scheme 4.5. Alternative Mechanism of Formation of 15 from 8-OH₂.**

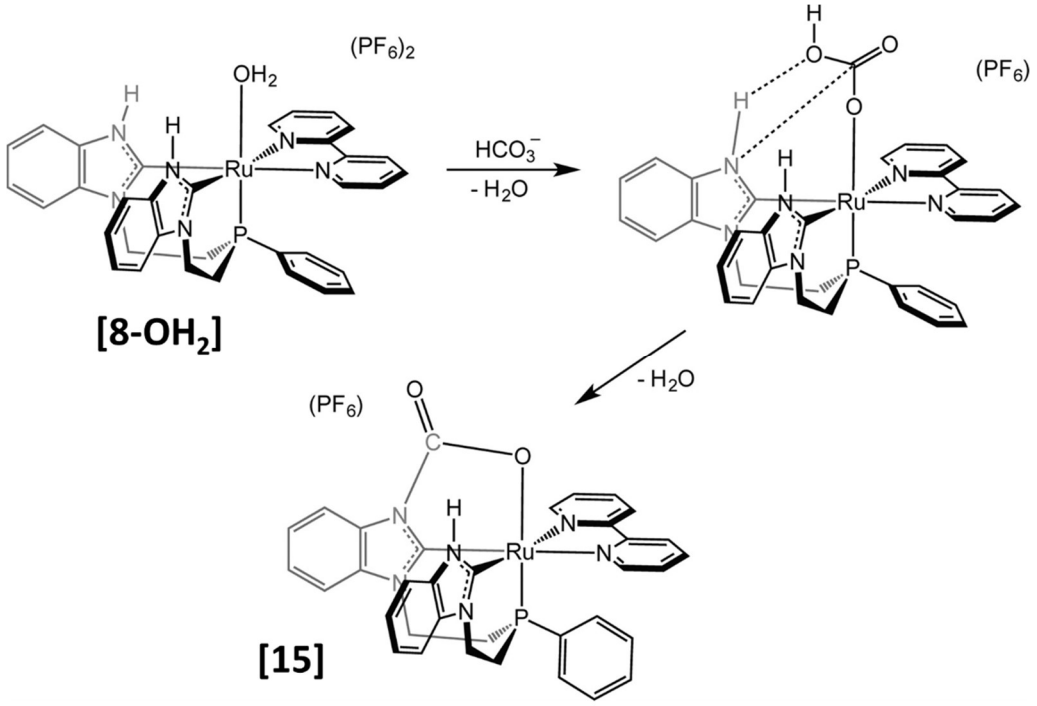


The $^{13}C$ NMR chemical shift of **15** and IR stretches are also consistent with those of other reported carbamates with an O atom bound to an adjacent metal center.[32, 33] Crystals suitable for X-ray diffraction were grown from slow evaporation of a solution of **15** in $CH_2Cl_2$ (Figure 4.1). The structure displays a carbamate moiety where the O atom is bound to the Ru center, which also removes a plane of symmetry in the molecule, making the benzimidazole arms of the $PhP(Etbim)_2$ ligand chemically distinct. This is reflected in the $^1H$ and $^{13}C$ NMR spectra, where the N–H (12.2 ppm) integrates for one proton, the diastereotopic – $CH_2$– protons of the

PhP(Etbim)$_2$ split into distinct resonances (Figure 4.15), and the $^{13}$C resonances for the C1 carbon atoms of the carbene ligands show up as distinct with chemical shifts of 202.9 ppm (s) and 193.6 (d, $^2J_{CC}$ = 15 Hz; Figure 4.16).

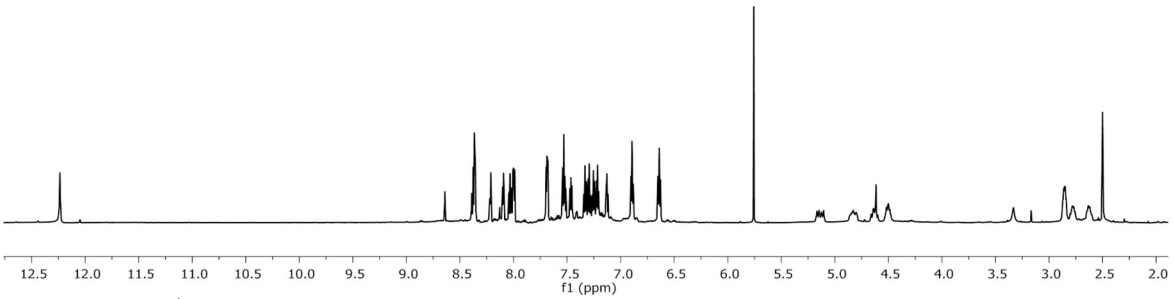


Figure 4.15. $^1$H NMR (500 MHz, DMSO-$d_6$) spectrum of **15** ($H_2$ also present at 4.6 ppm).

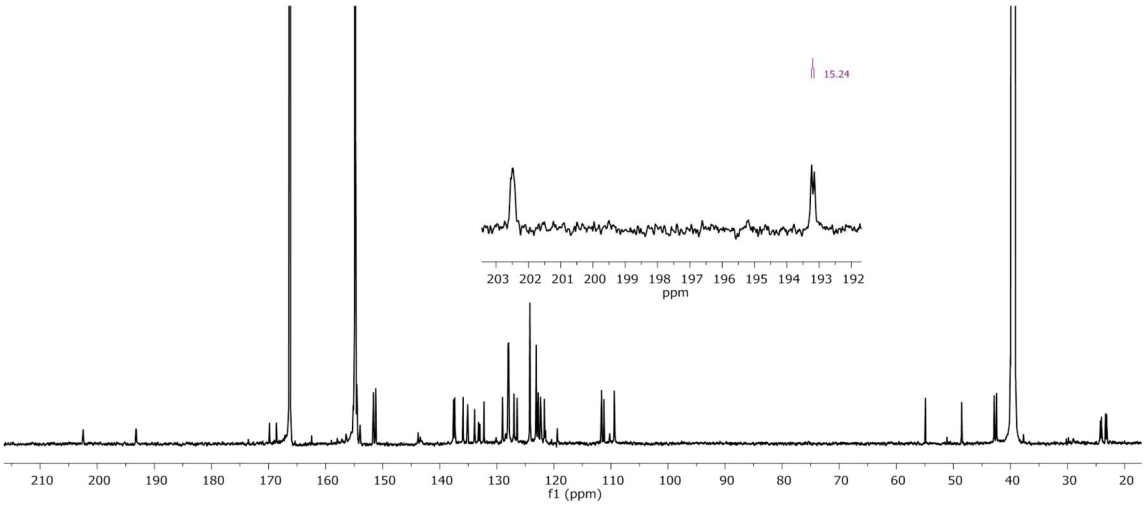


Figure 4.16. $^{13}$C NMR (176 MHz, DMSO-$d_6$) spectrum of **15** with inset showing the two distinct carbene carbon atoms with distinct $^{13}$C coupling to the one nearest the carbamate moiety.

### 4.2.2 *High Pressure reactions with **CCC***

Catalytic $CO_2$ hydrogenation using ruthenium complexes supported by tridentate ligands, as developed by Sanford[34, 35] and Leitner,[36] provided motivation for studying complex **9** as a catalyst for this transformation. Preliminary catalytic studies were performed with complex **9** (53 μmol) in THF under 20 bar $CO_2$ and 60 bar $H_2$, yielding formate in the presence of excess $K_3PO_4$, with an initial turn over number (TON) of 110 with un-optimized reaction conditions (Scheme 4.6).

Potassium formate precipitated out of solution, and the precipitate and solution were analyzed separately for formate formation using quantitative $^{1}H$ and $^{13}C$ NMR spectroscopy (Figure 4.17 and 4.18). Additionally, the pressure of the reaction vessel steadily decreased over the four-day reaction time, suggesting slow but consistent gas consumption (Figure 4.19). We hypothesize that further optimization of this class of complexes will result in robust catalytic activity. Optimization of the catalytic conditions and mechanistic investigations are currently underway in our lab.
with DMSO-$d^6$ and with mesitylene added as an internal standard taken.

**Scheme 4.6. Hydrogenation of $CO_2$ by $[(PNHC)_2P^{Ph}Ru(NCCH_3)_3][BF_4]_2$ (9) under basic conditions.**

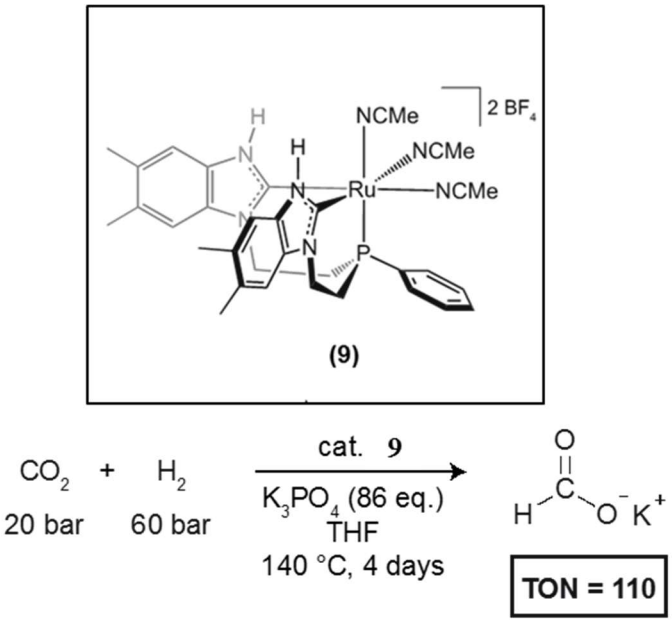

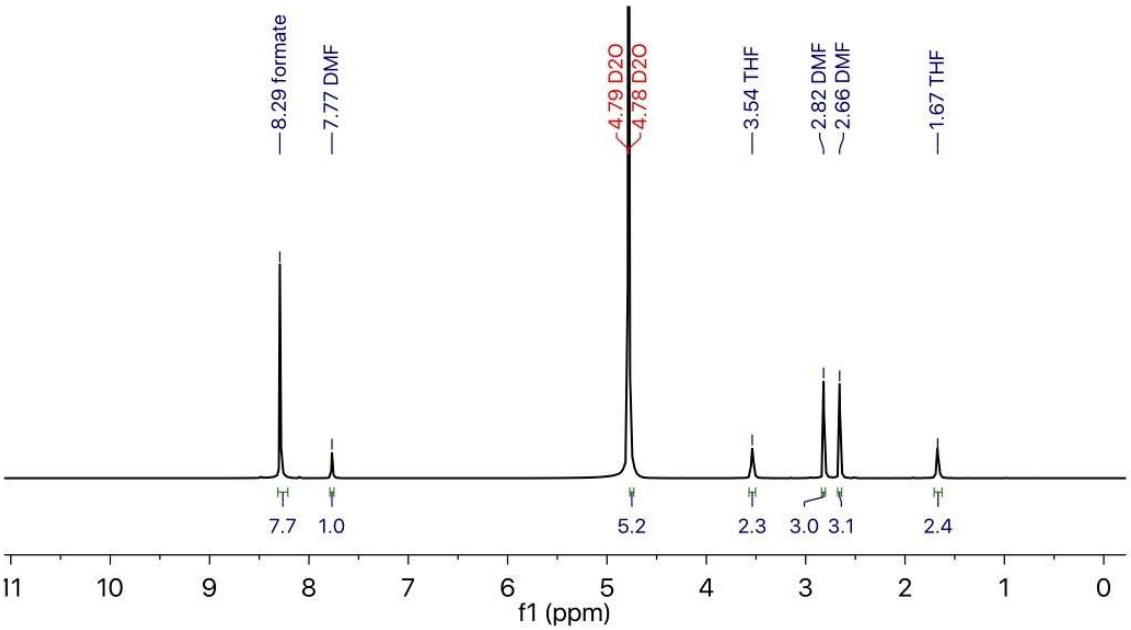


Figure 4.17. $^{1}$H NMR analysis of formate production under catalytic $CO_2$ hydrogenation conditions, using **9** as a catalyst. $^{1}$H NMR (298 K, 499.7 MHz) of precipitate dissolved in $D_2O$ and with dimethylformamide (DMF) added as an internal standard.

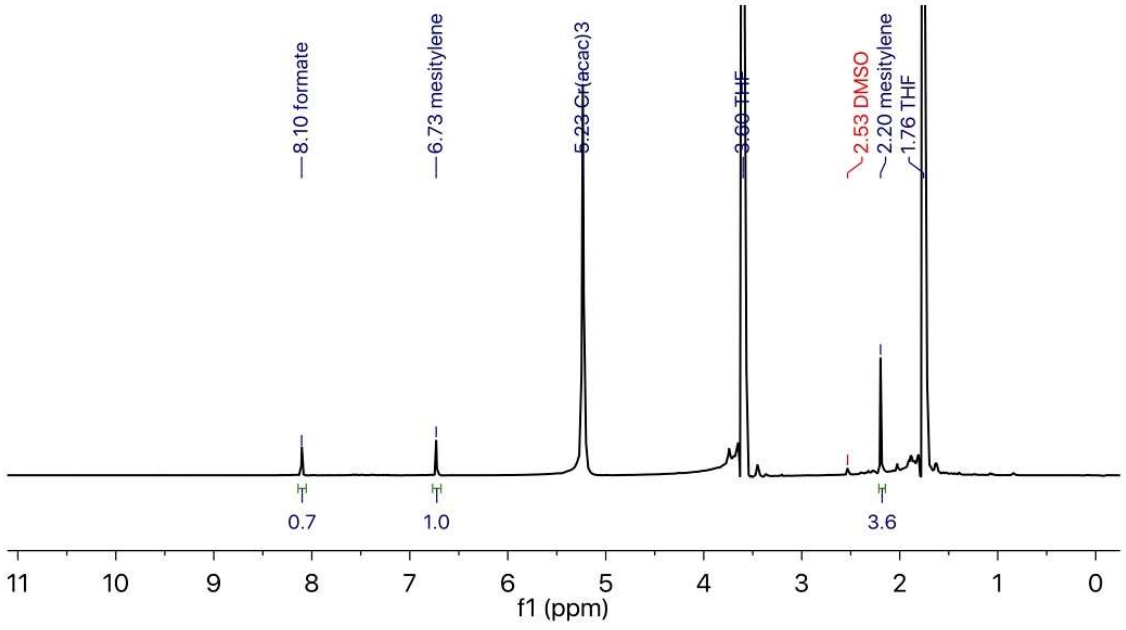


Figure 4.18**.** $^{1}$H NMR analysis of formate production under catalytic $CO_2$ hydrogenation conditions, using **9** as a catalyst. $^{1}$H NMR (298 K, 499.7 MHz) of crude solution, diluted with DMSO-$d^6$ and with mesitylene added as an internal standard taken.

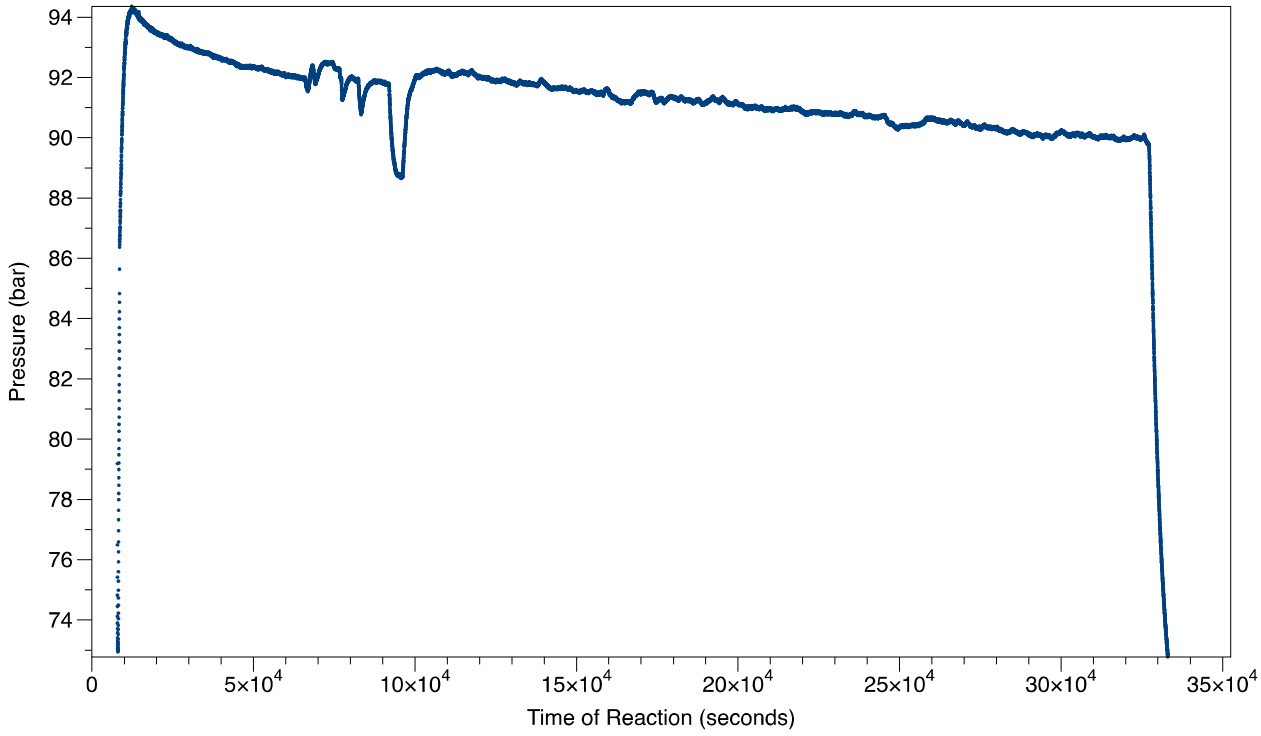


Figure 4.19**.** Pressure of Parr system vessel over the course of the reaction with catalyst **9**, shown in seconds. Unusual pressure spikes and dips between $6x10^4$ and $11x10^4$ seconds were consistent across multiple reactors on the Parr system manifold.

## 4.3 CONCLUSIONS

In our stoichiometric studies with **8-OH$_2$** and **8-Cl**, we have synthesized and characterized a new Ru complex that interacts with $CO_2$ via a unique pathway where $HCO_3^-$ is initially formed and then deoxygenated to give the $2e^-/2H^+$reduced formate. Dehydrogenation of formate, generating $H_2$ gas, then occurs spontaneously without loss of $CO_2$ from the complex. Further, $HCO_3^-$ can directly react with **8-OH$_2$** through a dehydration reaction to give an "activated" $CO_2$ in the form of a carbamate moiety. These results are significant, as they represent a spontaneous reduction of $CO_2$ without high-pressure $H_2$, electrochemical potential, or strong reducing agents. We are continuing to study the initial reduction reaction to better understand this mechanism and its potential to operate catalytically for reduced carbon products. Scheme 4.5 may also suggest a pathway to store $H_2$ if formal addition of $H_2O$ to **15** can generate a Ru–bicarbonate complex. This

overall scheme simplifies to a water-splitting reaction that is catalytic in **8-OH$_2$** and $CO_2$ ($H_2O$ + E → O = E + $H_2$) and provides a unique method of $H_2$ production from water. Initial results indicate that addition of strong acids remove the $CO_2$ from **15**, although studies remain ongoing in this area.

In the preliminary study of solvento complex **9** as a $CO_2$ hydrogenation catalyst, we observed a TON of 110 to formate and a small peak corresponding to trace amounts of synthesized methanol. We anticipate that further optimization of the reaction conditions will lead to robust catalytic activity from complex **9** and its derivatives. Future work in our lab will involve optimization of catalytic activity of **9** by altering the temperature, partial pressures, solvent, equivalents of external base, and possible pre-deprotonation of **9** before catalytic studies. Mechanistic and stoichiometric reactivity studies of **9** will also be performed. Further catalytic studies of $CO_2$ hydrogenation will be studied with complexes **8-OH$_2$**, **8-Cl,** and **15**.

## 4.4 EXPERIMENTAL

### General Information

Unless otherwise noted, all manipulations were carried out under a $N_2$ atmosphere using standard Schlenk technique. All solvents were purchased from Fisher Scientific. Benzimidazole (98%), sodium hydride (60% dispersion in mineral oil), phenylphosphine (10% wt. in hexanes), n-butyllithium solution (1.6 M in hexanes), 1,4-cyclohexadiene (97%), 2e,2'-bipyridyl, trimethylamine (≥99%), tetrabutylammonium hexafluorophosphate, and sodium formate-13C (99 atom %) were purchased from Sigma-Aldrich. 1,2-dichloroethane (certified ACS) was purchased from Fisher Scientific. Trifluoromethanesulfonic acid (98+%) and 1,1,3,3- tetramethyldisiloxane (97%) were purchased from Alfa Aesar. Ruthenium (III) chloride hydrate was purchased from Pressure Chemical. Sodium bicarbonate ($^{13}C$, 99%) was purchased from Cambridge Isotope Labs. $[Ru(Bz)Cl_2]_2$[37] and $[Ru(Bz)(bpy)(OTf)](OTf)$[38] were synthesized according to previously published literature procedures. $^1H$, $^{31}P$, and $^{13}C$ NMR were taken on either a Bruker AV500, Bruker AV700, Bruker DRX500, or Bruker AV300 spectrometer. Anhydrous DMSO-d6 was purchased from Sigma-Aldrich, all other NMR solvents were purchased from Cambridge Isotope Labs and were used as received. IR data were taken using a Bruker Vertex 70 FTIR with an ATR attachment. Headspace analysis for $H_2$ was performed on a SRI 8610C Gas Chromatograph using a 6' MS-13X column at 80 °C and Ar as the carrier gas. Microanalysis samples were weighed with

a PerkinElmer Model AD-6 Autobalance and their compositions were determined with a PerkinElmer 2400 Series II Analyzer. Time-resolved luminescence decay experiments were measured on a Fluorotime 100 lifetime spectrometer in a time-correlated single-photon-counting arrangement. A 375 nm LED with a pulse repetition rate of 500 KHz was used as the light source with a 490 nm long-pass filter. The instrument response function (FWHM~1.4 ns) was collected using a scatterer (non-dairy creamer). Dichloromethane, acetonitrile and diethyl ether were dried through columns of activated alumina and molecular sieves under $N_2$ gas. NMP, DMSO, DMSO-$d_6$, dichloro(p-cymene)ruthenium(II) dimer, and $AgBF_4$ were purchased anhydrous from Sigma Aldrich and were used without further purification. $CD_2Cl_2$ and $CD_3CN$ were purchased from Cambridge Isotope Labs, dried over calcium hydride, distilled before use, and stored over molecular sieves under $N_2$. Dichloro(benzene)ruthenium(II) dimer was prepared according to a published literature procedure.[39] **L** was prepared using a modified procedure from published in the literature.[1] All NMR spectra were taken on either a Bruker AV500, AV700, DRX500, or AV300 spectrometer at 298 K.

*Formate-bridge Ru Dimer crystals (**14**).* Open to air, a 20 ml glass vial equipt with a stir bar was charged with **8-OH$_2$** (24.8 mg, 0.0257 mmol, 1 eq), sodium bicarbonate (2.8 mg, 0.0333 mg, 1.3 eq), and DCM (2 ml). The reaction mixture was allowed to stir for 12 hours before the solution was filtered through a syringe filter into an nmr tube. Crystals formed after several days on the inside edge of the NMR tube.

Complex **14** was also made from $CO_2$ by addition of a small piece of dry ice to an NMR tube containing **8-OH$_2$** in DCM. Slow evaporation of the solution caused crystals of **14** to grow.

*Formate-Bridged Ru Monomer (**14-Monomer**).*

A mixture of **8-OH$_2$** (21 mg, 0.022 mmol, 1 eq) and $^{13}$C-formate (1.5 mg, 0.022 mmol, 1 eq) were added to $CD_2Cl_2$ (1.5 mL) and sonicated for 30 min. After standing for 16 h. at room temperature, a yellow-orange solid precipitated and an IR was obtained of the solid. The mother liquor was decanted and the solid was dissolved in DMSO-$d_6$ for $^1$H, $^{31}$P{H}, and $^{13}$C NMR analysis. $^1$H NMR (500 MHz, DMSO-$d_6$) δ 13.06 (s, 2H), 8.28 (d, $J$ = 4.6 Hz, 2H), 8.15 (d, $J$ = 8.3 Hz, 2H), 8.10 (dd, $J_{HC}$=193.8, $J_{HP}$= 6.2, 1H), 7.93 (t, $J$ = 7.9 Hz, 2H), 7.67 (d, $J$ = 7.6 Hz, 2H), 7.50 (dd, $J$ = 7.2, 1.7 Hz, 2H), 7.45 (t, $J$ = 6.6 Hz, 2H), 7.25 (p, $J$ = 7.0 Hz, 4H), 7.13 (t, $J$ = 7.7 Hz, 1H), 6.86

(t, $J$ = 7.3 Hz, 2H), 6.58 (t, $J$ = 8.5 Hz, 2H), 4.96 – 4.80 (m, 2H), 4.41 (q, $J$ = 13.2 Hz, 2H), 2.76 – 2.63 (m, 2H), 2.64 – 2.55 (m, 2H).$^{13}C\{^{1}H\}$ NMR (126 MHz, $CD_2Cl_2$) δ 170.30. $^{31}P\{^{1}H\}$ NMR (202 MHz, $CD_2Cl_2$) δ 51.9.

*Synthesis of Ruthenium carbamate in situ (**15**).* Before use $^{13}C$ labeled sodium formate was dried in a Schlenk bomb under vacuum at 100°C overnight before being transferred into an $N_2$ glove box. In an $N_2$ glovebox, a J-Young tube was charged with **8-Cl** (44.5 mg, 0.0532 mmol, 1 eq), $^{13}C$ labeled sodium formate (5.7 mg, 0.0826 mmol, 1.6 eq), and anhydrous DMSO-$d_6$ (1.4 ml). The reaction showed 100% conversion to **3** *in situ* after heating at 60°C for 68 hours or after 2 hours at 100°C. $^{1}H$ NMR (700 MHz, DMSO-$d_6$) δ 12.24 (s, 1H), 8.37 (tt, $J$ = 8.2, 1.0 Hz, 2H), 8.22 (ddd, $J$ = 5.5, 1.7, 0.8 Hz, 1H), 8.10 (ddd, $J$ = 5.4, 1.6, 0.8 Hz, 1H), 8.03 (td, $J$ = 7.8, 1.6 Hz, 1H), 8.01 (td, $J$ = 7.8, 1.6 Hz, 1H), 7.99 (ddd, $J$ = 7.8, 1.3, 0.6 Hz, 1H), 7.69 (dd, $J$ = 8.1, 4.8 Hz, 2H), 7.56 – 7.50 (m, 2H), 7.46 (ddd, $J$ = 7.7, 5.4, 1.3 Hz, 1H), 7.33 (td, $J$ = 7.8, 1.3 Hz, 1H), 7.29 (td, $J$ = 7.7, 1.2 Hz, 1H), 7.25 (td, $J$ = 7.7, 1.3 Hz, 1H), 7.22 (td, $J$ = 7.6, 1.1 Hz, 1H), 7.13 (tq, $J$ = 7.5, 1.1 Hz, 1H), 6.89 (td, $J$ = 7.9, 1.9 Hz, 2H), 6.64 (ddd, $J$ = 9.6, 8.1, 1.3 Hz, 2H), 5.14 (ddt, $J$ = 30.0, 14.4, 4.6 Hz, 1H), 4.83 (dddd, $J$ = 25.7, 14.7, 7.3, 4.1 Hz, 1H), 4.63 (dddd, $J$ = 17.2, 13.9, 10.3, 2.7 Hz, 1H), 4.50 (ddt, $J$ = 14.8, 9.8, 6.4 Hz, 1H), 2.89 – 2.83 (m, 2H), 2.78 (dddd, $J$ = 14.7, 10.3, 7.1, 3.1 Hz, 1H), 2.63 (dddd, $J$ = 14.7, 11.0, 7.7, 4.0 Hz, 1H). $^{31}P$ NMR (283 MHz, DMSO-$d_6$) δ 45.53 (d, $J_{PC}$ = 7.0 Hz).

*Reaction of $HCO_3^-$ with **8-OH$_2$** and added TMDS.* A J-Young tube was charged with **8-OH$_2$** (14 mg, 0.015 mmol, 1 eq), $NaH^{13}CO_3$ (12 mg, 0.15 mmol, 10 eq), and TMDS (26 µL, 0.15 mmol, 1 eq) in DMSO-$d_6$ and was heated at at 50 °C for 16 h. Complete conversion to **15** as observed by $^{13}C$ and $^{31}P$ NMR spectroscopy. Heating **8-OH$_2$** under $N_2$ with $NaH^{13}CO_3$ and TMDS on the same scale in DMSO also led to formation of **15.** Complex **15** could be isolated from the reaction by precipitation with an aqueous solution of $NH_4PF_6$ followed by centrifugation. The solid collect on a medium porosity frit and was washed with water and $Et_2O$. Crystals of **15** were grown by slow evaporation of a DCM solution of **15**. $^{1}H$ NMR (500 MHz, DMSO-$d_6$) δ 12.24 (s, 1H), 8.38 (t, $J$ = 6.5 Hz, 2H), 8.29 – 8.19 (m, 1H), 8.13 – 8.09 (m, 1H), 8.08 – 7.99 (m, 3H), 7.70 (d, $J$ = 7.8 Hz, 2H), 7.57 – 7.45 (m, 3H), 7.39 – 7.20 (m, 4H), 7.18 – 7.10 (m, 1H), 6.97 – 6.87 (m, 2H), 6.65 (t, $J$ = 8.7 Hz, 2H), 5.15 (dd, $J$ = 30.2, 13.7 Hz, 1H), 4.85 (s, 1H), 4.64 (d, $J$ = 14.4 Hz, 1H), 4.52 (d,

*J* = 12.7 Hz, 1H), 2.93 – 2.73 (m, 4H). $^{13}C\{^{1}H\}$ NMR (126 MHz, $CD_2Cl_2$) δ 155.25. $^{31}P\{^{1}H\}$ NMR (202 MHz, $CD_2Cl_2$) δ 47.5.

*Synthesis of **15** by dehydrogenation of **14** or deprotonation of **8-OH$_2$**.* Crystals of **14** formed from a DCM solution containing **8-OH$_2$** (14 mg, 0.015 mmol, 1 eq) and $NaH^{13}CO_2$ (1.0 mg, 0.015 mmol, 1 eq). The DCM was decanted and the crystals were dissolved into DMSO-$d_6$ for monitoring by NMR.

To test for $H_2$ evolution by GC analysis, **8-OH$_2$** (70 mg, 0.07 mmol, 1 eq) and $NaHCO_2$ (5 mg, 0.07 mmol, 1 eq) were dissolved in acetone (5 mL) and sealed in a gas-tight vial. The reaction mixture was allowed to stir at room temperature for 1 h before a sample of the reaction vessel headspace (1 mL) was taken and analyzed by GC.

Formation of **15** by deprotonation and reaction with $CO_2$ was done by first mixing a solution of **8-OH$_2$** (14 mg, 0.015 mmol) in $CD_2Cl_2$ with *n*BuLi (0.032 mmol) at -78 °C in a J-Young NMR tube in an $N_2$ glove box. The J-Young tube was evacuated with three freeze-pump-thaw cycles and then $^{13}CO_2$ was added to fill the headspace. Upon sitting at room temperature for 2 days a precipitate formed. The $CD_2Cl_2$ was decanted and the precipitate was dissolved in DMSO-$d_6$ for NMR analysis.

**Catalytic studies.** The $CO_2$ hydrogenation reaction was carried out in a PFTE lined 45 ml Parr Instruments 5000 Multiple Reactor system vessel. Under nitrogen atmosphere, **9** (45 mg, 53 μmol) and $K_3PO_4$ (962 mg, 4.53 mmol, 86 eq) were dissolved in THF (5 ml) and transferred to the Parr system vessel with a magnetic stir bar. The vessel was pressurized with $CO_2$ (20 bar) and $H_2$ (60 bar) and heated to 140 °C for four 4 days. The reaction solution was decanted away from the resulting precipitate, and both were analyzed via $^{1}H$ and $^{13}C$ NMR. To the decanted solution, mesitylene (27.4 mg, 0.2280 mmol) was added as an internal standard. The precipitate was dissolved in $D_2O$, and dimethylformamide (DMF; 50.9 mg, 0.6964 mmol) was added as an internal standard. The spin-lattice relaxation times (T1) were determined for standard solutions containing known amounts of mesitylene and formic acid in DMSO-$d^6$ and of DMF and sodium formate in $D_2O$ to determine the appropriate delay time for quantitative $^{1}H$ NMR. For the solution in DMSO-$d^6$, the formate C-H proton T1 = 7.2 seconds, the mesitylene arene-H T1 = 5.0 seconds, and the mesitylene methyl C-H T1 = 2.3 seconds. For the $D_2O$ solution, the formate C-H T1 = 9.5 seconds,

the DMF C-H T1 = 9.9 seconds, and the two inequivalent DMF methyl C-H T1 = 8.3 seconds and 4.7 seconds (See SI for details). These values are consistent with the literature.[40] The delay time for $^{1}H$ NMR analysis of the reaction solutions was set to 30 seconds. Turn over numbers were calculated independently for the solution and precipitate, and then added.

## 4.5 SUPPORTING INFORMATION

Table 4.1 Crystallographic Information for Complexes **14** and **15**.

| **Molecule** | **Complex 14** | **Complex 15** |
|---|---|---|
| Empirical formula | C71 H67 Cl4 F18 N12 O2 P5 Ru2 | C39 H42 F6 N6 O4 P2 Ru S2 |
| Formula weight | 1961.16 | 999.92 |
| Temperature | 100(2) K | 100(2) K |
| Wavelength | 0.71073 Å | 0.71073 Å |
| Crystal system | Monoclinic | Monoclinic |
| Space group | C 1 2/c 1 | P $2_1$/c |
| Unit cell dimensions | a = 27.5062(15) Å | a = 12.7105(10) Å |
| | b = 12.3658(6) Å | b = 25.453(2) Å |
| | c = 24.5908(13) Å | c = 12.5290(9) Å |
| | α= 90°. | α= 90°. |
| | β= 110.471(5)°. | β= 94.334(4)°. |
| | γ = 90°. | γ = 90°. |
| Volume | 7836.0(7) $Å^3$ | 4041.8(5) $Å^3$ |
| Z | 4 | 4 |
| Density (calculated) | 1.662 $Mg/m^3$ | 1.643 $Mg/m^3$ |
| Absorption coefficient | 0.721 $mm^{-1}$ | 0.649 $mm^{-1}$ |
| F(000) | 3944 | 2040 |
| Crystal size | 0.15 x 0.10 x 0.08 $mm^3$ | 0.15 x 0.08 x 0.03 $mm^3$ |
| Theta range for data collection | 1.58 to 25.69°. | 1.60 to 26.76°. |
| Index ranges | -33<=h<=33, -14<=k<=14, -29<=l<=30 | -15<=h<=16, -31<=k<=32, -15<=l<=15 |
| Reflections collected | 160385 | 117733 |
| Independent reflections | 7297 [R(int) = 0.0668] | 8457 [R(int) = 0.0817] |
| Completeness to theta = 25.00° | 99.50% | 100.00% |
| Absorption correction | Semi-empirical from equivalents | Semi-empirical from equivalents |
| Max. and min. transmission | 0.9446 and 0.8995 | 0.9808 and 0.9090 |
| Refinement method | Full-matrix least-squares on $F^2$ | Full-matrix least-squares on $F^2$ |
| Data / restraints / parameters | 7297 / 3 / 531 | 8457 / 0 / 545 |
| Goodness-of-fit on $F^2$ | 1.085 | 1.048 |
| Final R indices [I>2sigma(I)] | R1 = 0.0544, wR2 = 0.1162 | R1 = 0.0490, wR2 = 0.1255 |
| R indices (all data) | R1 = 0.0651, wR2 = 0.1209 | R1 = 0.0702, wR2 = 0.1387 |
| Largest diff. peak and hole | 1.251 and -1.141 $e.Å^{-3}$ | 0.982 and -1.115 $e.Å^{-3}$ |

# T1 Calculation Experimental Details

A variable delay time list was created with time ranging from 1 to 31 seconds on second intervals. Experiments were run on standard solutions of sodium formate and DMF in $D_2O$ (fig. S29) and of formic acid and mesitylene in DMSO-$d_6$ (fig. S30). Peak graphs were then created for the formate peaks and the internal standard peaks, and the data were fit with MestreNova's "Three Parameter Exponential Fit" function (eq. 1), where by comparison with equation 2,[1] we see $G = 1/T_1$.

$$B + Fe^{-xG} \qquad \text{eq. 1}$$

$$\Delta n(t) = \Delta n_{eq}[1 - \exp\left(-\frac{t}{T_1}\right)] \qquad \text{eq. 2}$$

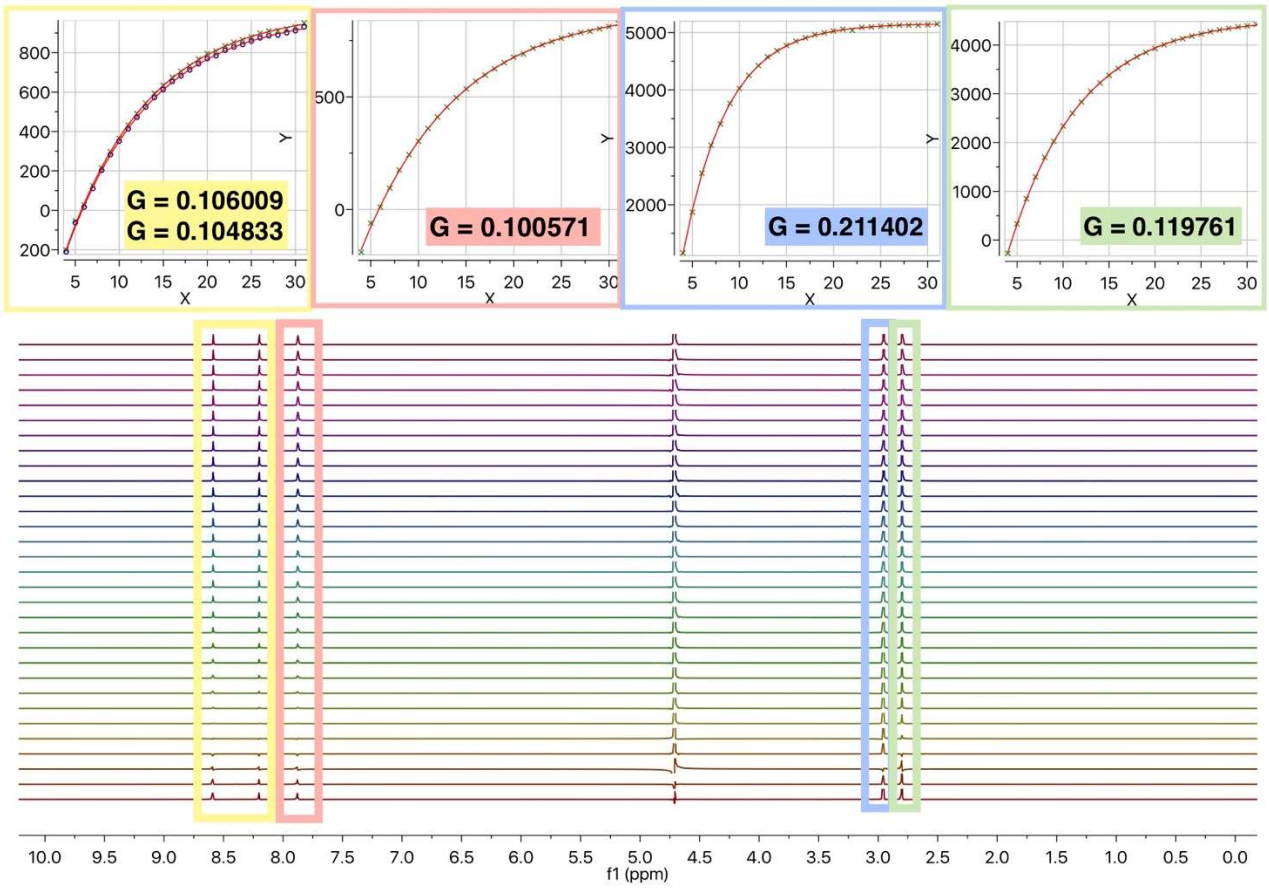


Figure 4.20. $^1$H NMR (298 K, 499.7 MHz) of $^{13}$C-labeled formic acid (yellow) and DMF (pink, blue, and green) in $D_2O$. Variable delay time list from 4 to 31 seconds.

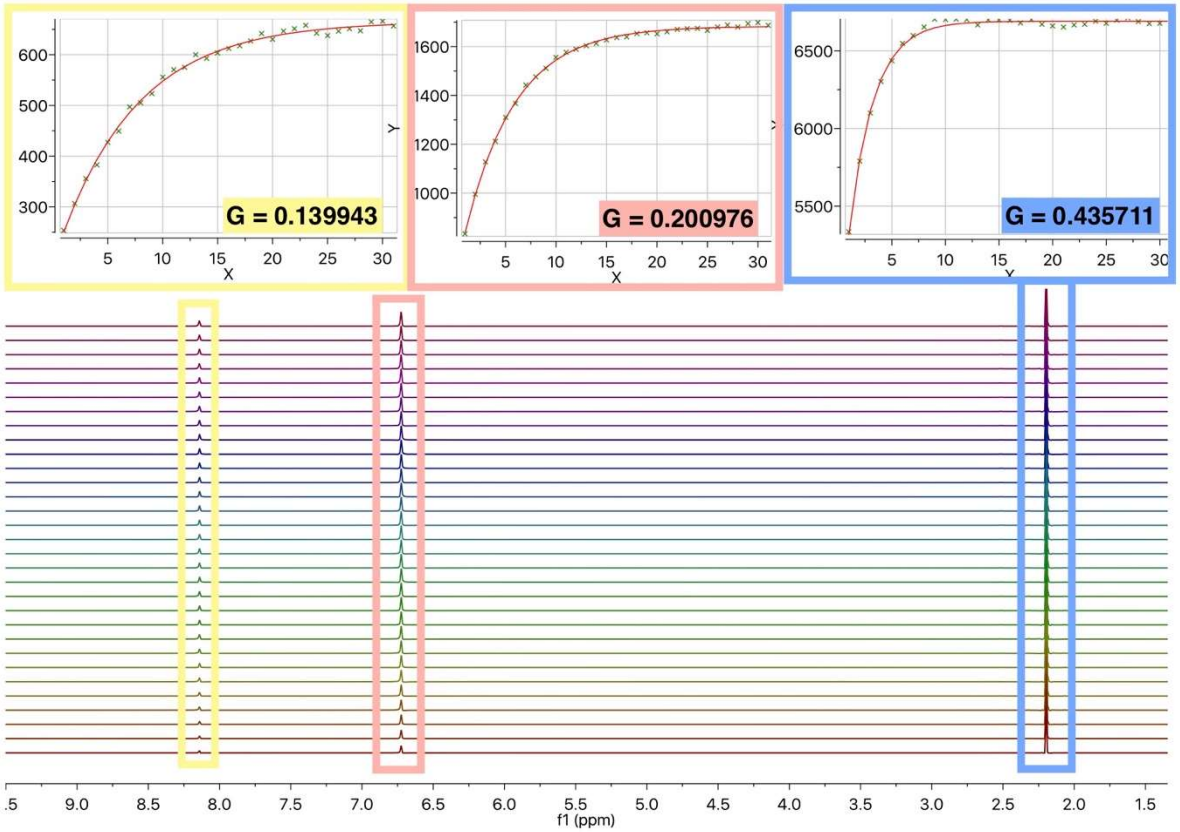


**Figure S30.** $^{1}$H NMR (298 K, 499.7 MHz) of formic acid (yellow) and mesitylene (pink and blue) in DMSO-$d_6$. Variable delay time list from 1 to 31 seconds.

## 4.6 NOTES TO THE CHAPTER


1. Adapted with permission from (M. R. Norris, S. E. Flowers, A. M. Mathews and B. M. Cossairt, *Organometallics*, 2016, **35**, 2778-2781.). Copyright (2016) American Chemical Society.
2. L. Barelli, G. Bidini, F. Gallorini and S. Servili, *Energy*, 2008, **33**, 554-570.
3. A. J. Morris, G. J. Meyer and E. Fujita, *Acc. Chem. Res.*, 2009, **42**, 1983-1994.
4. B. Kumar, M. Llorente, J. Froehlich, T. Dang, A. Sathrum and C. P. Kubiak, *Ann. Rev. Phys. Chem.*, 2012, **63**, 541-569.
5. Z. Chen, C. Chen, D. R. Weinberg, P. Kang, J. J. Concepcion, D. P. Harrison, M. S. Brookhart and T. J. Meyer, *Chem. Commun.*, 2011, **47**, 12607-12609.
6. E. Fujita, L. R. Furenlid and M. W. Renner, *J. Am. Chem. Soc.*, 1997, **119**, 4549-4550.
7. B. J. Fisher and R. Eisenberg, *J. Am. Chem. Soc.*, 1980, **102**, 7361-7363.
8. J. Hawecker, J.-M. Lehn and R. Ziessel, *Helv. Chim. Acta*, 1986, **69**, 1990-2012.
9. J. M. Smieja and C. P. Kubiak, *Inorg. Chem.*, 2010, **49**, 9283-9289.
10. J. W. Raebiger, J. W. Turner, B. C. Noll, C. J. Curtis, A. Miedaner, B. Cox and D. L. DuBois, *Organometallics*, 2006, **25**, 3345-3351.

11. I. Bhugun, D. Lexa and J.-M. Savéant, *J. Am. Chem. Soc.*, 1996, **118**, 1769-1776.
12. S. Ramakrishnan, K. M. Waldie, I. Warnke, A. G. De Crisci, V. S. Batista, R. M. Waymouth and C. E. D. Chidsey, *Inorg. Chem.*, 2016, **55**, 1623-1632.
13. Y. Tamaki, T. Morimoto, K. Koike and O. Ishitani, *Proc. Natl. Acad. Sci.*, 2012, **109**, 15673-15678.
14. A. M. Appel, J. E. Bercaw, A. B. Bocarsly, H. Dobbek, D. L. DuBois, M. Dupuis, J. G. Ferry, E. Fujita, R. Hille, P. J. A. Kenis, C. A. Kerfeld, R. H. Morris, C. H. F. Peden, A. R. Portis, S. W. Ragsdale, T. B. Rauchfuss, J. N. H. Reek, L. C. Seefeldt, R. K. Thauer and G. L. Waldrop, *Chem. Rev.*, 2013, **113**, 6621-6658.
15. N. M. Rezayee, C. A. Huff and M. S. Sanford, *J. Am. Chem. Soc.*, 2015, **137**, 1028-1031.
16. E. Barton Cole, P. S. Lakkaraju, D. M. Rampulla, A. J. Morris, E. Abelev and A. B. Bocarsly, *J. Am. Chem. Soc.*, 2010, **132**, 11539-11551.
17. J. F. Hull, Y. Himeda, W.-H. Wang, B. Hashiguchi, R. Periana, D. J. Szalda, J. T. Muckerman and E. Fujita, *Nature Chem.*, 2012, **4**, 383.
18. W.-H. Wang, Y. Himeda, J. T. Muckerman, G. F. Manbeck and E. Fujita, *Chem. Rev.*, 2015, **115**, 12936-12973.
19. M. Grasemann and G. Laurenczy, *Energy Environ. Sci.*, 2012, **5**, 8171-8181.
20. A. Boddien, F. Gärtner, C. Federsel, P. Sponholz, D. Mellmann, R. Jackstell, H. Junge and M. Beller, *Angew. Chem., Int. Ed.*, 2011, **50**, 6411-6414.
21. B. Mondal, J. Song, F. Neese and S. Ye, *Curr. Opin. Chem. Biol.*, 2015, **25**, 103-109.
22. S. Gambarotta, F. Arena, C. Floriani and P. F. Zanazzi, *J. Am. Chem. Soc.*, 1982, **104**, 5082-5092.
23. J. P. Krogman, B. M. Foxman and C. M. Thomas, *J. Am. Chem. Soc.*, 2011, **133**, 14582-14585.
24. R. Angamuthu, P. Byers, M. Lutz, A. L. Spek and E. Bouwman, *Science*, 2010, **327**, 313-315.
25. M. Vogt, M. Gargir, M. A. Iron, Y. Diskin-Posner, Y. Ben-David and D. Milstein, *Chem. Eur. J.*, 2012, **18**, 9194-9197.
26. C. A. Huff, J. W. Kampf and M. S. Sanford, *Organometallics*, 2012, **31**, 4643-4645.
27. A. Paparo, J. S. Silvia, C. E. Kefalidis, T. P. Spaniol, L. Maron, J. Okuda and C. C. Cummins, *Angew. Chem., Int. Ed.*, 2015, **54**, 9115-9119.
28. A. Looney, R. Han, K. McNeill and G. Parkin, *J. Am. Chem. Soc.*, 1993, **115**, 4690-4697.
29. W. Sattler and G. Parkin, *Catal. Sci. Technol.*, 2014, **4**, 1578-1584.
30. D. Chatterjee, N. Jaiswal and P. Banerjee, *Eur. J. Inorg. Chem.*, 2014, **2014**, 5856-5859.
31. M. Aresta, A. Dibenedetto and I. Tommasi, *Eur. J. Inorg. Chem.*, 2001, **2001**, 1801-1806.
32. S. Chakraborty, O. Blacque and H. Berke, *Dalton Trans.*, 2015, **44**, 6560-6570.
33. J. Sánchez-Nieves and P. Royo, *J. Organomet. Chem.*, 2001, **621**, 299-303.
34. C. A. Huff and M. S. Sanford, *ACS Catal.*, 2013, **3**, 2412-2416.
35. N. M. Rezayee, C. A. Huff and M. S. Sanford, *J. Am. Chem. Soc.*, 2015, **137**, 1028-1031.
36. S. Wesselbaum, V. Moha, M. Meuresch, S. Brosinski, K. M. Thenert, J. Kothe, T. vom Stein, U. Englert, M. Holscher, J. Klankermayer and W. Leitner, *Chem. Sci.*, 2015, **6**, 693-704.
37. M. A. Bennett and A. K. Smith, *J. Chem. Soc., Dalton Trans.*, 1974, 233-241.
38. M. R. Norris, J. J. Concepcion, C. R. K. Glasson, Z. Fang, A. M. Lapides, D. L. Ashford, J. L. Templeton and T. J. Meyer, *Inorg. Chem.*, 2013, **52**, 12492-12501.
39. M. A. Bennett and A. K. Smith, *J. Chem. Soc., Dalton Trans.*, 1974, **0**, 233-241.

40. I. D. Campbell and R. Freeman, *J. Magn. Reson.*, 1973, **11**, 143-162.

# Chapter 5. SINGLE-CRYSTAL STRUCTURE OF A 1.3 NM INDIUM PHOSPHIDE NANOCLUSTER

*The following have been previous published.*[1]
*Contributions to this were made by Dylan Gary, Werner Kaminsky, and Alessio Patrone.*

## 5.1 INTRODUCTION

Quantum-confined semiconductor nanocrystals (quantum dots, QDs) exhibit strongly size-dependent optical and electronic properties. As a result, considerable effort has been aimed at their integration into light-harvesting and -emitting devices both in the research laboratory and in the marketplace.[2, 3] Predicting the properties of QDs requires detailed knowledge of their size, shape, and composition. A longstanding challenge in this field has been to prepare a homogeneous sample and to grow a single crystal in order to determine a high-resolution structure that allows for unambiguous assignment of these three properties. While there is a rich history of structural interrogation of transition metal and main group cluster molecules,[4-10] to date a complete, atomically precise structural picture of a binary semiconductor QD remains elusive.

Magic-sized nanoclusters have emerged as an important class of intermediates at the interface of small molecules and QDs.[11-18] As a class of truly monodisperse nanomaterials, magic-sized nanoclusters can offer unique insight into the structure of their larger QD counterparts. Several group II-VI magic-sized clusters have been identified and structurally characterized; ,[4, 5, 9] however, these clusters do not appear to be directly involved in the high-temperature nucleation of group II-VI QDs since their thermal instability precludes their buildup in these traditional syntheses where kinetics are readily controlled by precursor conversion chemistry. [19-22] For group III-V QDs, on the other hand, precursor conversion chemistry does not appear to be the rate-determining step in the overall growth mechanism,[13, 23, 24] and magic-sized clusters have been implicated as kinetically persistent intermediates whose thermal transformation may be an important step in QD nucleation.[13, 25, 26] Given the potential significance of these cluster intermediates in elucidating the mechanism of III-V QD formation and in understanding the physical and electronic structure of carboxylate-terminated QDs, we sought to isolate and structurally characterize one such cluster.

Herein, we report the first single-crystal X-ray diffraction (XRD) structure of an indium phosphide (InP) magic-sized nanocluster with 0.83 Å resolution, including all ligands. This nanocrystal ($In_{37}P_{20}(O_2CCH_2Ph)_{51}$) exhibits a non-stoichiometric core, a geometry that does not correspond to that of bulk InP, and unanticipated ligand binding modes.

Solution-based syntheses of semiconductor nanocrystals typically yield an ensemble of particles that range in terms of size, shape, and surface composition. However, $In_{37}P_{20}(O_2CCH_2Ph)_{51}$ is the sole nanocrystalline product that we obtain from reaction of tris(trimethylsilyl)phosphine, indium acetate, and carboxylic acid at 100 °C, as evident from elemental analysis and $^{31}P$ NMR spectroscopy. This cluster has previously been identified by its spectroscopic signatures as a magic size in the growth profile of InP QDs. [13, 25] Crystals suitable for single-crystal X-ray analysis were grown from a supersaturated solution of particles (R = $CH_2Ph$) in ethyl acetate and formed as yellow prisms.

## 5.2 Results and Discussion

### 5.2.1 *Physical Structure- Core*

The structure of $In_{37}P_{20}(O_2CCH_2Ph)_{51}$ (Figure 5.1) exhibits several unanticipated features that deviate from the conventional model of a nanoparticle. Binary semiconductor nanocrystals are typically envisioned as possessing a crystalline, stoichiometric core structure that corresponds to a known bulk phase and is unaltered during ligand exchange reactions post-synthesis.[27, 28] Additionally, this core would be surrounded by a shell of neutral, datively bound ligands or by a shell of excess metal cations charge-balanced by anionic ligands.[28, 29] In the structure of $In_{37}P_{20}(O_2CCH_2Ph)_{51}$ there is no subset of atoms that can accurately be described as a stoichiometric, charge-neutral core of InP. The nanocrystal core, which consists solely of fused 6-membered rings with all phosphorus atoms coordinated to four indium atoms in a pseudo-tetrahedral arrangement (Figure 5.1A), has the formula $[In_{21}P_{20}]^{3+}$. This subset of atoms possesses a C2 rotation axis that bisects two phosphorus atoms and a single indium atom located at the center of the particle, and measures approximately 1.3 nm × 1.0 nm × 1.0 nm. This arrangement of core atoms deviates from that of the known bulk phases of InP.[30] A dihedral angle of 160 ± 3° is consistent along the longest straight In–P chain and demonstrates a clear deviation from zincblende ($\phi = \pm 60°$ or $\pm 180°$) and wurtzite ($\phi = \pm 120°$) (Figure 5.2). The average In–P bond length in the

$[In_{21}P_{20}]^{3+}$ core is 2.528 Å (min 2.479 Å, max 2.624 Å), and the average P–In–P bond angle is 109.2° (min 97.7°, max 119.9°), while those of the zincblende lattice are 2.541 Å and 109.5°, respectively. An additional 16 indium atoms are singly bound to this core through surface-exposed phosphorus atoms (Figure 5.1B), with an average bond length of 2.482 Å (min 2.450 Å, max 2.515 Å). Since the sum of the single-bond covalent radii for In and P is 2.53 Å, it is inferred that the bonding in the inorganic core of this cluster may be best viewed as covalent in nature, with differences in bond lengths between In–P in the core and In–P at the surface arising from internal strain.[31]

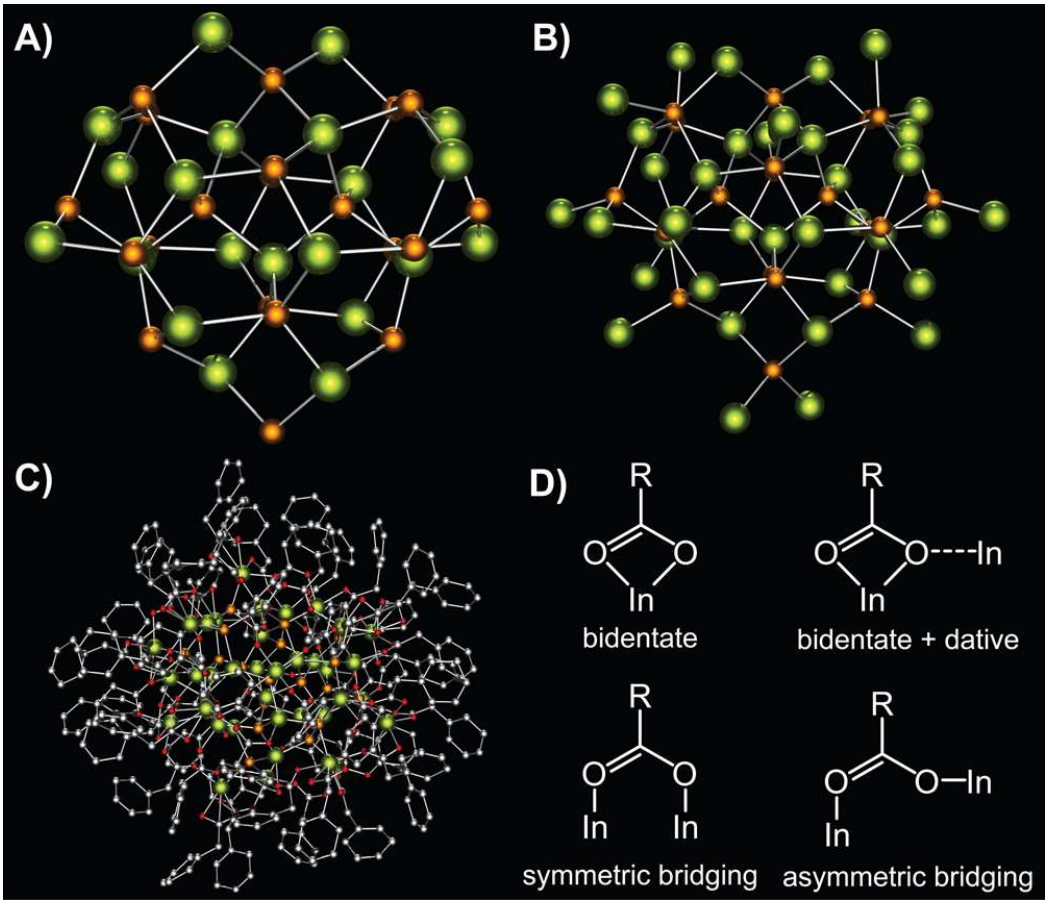


Figure 5.1. Molecular structure of $In_{37}P_{20}(O_2CCH_2Ph)_{51}$ (hydrogen atoms omitted for clarity). (A) $[In_{21}P_{20}]3+$ core. (B) Core plus 16 surface indium atoms. (C) Complete single-crystal XRD structure including all ligands. (D) Schematic representation of all observed ligand binding modes. Of the 51 phenylacetate ligands, 12 are identified as bidentate, 1 is identified as bidentate + dative, 5 are identified as symmetric bridging, and 33 are identified as asymmetric bridging. Color legend: green, indium; orange, phosphorus; red, oxygen; gray, carbon.

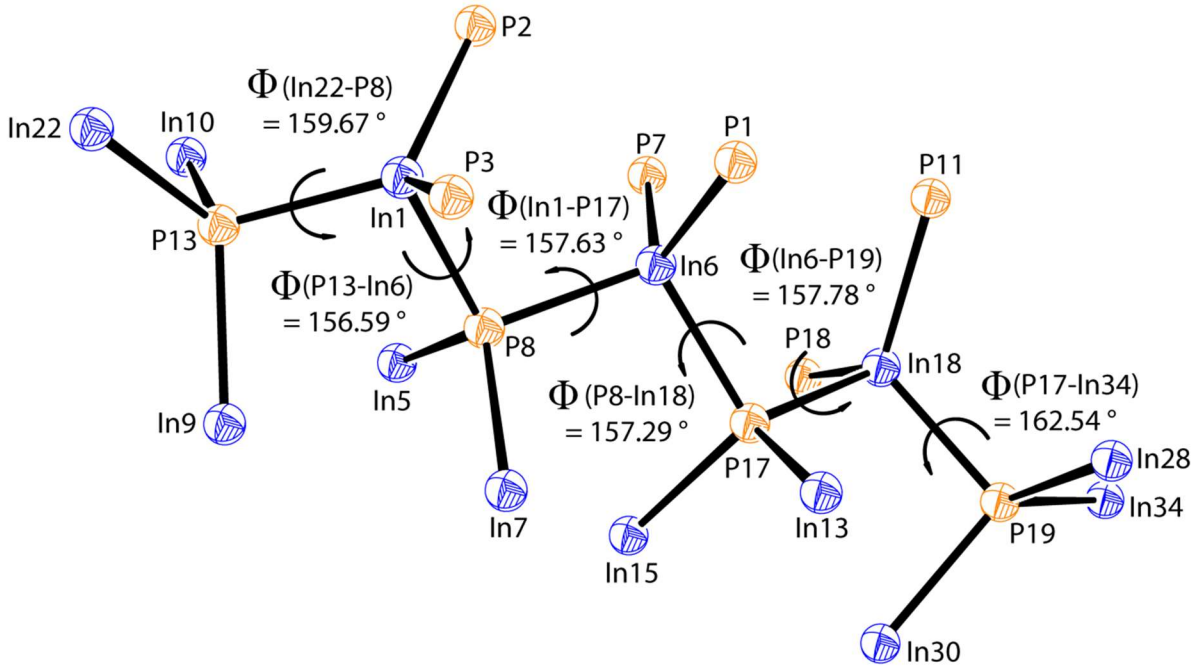


Figure 5.2 Dihedral angles between In and P atoms in the longest chain in $In_{37}P_{20}(O_2CCH_2Ph)_{51}$. In6 is the central indium atom that is bisected by the C2 axis for the $[In_{21}P_{20}]^{3+}$ core. All dihedral angles measure 160 ± 3 °. Note, the subset of atoms In1, In5, In7, P8, In6, P17, In15, In13, In18 is a unique subset of atoms of the cluster core in which no indium atom has a bond to an oxygen atom from surface carboxylates. These are the only indium atoms in the structure for which this is true. Color legend: orange = phosphorus, blue = indium.

### 5.2.2 *Physical Structure - Surface*

An accurate picture of the surface chemistry of InP nanoparticles is essential for understanding their optoelectronic properties and for designing methods to alter their surfaces post-synthetically, a crucial step for applications requiring high photoluminescence quantum yield or efficient charge extraction.[28, 29, 32-35] $In_{37}P_{20}(O_2CCH_2Ph)_{51}$ is an In-rich nanoparticle that is completely passivated by a phenylacetate ligand set with highly variable coordination modes (Figure 5.1C,D and Table 5.1, See section 5.5 Supporting information). Each surface indium atom is bound to at least two other indium atoms through bridging carboxylate ligands, and as such this ligand set is best described as entirely anionic in nature (i.e., X-type), with no neutral, datively bound ligands.[28] This stands in contrast to the prevailing model of QD surfaces wherein the

dominant coordination modes are thought to be labile, neutral Lewis bases such as primary amines acting as two-electron donors (L-type) or neutral Lewis acids acting as two-electron acceptors (Z-type).[33] Retention of this tightly bound and dense ligand packing in solution is confirmed via NMR spectroscopy. A $^{1}H–^{1}H$ COSY spectrum revealed that the methylene protons on a common carbon atom are chemically inequivalent, separated by up to 1.3 ppm. This large difference in chemical shift may be indicative of both hindered rotation about the C–C bonds of the methylene linker and CH–π interactions with nearby aromatic rings (Figure 5.3). Similar interactions have been observed for phenylalanine residues in small proteins.[36]

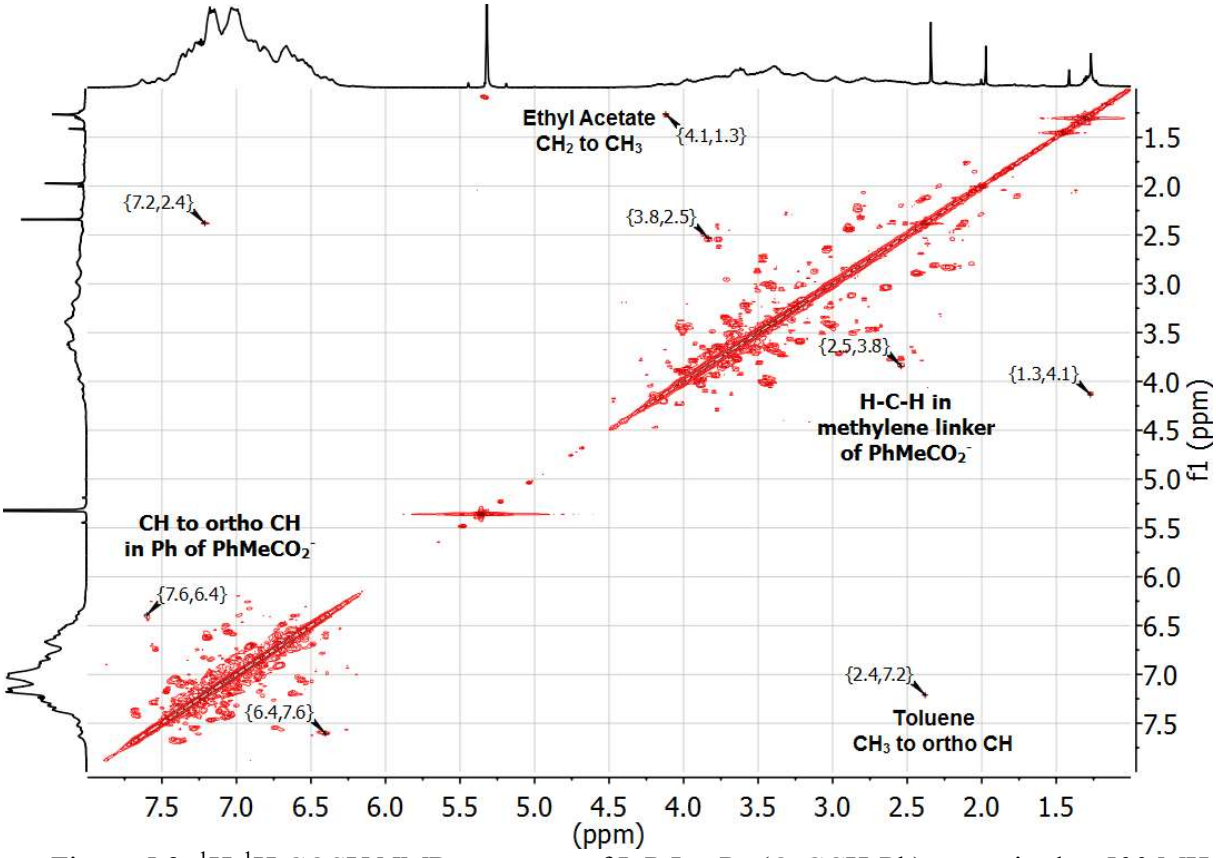


Figure 5.3. $^{1}H$-$^{1}H$ COSY NMR spectrum of InP $In_{37}P_{20}(O_2CCH_2Ph)_{51}$ acquired at 500 MHz in $C_6D_6$. Protons in the methylene region on each phenylacetate ligand are inequivalent indicative of hindered rotation and CH-π interactions.

We discovered that single crystals of $In_{37}P_{20}(O_2CCH_2Ph)_{51}$ are sensitive to air exposure,(12) suggesting a chemical transformation of the particles under these conditions. When these crystals are exposed to air they begin to fracture within 30 min, and a change is observed in

the dimensions of the unit cell. In a separate single-crystal XRD study on crystals exposed to moist air, we have identified a stoichiometric reaction with water wherein a single carboxylate ligand adopts a monodentate binding motif with the resulting open coordination site filled by a water molecule (Figure 5.4). This structural change has minimal impact on the frontier orbitals of the cluster, and hence its electronic structure shows little change, as indicated by TDDFT calculations (Figure 5.5). Interestingly, the reaction with water is selective for a single indium site (likely due to small differences in the Lewis acidity of the indium sites). This result suggests that stoichiometric and site-specific ligand chemistry may be achieved at the surfaces of semiconductor QDs.

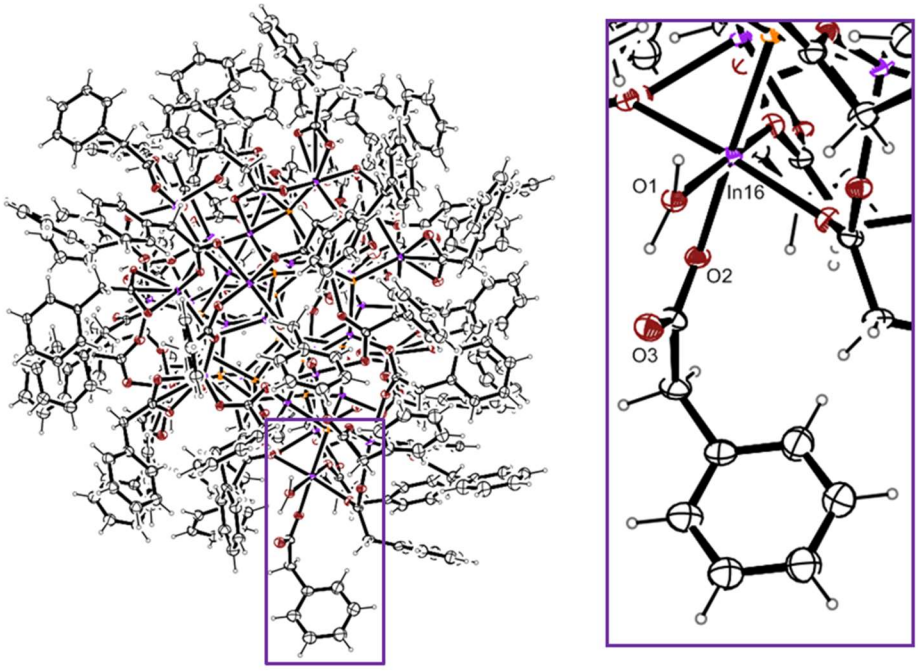


Figure 5.4. Single crystal X-ray diffraction structure of the reaction product of $In_{37}P_{20}(O_2CCH_2Ph)_{51}$ with one equivalent of water including a zoom-in of the specific indium center (16) that has been transformed through coordination of water and a transition of the phenylacetate ligand from bidentate to monodentate.

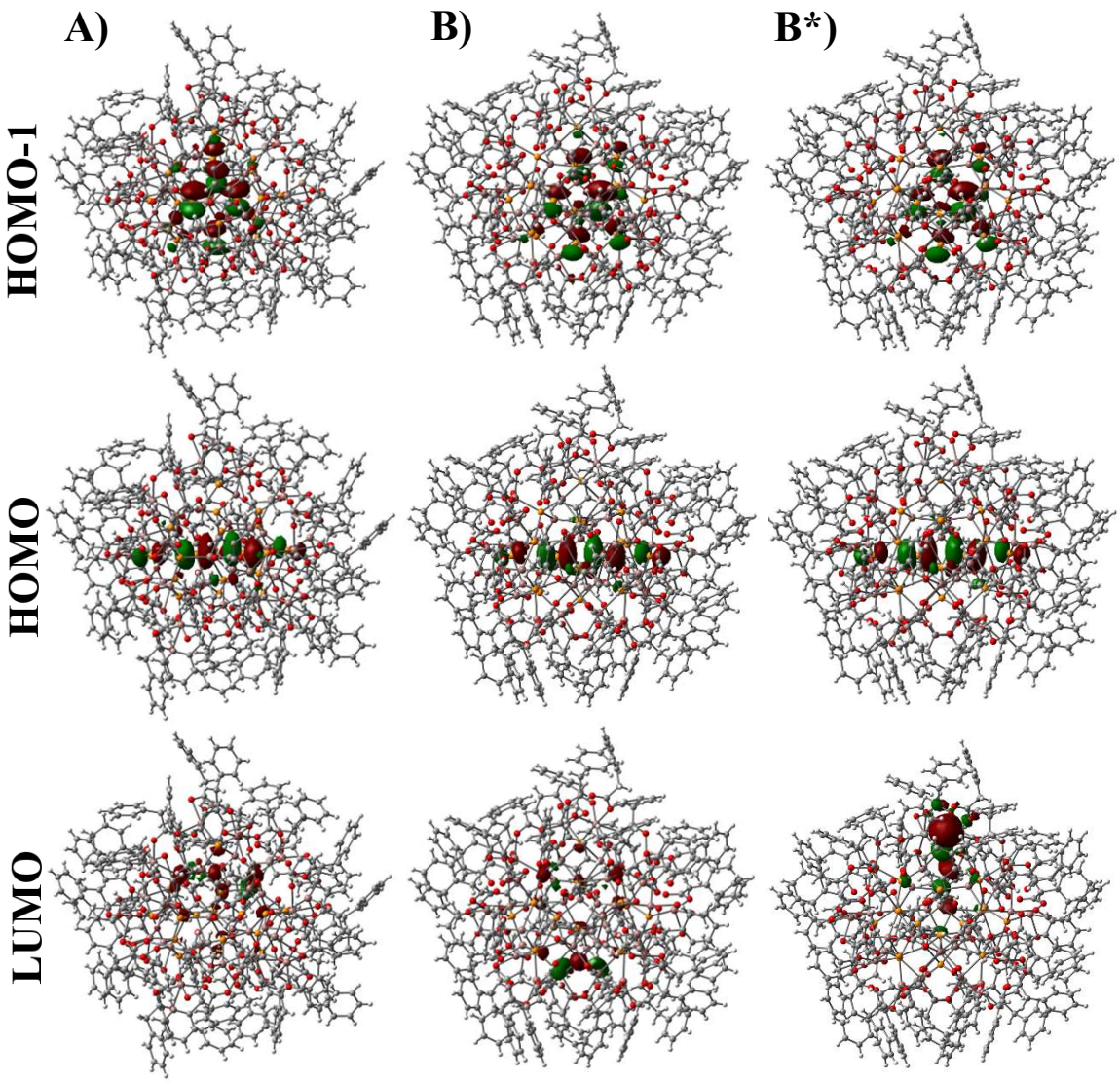


Figure 5.5. HSE06/LANL2DZ molecular orbital (MO) diagrams of the occupied (HOMO-1 and HOMO) and unoccupied (LUMO) orbitals involved in the two brightest transitions calculated for the air-free crystal A $In_{37}P_{20}(O_2CCH_3)_{51}$ and corresponding MOs in the air exposed crystal B $In_{37}P_{20}(O_2CCH_2Ph)_{51}(H_2O)$ and crystal B* $In_{37}P_{20}(O_2CCH_2Ph)_{51}$ . The MOs were plotted with an isosurface value of 0.025.

## 5.3 CONCLUSIONS

In conclusion, we have characterized the physical and electronic structure of an indium phosphide magic-sized cluster, $In_{37}P_{20}(O_2CR)_{51}$, which is a key intermediate in the synthesis of InP

quantum dots. Since this structure does not correspond to a known bulk phase or a magic number for a closed shell of valence electrons, it may be that the selectivity for and stability of this cluster can be attributed to the dense, interconnected network of supporting ligands passivating the particle surface. Not only does this result allow us insight into the structure of III-V QDs and nanocluster intermediates, it also leads us to propose several new structural principles to the field of semiconductor QDs. First, the cores of semiconductor nanocrystals need not be stoichiometric (neutral), as is seen for the $[In_{21}P_{20}]^{3+}$ fragment in $In_{37}P_{20}(O_2CR)_{51}$. Second, observations of differential ligand exchange on QDs need not be related to coordination at different facets, but rather may be due to the presence of different and often interlinked coordination networks. As a consequence of this interconnected ligand set, which has predominately bridging binding modes and is free of any neutral, datively bound metal carboxylate complexes, ligand exchange reactions that displace $M(O_2CR)_x$ complexes are likely coupled with significant structural changes. In contrast, X- and L-type ligand exchange reactions can be site specific, allowing for subtle changes to the surface coordination in a controlled manner, as is observed for the reaction of $In_{37}P_{20}(O_2CCH_2Ph)_{51}$ with 1 equiv of water.

## 5.4 EXPERIMENTAL

*General Considerations.* Indium acetate (99.99%), phenylacetic acid (99%), and oleic acid (90%) were purchased from Sigma-Aldrich and used without further purification. NMR solvents were purchased from Cambridge Isotope Laboratories. All solvents were dried over calcium hydride, distilled, and stored over 4 Å molecular sieves prior to use. $P(SiMe_3)_3$ was prepared according to literature procedures.[37] All manipulations were performed under an inert atmosphere of dry $N_2$ using standard Schlenk or glovebox techniques unless otherwise stated. Optical spectra were acquired on a Cary 5000 UV-Vis-NIR spectrophotometer from Agilent Technologies. NMR spectra were acquired on 300, 500, and 700 MHz Bruker Avance spectrometers.

*Synthesis of $In_{37}P_{20}(O_2CCH_2Ph)_{51}$.* $In_{37}P_{20}(O_2CCH_2Ph)_{51}$ was prepared by modification of a reported procedure for myristate-capped particles using $In(O_2CCH_3)_3$ (934 mg, 3.20 mmol) and phenylacetic acid (1.58 g, 11.6 mmol) in toluene (10 mL), and $P(SiMe_3)_3$ (465 μL, 1.60 mmol) in toluene (5 mL).[13] The workup procedure was modified from that of the particles with a myristate ligand set by substituting pentane for acetonitrile to selectively precipitate the particles (three

cycles). $In_{37}P_{20}(O_2CCH_2Ph)_{51}$ was isolated in 25% yield (238 mg, 0.02 mmol) based on $P(SiMe_3)_3$ as the limiting reagent. Elemental analysis $In_{37}P_{20}O_{102}C_{408}H_{357}$: calculated C 41.67%, H 3.06%, N 0.00%; actual C 41.872%, H 3.053%, N −0.227%. Extinction coefficient: 75,900 L $mol^{-1}$ $cm^{-1}$ (300 nm).

For crystallization, under a nitrogen atmosphere $In_{37}P_{20}(O_2CCH_2Ph)_{51}$ (200 mg) was dissolved in ethyl acetate (0.5 mL) and was filtered into a J-Young tube using a 1 mL syringe outfitted with a PFTE filter with a 0.45 μm pore size. Single crystals grew in the J-Young tube overnight at room temperature.

*Single Crystal X-Ray Diffraction Methods.* Two separate crystals were mounted with oil on a nylon loop and data was collected at −173 °C on a Bruker APEX II single crystal X-ray diffractometer using Mo radiation. Specific details on these crystals are summarized in **Table S2**. Solvent analysis discovered two distinct voids filled with ethyl acetate; this contribution to the diffraction pattern was removed with SQUEEZE. With this size of molecule comes the possibility of disorder, which may have contributed to larger than expected positive as well as negative rest electron densities near the indium atoms, estimated to be about 5%. Some disorder of the aromatic groups was treated explicitly as some inter molecular 'squeezing' occurs. As a result of the large molecular size (11.7 kD) and strong scattering of the In-P cluster core, carbon atoms were weakly represented in the data, requiring DELU (In-O-C) and ISOR (O, C) restraints. In addition, the general geometry of the organic ligands was linked via SAME commands. The crystallographic data for the two structures have been deposited in the Cambridge Crystallographic Database under deposition numbers 1417965 and 1417966.

## 5.5 SUPPORTING INFORMATION

Table 5.1. Details on the indium coordination environments in $In_{37}P_{20}(O_2CCH_2Ph)_{51}$. Briefly, there are 7 indium atoms that are pseudo tetrahedral and are each bound to four phosphorus atoms in the core. There are 8 indium atoms that are pseudo tetrahedral with each atom bound to three phosphorus atoms and one oxygen atom. There are 9 indium atoms that are five coordinate and of these 6 are bound to one phosphorus and four bridging oxygens; 2 are bound to two phosphorus atoms and three bridging oxygen atoms; and 1 indium atom is bound to two phosphorus, 1 bridging oxygen, and one bidentate carboxylate. Finally, there are 12 indium atoms that are six coordinate and of these 9 are bound to one phosphorus, three bridging oxygens, and one bidentate carboxylate; 2 are bound to two phosphorus atoms two bridging oxygens, and one bidentate carboxylate (this is the position where we see reactivity with water): and 1 is bound to two phosphorus atoms and four bridging oxygen atoms.

| | Coordination number | | Bond lengths | | Bond Angles |
|---|---|---|---|---|---|
| In1 | 4 | P(2)-In(1) | 2.529(4) | P(8)-In(1)-P(13) | 98.11(16) |
| | | P(3)-In(1) | 2.527(4) | P(8)-In(1)-P(3) | 104.54(13) |
| | | P(8)-In(1) | 2.506(4) | P(13)-In(1)-P(3) | 112.55(14) |
| | | P(13)-In(1) | 2.509(5) | P(8)-In(1)-P(2) | 103.71(12) |
| | | | | P(13)-In(1)-P(2) | 116.99(14) |
| | | | | P(3)-In(1)-P(2) | 117.48(16) |
| In2 | 4 | O(71)-In(2) | 2.135(8) | O(71)-In(2)-P(7) | 118.1(3) |
| | | P(2)-In(2) | 2.579(4) | O(71)-In(2)-P(9) | 100.9(3) |
| | | P(7)-In(2) | 2.503(4) | P(7)-In(2)-P(9) | 116.49(13) |
| | | P(9)-In(2) | 2.514(5) | O(71)-In(2)-P(2) | 106.1(3) |
| | | | | P(7)-In(2)-P(2) | 106.96(13) |
| | | | | P(9)-In(2)-P(2) | 107.5(14) |
| In3 | 4 | O(53)-In(3) | 2.136(9) | O(53)-In(3)-P(10) | 101.0(3) |
| | | P(7)-In(3) | 2.531(4) | O(53)-In(3)-P(7) | 114.0(3) |
| | | P(10)-In(3) | 2.519(5) | P(10)-In(3)-P(7) | 105.20(14) |
| | | P(11)-In(3) | 2.532(4) | O(53)-In(3)-P(11) | 115.1(3) |
| | | | | P(10)-In(3)-P(11) | 114.02(15) |
| | | | | P(7)-In(3)-P(11) | 107.12(13) |

| | | | | | |
|---|---|---|---|---|---|
| In4 | 5 | O(15)-In(4) | 2.292(11) | O(93)-In(4)-O(88) | 76.6(8) |
| | | C(369)-In(4) | 2.534(18) | O(93)-In(4)-O(15) | 93.9(8) |
| | | O(93)-In(4) | 2.17(2) | O(88)-In(4)-O(15) | 170.3(4) |
| | | O(94)-In(4) | 2.30(2) | O(93)-In(4)-O(94) | 59.0(5) |
| | | P(3)-In(4) | 2.540(5) | O(88)-In(4)-O(94) | 92.9(8) |
| | | P(5)-In(4) | 2.575(6) | O(15)-In(4)-O(94) | 83.9(8) |
| | | | | O(93)-In(4)-P(3) | 106.2(5) |
| | | | | O(88)-In(4)-P(3) | 95.2(3) |
| | | | | O(15)-In(4)-P(3) | 85.3(3) |
| | | | | O(94)-In(4)-P(3) | 160.9(6) |
| | | | | O(93)-In(4)-P(5) | 147.9(5) |
| | | | | O(88)-In(4)-P(5) | 92.0(4) |
| | | | | O(15)-In(4)-P(5) | 97.2(3) |
| | | | | O(94)-In(4)-P(5) | 92.3(5) |
| | | | | P(3)-In(4)-P(5) | 104.63(14) |
| | | | | O(93)-In(4)-C(369) | 29.6(4) |
| | | | | O(88)-In(4)-C(369) | 82.0(8) |
| | | | | O(15)-In(4)-C(369) | 90.8(8) |
| | | | | O(94)-In(4)-C(369) | 29.5(4) |
| | | | | C(369)-In(4)-P(3) | 135.4(5) |
| | | | | C(369)-In(4)-P(5) | 120.0(5) |
| In5 | 4 | P(6)-In(5) | 2.516(4) | P(9)-In(5)-P(6) | 119.45(14) |
| | | P(8)-In(5) | 2.540(4) | P(9)-In(5)-P(8) | 103.97(14) |
| | | P(9)-In(5) | 2.513(4) | P(6)-In(5)-P(8) | 98.64(15) |
| | | P(16)-In(5) | 2.543(4) | P(9)-In(5)-P(16) | 115.09(12) |
| | | | | P(6)-In(5)-P(16) | 113.12(15) |
| | | | | P(8)-In(5)-P(16) | 102.92(13) |
| In6 | 4 | P(1)-In(6) | 2.549(4) | P(17)-In(6)-P(8) | 102.74(13) |
| | | P(7)-In(6) | 2.559(3) | P(17)-In(6)-P(1) | 109.68(13) |
| | | P(8)-In(6) | 2.479(4) | P(8)-In(6)-P(1) | 109.34(14) |
| | | P(17)-In(6) | 2.479(4) | P(17)-In(6)-P(7) | 108.78(12) |
| | | | | P(8)-In(6)-P(7) | 109.47(12) |
| | | | | P(1)-In(6)-P(7) | 116.01(13) |
| In7 | 4 | P(4)-In(7) | 2.532(5) | P(12)-In(7)-P(5) | 111.96(16) |
| | | P(5)-In(7) | 2.527(4) | P(12)-In(7)-P(4) | 114.27(15) |
| | | P(8)-In(7) | 2.541(3) | P(5)-In(7)-P(4) | 116.64(17) |
| | | P(12)-In(7) | 2.523(5) | P(12)-In(7)-P(8) | 105.44(14) |
| | | | | P(5)-In(7)-P(8) | 101.94(13) |
| | | | | P(4)-In(7)-P(8) | 104.82(13) |

| | | | | | |
|---|---|---|---|---|---|
| In8 | 4 | O(70)-In(8) | 2.147(9) | O(70)-In(8)-P(7) | 103.4(3) |
| | | P(7)-In(8) | 2.521(4) | O(70)-In(8)-P(18) | 104.3(3) |
| | | P(16)-In(8) | 2.532(4) | P(7)-In(8)-P(18) | 111.87(14) |
| | | P(18)-In(8) | 2.526(4) | O(70)-In(8)-P(16) | 118.2(3) |
| | | | | P(7)-In(8)-P(16) | 106.44(13) |
| | | | | P(18)-In(8)-P(16) | 112.39(13) |
| In9 | 4 | O(46)-In(9) | 2.131(12) | O(46)-In(9)-P(5) | 101.8(4) |
| | | P(5)-In(9) | 2.495(5) | O(46)-In(9)-P(6) | 108.0(4) |
| | | P(6)-In(9) | 2.506(5) | P(5)-In(9)-P(6) | 116.75(17) |
| | | P(13)-In(9) | 2.540(5) | O(46)-In(9)-P(13) | 103.1(4) |
| | | | | P(5)-In(9)-P(13) | 114.85(19) |
| | | | | P(6)-In(9)-P(13) | 110.73(15) |
| In10 | 6 | O(73)-In(10) | 2.163(11) | O(73)-In(10)-O(78) | 100.8(4) |
| | | C(305)-In(10) | 2.706(15) | O(73)-In(10)-O(89) | 84.9(5) |
| | | O(77)-In(10) | 2.472(13) | O(78)-In(10)-O(89) | 77.4(5) |
| | | O(78)-In(10) | 2.203(12) | O(73)-In(10)-O(77) | 155.5(4) |
| | | O(89)-In(10) | 2.271(11) | O(78)-In(10)-O(77) | 54.8(4) |
| | | P(9)-In(10) | 2.587(4) | O(89)-In(10)-O(77) | 87.6(5) |
| | | P(13)-In(10) | 2.507(4) | O(73)-In(10)-P(13) | 103.1(3) |
| | | | | O(78)-In(10)-P(13) | 150.4(3) |
| | | | | O(89)-In(10)-P(13) | 87.7(3) |
| | | | | O(77)-In(10)-P(13) | 99.8(3) |
| | | | | O(73)-In(10)-P(9) | 90.8(3) |
| | | | | O(78)-In(10)-P(9) | 91.6(3) |
| | | | | O(89)-In(10)-P(9) | 167.1(3) |
| | | | | O(77)-In(10)-P(9) | 91.5(3) |
| | | | | P(13)-In(10)-P(9) | 105.10(13) |
| | | | | O(73)-In(10)-C(305) | 127.8(4) |
| | | | | O(78)-In(10)-C(305) | 27.0(3) |
| | | | | O(89)-In(10)-C(305) | 82.1(6) |
| | | | | O(77)-In(10)-C(305) | 27.8(3) |
| | | | | P(13)-In(10)-C(305) | 126.4(3) |
| | | | | P(9)-In(10)-C(305) | 91.1(4) |
| In11 | 4 | O(13)-In(11) | 2.140(10) | O(13)-In(11)-P(1) | 109.1(3) |
| | | P(1)-In(11) | 2.524(4) | O(13)-In(11)-P(3) | 104.3(3) |
| | | P(3)-In(11) | 2.535(4) | P(1)-In(11)-P(3) | 111.67(13) |
| | | P(12)-In(11) | 2.536(5) | O(13)-In(11)-P(12) | 113.1(3) |
| | | | | P(1)-In(11)-P(12) | 106.05(13) |
| | | | | P(3)-In(11)-P(12) | 112.77(16) |

| | | | | | |
|---|---|---|---|---|---|
| In12 | 4 | O(38)-In(12) | 2.113(11) | O(38)-In(12)-P(14) | 94.9(3) |
| | | P(1)-In(12) | 2.517(4) | O(38)-In(12)-P(1) | 111.7(4) |
| | | P(11)-In(12) | 2.573(4) | P(14)-In(12)-P(1) | 115.53(13) |
| | | P(14)-In(12) | 2.515(4) | O(38)-In(12)-P(11) | 119.3(4) |
| | | | | P(14)-In(12)-P(11) | 109.51(14) |
| | | | | P(1)-In(12)-P(11) | 106.06(13) |
| In13 | 4 | P(12)-In(13) | 2.534(4) | P(15)-In(13)-P(14) | 119.88(15) |
| | | P(14)-In(13) | 2.511(5) | P(15)-In(13)-P(12) | 113.83(14) |
| | | P(15)-In(13) | 2.511(5) | P(14)-In(13)-P(12) | 114.77(16) |
| | | P(17)-In(13) | 2.536(4) | P(15)-In(13)-P(17) | 97.73(14) |
| | | | | P(14)-In(13)-P(17) | 104.02(13) |
| | | | | P(12)-In(13)-P(17) | 102.57(13) |
| In14 | 4 | O(59)-In(14) | 2.137(12) | O(59)-In(14)-P(10) | 96.8(3) |
| | | P(1)-In(14) | 2.521(4) | O(59)-In(14)-P(2) | 119.1(4) |
| | | P(2)-In(14) | 2.521(5) | P(10)-In(14)-P(2) | 114.81(14) |
| | | P(10)-In(14) | 2.518(4) | O(59)-In(14)-P(1) | 110.5(3) |
| | | | | P(10)-In(14)-P(1) | 104.93(14) |
| | | | | P(2)-In(14)-P(1) | 109.38(14) |
| In15 | 4 | P(4)-In(15) | 2.543(4) | P(16)-In(15)-P(20) | 111.67(14) |
| | | P(16)-In(15) | 2.523(4) | P(16)-In(15)-P(17) | 106.25(13) |
| | | P(17)-In(15) | 2.538(4) | P(20)-In(15)-P(17) | 101.85(15) |
| | | P(20)-In(15) | 2.529(5) | P(16)-In(15)-P(4) | 113.45(14) |
| | | | | P(20)-In(15)-P(4) | 116.65(14) |
| | | | | P(17)-In(15)-P(4) | 105.50(14) |
| In16 | 6 | O(33)-In(16) | 2.169(13) | O(33)-In(16)-O(36) | 89.9(5) |
| | | C(137)-In(16) | 2.524(16) | O(33)-In(16)-O(37) | 82.7(5) |
| | | O(35)-In(16) | 2.256(15) | O(36)-In(16)-O(37) | 90.7(5) |
| | | O(36)-In(16) | 2.190(14) | O(33)-In(16)-O(97) | 99.6(5) |
| | | O(37)-In(16) | 2.197(12) | O(36)-In(16)-O(97) | 81.5(6) |
| | | O(97)-In(16) | 2.210(13) | O(37)-In(16)-O(97) | 171.8(5) |
| | | P(10)-In(16) | 2.474(5) | O(33)-In(16)-O(35) | 149.8(5) |
| | | | | O(36)-In(16)-O(35) | 60.5(4) |
| | | | | O(37)-In(16)-O(35) | 91.0(6) |
| | | | | O(97)-In(16)-O(35) | 83.0(6) |
| | | | | O(33)-In(16)-P(10) | 95.6(4) |
| | | | | O(36)-In(16)-P(10) | 173.5(4) |
| | | | | O(37)-In(16)-P(10) | 93.5(3) |
| | | | | O(97)-In(16)-P(10) | 94.1(4) |
| | | | | O(35)-In(16)-P(10) | 114.3(4) |

| | | | | | |
|---|---|---|---|---|---|
| | | | | O(33)-In(16)-C(137) | 120.5(5) |
| | | | | O(36)-In(16)-C(137) | 30.7(4) |
| | | | | O(37)-In(16)-C(137) | 92.6(7) |
| | | | | O(97)-In(16)-C(137) | 79.4(7) |
| | | | | O(35)-In(16)-C(137) | 30.0(3) |
| | | | | P(10)-In(16)-C(137) | 143.9(4) |
| In17 | 5 | O(16)-In(17) | 2.136(11) | O(21)-In(17)-O(16) | 108.5(4) |
| | | O(18)-In(17) | 2.262(12) | O(21)-In(17)-O(24) | 85.4(5) |
| | | O(21)-In(17) | 2.127(11) | O(16)-In(17)-O(24) | 91.1(5) |
| | | O(24)-In(17) | 2.179(13) | O(21)-In(17)-O(18) | 84.9(5) |
| | | P(12)-In(17) | 2.465(3) | O(16)-In(17)-O(18) | 79.6(5) |
| | | | | O(24)-In(17)-O(18) | 163.7(4) |
| | | | | O(21)-In(17)-P(12) | 126.4(3) |
| | | | | O(16)-In(17)-P(12) | 123.0(3) |
| | | | | O(24)-In(17)-P(12) | 105.8(3) |
| | | | | O(18)-In(17)-P(12) | 90.5(3) |
| In18 | 4 | P(11)-In(18) | 2.535(5) | P(17)-In(18)-P(19) | 98.40(13) |
| | | P(17)-In(18) | 2.507(4) | P(17)-In(18)-P(18) | 103.83(13) |
| | | P(18)-In(18) | 2.526(4) | P(19)-In(18)-P(18) | 111.91(14) |
| | | P(19)-In(18) | 2.509(4) | P(17)-In(18)-P(11) | 103.76(13) |
| | | | | P(19)-In(18)-P(11) | 117.89(16) |
| | | | | P(18)-In(18)-P(11) | 117.48(13) |
| In19 | 6 | O(61)-In(19) | 2.130(11) | O(61)-In(19)-O(92) | 93.5(5) |
| | | O(69)-In(19) | 2.331(10) | O(61)-In(19)-O(81) | 87.9(4) |
| | | C(321)-In(19) | 2.592(11) | O(92)-In(19)-O(81) | 143.1(4) |
| | | O(81)-In(19) | 2.258(10) | O(61)-In(19)-O(82) | 87.0(4) |
| | | O(82)-In(19) | 2.266(11) | O(92)-In(19)-O(82) | 85.2(4) |
| | | O(92)-In(19) | 2.248(11) | O(81)-In(19)-O(82) | 58.0(3) |
| | | P(9)-In(19) | 2.488(4) | O(61)-In(19)-O(69) | 83.0(4) |
| | | | | O(92)-In(19)-O(69) | 127.4(4) |
| | | | | O(81)-In(19)-O(69) | 89.3(4) |
| | | | | O(82)-In(19)-O(69) | 146.2(4) |
| | | | | O(61)-In(19)-P(9) | 160.5(3) |
| | | | | O(92)-In(19)-P(9) | 83.9(3) |
| | | | | O(81)-In(19)-P(9) | 105.8(3) |
| | | | | O(82)-In(19)-P(9) | 112.0(3) |
| | | | | O(69)-In(19)-P(9) | 83.3(3) |
| | | | | O(61)-In(19)-C(321) | 86.4(5) |
| | | | | O(92)-In(19)-C(321) | 114.3(4) |
| | | | | O(81)-In(19)-C(321) | 29.0(3) |

| | | | | | |
|---|---|---|---|---|---|
| | | | | O(82)-In(19)-C(321) | 29.1(3) |
| | | | | O(69)-In(19)-C(321) | 117.8(4) |
| | | | | P(9)-In(19)-C(321) | 112.3(4) |
| In20 | 5 | O(31)-In(20) | 2.187(13) | O(66)-In(20)-O(31) | 77.0(5) |
| | | O(66)-In(20) | 2.142(12) | O(66)-In(20)-O(75) | 88.7(5) |
| | | O(75)-In(20) | 2.201(12) | O(31)-In(20)-O(75) | 101.4(5) |
| | | P(4)-In(20) | 2.554(5) | O(66)-In(20)-P(4) | 94.6(4) |
| | | P(6)-In(20) | 2.621(5) | O(31)-In(20)-P(4) | 148.0(4) |
| | | | | O(75)-In(20)-P(4) | 109.4(3) |
| | | | | O(66)-In(20)-P(6) | 161.4(4) |
| | | | | O(31)-In(20)-P(6) | 87.4(4) |
| | | | | O(75)-In(20)-P(6) | 84.5(4) |
| | | | | P(4)-In(20)-P(6) | 103.96(15) |
| In21 | 5 | O(11)-In(21) | 2.237(11) | O(20)-In(21)-O(34) | 93.4(4) |
| | | O(20)-In(21) | 2.095(11) | O(20)-In(21)-O(11) | 84.3(5) |
| | | O(26)-In(21) | 2.272(11) | O(34)-In(21)-O(11) | 89.7(5) |
| | | O(34)-In(21) | 2.133(11) | O(20)-In(21)-O(26) | 87.4(5) |
| | | P(11)-In(21) | 2.476(4) | O(34)-In(21)-O(26) | 89.0(5) |
| | | | | O(11)-In(21)-O(26) | 171.5(4) |
| | | | | O(20)-In(21)-P(11) | 148.7(3) |
| | | | | O(34)-In(21)-P(11) | 117.2(3) |
| | | | | O(11)-In(21)-P(11) | 101.3(3) |
| | | | | O(26)-In(21)-P(11) | 86.8(3) |
| In22 | 5 | O(11)-In(21) | 2.237(11) | O(85)-In(22)-O(90) | 99.1(6) |
| | | O(20)-In(21) | 2.095(11) | O(85)-In(22)-O(87) | 85.9(5) |
| | | O(26)-In(21) | 2.272(11) | O(90)-In(22)-O(87) | 85.5(5) |
| | | O(34)-In(21) | 2.133(11) | O(85)-In(22)-O(84) | 83.9(5) |
| | | P(11)-In(21) | 2.476(4) | O(90)-In(22)-O(84) | 92.1(5) |
| | | | | O(87)-In(22)-O(84) | 169.0(5) |
| | | | | O(85)-In(22)-P(13) | 152.6(4) |
| | | | | O(90)-In(22)-P(13) | 107.5(4) |
| | | | | O(87)-In(22)-P(13) | 102.4(4) |
| | | | | O(84)-In(22)-P(13) | 88.5(3) |
| In23 | 6 | C(217)-In(23) | 2.46(2) | O(57)-In(23)-O(55) | 95.5(8) |
| | | O(55)-In(23) | 2.18(3) | O(57)-In(23)-O(56) | 93.0(9) |
| | | O(56)-In(23) | 2.20(2) | O(55)-In(23)-O(56) | 60.7(6) |
| | | O(57)-In(23) | 2.112(12) | O(57)-In(23)-O(86) | 84.4(6) |
| | | O(60)-In(23) | 2.328(13) | O(55)-In(23)-O(86) | 136.3(7) |
| | | O(86)-In(23) | 2.321(14) | O(56)-In(23)-O(86) | 75.6(6) |

| | | | | | |
|---|---|---|---|---|---|
| | | P(3)-In(23) | 2.470(5) | O(57)-In(23)-O(60) | 83.4(5) |
| | | | | O(55)-In(23)-O(60) | 87.9(7) |
| | | | | O(56)-In(23)-O(60) | 148.0(7) |
| | | | | O(86)-In(23)-O(60) | 135.1(5) |
| | | | | O(57)-In(23)-P(3) | 153.6(3) |
| | | | | O(55)-In(23)-P(3) | 108.0(8) |
| | | | | O(56)-In(23)-P(3) | 108.8(8) |
| | | | | O(86)-In(23)-P(3) | 86.7(4) |
| | | | | O(60)-In(23)-P(3) | 85.5(4) |
| | | | | C(217)-In(23)-P(3) | 116.4(10) |
| | | | | O(57)-In(23)-C(217) | 90.0(11) |
| | | | | O(55)-In(23)-C(217) | 30.6(4) |
| | | | | O(56)-In(23)-C(217) | 30.8(4) |
| | | | | O(86)-In(23)-C(217) | 105.9(6) |
| | | | | O(60)-In(23)-C(217) | 117.2(7) |
| In24 | 6 | O(23)-In(24) | 2.178(13) | O(30)-In(24)-O(23) | 87.8(5) |
| | | C(105)-In(24) | 2.586(14) | O(30)-In(24)-O(28) | 98.3(5) |
| | | O(27)-In(24) | 2.274(13) | O(23)-In(24)-O(28) | 81.5(5) |
| | | O(28)-In(24) | 2.230(13) | O(30)-In(24)-O(27) | 156.3(5) |
| | | O(30)-In(24) | 2.172(13) | O(23)-In(24)-O(27) | 86.2(6) |
| | | O(32)-In(24) | 2.282(14) | O(28)-In(24)-O(27) | 58.2(4) |
| | | P(5)-In(24) | 2.503(5) | O(30)-In(24)-O(32) | 79.6(5) |
| | | | | O(23)-In(24)-O(32) | 160.8(5) |
| | | | | O(28)-In(24)-O(32) | 85.9(5) |
| | | | | O(27)-In(24)-O(32) | 99.6(6) |
| | | | | O(30)-In(24)-P(5) | 103.0(3) |
| | | | | O(23)-In(24)-P(5) | 105.8(4) |
| | | | | O(28)-In(24)-P(5) | 157.7(4) |
| | | | | O(27)-In(24)-P(5) | 100.7(3) |
| | | | | O(32)-In(24)-P(5) | 91.3(3) |
| | | | | O(30)-In(24)-C(105) | 127.3(5) |
| | | | | O(23)-In(24)-C(105) | 82.2(7) |
| | | | | O(28)-In(24)-C(105) | 29.1(3) |
| | | | | O(27)-In(24)-C(105) | 29.1(3) |
| | | | | O(32)-In(24)-C(105) | 93.9(7) |
| | | | | P(5)-In(24)-C(105) | 129.6(4) |
| In25 | 5 | O(58)-In(25) | 2.268(10) | O(83)-In(25)-O(74) | 84.5(4) |
| | | O(74)-In(25) | 2.208(9) | O(83)-In(25)-O(99) | 93.4(8) |
| | | O(83)-In(25) | 2.131(11) | O(74)-In(25)-O(99) | 90.8(7) |
| | | O(99)-In(25) | 2.23(2) | O(83)-In(25)-O(58) | 86.1(5) |
| | | P(2)-In(25) | 2.487(4) | O(74)-In(25)-O(58) | 170.1(4) |

| | | | | | |
|---|---|---|---|---|---|
| | | | | O(99)-In(25)-O(58) | 86.7(7) |
| | | | | O(83)-In(25)-P(2) | 151(3) |
| | | | | O(74)-In(25)-P(2) | 102.2(3) |
| | | | | O(99)-In(25)-P(2) | 114.4(7) |
| | | | | O(58)-In(25)-P(2) | 87.5(3) |
| In26 | 6 | O(45)-In(26) | 2.247(15) | O(91)-In(26)-O(79) | 89.2(5) |
| | | O(77)-In(26) | 2.240(12) | O(91)-In(26)-O(77) | 94.7(5) |
| | | C(313)-In(26) | 2.562(14) | O(79)-In(26)-O(77) | 149.8(5) |
| | | O(79)-In(26) | 2.239(13) | O(91)-In(26)-O(45) | 159.2(5) |
| | | O(80)-In(26) | 2.255(13) | O(79)-In(26)-O(45) | 88.7(6) |
| | | O(91)-In(26) | 2.181(14) | O(77)-In(26)-O(45) | 77.2(5) |
| | | P(6)-In(26) | 2.515(5) | O(91)-In(26)-O(80) | 81.6(5) |
| | | | | O(79)-In(26)-O(80) | 58.6(4) |
| | | | | O(77)-In(26)-O(80) | 92.3(5) |
| | | | | O(45)-In(26)-O(80) | 79.6(6) |
| | | | | O(91)-In(26)-P(6) | 103.5(4) |
| | | | | O(79)-In(26)-P(6) | 105.9(3) |
| | | | | O(77)-In(26)-P(6) | 102.3(3) |
| | | | | O(45)-In(26)-P(6) | 97.0(4) |
| | | | | O(80)-In(26)-P(6) | 164.0(4) |
| | | | | O(91)-In(26)-C(313) | 83.5(6) |
| | | | | O(79)-In(26)-C(313) | 29.1(3) |
| | | | | O(77)-In(26)-C(313) | 121.7(5) |
| | | | | O(45)-In(26)-C(313) | 84.7(7) |
| | | | | O(80)-In(26)-C(313) | 29.6(3) |
| | | | | P(6)-In(26)-C(313) | 135.0(4) |
| In27 | 6 | C(169)-In(27) | 2.595(13) | O(100)-In(27)-O(72) | 85.4(10) |
| | | O(43)-In(27) | 2.220(13) | O(100)-In(27)-O(43) | 155.1(11) |
| | | O(44)-In(27) | 2.250(12) | O(72)-In(27)-O(43) | 93.0(5) |
| | | O(72)-In(27) | 2.218(11) | O(100)-In(27)-O(98) | 89.3(10) |
| | | O(98)-In(27) | 2.231(13) | O(72)-In(27)-O(98) | 170.4(4) |
| | | O(100)-In(27) | 2.19(3) | O(43)-In(27)-O(98) | 88.4(5) |
| | | P(10)-In(27) | 2.487(4) | O(100)-In(27)-O(44) | 97.5(10) |
| | | | | O(72)-In(27)-O(44) | 91.7(5) |
| | | | | O(43)-In(27)-O(44) | 57.7(4) |
| | | | | O(98)-In(27)-O(44) | 81.0(5) |
| | | | | O(100)-In(27)-P(10) | 97.6(10) |
| | | | | O(72)-In(27)-P(10) | 90.7(3) |
| | | | | O(43)-In(27)-P(10) | 107.2(4) |
| | | | | O(98)-In(27)-P(10) | 98.0(4) |
| | | | | O(44)-In(27)-P(10) | 164.9(4) |

| | | | | | |
|---|---|---|---|---|---|
| | | | | O(100)-In(27)-C(169) | 126.4(10) |
| | | | | O(72)-In(27)-C(169) | 94.4(6) |
| | | | | O(43)-In(27)-C(169) | 28.9(3) |
| | | | | O(98)-In(27)-C(169) | 82.2(7) |
| | | | | O(44)-In(27)-C(169) | 28.9(3) |
| | | | | P(10)-In(27)-C(169) | 136.0(4) |
| In28 | 6 | O(1)-In(28) | 2.185(11) | O(12)-In(28)-O(1) | 105.4(4) |
| | | O(2)-In(28) | 2.561(11) | O(12)-In(28)-O(10) | 76.5(7) |
| | | O(10)-In(28) | 2.27(2) | O(1)-In(28)-O(10) | 77.5(8) |
| | | O(12)-In(28) | 2.181(11) | O(12)-In(28)-P(19) | 103.1(3) |
| | | P(14)-In(28) | 2.596(4) | O(1)-In(28)-P(19) | 146.5(3) |
| | | P(19)-In(28) | 2.521(5) | O(10)-In(28)-P(19) | 92.5(7) |
| | | | | O(12)-In(28)-O(2) | 159.2(4) |
| | | | | O(1)-In(28)-O(2) | 53.7(3) |
| | | | | O(10)-In(28)-O(2) | 96.4(7) |
| | | | | P(19)-In(28)-O(2) | 96.8(3) |
| | | | | O(12)-In(28)-P(14) | 90.5(3) |
| | | | | O(1)-In(28)-P(14) | 92.2(3) |
| | | | | O(10)-In(28)-P(14) | 160.3(6) |
| | | | | P(19)-In(28)-P(14) | 104.93(14) |
| | | | | O(2)-In(28)-P(14) | 90.7(3) |
| In29 | 5 | O(22)-In(29) | 2.206(12) | O(48)-In(29)-O(29) | 76.0(5) |
| | | O(29)-In(29) | 2.188(12) | O(48)-In(29)-O(22) | 102.9(5) |
| | | O(48)-In(29) | 2.144(12) | O(29)-In(29)-O(22) | 89.3(5) |
| | | P(4)-In(29) | 2.544(4) | O(48)-In(29)-P(4) | 147.2(4) |
| | | P(15)-In(29) | 2.624(5) | O(29)-In(29)-P(4) | 94.3(3) |
| | | | | O(22)-In(29)-P(4) | 108.3(3) |
| | | | | O(48)-In(29)-P(15) | 87.1(4) |
| | | | | O(29)-In(29)-P(15) | 160.4(3) |
| | | | | O(22)-In(29)-P(15) | 85.0(3) |
| | | | | P(4)-In(29)-P(15) | 105.26(13) |
| In30 | 4 | O(63)-In(30) | 2.150(12) | O(63)-In(30)-P(15) | 108.4(4) |
| | | P(15)-In(30) | 2.505(4) | O(63)-In(30)-P(20) | 99.7(4) |
| | | P(19)-In(30) | 2.537(5) | P(15)-In(30)-P(20) | 113.89(15) |
| | | P(20)-In(30) | 2.510(5) | O(63)-In(30)-P(19) | 108.0(4) |
| | | | | P(15)-In(30)-P(19) | 110.64(16) |
| | | | | P(20)-In(30)-P(19) | 115.31(14) |
| In31 | 5 | O(40)-In(31) | 2.21(4) | O(76)-In(31)-O(68) | 108.8(5) |

| | | | | | |
|---|---|---|---|---|---|
| | | O(62)-In(31) | 2.241(12) | O(76)-In(31)-O(40) | 85.4(12) |
| | | O(68)-In(31) | 2.135(13) | O(68)-In(31)-O(40) | 93.3(11) |
| | | O(76)-In(31) | 2.126(12) | O(76)-In(31)-O(62) | 84.0(5) |
| | | P(16)-In(31) | 2.450(5) | O(68)-In(31)-O(62) | 80.8(5) |
| | | | | O(40)-In(31)-O(62) | 165.5(11) |
| | | | | O(76)-In(31)-P(16) | 119.6(4) |
| | | | | O(68)-In(31)-P(16) | 129.3(4) |
| | | | | O(40)-In(31)-P(16) | 103.9(10) |
| | | | | O(62)-In(31)-P(16) | 90.0(4) |
| In32 | 6 | O(3)-In(32) | 2.267(11) | O(17)-In(32)-O(3) | 87.3(4) |
| | | C(17)-In(32) | 2.623(14) | O(17)-In(32)-O(5) | 87.4(5) |
| | | O(5)-In(32) | 2.271(12) | O(3)-In(32)-O(5) | 83.9(5) |
| | | O(6)-In(32) | 2.278(14) | O(17)-In(32)-O(6) | 84.1(5) |
| | | O(14)-In(32) | 2.292(10) | O(3)-In(32)-O(6) | 140.5(4) |
| | | O(17)-In(32) | 2.130(11) | O(5)-In(32)-O(6) | 57.3(4) |
| | | P(14)-In(32) | 2.494(4) | O(17)-In(32)-O(14) | 83.5(4) |
| | | | | O(3)-In(32)-O(14) | 126.9(4) |
| | | | | O(5)-In(32)-O(14) | 147.1(5) |
| | | | | O(6)-In(32)-O(14) | 90.3(4) |
| | | | | O(17)-In(32)-P(14) | 157.0(3) |
| | | | | O(3)-In(32)-P(14) | 84.9(3) |
| | | | | O(5)-In(32)-P(14) | 113.1(4) |
| | | | | O(6)-In(32)-P(14) | 115.2(4) |
| | | | | O(14)-In(32)-P(14) | 84.1(3) |
| | | | | O(17)-In(32)-C(17) | 86.0(6) |
| | | | | O(3)-In(32)-C(17) | 112.0(5) |
| | | | | O(5)-In(32)-C(17) | 28.2(3) |
| | | | | O(6)-In(32)-C(17) | 29.1(3) |
| | | | | O(14)-In(32)-C(17) | 119.3(5) |
| | | | | P(14)-In(32)-C(17) | 117.0(5) |
| In33 | 6 | O(25)-In(33) | 2.107(11) | O(25)-In(33)-O(41) | 91.9(5) |
| | | C(161)-In(33) | 2.549(13) | O(25)-In(33)-O(42) | 90.8(5) |
| | | O(41)-In(33) | 2.259(13) | O(41)-In(33)-O(42) | 57.8(4) |
| | | O(42)-In(33) | 2.264(12) | O(25)-In(33)-O(54) | 86.6(4) |
| | | O(52)-In(33) | 2.346(11) | O(41)-In(33)-O(54) | 139.6(4) |
| | | O(54)-In(33) | 2.292(10) | O(42)-In(33)-O(54) | 81.8(4) |
| | | P(18)-In(33) | 2.475(4) | O(25)-In(33)-O(52) | 81.8(4) |
| | | | | O(41)-In(33)-O(52) | 82.7(5) |
| | | | | O(42)-In(33)-O(52) | 139.7(4) |
| | | | | O(54)-In(33)-O(52) | 136.6(4) |
| | | | | O(25)-In(33)-P(18) | 153.1(3) |

| | | | | | |
|---|---|---|---|---|---|
| | | | | O(41)-In(33)-P(18) | 110.1(4) |
| | | | | O(42)-In(33)-P(18) | 113.7(4) |
| | | | | O(54)-In(33)-P(18) | 86.2(2) |
| | | | | O(52)-In(33)-P(18) | 85.8(3) |
| | | | | O(25)-In(33)-C(161) | 91.3(5) |
| | | | | O(41)-In(33)-C(161) | 29.3(3) |
| | | | | O(42)-In(33)-C(161) | 28.5(3) |
| | | | | O(54)-In(33)-C(161) | 110.3(4) |
| | | | | O(52)-In(33)-C(161) | 111.7(4) |
| | | | | P(18)-In(33)-C(161) | 115.5(4) |
| In34 | 5 | O(9)-In(34) | 2.17(3) | O(9A)-In(34)-O(51) | 98.5(9) |
| | | O(19)-In(34) | 2.318(12) | O(51)-In(34)-O(9) | 100.5(8) |
| | | O(51)-In(34) | 2.119(11) | O(51)-In(34)-O(96) | 83.9(5) |
| | | O(96)-In(34) | 2.246(13) | O(9)-In(34)-O(96) | 90.4(7) |
| | | P(19)-In(34) | 2.460(4) | O(51)-In(34)-O(19) | 84.4(5) |
| | | | | O(9)-In(34)-O(19) | 89.2(7) |
| | | | | O(96)-In(34)-O(19) | 167.9(5) |
| | | | | O(51)-In(34)-P(19) | 153.3(3) |
| | | | | O(9)-In(34)-P(19) | 105.0(7) |
| | | | | O(96)-In(34)-P(19) | 103.3(4) |
| | | | | O(19)-In(34)-P(19) | 88.4(3) |
| In35 | 6 | O(39)-In(35) | 2.23(4) | O(65)-In(35)-O(50) | 98.6(5) |
| | | O(47)-In(35) | 2.276(14) | O(65)-In(35)-O(39) | 90.0(10) |
| | | C(193)-In(35) | 2.580(15) | O(50)-In(35)-O(39) | 82.6(10) |
| | | O(49)-In(35) | 2.302(14) | O(65)-In(35)-O(47) | 79.7(6) |
| | | O(50)-In(35) | 2.217(13) | O(50)-In(35)-O(47) | 85.6(5) |
| | | O(65)-In(35) | 2.164(14) | O(39)-In(35)-O(47) | 163.0(11) |
| | | P(20)-In(35) | 2.493(5) | O(65)-In(35)-O(49) | 155.7(5) |
| | | | | O(50)-In(35)-O(49) | 57.5(4) |
| | | | | O(39)-In(35)-O(49) | 82.5(10) |
| | | | | O(47)-In(35)-O(49) | 101.3(6) |
| | | | | O(65)-In(35)-P(20) | 104.2(4) |
| | | | | O(50)-In(35)-P(20) | 155.7(4) |
| | | | | O(39)-In(35)-P(20) | 105.4(10) |
| | | | | O(47)-In(35)-P(20) | 90.3(4) |
| | | | | O(49)-In(35)-P(20) | 100.1(4) |
| | | | | O(65)-In(35)-C(193) | 127.0(5) |
| | | | | O(50)-In(35)-C(193) | 28.6(3) |

| | | | | | |
|---|---|---|---|---|---|
| | | | | O(39)-In(35)-C(193) | 80.4(10) |
| | | | | O(47)-In(35)-C(193) | 94.9(7) |
| | | | | O(49)-In(35)-C(193) | 28.9(3) |
| | | | | P(20)-In(35)-C(193) | 128.7(4) |
| In36 | 6 | O(2)-In(36) | 2.218(12) | O(4)-In(36)-O(2) | 96.7(4) |
| | | O(4)-In(36) | 2.167(11) | O(4)-In(36)-O(7) | 86.6(5) |
| | | C(25)-In(36) | 2.567(14) | O(2)-In(36)-O(7) | 150.1(4) |
| | | O(7)-In(36) | 2.233(13) | O(4)-In(36)-O(8) | 81.2(5) |
| | | O(8)-In(36) | 2.252(12) | O(2)-In(36)-O(8) | 92.7(4) |
| | | O(64)-In(36) | 2.258(14) | O(7)-In(36)-O(8) | 58.3(4) |
| | | P(15)-In(36) | 2.508(4) | O(4)-In(36)-O(64) | 160.2(5) |
| | | | | O(2)-In(36)-O(64) | 77.9(5) |
| | | | | O(7)-In(36)-O(64) | 89.0(6) |
| | | | | O(8)-In(36)-O(64) | 80.1(5) |
| | | | | O(4)-In(36)-P(15) | 104.4(3) |
| | | | | O(2)-In(36)-P(15) | 102.1(3) |
| | | | | O(7)-In(36)-P(15) | 105.9(3) |
| | | | | O(8)-In(36)-P(15) | 163.3(4) |
| | | | | O(64)-In(36)-P(15) | 95.4(4) |
| | | | | O(4)-In(36)-C(25) | 80.9(6) |
| | | | | O(2)-In(36)-C(25) | 121.6(5) |
| | | | | O(7)-In(36)-C(25) | 29.4(3) |
| | | | | O(8)-In(36)-C(25) | 29.0(3) |
| | | | | O(64)-In(36)-C(25) | 85.9(6) |
| | | | | P(15)-In(36)-C(25) | 135.3(4) |
| In37 | 6 | O(67)-In(37) | 2.346(14) | O(2B)-In(37)-O(95) | 90.1(10) |
| | | O(95)-In(37) | 2.232(13) | O(101)-In(37)-O(95) | 95.3(8) |
| | | C(401)-In(37) | 2.56(2) | O(101)-In(37)-O(102) | 57.7(6) |
| | | O(101)-In(37) | 2.16(2) | O(95)-In(37)-O(102) | 77.0(7) |
| | | O(102)-In(37) | 2.32(2) | O(101)-In(37)-O(67) | 80.6(9) |
| | | P(18)-In(37) | 2.534(4) | O(95)-In(37)-O(67) | 168.0(5) |
| | | P(20)-In(37) | 2.549(4) | O(102)-In(37)-O(67) | 91.3(7) |
| | | | | O(101)-In(37)-P(18) | 148.1(7) |
| | | | | O(95)-In(37)-P(18) | 95.7(4) |
| | | | | O(102)-In(37)-P(18) | 96.1(5) |
| | | | | O(67)-In(37)-P(18) | 82.4(4) |
| | | | | O(101)-In(37)-P(20) | 105.0(6) |
| | | | | O(95)-In(37)-P(20) | 91.5(3) |
| | | | | O(102)-In(37)-P(20) | 157.4(5) |
| | | | | O(67)-In(37)-P(20) | 100.4(4) |
| | | | | P(18)-In(37)-P(20) | 104.51(14) |

| | |
|---|---|
| O(101)-In(37)-C(401) | 29.1(4) |
| O(95)-In(37)-C(401) | 81.0(9) |
| O(102)-In(37)-C(401) | 29.5(4) |
| O(67)-In(37)-C(401) | 90.3(9) |
| P(18)-In(37)-C(401) | 125.1(6) |
| P(20)-In(37)-C(401) | 130.2(6) |

Table 5.2 Crystal data and structure refinement specifics for $In_{37}P_{20}(O_2CCH_2Ph)_{51}$ and $In_{37}P_{20}(O_2CCH_2Ph)_{51}(H_2O)$.

| Crystallographic information | | |
|---|---|---|
| Compound | $In_{37}P_{20}(O_2CCH_2Ph)_{51}$ | $In_{37}P_{20}(O_2CCH_2Ph)_{51}(H_2O)$ |
| Empirical formula | C408 H357 In37 O102 P20 | C408 H359 In37 O103 P20 |
| Formula weight | 11759.65 | 11775.68 |
| Temperature | 100(2) K | 100(2) K |
| Wavelength | 0.71073 Å | 0.71073 Å |
| Crystal system | Triclinic | Triclinic |
| Space group | P -1 | P -1 |
| Unit cell dimensions | a = 24.2059(13) Å | a = 23.5228(11) Å |
| | b = 25.0500(11) Å | b = 24.1862(12) Å |
| | c = 42.7930(19) Å | c = 43.0370(19) Å |
| | α = 94.394(3)° | α = 84.905(3)°. |
| | β = 91.966(3)° | β = 88.006(3)°. |
| | γ = 115.651(2)° | γ = 63.079(3)°. |
| Volume | 23256(2) Å3 | 21744.9(18) Å3 |
| Z | 2 | 2 |
| Density (calculated) | 1.679 Mg/m3 | 1.799 Mg/m3 |
| Absorption coefficient | 1.933 mm-1 | 2.067 mm-1 |
| F(000) | 11468 | 11488 |
| Crystal size | 0.300 x 0.190 x 0.180 mm3 | 0.19 x 0.15 x 0.15 mm3 |
| Theta range for data collection | 1.383 to 25.350°. | 1.63 to 25.47°. |
| Index ranges | -29<=h<=29, -30<=k<=30, -51<=l<=51 | -28<=h<=28, -29<=k<=29, -51<=l<=51 |
| Reflections collected | 382918 | 254930 |
| Independent reflections | 84779 [R(int) = 0.0785] | 80158 [R(int) = 0.0708] |
| Completeness to theta = 25.000° | 99.50% | 99.97% |
| Absorption correction | Semi-empirical from equivalents | |
| Max. and min. transmission | 0.722 and 0.595 | 0.7468 and 0.6948 |
| Refinement method | Full-matrix least-squares on F2 | Full-matrix least-squares on F2 |
| Data / restraints / parameters | 84779 / 58044 / 5798 | 80008 / 34585 / 4771 |
| Goodness-of-fit on F2 | 1.133 | 1.329 |

| | | |
|---|---|---|
| Final R indices [I>2sigma(I)] | R1 = 0.1109, wR2 = 0.2992 | R1 = 0.1283, wR2 = 0.3359 |
| R indices (all data) | R1 = 0.1790, wR2 = 0.3499 | R1 = 0.1935, wR2 = 0.3771 |
| Largest diff. peak and hole | 4.011 and -1.679 e.Å-3 | 7.109 and -1.793 e.Å-3 |

## 5.6 NOTES TO THE CHAPTER


1. Adapted with permission from (D. C. Gary, S. E. Flowers, W. Kaminsky, A. Petrone, X. Li and B. M. Cossairt, *J. Am. Chem. Soc.*, 2016, **138**, 1510-1513.). Copyright (2016) American Chemical Society.
2. R. R. Lunt, T. P. Osedach, P. R. Brown, J. A. Rowehl and V. Bulović, *Adv. Mater.*, 2011, **23**, 5712-5727.
3. Y. Shirasaki, G. J. Supran, M. G. Bawendi and V. Bulović, *Nature Photon.*, 2013, **7**, 13-23.
4. T. Vossmeyer, G. Reck, L. Katsikas, E. T. K. Haupt, B. Schulz and H. Weller, *Science*, 1995, **267**, 1476-1479.
5. N. Herron, J. C. Calabrese, W. E. Farneth and Y. Wang, *Science*, 1993, **259**, 1426-1428.
6. H. Schnockel, *Chem. Rev.*, 2010, **110**, 4125-4163.
7. J. F. Corrigan and M. W. DeGroot, in *The Chemistry of Nanomaterials: Synthesis, Properties and Applications*, eds. C. N. R. Rao, A. Muller and A. K. Cheetham, Wiley-VCH, Weinheim, 2004, vol. 2, ch. 13, pp. 418-451.
8. J. G. Brennan, T. Siegrist, S. M. Stuczynski and M. L. Steigerwald, *J. Am. Chem. Soc.*, 1989, **111**, 9241-9242.
9. A. N. Beecher, X. Yang, J. H. Palmer, A. L. LaGrassa, P. Juhas, S. J. L. Billinge and J. S. Owen, *J. Am. Chem. Soc.*, 2014, **136**, 10645-10653.
10. P. D. Jadzinsky, G. Calero, C. J. Ackerson, D. A. Bushnell and R. D. Kornberg, *Science*, 2007, **318**, 430-433.
11. J. R. McBride, A. D. I. Dukes, M. A. Schreuder and S. J. Rosenthal, *Chem. Phys. Lett.*, 2010, **498**, 1-9.
12. C. Evans, L. Guo, J. Peterson, S. Maccagnano-Zacher and T. Krauss, *Nano Lett.*, 2008, **8**, 2896-2899.
13. D. C. Gary, M. Terban, S. J. L. Billinge and B. M. Cossairt, *Chem. Mater.*, 2015, **27**, 1432-1441.
14. S. Kudera, M. Zanella, C. Giannini, A. Rizzo, Y. Li, G. Gigli, R. Cingolani, G. Ciccarella, W. Spahl, W. J. Parak and L. Manna, *Adv. Mater.*, 2007, **19**, 548-552.
15. Y. Wang, Y. Zhang, F. Wang, D. E. Giblin, J. Hoy, H. W. Rohrs, R. A. Loomis and W. E. Buhro, *Chem. Mater.*, 2014, **26**, 2233-2243.
16. Q. Yu and C.-Y. Liu, *J. Phys. Chem. C*, 2009, **113**, 12766-12771.
17. J. Zhang, C. Rowland, Y. Liu, H. Xiong, S. Kwon, E. Shevchenko, R. D. Schaller, V. B. Prakapenka, S. Tkachev and T. Rajh, *J. Am. Chem. Soc.*, 2015, **137**, 742-749.
18. A. Kasuya, R. Sivamohan, Y. A. Barnakov, I. M. Dmitruk, T. Nirasawa, V. R. Romanyuk, V. Kumar, S. V. Mamykin, K. Tohji, B. Jeyadevan, K. Shinoda, T. Kudo, O. Terasaki, Z. Liu, R. V. Belosludov, V. Sundararajan and Y. Kawazoe, *Nature Mater.*, 2004, **3**, 99-102.

19. E. Chan, C. Xu, A. Mao, G. Han, J. Owen, B. Cohen and D. Milliron, *Nano Lett.*, 2010, **10**, 1874-1885.
20. M. D. Clark, S. K. Kumar, J. S. Owen and E. M. Chan, *Nano Lett.*, 2011, **11**, 1976-1980.
21. M. P. Hendricks, M. P. Campos, G. T. Cleveland, I. Jen-La Plante and J. S. Owen, *Science*, 2015, **348**, 1226-1230.
22. M. P. Hendricks, B. M. Cossairt and J. S. Owen, *ACS Nano*, 2012, **6**, 10054-10062.
23. D. C. Gary, B. A. Glassy and B. M. Cossairt, *Chem. Mater.*, 2014, **26**, 1734–1744.
24. D. Franke, D. H. Harris, L. Xie, K. F. Jensen and M. G. Bawendi, *Angew. Chem., Int. Ed.*, 2015, **54**, 14299-14503.
25. R. Xie, Z. Li and X. Peng, *J. Am. Chem. Soc.*, 2009, **131**, 15457-15466.
26. R. Xie and X. Peng, *Angew. Chem., Int. Ed.*, 2008, **47**, 7677-7680.
27. C. B. Murray, C. R. Kagan and M. G. Bawendi, *Annu. Rev. Mater. Sci.*, 2000, **30**, 545-610.
28. J. S. Owen, *Science*, 2015, **347**, 615-616.
29. J. S. Owen, J. Park, P.-E. Trudeau and A. P. Alivisatos, *J. Am. Chem. Soc.*, 2008, **130**, 12279-12281.
30. S. Adachi, *Properties of Group-IV, III-V and II-VI Semiconductors*, John Wiley & Sons, West Sussex, 2005.
31. P. Pyykkö and M. Atsumi, *Chem. Eur. J.*, 2009, **15**, 186-197.
32. A. Cros-Gagneux, F. Delpech, C. Nayral, A. Cornejo, Y. Coppel and B. Chaudret, *J. Am. Chem. Soc.*, 2010, **132**, 18147-18157.
33. B. M. Cossairt and J. S. Owen, *Chem. Mater.*, 2011, **23**, 3114-3119.
34. M. V. Kovalenko, M. Scheele and D. V. Talapin, *Science*, 2009, **324**, 1417-1420.
35. X. Lan, S. Masala and E. H. Sargent, *Nature Mater.*, 2014, **13**, 233-240.
36. W. B. Jennings, N. J. P. McCarthy, P. Kelly and J. F. Malone, *Org. Biomol. Chem.*, 2009, **7**, 5156-5162.
37. D. C. Gary and B. M. Cossairt, *Chem. Mater.*, 2013, **25**, 2463-2469.

# BIBLIOGRAPHY


Annual Energy Review 2009; U.S. Energy Information Administration: Washington, DC, **2010**; Tables 12.2–12.4, pp 349– 353.

S. Adachi, *Properties of Group-IV, III-V and II-VI Semiconductors*, John Wiley & Sons, West Sussex, 2005.

F. H. Allen, *Acta. Cryst.*, 2002, **58**, 380-388.

T. L. Amyes, S. T. Diver, J. P. Richard, F. M. Rivas and K. Toth, *J. Am. Chem. Soc.*, 2004, **126**, 4366-4374.

R. Angamuthu, P. Byers, M. Lutz, A. L. Spek and E. Bouwman, *Science*, 2010, **327**, 313-315.

A. M. Appel, J. E. Bercaw, A. B. Bocarsly, H. Dobbek, D. L. DuBois, M. Dupuis, J. G. Ferry, E. Fujita, R. Hille, P. J. A. Kenis, C. A. Kerfeld, R. H. Morris, C. H. F. Peden, A. R. Portis, S. W. Ragsdale, T. B. Rauchfuss, J. N. H. Reek, L. C. Seefeldt, R. K. Thauer and G. L. Waldrop, *Chem. Rev.*, 2013, **113**, 6621-6658.

K. Araki, S. Kuwata and T. Ikariya, *Organometallics*, 2008, **27**, 2176-2178.

A. J. Arduengo, H. V. R. Dias, J. C. Calabrese and F. Davidson, *Organometallics*, 1993, **12**, 3405-3409.

M. Aresta, A. Dibenedetto and I. Tommasi, *Eur. J. Inorg. Chem.*, 2001, **2001**, 1801-1806.

Y. Arikawa, T. Asayama, Y. Moriguchi, S. Agari and M. Onishi, *J. Am. Chem. Soc.*, 2007, **129**, 14160-14161.

L. Barelli, G. Bidini, F. Gallorini and S. Servili, *Energy*, 2008, **33**, 554-570.

E. Becker, S. Pavlik and K. Kirchner, *Adv. Organomet. Chem.*, 2008, **56**, 155-197.

A. N. Beecher, X. Yang, J. H. Palmer, A. L. LaGrassa, P. Juhas, S. J. L. Billinge and J. S. Owen, *J. Am. Chem. Soc.*, 2014, **136**, 10645-10653.

M. A. Bennett and A. K. Smith, *J. Chem. Soc., Dalton Trans.*, 1974, 233-241.

I. Bhugun, D. Lexa and J.-M. Savéant, *J. Am. Chem. Soc.*, 1996, **118**, 1769-1776.

A. Boddien, F. Gärtner, C. Federsel, P. Sponholz, D. Mellmann, R. Jackstell, H. Junge and M. Beller, *Angew. Chem., Int. Ed.*, 2011, **50**, 6411-6414.

F. Bonati, A. Burini, B. R. Pietroni and B. Bovio, *J. Organomet. Chem.*, 1989, **375**, 147-160.

J. G. Brennan, T. Siegrist, S. M. Stuczynski and M. L. Steigerwald, *J. Am. Chem. Soc.*, 1989, **111**, 9241-9242.

M. Brill, J. Díaz, M. A. Huertos, R. López, J. Pérez and L. Riera, *Chem. Eur. J.*, 2011, **17**, 8584-8595.

I. D. Campbell and R. Freeman, *J. Magn. Reson.*, 1973, **11**, 143-162.

K. J. Cavell and D. S. McGuinness, *Coord. Chem. Rev.*, 2004, **248**, 671-681.

S. Chakraborty, O. Blacque and H. Berke, *Dalton Trans.*, 2015, **44**, 6560-6570.

E. Chan, C. Xu, A. Mao, G. Han, J. Owen, B. Cohen and D. Milliron, *Nano Lett.*, 2010, **10**, 1874-1885.

J. T. Chantson and S. Lotz, *J. Organomet. Chem.*, 2004, **689**, 1315-1324.

D. Chatterjee, N. Jaiswal and P. Banerjee, *Eur. J. Inorg. Chem.*, 2014, **2014**, 5856-5859.

Z. Chen, C. Chen, D. R. Weinberg, P. Kang, J. J. Concepcion, D. P. Harrison, M. S. Brookhart and T. J. Meyer, *Chem. Commun.*, 2011, **47**, 12607-12609.
M. D. Clark, S. K. Kumar, J. S. Owen and E. M. Chan, *Nano Lett.*, 2011, **11**, 1976-1980.
J. Coetzee, D. L. Dodds, J. Klankermayer, S. Brosinski, W. Leitner, A. M. Z. Slawin and D. J. Cole-Hamilton, *Chem. Eur. J.*, 2013, **19**, 11039-11050.
E. Barton Cole, P. S. Lakkaraju, D. M. Rampulla, A. J. Morris, E. Abelev and A. B. Bocarsly, *J. Am. Chem. Soc.*, 2010, **132**, 11539-11551.
J. F. Corrigan and M. W. DeGroot, in *The Chemistry of Nanomaterials: Synthesis, Properties and Applications*, eds. C. N. R. Rao, A. Muller and A. K. Cheetham, Wiley-VCH, Weinheim, 2004, vol. 2, ch. 13, pp. 418-451.
B. M. Cossairt and J. S. Owen, *Chem. Mater.*, 2011, **23**, 3114-3119.
A. Cros-Gagneux, F. Delpech, C. Nayral, A. Cornejo, Y. Coppel and B. Chaudret, *J. Am. Chem. Soc.*, 2010, **132**, 18147-18157.
A. F. Dalebrook, W. Gan, M. Grasemann, S. Moret and G. Laurenczy, *Chem. Commun.*, 2013, **49**, 8735-8751.
A. Demonceau, A. W. Stumpf, E. Saive and A. F. Noels, *Macromolecules*, 1997, **30**, 3127-3136.
J. DePasquale, M. Kumar, M. Zeller and E. T. Papish, *Organometallics*, 2013, **32**, 966-979.
S. Díez-González and S. P. Nolan, *Coord. Chem. Rev.*, 2007, **251**, 874-883.
G. E. Dobereiner, C. A. Chamberlin, N. D. Schley and R. H. Crabtree, *Organometallics*, 2010, **29**, 5728-5731.
V. Dragutan, I. Dragutan, L. Delaude and A. Demonceau, *Coord. Chem. Rev.*, 2007, **251**, 765-794.
E. W. Team, "ESRL Global Monitoring Division - Global Greenhouse Gas Reference Network.", web.archive.org/web/20170918142645/http://www.esrl.noaa.gov/gmd/ccgg/trends/full.html, (accessed 26 Nov. 2017).
P. G. Edwards and F. E. Hahn, *Dalton Trans.*, 2011, **40**, 10278-10288.
J. M. C. and H. F. Ekkehardt, *Chem. Lett.*, 2015, **44**, 226-237.
A. S. El-Tabl, M. Mohamed Abd El-Waheed, M. A. Wahba and N. Abd El-Halim Abou El-Fadl, *Bioinorg. Chem. Appl.*, 2015, **2015**, 126023.
C. Evans, L. Guo, J. Peterson, S. Maccagnano-Zacher and T. Krauss, *Nano Lett.*, 2008, **8**, 2896-2899.
P. J. Fagan, M. D. Ward and J. C. Calabrese, *J. Am. Chem. Soc.*, 1989, **111**, 1698-1719.
J. D. Figueroa, T. Fout, S. Plasynski, H. McIlvried and R. D. Srivastava, *Int. J. Greenhouse Gas Control*, 2008, **2**, 9-20.
G. A. Filonenko, M. J. B. Aguila, E. N. Schulpen, R. van Putten, J. Wiecko, C. Müller, L. Lefort, E. J. M. Hensen and E. A. Pidko, *J. Am. Chem. Soc.*, 2015, **137**, 7620-7623.
B. J. Fisher and R. Eisenberg, *J. Am. Chem. Soc.*, 1980, **102**, 7361-7363.
A. Flores-Figueroa, T. Pape, K.-O. Feldmann and F. E. Hahn, *Chem. Commun.*, 2010, **46**, 324-326.
S. E. Flowers and B. M. Cossairt, *Organometallics*, 2014, **33**, 4341-4344.

N. A. Foley, M. Lail, J. P. Lee, T. B. Gunnoe, T. R. Cundari and J. L. Petersen, *J. Am. Chem. Soc.*, 2007, **129**, 6765-6781.
D. Franke, D. H. Harris, L. Xie, K. F. Jensen and M. G. Bawendi, *Angew. Chem., Int. Ed.*, 2015, **54**, 14299-14503.
E. Fujita, L. R. Furenlid and M. W. Renner, *J. Am. Chem. Soc.*, 1997, **119**, 4549-4550.
S. Gaillard and J.-L. Renaud, *Dalton Trans.*, 2013, **42**, 7255-7270.
S. Gambarotta, F. Arena, C. Floriani and P. F. Zanazzi, *J. Am. Chem. Soc.*, 1982, **104**, 5082-5092.
D. C. Gary and B. M. Cossairt, *Chem. Mater.*, 2013, **25**, 2463-2469.
D. C. Gary, B. A. Glassy and B. M. Cossairt, *Chem. Mater.*, 2014, **26**, 1734–1744.
D. C. Gary, M. Terban, S. J. L. Billinge and B. M. Cossairt, *Chem. Mater.*, 2015, **27**, 1432-1441.
D. C. Gary, S. E. Flowers, W. Kaminsky, A. Petrone, X. Li and B. M. Cossairt, *J. Am. Chem. Soc.*, 2016, **138**, 1510-1513.
J. L. Gomez-Lopez, D. Chávez, M. Parra-Hake, A. T. Royappa, A. L. Rheingold, D. B. Grotjahn and V. Miranda-Soto, *Organometallics*, 2016, **35**, 3148-3153.
M. Grasemann and G. Laurenczy, *Energy Environ. Sci.*, 2012, **5**, 8171-8181.
F. E. Hahn and M. C. Jahnke, *Angew. Chem., Int. Ed.*, 2008, **47**, 3122-3172.
F. E. Hahn, A. R. Naziruddin, A. Hepp and T. Pape, *Organometallics*, 2010, **29**, 5283-5288.
F. E. Hahn, *ChemCatChem*, 2013, **5**, 419-430.
F. E. Hahn, in *Advances in Organometallic Chemistry and Catalysis*, John Wiley & Sons, Inc., 2013, DOI: 10.1002/9781118742952.ch9, pp. 111-132.
F. E. Hahn, V. Langenhahn, T. Lugger, T. Pape and D. Le Van, *Angew. Chem., Int. Ed.*, 2005, **44**, 3759-3763.
J. Hawecker, J.-M. Lehn and R. Ziessel, *Helv. Chim. Acta*, 1986, **69**, 1990-2012.
C. Heinemann, T. Müller, Y. Apeloig and H. Schwarz, *J. Am. Chem. Soc.*, 1996, **118**, 2023-2038.
M. P. Hendricks, B. M. Cossairt and J. S. Owen, *ACS Nano*, 2012, **6**, 10054-10062.
M. P. Hendricks, M. P. Campos, G. T. Cleveland, I. Jen-La Plante and J. S. Owen, *Science*, 2015, **348**, 1226-1230.
W. A. Herrmann, *Angew. Chem., Int. Ed.*, 2002, **41**, 1290-1309.
N. Herron, J. C. Calabrese, W. E. Farneth and Y. Wang, *Science*, 1993, **259**, 1426-1428.
M. N. Hopkinson, C. Richter, M. Schedler and F. Glorius, *Nature*, 2014, **510**, 485-496.
H. Horvath, G. Laurenczy and A. Katho, *J. Organomet. Chem.*, 2004, **689**, 1036-1045.
M. A. Huertos, J. Pérez, L. Riera, J. Díaz and R. López, *Chem. Eur. J.*, 2010, **16**, 8495-8507.
C. A. Huff and M. S. Sanford, *ACS Catal.*, 2013, **3**, 2412-2416.
C. A. Huff, J. W. Kampf and M. S. Sanford, *Organometallics*, 2012, **31**, 4643-4645.
J. F. Hull, Y. Himeda, W.-H. Wang, B. Hashiguchi, R. Periana, D. J. Szalda, J. T. Muckerman and E. Fujita, *Nature Chem.*, 2012, **4**, 383.
Y. Inoue, H. Izumida, Y. Sasaki and H. Hashimoto, *Chem. Lett.*, 1976, **5**, 863-864.

H. Jacobsen, A. Correa, A. Poater, C. Costabile and L. Cavallo, *Coord. Chem. Rev.*, 2009, **253**, 687-703.
P. D. Jadzinsky, G. Calero, C. J. Ackerson, D. A. Bushnell and R. D. Kornberg, *Science*, 2007, **318**, 430-433.
M. C. Jahnke and F. E. Hahn, *Coord. Chem. Rev.*, 2015, **293**, 95-115.
M. S. Jeletic, E. B. Hulley, M. L. Helm, M. T. Mock, A. M. Appel, E. S. Wiedner and J. C. Linehan, *ACS Catal.*, 2017, **7**, 6008-6017.
W. B. Jennings, N. J. P. McCarthy, P. Kelly and J. F. Malone, *Org. Biomol. Chem.*, 2009, **7**, 5156-5162.
A. Kasuya, R. Sivamohan, Y. A. Barnakov, I. M. Dmitruk, T. Nirasawa, V. R. Romanyuk, V. Kumar, S. V. Mamykin, K. Tohji, B. Jeyadevan, K. Shinoda, T. Kudo, O. Terasaki, Z. Liu, R. V. Belosludov, V. Sundararajan and Y. Kawazoe, *Nature Mater.*, 2004, **3**, 99-102.
T. J. Korstanje, J. Ivar van der Vlugt, C. J. Elsevier and B. de Bruin, *Science*, 2015, **350**, 298-302.
T. Kösterke, T. Pape and F. E. Hahn, *J. Am. Chem. Soc.*, 2011, **133**, 2112-2115.
K. Kottsieper, O. Stelzer and P. Wasserscheid, *J. Mol. Catal. A*, 2001, **175**, 285-288.
M. V. Kovalenko, M. Scheele and D. V. Talapin, *Science*, 2009, **324**, 1417-1420.
J. P. Krogman, B. M. Foxman and C. M. Thomas, *J. Am. Chem. Soc.*, 2011, **133**, 14582-14585.
S. Kudera, M. Zanella, C. Giannini, A. Rizzo, Y. Li, G. Gigli, R. Cingolani, G. Ciccarella, W. Spahl, W. J. Parak and L. Manna, *Adv. Mater.*, 2007, **19**, 548-552.
B. Kumar, M. Llorente, J. Froehlich, T. Dang, A. Sathrum and C. P. Kubiak, *Ann. Rev. Phys. Chem.*, 2012, **63**, 541-569.
S. Kuwata and T. Ikariya, *Chem. Commun.*, 2014, **50**, 14290-14300.
X. Lan, S. Masala and E. H. Sargent, *Nature Mater.*, 2014, **13**, 233-240.
C. W. Leung, W. Zheng, Z. Zhou, Z. Lin and C. P. Lau, *Organometallics*, 2008, **27**, 4957-4969.
N. S. Lewis and D. G. Nocera, *Proc. Natl. Acad. Sci.*, 2006, **103**, 15729-15735.
J. C. Lewis, S. H. Wiedemann, R. G. Bergman and J. A. Ellman, *Org. Lett.*, 2004, **6**, 35-38.
Y. Li, I. Sorribes, T. Yan, K. Junge and M. Beller, *Angew. Chem., Int. Ed.*, 2013, **52**, 12156-12160.
A. Looney, R. Han, K. McNeill and G. Parkin, *J. Am. Chem. Soc.*, 1993, **115**, 4690-4697.
R. R. Lunt, T. P. Osedach, P. R. Brown, J. A. Rowehl and V. Bulović, *Adv. Mater.*, 2011, **23**, 5712-5727.
N. MacDowell, N. Florin, A. Buchard, J. Hallett, A. Galindo, G. Jackson, C. S. Adjiman, C. K. Williams, N. Shah and P. Fennell, *Energy Environ. Sci.*, 2010, **3**, 1645-1669.
A. M. Magill, K. J. Cavell and B. F. Yates, *J. Am. Chem. Soc.*, 2004, **126**, 8717-8724.
D. C. Marelius, E. H. Darrow, C. E. Moore, J. A. Golen, A. L. Rheingold and D. B. Grotjahn, *Chem. Eur. J.*, 2015, **21**, 10988-10992.
A. A. N. Magro, G. R. Eastham and D. J. Cole-Hamilton, *Chem. Commun.*, 2007, 3154-3156.
N. Marion, S. Díez-González and S. P. Nolan, *Angew. Chem., Int. Ed.*, 2007, **46**, 2988-3000.

J. Masuda, W. Schoeller, B. Donnadieu and G. Bertrand, *J. Am. Chem. Soc.*, 2007, **129**, 14180-14181.
J. R. McBride, A. D. I. Dukes, M. A. Schreuder and S. J. Rosenthal, *Chem. Phys. Lett.*, 2010, **498**, 1-9.
N. Meier, F. E. Hahn, T. Pape, C. Siering and S. R. Waldvogel, *Eur. J. Inorg. Chem.*, 2007, **2007**, 1210-1214.
D. Mellmann, P. Sponholz, H. Junge and M. Beller, *Chem. Soc. Rev.*, 2016, **45**, 3954-3988.
I. Mellone, M. Peruzzini, L. Rosi, D. Mellmann, H. Junge, M. Beller and L. Gonsalvi, *Dalton Trans.*, 2013, **42**, 2495-2501.
V. Miranda-Soto, D. B. Grotjahn, A. L. Cooksy, J. A. Golen, C. E. Moore and A. L. Rheingold, *Angew. Chem., Int. Ed.*, 2011, **50**, 631-635.
V. Miranda-Soto, D. B. Grotjahn, A. G. DiPasquale and A. L. Rheingold, *J. Am. Chem. Soc.*, 2008, **130**, 13200-13201.
V. Miranda-Soto, D. B. Grotjahn, A. L. Cooksy, J. A. Golen, C. E. Moore and A. L. Rheingold, *Angew. Chem., Int. Ed.*, 2011, **50**, 631-635.
I. Moldes, E. de la Encarnacion, J. Ros, A. Alvarez-Larena and J. F. Piniella, *J. Organomet. Chem.*, 1998, **566**, 165-174.
B. Mondal, J. Song, F. Neese and S. Ye, *Curr. Opin. Chem. Biol.*, 2015, **25**, 103-109.
A. J. Morris, G. J. Meyer and E. Fujita, *Acc. Chem. Res.*, 2009, **42**, 1983-1994.
C. B. Murray, C. R. Kagan and M. G. Bawendi, *Annu. Rev. Mater. Sci.*, 2000, **30**, 545-610.
N. Nakagawa, E. J. Derrah, M. Schelwies, F. Rominger, O. Trapp and T. Schaub, *Dalton Trans.*, 2016, **45**, 6856-6865.
A. R. Naziruddin, A. Hepp, T. Pape and F. E. Hahn, *Organometallics*, 2011, **30**, 5859-5866.
M. R. Norris, J. J. Concepcion, C. R. K. Glasson, Z. Fang, A. M. Lapides, D. L. Ashford, J. L. Templeton and T. J. Meyer, *Inorg. Chem.*, 2013, **52**, 12492-12501.
M. R. Norris, S. E. Flowers, A. M. Mathews and B. M. Cossairt, *Organometallics*, 2016, **35**, 2778-2781.
K. Öfele, *J. Organomet. Chem.*, 1968, **12**, P42-P43.
J. S. Owen, J. Park, P.-E. Trudeau and A. P. Alivisatos, *J. Am. Chem. Soc.*, 2008, **130**, 12279-12281.
J. S. Owen, *Science*, 2015, **347**, 615-616.
A. Paparo, J. S. Silvia, C. E. Kefalidis, T. P. Spaniol, L. Maron, J. Okuda and C. C. Cummins, *Angew. Chem., Int. Ed.*, 2015, **54**, 9115-9119.
D. Pugh and A. A. Danopoulos, *Coord. Chem. Rev.*, 2007, **251**, 610-641.
P. Pyykkö and M. Atsumi, *Chem. Eur. J.*, 2009, **15**, 186-197.
R. Sundburg, R. Shepherd and H. Taube, *J. Am. Chem. Soc.*, 1972, **94**, 6558-6559.
J. W. Raebiger, J. W. Turner, B. C. Noll, C. J. Curtis, A. Miedaner, B. Cox and D. L. DuBois, *Organometallics*, 2006, **25**, 3345-3351.
S. Ramakrishnan, K. M. Waldie, I. Warnke, A. G. De Crisci, V. S. Batista, R. M. Waymouth and C. E. D. Chidsey, *Inorg. Chem.*, 2016, **55**, 1623-1632.
H. G. Raubenheimer, F. Scott, G. J. Kruger, J. G. Toerien, R. Otte, W. van Zyl, I. Taljaard, P. Olivier and L. Linford, *J. Chem. Soc., Dalton Trans.*, 1994, 2091-2097.
N. M. Rezayee, C. A. Huff and M. S. Sanford, *J. Am. Chem. Soc.*, 2015, **137**, 1028-1031.

J. Ruiz and B. F. Perandones, *J. Am. Chem. Soc.*, 2007, **129**, 9298-9299.

J. Ruiz, D. Sol, J. F. Van der Maelen and M. Vivanco, *Organometallics*, 2017, **36**, 1035-1041.

J. Ruiz, A. Berros, B. F. Perandones and M. Vivanco, *Dalton Trans.*, 2009, 6999-7007.

J. S. M. Samec, J.-E. Backvall, P. G. Andersson and P. Brandt, *Chem. Soc. Rev.*, 2006, **35**, 237-248.

J. Sánchez-Nieves and P. Royo, *J. Organomet. Chem.*, 2001, **621**, 299-303.

S. Sanz, M. Benítez and E. Peris, *Organometallics*, 2010, **29**, 275-277.

W. Sattler and G. Parkin, *Catal. Sci. Technol.*, 2014, **4**, 1578-1584.

M. F. Schettini, G. Wu and T. W. Hayton, *Chem. Commun.*, 2012, **48**, 1484-1486.

H. Schnockel, *Chem. Rev.*, 2010, **110**, 4125-4163.

Y. Shirasaki, G. J. Supran, M. G. Bawendi and V. Bulović, *Nature Photon.*, 2013, **7**, 13-23.

A. K. Singh, S. Singh and A. Kumar, *Catal. Sci. Technol.*, 2016, **6**, 12-40.

G. Sini, O. Eisenstein and R. H. Crabtree, *Inorg. Chem.*, 2002, **41**, 602-604.

J. M. Smieja and C. P. Kubiak, *Inorg. Chem.*, 2010, **49**, 9283-9289.

R. J. Sundberg, R. F. Bryan, I. F. Taylor and H. Taube, *J. Am. Chem. Soc.*, 1974, **96**, 381-392.

Y. Tamaki, T. Morimoto, K. Koike and O. Ishitani, *Proc. Natl. Acad. Sci.*, 2012, **109**, 15673-15678.

K. L. Tan, R. G. Bergman and J. A. Ellman, *J. Am. Chem. Soc.*, 2002, **124**, 3202-3203.

R. Tanaka, M. Yamashita and K. Nozaki, *J. Am. Chem. Soc.*, 2009, **131**, 14168-14169.

T. Toda, S. Kuwata and T. Ikariya, *Chem. Eur. J.*, 2014, **20**, 9539-9542.

T. M. Trnka and R. H. Grubbs, *Acc. Chem. Res.*, 2001, **34**, 18-29.

M. Vogt, M. Gargir, M. A. Iron, Y. Diskin-Posner, Y. Ben-David and D. Milstein, *Chem. Eur. J.*, 2012, **18**, 9194-9197.

T. Vossmeyer, G. Reck, L. Katsikas, E. T. K. Haupt, B. Schulz and H. Weller, *Science*, 1995, **267**, 1476-1479.

W.-H. Wang, Y. Himeda, J. T. Muckerman, G. F. Manbeck and E. Fujita, *Chem. Rev.*, 2015, **115**, 12936-12973.

Y. Wang, Y. Zhang, F. Wang, D. E. Giblin, J. Hoy, H. W. Rohrs, R. A. Loomis and W. E. Buhro, *Chem. Mater.*, 2014, **26**, 2233-2243.

H. W. Wanzlick and H. J. Schönherr, *Angew. Chem., Int. Ed.*, 1968, **7**, 141-142.

S. Wesselbaum, V. Moha, M. Meuresch, S. Brosinski, K. M. Thenert, J. Kothe, T. vom Stein, U. Englert, M. Holscher, J. Klankermayer and W. Leitner, *Chem. Sci.*, 2015, **6**, 693-704.

S. H. Wiedemann, J. C. Lewis, J. A. Ellman and R. G. Bergman, *J. Am. Chem. Soc.*, 2006, **128**, 2452-2462.

L. Xiang, J. Xiao and L. Deng, *Organometallics*, 2011, **30**, 2018-2025.

R. Xie and X. Peng, *Angew. Chem., Int. Ed.*, 2008, **47**, 7677-7680.

R. Xie, Z. Li and X. Peng, *J. Am. Chem. Soc.*, 2009, **131**, 15457-15466.

C. Yin, Z. Xu, S.-Y. Yang, S. M. Ng, K. Y. Wong, Z. Lin and C. P. Lau, *Organometallics*, 2001, **20**, 1216-1222.

Q. Yu and C.-Y. Liu, *J. Phys. Chem. C*, 2009, **113**, 12766-12771.

G. Zassinovich, G. Mestroni and S. Gladiali, *Chem. Rev.*, 1992, **92**, 1051-1069.

J. Zhang, C. Rowland, Y. Liu, H. Xiong, S. Kwon, E. Shevchenko, R. D. Schaller, V. B. Prakapenka, S. Tkachev and T. Rajh, *J. Am. Chem. Soc.*, 2015, **137**, 742-749.

E. Mas-Marzá, M. Sanaú and E. Peris, *Inorg. Chem.*, 2005, **44**, 9961-9967.

V. T. Annibale, R. Batcup, T. Bai, S. J. Hughes and D. Song, *Organometallics*, 2013, **32**, 6511-6521.

# VITA

Sarah Elizabeth Flowers was born in 1989 in Houston, Texas, and since that time she has gone by the nick-name “Betsy”. She attended high school at St. John’s School in Houston, TX. In 2012 she received her Bachelors of Science in Chemistry with a Minor in Music from the Massachusetts Institute of Technology in Cambridge, MA. While at MIT she worked as an undergraduate researcher in Prof. Richard Schrock’s laboratory. Betsy attended graduate school at the University of Washington in Seattle, and her research was conducted under Professor Brandi Cossairt. Betsy received her PhD in Chemistry from the University of Washington in 2017.